2015-07-13

Optimal Design of Solar Photovoltaic Systems

Hoe-Gil Lee
University of Miami, hoegillee@yahoo.com

UNIVERSITY OF MIAMI

OPTIMAL DESIGN OF SOLAR PHOTOVOLTAIC SYSTEMS

By

Hoe-Gil Lee

A DISSERTATION

Submitted to the Faculty
of the University of Miami
in partial fulfillment of the requirements for
the degree of Doctor of Philosophy

Coral Gables, Florida

August 2015

UNIVERSITY OF MIAMI

A dissertation submitted in partial fulfillment of
the requirements for the degree of
Doctor of Philosophy

OPTIMAL DESIGN OF SOLAR PHOTOVOLTAIC SYSTEMS

Hoe-Gil Lee

Approved:

_____	_____
Singiresu S. Rao, Ph.D. Professor of Mechanical and Aerospace Engineering	Hongtan Liu, Ph.D. Professor of Mechanical and Aerospace Engineering
_____	_____
Shihab S. Asfour, Ph.D. Professor of Industrial Engineering	Dean of the Graduate School
_____	
Michael R. Swain, Ph.D. Associate Professor of Mechanical and Aerospace Engineering	

HOE-GIL, LEE (Ph.D., Mechanical Engineering)

Optimal Design of Solar Photovoltaic Systems (August 2015)

Abstract of a dissertation at the University of Miami.

Dissertation supervised by Professor Singiresu S. Rao
No. of pages in text. (278)

A solar PV array system is comprised of the following components - solar cells, panel modules, and an array system. Thus, overall optimal design of a solar PV system involves the optimal design of the components at three levels - solar cell, panel module, and array. The conversion efficiency, power output, and incident solar energy pertaining to the requirements of seasonal demands are to be considered in the process. At the solar cell level, cell performance depends on solar cell structure, top contact design, and cell size. The correlations between cell structure, cell size and top contact design are investigated. At the PV panel module level, the optimization of a PV panel module is investigated based on the optimal design of individual solar cells for maximizing the power output. The role of the PV panel module is interactive between solar cells and the array system and is composed of a number of solar cells and panel modules. In designing a solar PV array system with cost considerations, the performance of a solar PV array system is investigated based on the performance of its subsystems - the solar cell and the panel module – as well as the cost of the array system. The optimal design of an array system is considered by formulating six single-objective optimization problems – the maximization of the conversion efficiency of the cells, power output of the arrays, annual monthly

average incident solar energy, lowest month's and highest month's incident solar energy and minimization of cost.

Multi-objective optimum designs of a solar cell, flat plate solar PV array system and compound parabolic concentrator (CPC) PV collector system are also considered by using mathematical techniques. Game theory and fuzzy set theory methodologies are used for finding the solution of multi-objective optimization problems derived from the results of single-objective problems using genetic algorithms of *ga* (program MATLAB). For a solar cell, the multi-objective optimization is constructed using two objectives – the maximization of the conversion efficiency and power output. The resulting multi-objective optimization (of a solar cell) is investigated with varying intensities of sunlight and by placing constraints on the minimum permissible conversion efficiency while maximizing efficiency and power output. Multilevel system optimization problems are solved using game theory and fuzzy set theory for finding a compromise solution of the six-objective optimization problems which are related to conversion efficiency, power output, annual incident solar energy, winter incident solar energy, summer incident solar energy and total cost of the PV array system. In the case of a solar CPC collector system, there are three single-objective problems: annual monthly average of incident solar energy, lowest month's incident solar energy and cost. Game theory methodology is used for finding a compromise solution in the process of constraints stated.

The aim of uncertainty analysis is to predict the performance of a component or system in the presence of uncertain parameters. Uncertainty analyses of a solar cell, flat plate PV array system and CPC PV collector system are considered using probabilistic and fuzzy analysis methodologies. In probabilistic analysis, the random variables of a solar cell and

solar PV array system include geometric design variables (except for integer values) and uncertain design parameters of top metallic contact. The solar cell and solar PV array system have been investigated by varying the values of the weight of mean and coefficient variations and illustrations by applying the parametric study related to the probabilistic efficiency of a solar cell and solar PV array system. The fuzzy membership functions are used for modeling the uncertain or imprecise design parameters of a solar PV system. Triangular membership functions are used to represent the uncertain parameters as fuzzy quantities. Fuzzy arithmetic operations and extension principles are used for finding the membership functions of the fuzzy response parameters of the system. In the case of a solar cell, the deviations of solar cell performance including the conversion efficiency and power output from the crisp value are investigated by varying α-cut interval levels and uncertain input parameters of different fuzzy confidence intervals. In the case of a CPC PV collector system, the responses from applying uncertain input parameters of different fuzzy confidence interval levels are investigated by using the crisp values of annual monthly average incident solar energy, lowest month incident solar energy, and cost. Also, the variations of three single-objective problems are represented by using a triangular shape with respect to various fuzzy interval confidence levels.

ACKNOWLEDGEMENTS

I would like to extend my sincere gratitude and appreciation to my Ph.D. dissertation advisor and chairman of the committee, Dr. Singiresu S. Rao. He demonstrated exemplary guidance, patience and encouragement throughout the entire research and dissertation process. Working closely with him over the past four years has been a marvelous and enriching experience. My thanks also go to University of Miami faculty members, namely the members of my dissertation committee: Dr. Michael R. Swain and Dr. Hongtan Liu in the Department of Mechanical & Aerospace Engineering, and Dr. Shihab S. Asfour in the Department of Industrial Engineering. Their constructive criticism and input have been invaluable. I would also like thank Dr. Jaedal Jung in the Department of Mechanical and Aerospace Engineering for his consistent support and insight when I encountered academic obstacles. Above all, I would like to thank my parents, brothers, and especially my dear, selfless sister. I have the deepest gratitude to my inspirational wife, Devon, and our beautiful baby girl, Arabella Nari. I also appreciate the unrelenting advocacy and sacrifices made by my mother-in-law, Janet, and sister-in-law, Dana.

CONTENTS

LIST OF TABLES

LIST OF FIGURES

LIST OF NOMENCLATURE

C = Intensity of sunlight (an integer)

D_b= Spacing between the busbars (cm)

D_f = Spacing between the fingers (cm)

D_p = Minority electron diffusion coefficient (cm^2/s)

D_n = Minority hole diffusion coefficient (cm^2/s)

F_b =Fractional power loss of the resistivity of the busbars (%)

F_c = Fractional power loss of contact resistance (%)

F_f = Fractional power loss of the resistivity of the fingers (%)

F_{sum} = Total fractional power losses (%)

F_s = Fractional power loss of shadowing (%)

F_{sr} = Fractional power loss of sheet resistance (%)

H_c = Height of cell (cm)

J_B = Current density of base (mA/cm^2)

J_E = Current density of emitter (mA/cm^2)

J_L= Light-generated current density (mA/cm^2)

J_m = Maximum operating current density (mA/cm^2)

J_{SCR} = Current density of space-charge region (mA/cm^2)

J_S = Saturation current density (mA/cm^2)

J_{sc} = Short-circuit density (mA/cm^2)

k = Boltzmann constant (8.617×10^{-5} eV/K)

L_p = Minority electron diffusion length (μm)

L_n = Minority hole diffusion length (μm)

L_T = Current transfer length (μm)

L_c = Length of cell (cm)

N_a = Acceptor concentration (cm^3)

N_d = Donor concentration (cm^3)

n_i = Intrinsic carrier concentration (cm^3)

n_{ph} = Photon flux ($cm^{-2}\ s^{-1}$)

P_m = Maximum operating power density (W/cm^2)

P_{in} = Input incident power density (W/m^2)

P_o = Power output (W)

q = Electron charge ($1.602\times10^{-19}\ colulomb$)

R = Reflection coefficient of the anti-reflective coating

R_c = Contact resistance ($\Omega\cdot cm^2$)

R_{sh} =Sheet resistance (Ω/cm^2)

S_p = Recombination velocity of the front surface (cm/s)

S_n = Recombination velocity of the back surface (cm/s)

t_{scr} = Width of the space charge region (μm)

T = Temperature (K)

T_e = Thickness of the emitter region (μm)

T_b = Thickness of the base region (μm)

V_{oc} = Open-circuit voltage (mV)

V_m = Maximum operating voltage (mV)

L_c = Length of cell (cm)

α = Absorption coefficient (cm^{-1})

η= Conversion efficiency of a solar cell (%)

η_{ma} = Maximum conversion efficiency of a solar cell (%)

τ_p = Minority carrier lifetime in the emitter region (μs)

τ_n= Minority carrier lifetime in the base region (μs)

δE_g = Shrinkage of the energy gap (eV)

ρ_m = Metal resistivity ($\Omega\cdot cm$)

λ = Wavelength (μm)

CHAPTER 1

Introduction

1.1 Overview of Solar Energy

The effects of climate change have become a cumbersome reality of the 21st century. No society is completely safe from the rapid changes in the climate, and its consequences are seen in rising sea levels, warming oceans, shrinking ice, and glacial retreat. Summers are longer and hotter while winters are shorter and warmer. An overwhelming majority of scientists believe that climate change is caused by human-induced emissions of heat-trapping gases, such as carbon dioxide (CO_2) and water vapor (H_2O) in the atmosphere. The greenhouse effect, as it is commonly known, is a result of the burning of mass amounts of fossil fuels. If we do not want future generations to be burdened with the catastrophic impact of climate change, we must act now to enforce drastic change in how we obtain and use energy.

We are thus turning to renewable energy sources; they are considered renewable because they come from resources such as sunlight, wind, ocean energy, hydrogen, waves, and geothermal heat. They can potentially offer several benefits that conventional sources of energy cannot because they are clean and guarantee energy security. Therefore, we should strive to replace the conventional plant in electricity energy generation with sources of renewable energy. Since regulatory or policy efforts aimed at reducing emissions would also affect the energy supply system, vigorous research into the

application of alternative and green energy sources must be conducted. Table 1-1 shows the growth of renewable energy [www,eig.gov/aer: Annual Energy Review 2011].

Table 1-1 U.S. renewable electricity nameplate capacity (MW)

	Hydro	Solar PV	CSP	Wind	Geothermal	Biomass	Total Renewables
2001	76,91 (0%)	29 (62.4%)	354 (0%)	4,275 (65.8%)	2,798 (0%)	10,576 (-0.9%)	94,943 (1.7%)
2002	77,04 (0.2%)	52 (76.9%)	354 (0%)	4,686 (9.6%)	2,798 (0%)	10,867 (2.8%)	95,804 (0.9%)
2003	77,02 (0%)	97 (87.3%)	354 (0%)	6,353 (36.6%)	2,798 (0%)	10,856 (-0.1%)	97,478 (1.7%)
2004	77,13 (0.1%)	155 (59.2%)	354 (0%)	6,725 (5.9%)	2,798 (0%)	11,033 (1.6%)	98,195 (0.7%)
2005	7,354 (0.3%	234 (51.0%)	354 (0%)	9,121 (35.6%)	2,828 (1.1%)	11,222 (1.7%)	101,113 (3.0%)
2006	7,419 (0.1%	339 (44.7%)	355 (0.3%)	11,575 (26.9)	2,831 (0.1%)	11,553 (2.9%)	104,072 (2.9%)
2007	77,432 (0%)	508 (49.8%)	419 (18%)	16,812 (45.2%)	2,937(3.7%)	11,738(1.6%)	109,845 (5.5%)
2008	7,640 (0.3%	819 (61.2%)	419 (18%)	25,237 (50.1%)	3,040 (3.5%)	12,485 (6.4%)	119,6393 (8.9%)
2009	7,910 (0.3%	1,257 (53.5%)	430 (2.6%)	35,159 (39.3%)	3086 (1.5%)	12,836 (2.8%)	130,677 (9.2%)
2010	8,204 (0.4%	2,153 (71.3%)	507 (18.0%)	40,267 (14.5%)	3,101 (0.5%)	13,053 (1.7%)	137,286 (5.1%)
2011	78,237 (0%)	4,011 (86,3%)	516 (1.7%)	46,916 (16,5%)	3,187 (2.8%)	13,276 (1.7%)	146,412 (6.5%)

Wind and solar energy are the fastest growing renewable electricity methods, and their capacities are being widely investigated and debated. Remarkably, solar photovoltaic installed capacity grew more than 86% in the beginning of the 21st century.

Solar energy is simply energy that comes from the sun. There are a variety of technologies that have been developed to take advantage of the different forms of capturing solar energy, such as solar photovoltaic (PV), thermal electricity, and heating systems. In general, solar PV and thermal electricity systems have experienced phenomenal growth in recent years due to both technological improvements resulting in cost reductions and government policies supportive of renewable energy development and utilization. While early solar technologies consisted of small-scale photovoltaic cells, recent technologies are represented by concentrated solar power (CSP) and by large-scale PV systems that feed into electricity grids. Table 1-2 shows solar electricity capacity and

increases from previous years [U.S department of Energy: 2011 Renewable Energy Data Book].

Table 1-2 U.S. total installed solar electricity capacity and generation

	U.S. Solar Energy Generation (Million kWh)	U.S. Solar Energy Capacity (MW) and % Increase form Previous Year			
		PV	CSP	Total	Increase
2000	804	18	354	372	4.3%
2001	822	29	354	383	3.0%
2002	857	52	354	406	5.9%
2003	929	97	354	451	11.2%
2004	1,020	155	354	509	12.8%
2005	1,145	234	354	588	15.5%
2006	1,312	339	355	694	18.0%
2007	1,718	508	419	927	33.5%
2008	2,208	819	419	1237	33.5%
2009	2,922	1257	430	1686	36.3%
2010	4,505	2153	507	2660	57.7%
2011	7,454	4011	516	4527	70.2%

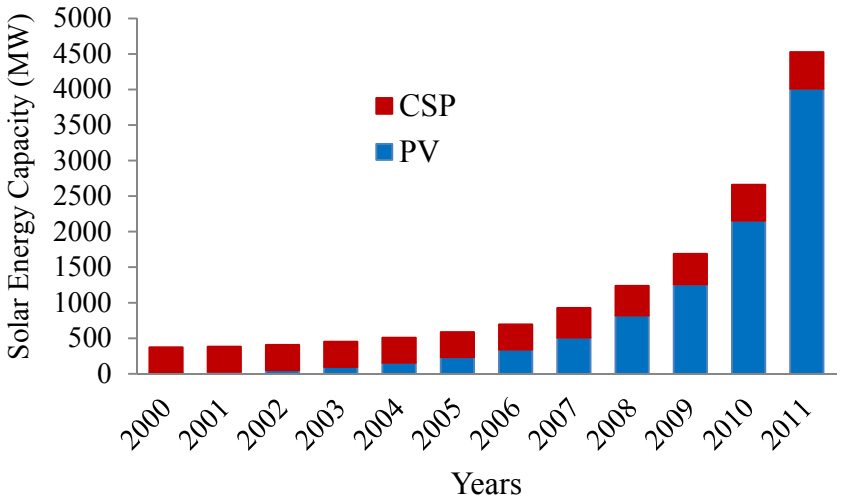

As seen in Tables 1-1 and 1-2, solar energy is growing exponentially as more and more people recognize its potential; simultaneously, the costs of solar energy technologies have dropped substantially. Solar energy is almost infinite as a resource, and has the possibility to far exceed the entire global energy demand. Despite this technical potential and the recent growth of the market, the contribution of solar energy to the global energy supply mix is still relatively insignificant.

Solar thermal electricity is a proven technology that has been in existence for close to 30 years. Its strengths rest in its ability to make electric capacities firm and to time-shift electricity generation, thanks to thermal storage. Low concentration power systems may offer new options with storage under a greater variety of climates, but high concentration power plants such as parabolic trough and dish engine systems can be installed in desert regions in order to collect more sun's heat energy. The trend is to increase working temperatures, and to set up towers with a great variety of designs and applications.

Concentrating the solar rays allows for higher working temperatures with good efficiency at the collector level, leading to improved efficiency in the conversion of the heat into mechanical energy. The ideal efficiency is defined as the ratio of the difference in temperatures of the hot and the cold source, divided by the absolute temperature as well as hot source. Receiver efficiency is a function of the working fluid temperature for various the concentration ratio. Accordingly, the efficiency of the receiver depends on the working fluid temperature.

Photovoltaic (PV) system materials and devices convert sunlight into electrical energy, and PV cells are commonly known as solar cells. In fact, the term "photovoltaic system" can literally be translated as *light-electricity*. Simple PV systems provide power for small

consumer items, such as calculators and wristwatches. More complicated systems provide power for communication satellites, water pumps, lights, appliances, and machines in residential and commercial buildings. Now a days, many road and traffic signs are also powered by PV systems.

Solar PV cells come in many different shapes and sizes, from sizes smaller than a postage stamp to sizes over several inches across. They are often connected together to form PV modules that may be up to several feet long and a few feet wide. The PV modules, in turn, can be combined and connected to form PV arrays of varying sizes and power outputs. The modules of the array make up the major part of a PV system, which can also include electrical connections, mounting hardware, power-conditioning equipment, and energy storage systems that store solar energy for use when the sunlight is not immediately available.

The PV system market is currently dominated by crystalline silicon-based PV cells, which accounted for more than 80 % of the market in 2011. The remainder of the market almost entirely consists of thin film technologies that use cells made by directly depositing a photovoltaic layer on a supporting substrate.

1.2 Types of Solar Power Systems

The solar energy conversion systems can be largely divided into 2 types: concentrating solar power systems (CSP), which is accomplished through heat transfer, and solar PV systems (PV), which is accomplished through light energy.

1.2.1 Concentrating solar power system

A solar thermal conversion system is a technology that converts heat to generate electricity on demand. In this process, a heat transfer fluid is heated as it circulates through the receivers within the collectors. It operates through heat exchange to generate high-pressure heated steam. The working fluid is fed into a separate section to provide power to rotate a conventional turbine system. The heated working fluid from the turbine is condensed by a condenser and transferred into a liquid state from a vapor state to be re-heated in the solar steam generator to complete the cycle.

A solar thermal power system is composed of three sub-systems: solar energy collector, thermal energy storage, and power generation systems as shown in Fig. 1-1.

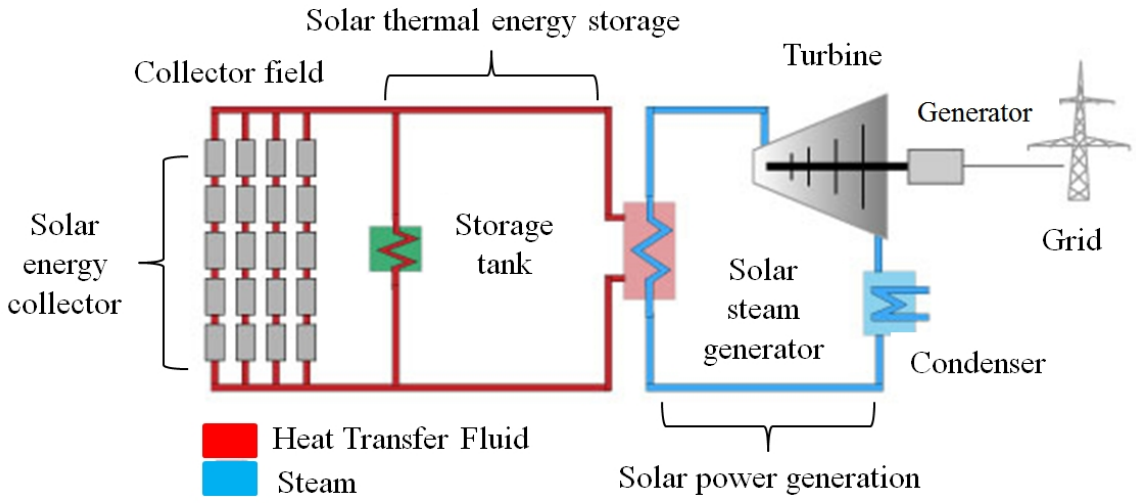

Figure 1-1 Stand-alone solar rankine system

(Source: Green Rhino Energy (www.greenrhinoenergy.com)

For collecting solar energy, a solar field is comprised of rows of solar thermal systems. A working fluid is transported to thermal energy storage tanks and used to boil water to generate steam for use in a conventional steam generator to produce electricity. The solar thermal conversion process of solar energy is based on heat transfer.

Solar thermal technologies use mirrors or lenses to reflect and concentrate a large area of sunlight onto small surfaces that collect solar thermal energy and convert it to electricity. Solar thermal systems use a different technology than photovoltaic systems because higher temperatures are ultimately used to convert heated energy into electricity. Solar thermal energy systems can be classified according to the temperatures of the working fluid. In case of low temperature collectors, compound parabolic concentrator (CPC) solar power system allows an efficient conversion of sunlight to thermal energy at temperatures of 130 °C to 160 °C in stationary collectors. The other types of concentrating solar thermal collectors include Fresnel collectors, parabolic troughs, dishes, and towers allow much higher working temperatures up to 2500°C. Figure 1-2 shows different types of concentration solar power systems.

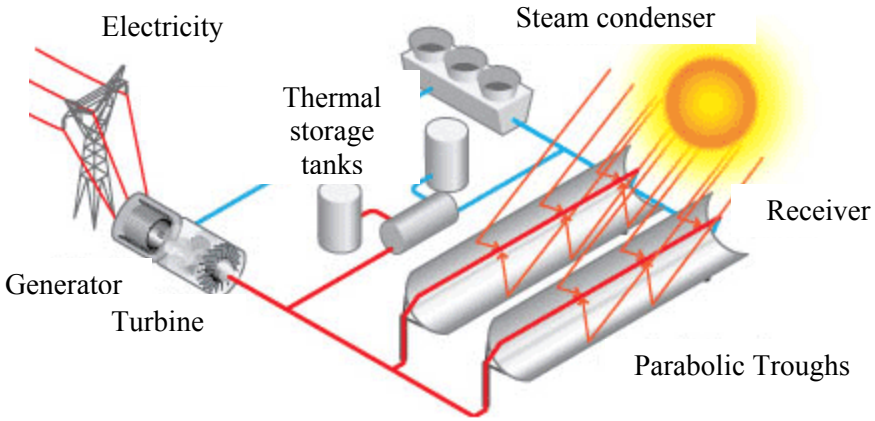

(a) Parabolic trough system

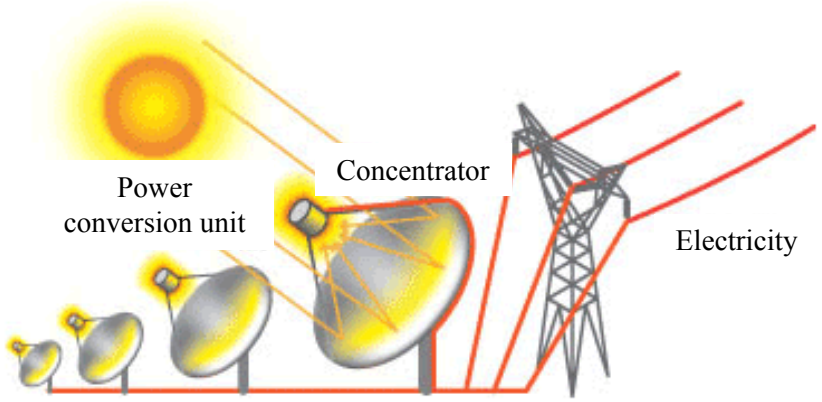

(b) Dish/engine system

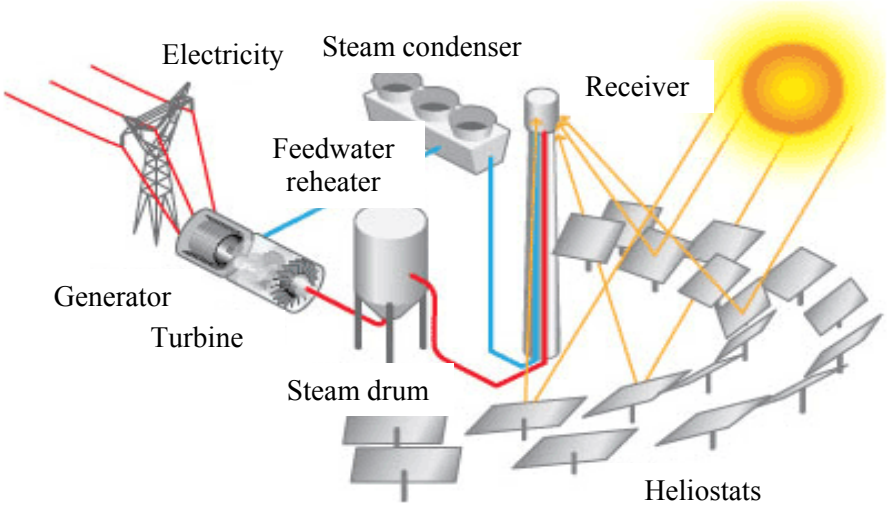

(c) Power tower system

Figure 1-2 Parabolic trough system, dish/engine system, and power tower system

(Source: Energy.gov, Office of Energy Efficiency & Renewable Energy)

The efficiency of parabolic shape of collectors can be explained by its relation to a high geometric concentration ratio. The reason that some collectors have a flat shape is to enable focus on solar thermal energy by tracking the sun's movement. A parabolic trough consists of multiple collectors arranged in parallel rows. These are typically aligned in a

north-south position for the purpose of maximizing the annual and summer energy collection with one-axis tracking. The concentration ratio is 200x for maximum concentration and around 100x in practice. The parabolic trough is typically a linear concentrating solar power (CSP) collector. Once ultra-heated steam is generated by the solar collector, it spins a turbine that triggers a generator to produce electricity. Alternatively, steam can be generated directly in the solar field; in some ways, this is ideal since it eliminates the need for costly heat exchangers. With a single-axis sun-tracking system, this configuration enables the mirrors to track the sun from east to west during the day, which ensures that the sun reflects continuously onto the receiver tubes.

Because the dish/engine system consists of a thermal concentrator and power conversion unit, this system can only produce relatively small amounts of electricity compared to parabolic trough applications. The concentration ratio, also, is 4,600x for maximum concentration and 1000x in practice with two-axis tracking and gathers the solar thermal energy coming directly from the sun raises temperature up to 1,000°C. The resulting beam of concentrated sunlight is reflected onto a thermal receiver that collects the solar heat. The dish is mounted on a tracking structure which monitors the sun continuously throughout the day to acquire the highest percentage of sunlight possible onto the thermal receiver.

A tower system is a type of solar furnace using a tower to receive thermal solar energy through many flat reflectors. A characteristic of this system is the sun-tracking mirrors that are designed to collect energy found at the top of the tall tower. A heat-transfer fluid heated in the receiver is used to generate steam, which, in turn, is used in a conventional turbine generator to produce electricity. While some power tower systems use

water/steam as the heat-transfer fluid, advanced designs are experimenting with molten nitrate salt due to its superior heat-transfer and energy-storage capabilities.

1.2.2 Photovoltaic solar power system

Photovoltaic (PV) cells use the energy in sunlight to produce electricity. However, the amount of electricity produced depends on the quality of the light available and the performance of the PV cells. The conversion efficiency of a photovoltaic (PV) cell is the percentage of the solar energy shining on a PV device that is converted into electricity. Improving this conversion efficiency is a key goal of research and helps make PV technologies cost-competitive with more conventional sources of energy. Much of the energy from sunlight reaching a PV cell is lost before it can be converted into electricity. But certain characteristics of solar cell materials also limit the cell's efficiency to convert the sunlight it receives. Figure 1-3 shows how a photovoltaic (PV) system functions.

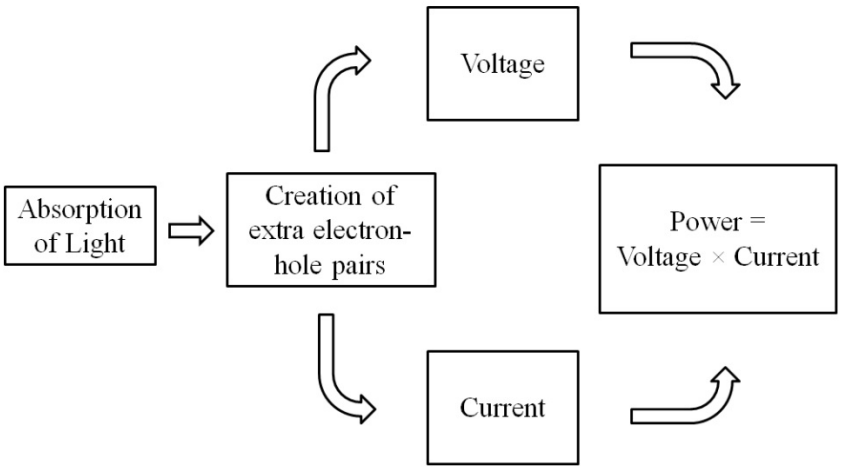

Figure 1-3 Diagram of photovoltaic effect

Light is composed of photons or packets of energy that range in wavelength. When light strikes the surface of a solar cell, some photons are reflected and do not enter the cell. Other photons pass through the material. Of these, some are absorbed but only have enough energy to generate heat, and some have enough energy to separate electrons from their atomic bonds to produce charge carriers negative electrons and positive holes.

Photovoltaic systems can be divided into flat plate PV systems and CPV systems. The most common photovoltaic (PV) array design uses flat plate PV panels. These panels-based solar cells can be fixed in place. Their response to sunlight accounts for between 10% and 20% of the total solar radiation on a horizontal surface. On partly sunny days, up to 50% of that radiation is diffused, and on cloudy days, 100% of the radiation is diffused. Therefore, the design of a flat-plate solar PV system should take into account the relationships among the cell parameters, panel parameters, location and solar energy. A flat-plate PV system can be divided into three levels: the cell, panel and array system, as shown in Fig.1-4.

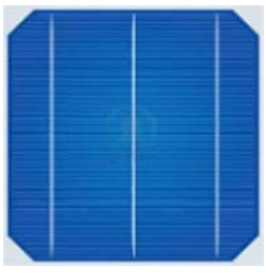

(a) Solar cell

(b) Panel module

(c) PV array system

Figure 1-4 Levels of a Flat Plate Photovoltaic System

At the cell level, the basic PV cells produce electricity from sunlight. The main consideration is the energy conversion efficiency, which varies with the material used, structure, contact design and intensity of sunlight. Within the panel, the main consideration is the nature in which the cells are interconnected because this dictates how much power is produced. Based on the optimized cell and panel, designs made at the array level of the PV system are dependent upon customer requirements, and factors such as energy usage, budget, and location also play a role. The cell and array sizes are flexible and can be modified on a case-by-case basis according to customer needs. However, the panel is regulated according to the power output needs.

Concentrator PV (CPV) systems use lenses or reflectors to concentrate sunlight onto PV cells. This technique leads to a reduction in the cell area required for generating a desired amount of power. The goal is to significantly reduce the cost of electricity generated by replacing expensive PV converter areas with less expensive optical material. Figure 1-5 demonstrates the two types of concentrator technologies.

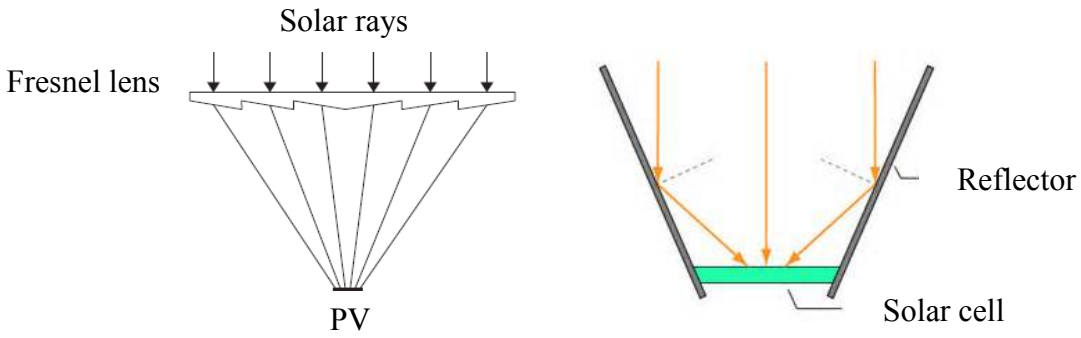

(a) Fresnel lens (b) Reflector

Figure 1-5 Types of concentrating PV systems

A Fresnel lens uses different angles to increase the collection of solar rays. As a high concentration ratio, it is possible to use a multi-junction photovoltaic cell with maximum efficiency. Reflector technology can be applied to low concentration photovoltaic module systems to collect sunlight by a solar cell. Determining the angle of the mirrors is dependent on the direction of a photovoltaic module system, which is fixed, including inclination of installation and location. The concentration ratios range between 1.5 and 2.5. This approach also provides the opportunity to use higher performance PV cells that

would be prohibitively expensive. As a result, concentrator modules can easily exceed 20% in energy conversion efficiency. While the concept is simple and has been examined since terrestrial photovoltaics first gained scientific attention, the practice has proven to be challenging and unreliable. Concentrator research has focused much effort on the PV cells. The main concern is to collect point-focus-optics based on two axes of azimuth and elevation, as shown in Fig. 1-6.

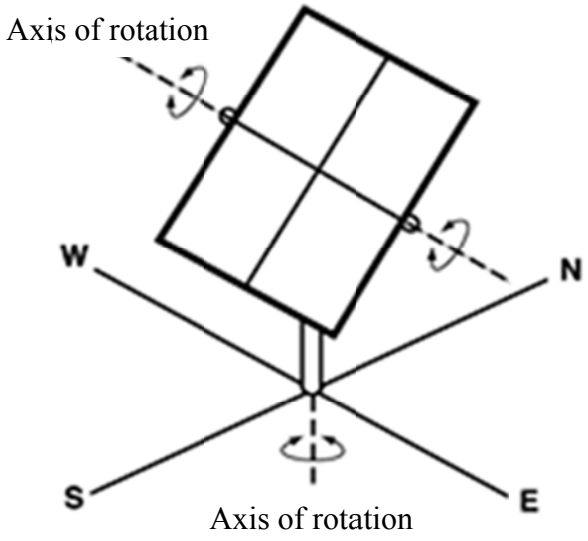

Figure 1-6 Two-axis tracking configurations

Even though evidence shows that the two-axis system is more complex than the one-axis tracking, the resulting point focus systems are capable of achieving higher concentration ratios and lower cell costs. The two main obstacles that research seeks to overcome are: first the difficult cell packaging requirements stemming from the high heat flux and electrical current density, and the second need for more cost-effective and reliable tracking system and module designs. There are four common types of one-and two-axis tracking systems, as shown in Fig. 1-7.

(a) Horizontal axis tracker

(Sorce: www.cleantick.com)

(b) Vertical axis tracker

(Sorce: www.tradekorea.com)

(c) Tilted axis tracker

(Sorce: www.tradekorea.com)

(d) Dual axis tracker

(Sorce: www.solarpowerportal.co.uk)

Figure 1-7 Tracking types of concentrator photovoltaic system

Ground-mounted solar installations may make use of tracking platforms that can tilt the surface along one or two axes with the help of a motor.

1.3 How to Approach the Optimal Design of Solar PV Systems

When sunlight reaches a solar energy system, the solar energy system generates electricity through thermal and optical energy conversion. If there are no energy losses, the input (solar energy) is proportional to the output (electricity). However, due to noise factors, which are non-design variables, and controlled factors, which include design variables, the output is reduced. Therefore, the output is lower than the theoretical value because of energy losses, as shown in Fig. 1-8.

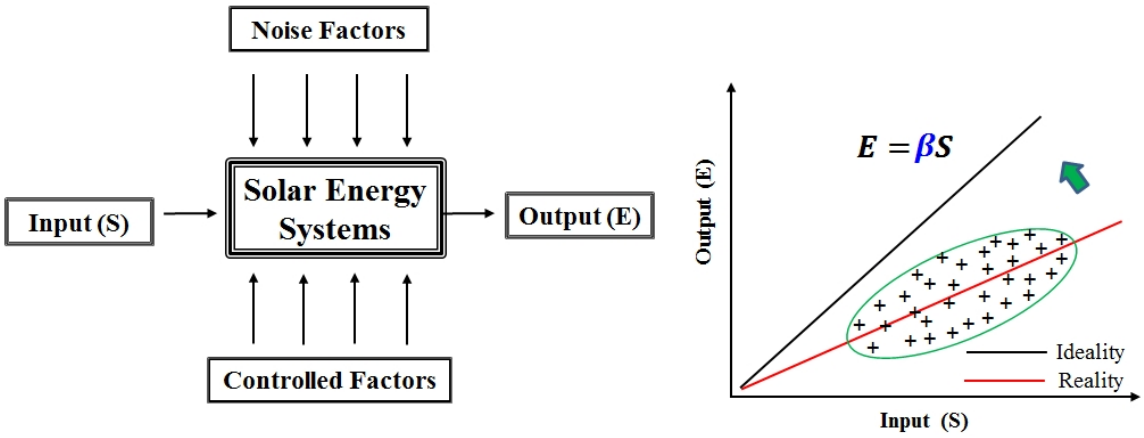

Figure 1-8 Optimal design of solar energy systems and how to approach optimization

The amount of solar energy, known as solar radiation, is reliant upon the motion of the earth around the sun, the motion of the earth around its own axis, and the angle between the earth's equator and the plane of the sun-earth orbital system. Figure 1-9 shows the position of the sun at any given point on earth.

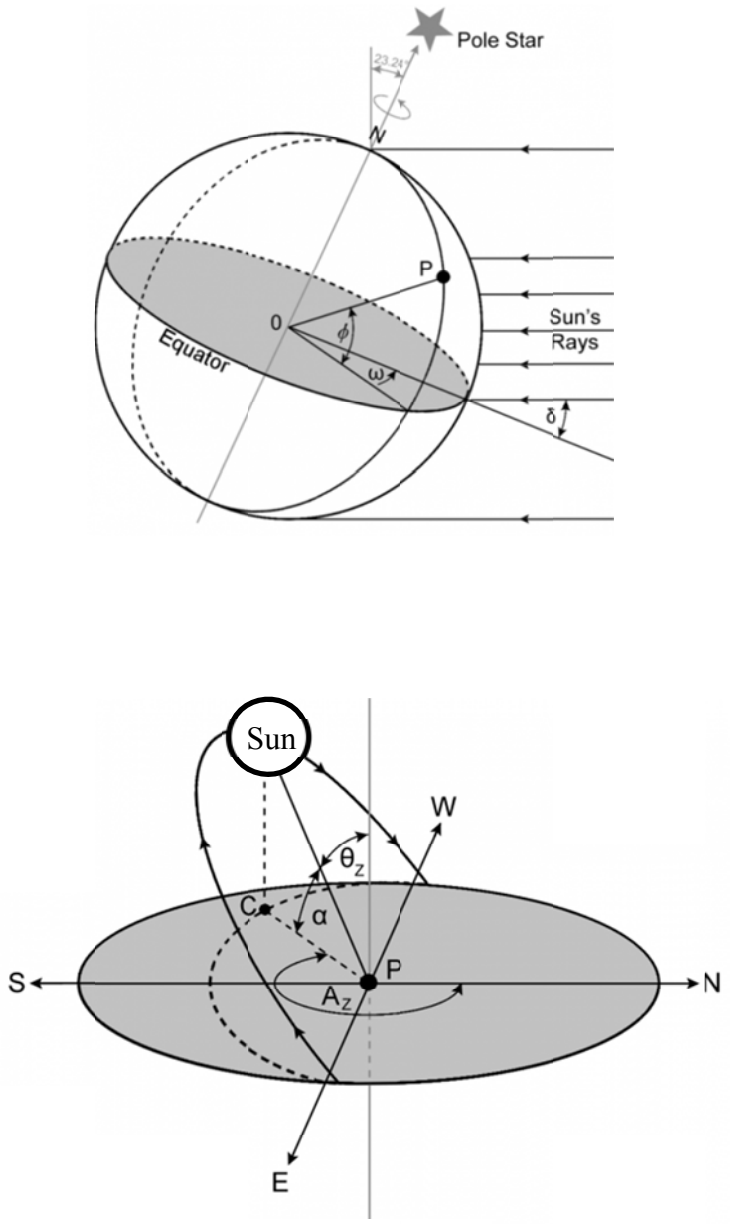

Figure 1-9 Definitions of declination angle (δ), latitude (φ), the hour angle (ω) for point P, sun's zenith (θ_z), altitude (α), and azimuth angles (A_z) for the sun.

To calculate the amount of solar radiation, due to sun's rays reaching the earth, it is necessary to understand the solar angles, angle (δ), latitude (φ), hour angle (ω), sun's zenith (θ_z), altitude (α), and azimuth angle (A_z). Chapter 2 will closely examine the

approaches to calculating solar radiation. The three major concerns for optimization of solar energy systems are identified as the annual monthly average incident solar energy and incident solar energy in the lowest and highest months.

a) Annual monthly average incident solar energy

The aim of a fixed solar energy system is to collect the maximum amount of solar energy in a given year. From a fixed perspective on Earth, the sun appears to move across the sky. Although the sun does not actually move, rotation of the Earth about its axis instigates changes in the angle at which the direct component of light will strike the Earth. The position of the sun depends on the geographical location of a point on Earth, the time of day, and the time of year. This apparent motion of the sun has a major impact on the amount of power received by a solar collector. When the sun's rays are perpendicular to the absorbing surface, the power density on the surface is equal to the incident power density. However, as the angle between the sun and the absorbing surface is diversified, the intensity on the surface is reduced. In fact, when the module is parallel to the sun's rays, the intensity of light essentially falls to zero. For intermediate angles, the relative power density is the angle between the sun's rays and the solar collectors. Therefore, annual average of hourly, daily and monthly solar incident solar energy on tilted collectors is needed to calculate the solar energy based on solar angles.

b) Incident solar energy of the lowest month

The variation in solar angles has a major impact on the amount of incident solar energy that is collected by a solar collector. The angle between the absorbing surface of a collector on ground and sunlight’s direction can be determined for any particular location

in view of the length of hourly, daily, monthly and yearly sunlight, and longitude. The most important design parameters in a solar energy system are elevation, declination, and azimuth angles to collect the maximum amount of solar energy.

Solar collectors can collect more incident solar energy in summer than in winter due to the tilt angle of the earth. The tilt angle varies seasonally because of the rotation of the earth around the sun as shown Fig. 1-10.

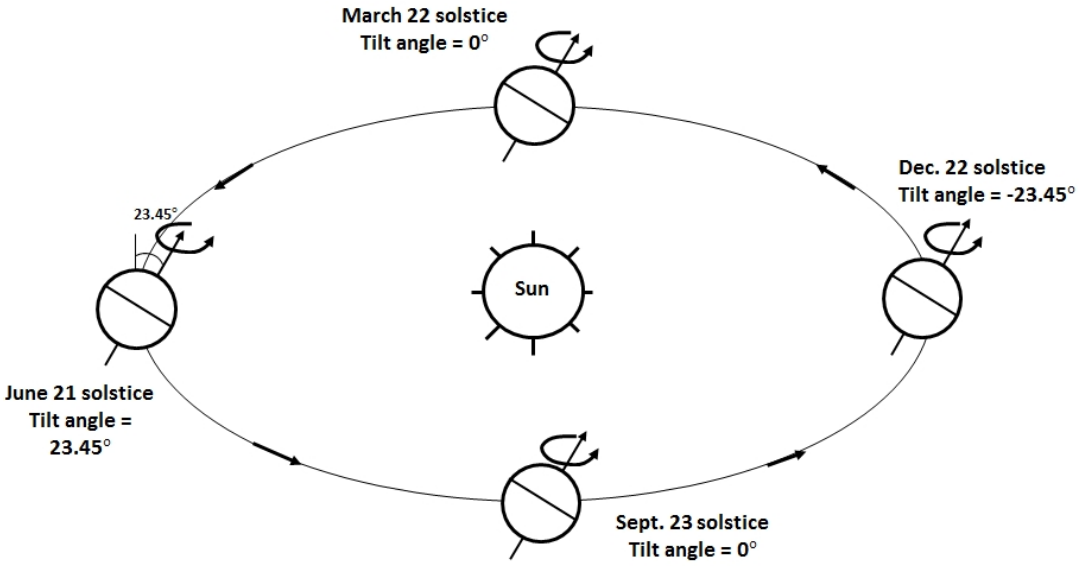

Figure 1-10 (a) Tilt angle changes from summer to winter in the northern hemisphere

Although the horizontal face of the solar energy system absorbs the solar energy for maximum performance in summer, the amount of solar radiation is not always maximum due to the particular location and the season.

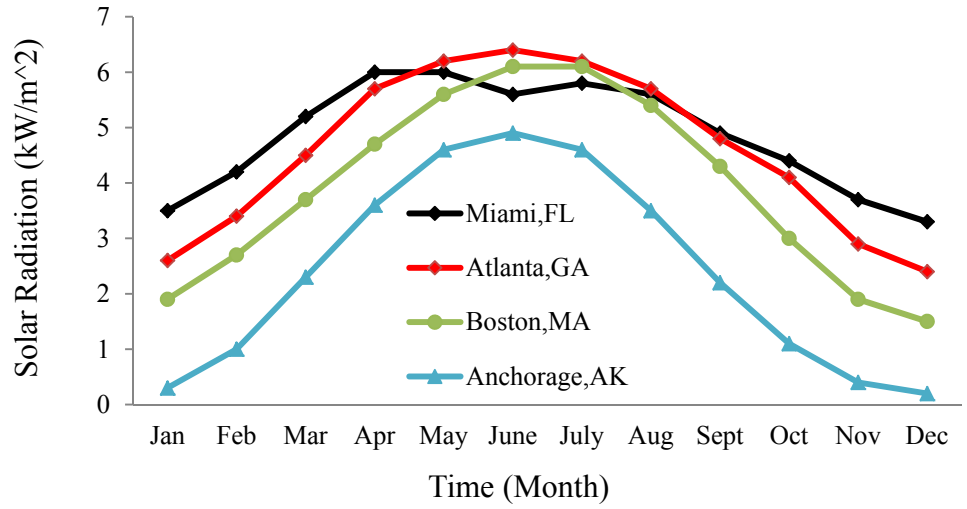

Figure 1-10 (b) Solar radiation and length of day on horizontal surface by region

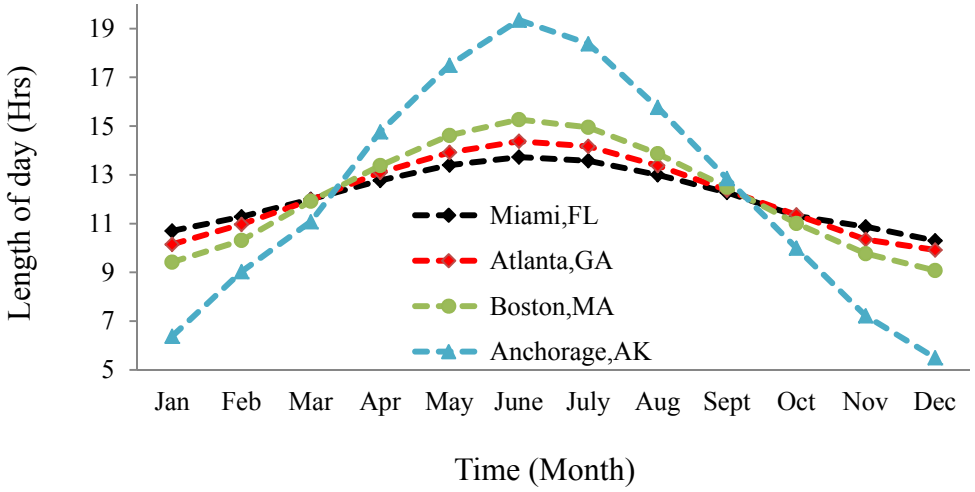

Figure 10 (c) Solar radiation and length of day on horizontal surface by region

c) Incident solar energy of the highest month

Climate change and seasonal energy demands have an influence on solar energy systems because a higher temperature during summer requires the use of more electricity (for cooling), while a warmer winter decreases the energy demand (for heating). According to the U.S. National Climate Assessment, the annual average temperatures have been higher

than the long-term average. Table 1-3 shows a comparison of the estimated amount of electricity required to operate the HVAC systems between hotter and longer summers and warmer winters, for different regions.

[Source: nca2014.globalchange.gov: U.S. National Climate Assessment- Climate Change Impacts in the United States].

Table 1-3 Variations in energy use for heating and cooling by region

Region	Cooling	Heating
Physical Impacts - High Likelihood	**Hotter and Longer Summers** Number of additional extreme hot days (> 95°F) and % increase in cooling degree days per year in 2041-2070 above 1971-2000 level	**Warmer Winters** Number of fewer extreme cold days (< 10°F) and % decrease in heating degree days per year in 2041-2070 below 1971-2000 level
Northeast	+10 days, +77%	-12 days, -17%
Southeast	+23 days, +43%	-2 days, -19%
Midwest	+14 days, +64%	-14 days, -15%
Great Plains	+22 days, +37%	-4 days, -18%
Southwest	+20 days, +44%	-3 days, -20%
Northwest	+5 days, +89%	-7 days, -15%
Alaska	Not studied	Not studied
Pacific Islands	Not studied	Not studied

The data indicates that more energy is necessary to cool buildings in summer, while less energy is required to heat buildings in winter. The climate changes result in new regional trends in energy supply and use because the temperature changes impact residential electricity use. Hotter summers can be directly linked to spikes in electricity use because there are a higher number of additional extreme hot days. Demands for electricity for cooling are expected to continue to rise virtually everywhere as a result of climate change.

Thermal CPC collectors are related to the direction of the sun's rays in gathering the maximized amount of solar radiation. The direction of the rays affects the design variables of the CPC collectors, receiver, reflector and size of land, as shown in Figs.1-11.

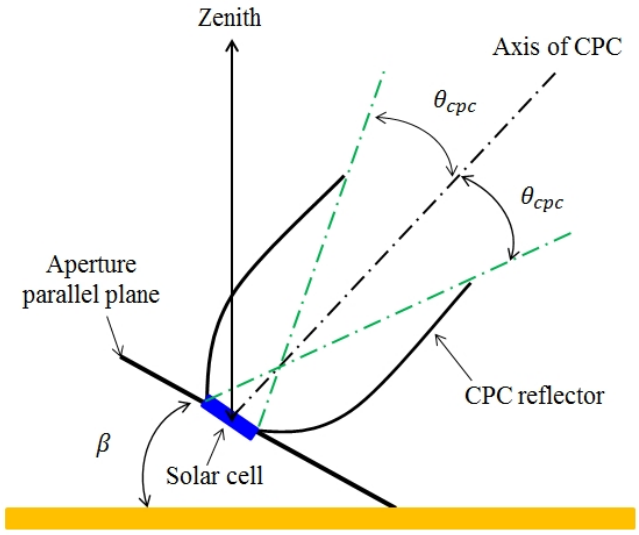

(a) CPC Collector

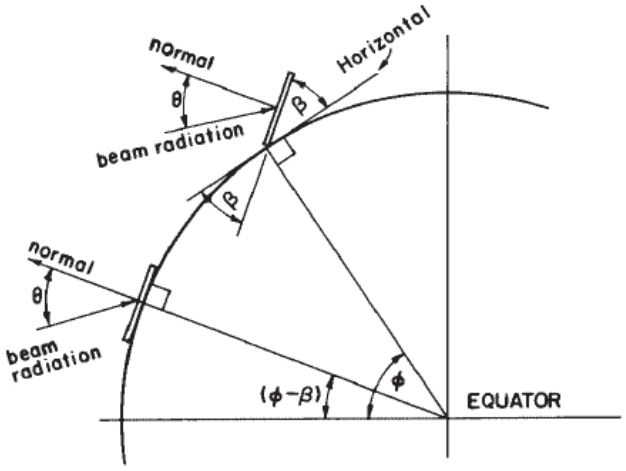

(b) Solar angles for a collector surface

Figure 1-11 Maximization of CPC PV array system performance

The cost analysis involves three different cost factors- solar receiver, reflectors and land for installation-for minimization. These factors are related to the design variables, and the costs vary with the values of the design variables. Thus, interactive relations between costs and sizes of receiver, reflector and land are considered with known or assumed unit values of receiver, reflector and land. Figures 1-12 show the sequential design process involved in an integrated PV system.

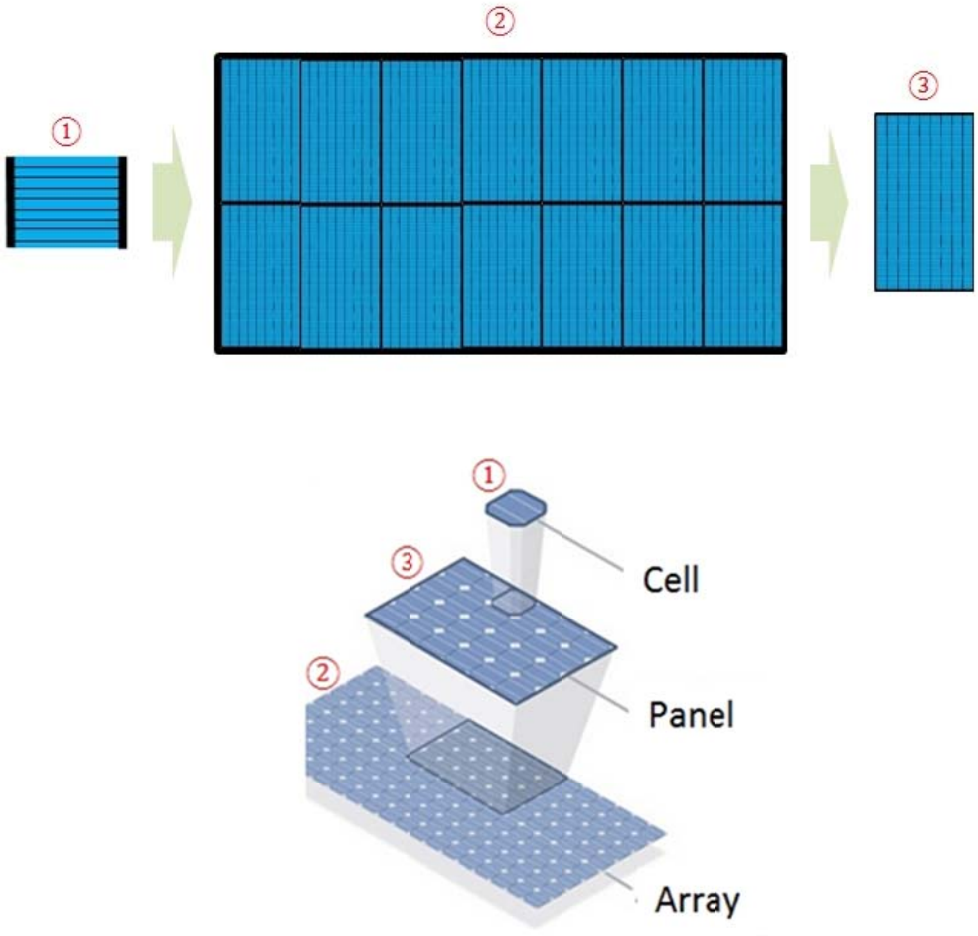

Figure 1-12 Optimal design of PV system approach order

The main concern in a PV system is to collect solar radiation by the collectors. Thus, the maximizations of annual monthly average incident solar energy and average incident solar energy for the lowest and highest months are determined by the design of solar PV collector. The maximization of PV performance is essential in the design of any solar collector. At the cell level, the conversion efficiency depends on four factors: material, cell structure, incident light and contact design. At the panel level, the main concern is how to connect individual solar cells and assemble the components. However, utilizing a solar cell reference model does not offer flexibility in the design of panel or array system. By treating the solar cell size as geometric design parameters, links can be made between the cell, panel and array. There are benefits to considering design parameters for the three systems. Instead of optimizing each level or system separately, an approach most utilized in the past, they can be optimized as an integrated system through the use of optimization techniques. Optimizing all parts (systems) simultaneously (rather than optimizing them separately and then assembling them) is likely to improve each level's objective function as well as that of the integrated system.

Solar PV systems usually require an inverter to transforms the direct current (DC) of the PV modules into an alternate current (AC); it should be noted that most equipment at the user end require AC power. The components associated with this delivery process, such as inverters, transformers, electrical protection devices, wiring, and monitoring equipment, are all considered part of the balance of system (BOS) for fixed mounting system. In addition, the BOS includes structural components for installing PV modules. Installation costs have decreased at different rates depending on the type of application and maturity of the market. Reductions in prices for materials (such as mounting

structures), cables, land use and installation account for much of the decrease in BOS costs. Another contributor to the decrease of BOS and installation-related costs is the increased efficiency at the module level. More efficient modules imply lower costs for BOS equipment, installation and land use.

Solar PV systems should be simultaneously optimized based on the conversion efficiency of cells, power output of panels, maximized collection of solar energy by an array system, and costs, including the entire solar PV system, through optimization techniques as shown in Fig. 1-13.

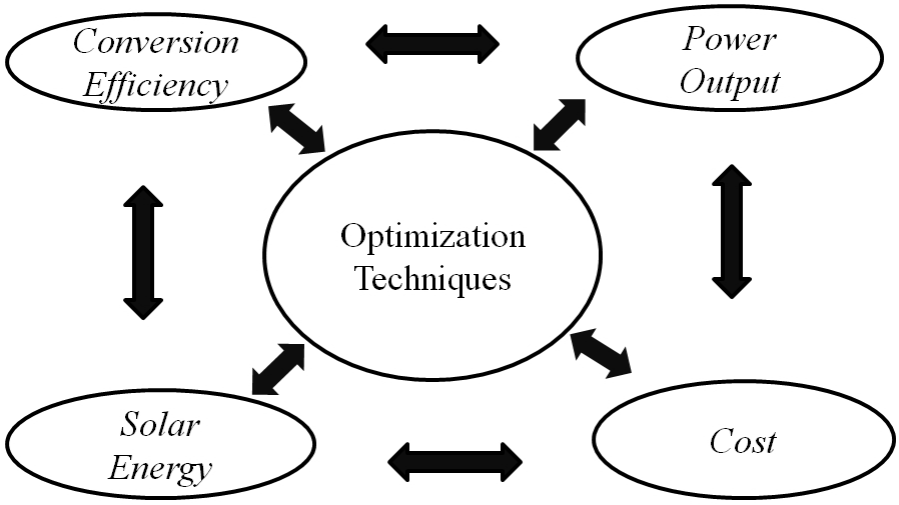

Figure 1-13 Optimization of single level and integrated PV systems

An integrated solar PV array system can be simultaneously optimized by treating the solar cell size as geometric design parameters with links established between the cell, panel and the array.

1.4 Literature Review

A solar PV array system is comprised of solar cells, panel modules and array systems. In order to progressively optimize solar PV systems, literature reviews centered on each level of PV systems individually and entire PV systems encompassing all parts need to be examined.

- Literature review of the solar cell

To achieve the maximum conversion efficiency, it is necessary to optimize the structure of a solar cell as well as the collecting grid contact design under concentrated sunlight. Arturo (1985) described a method for the optimization of the concentration factor in terms of size and nominal efficiency (at an intensity of 1sun) by assuming practical values of the specific resistance between the grid contact patterns and the semiconductor. However, factors such as the properties of materials, the metallic value of geometric grid contact factors, and the interactions among these factors were not considered; only the relationship between the conversion efficiency (η_c) and concentrated sunlight (C) to the length of a cell was taken into account. Arturo (1985) did not indicate a procedure to optimize solar cells. Gessert (1992) reviewed the models and techniques utilized to design and optimize metal contacts and antireflective coatings and identified the differences between grid metallization of cells used under electrical resistivity by using a computer program. A limitation of Gessert's study is that it did not examine the design the presence of constraints on design variables. Liu (2010) showed the influence of metal grid lines and power losses under concentrated sunlight (C) in the optimization of grid contact design of a solar cell by using computer simulations. Unfortunately, the study

failed to establish how to obtain individual optimal design values when geometric grid contact values are fixed as constrained parameters based on the variation of metal grid properties. In addition, the thickness of the solar cell was not factored in the power output, even though these thicknesses are related to sheet resistivity due to the doping level.

Reeves and Harrison (1982) obtained the specific contact resistance from the transmission line model measurements. In top contact design, it is necessary to find values of specific contact resistance for planar ohmic contacts between metallic parts and the top surface of a solar cell because the contact resistance influences conversion efficiency of a solar cell. Two different sheet resistances of GaAs and Si were compared and measured. Kulushich (2013) presented a method to optimize the front geometric parameters with a consideration of power losses, such as the optical, electronic, and electrical losses of metal grids. In this work, solar cell structure and concentration ratio were not considered. In addition, although the optimization was performed by adjusting the values of the geometric grid contact parameters through a trial and error process, the resulting value of maximum conversion efficiency (η_c) is expected to be lower compared to the value obtainable through the application of mathematical programming techniques. Shabana (1989) attempted to reduce the cost of photovoltaic systems by considering the internal loss under the metallic finger. Optimization of the top contact design for p-n junction silicon solar cells was conducted with illumination intensities of sunlight and fractional power loss. In this study, solar cell structure and size of cell were not considered as design variables; only grid dimensions were treated as design factors. Singal (1981) studied the photovoltaic power conversion efficiency of a silicon solar cell under varying intensities of sunlight. Given the solar cell size, the sunlight concentration

was considered as the design factor with a pre-specified grid structure and cell structure for optimization.

Caballero, Martinez, Sanchez-Friera, and Alonso (2008) examined the front grid design in industrial silicon solar cells. They investigated the characteristics of series resistance because they are the critical factors in the field of cell and panel module fabrication. Three different models of top contact design with varying numbers of busbars were compared to the performance of solar cells with given grid parameters. Liou and Wong (1992) focused on improvements in Si and GaAs solar cell performance. They investigated optimal solar cell efficacy by directing their study on the semiconductor layer thickness and impurity doping concentration. Also, the minority-carrier lifetime, the minority-carrier diffusion coefficient, and the surface recombination velocity were reflected in solar cell design. Theoretical cell performance was only considered without applying front contact grid design.

Rault (2002) investigated the probabilistic generation of an electron–hole pair to analyze the performance of solar conversion efficiency. It is a known that quantum mechanics is a probability-based approach. The key is which probability distribution function (PDF) and cumulative distribution function (CDF) best fits the physical mechanics of recombination at the sub-atomic level. There are a number of possible distributions, but overall the one that seems to fit best is the Burr distribution. This approach is used to determine the radiative lifetime, and the results are compared to an existing device. Zulkifli (2014) claimed that PV output is dependent on the solar radiation intermittency and the location of installation. A solar photovoltaic system was analyzed under probabilistic distribution function of the hourly solar radiation in between two different locations for the purposes

of inspecting I-V characteristics and evaluating solar photovoltaic power systems. At the solar cell level, the optimized solar cell factors include materials, cell structure, intensity of sunlight, and contact design to generate electricity. Chen (1985) and Pelanchon (1990) studied solar cell performance with cell structure parameters and utilized mathematical optimization techniques for optimization of conversion efficiency. A limitation to this approach is that it only involves solar cell structures such as thicknesses of the solar cell, recombination velocity and dopant concentration. Djeffal (2012) presented a new multi-objective generic algorithm to optimize the front metal design of a solar cell with intent to improve electrical and conversion efficiency under concentrated sunlight without considerations of geometric design variables (fixed data).

- Literature review of the panel module

A PV module is comprised of individual solar cells necessary to generate power output. The solar cells are electrically interconnected and protected from environmental conditions. The most critical consequences of PV module performance are related to losses caused by the interconnection of mismatched solar cells, temperature of the panel module, and encapsulation to prevent the mechanical damage and the electrical contacts.

Tian, H., el al. (2012) presented a cell-to-module-to-array details for photovoltaic panels. The paper considered a PV module focused on a number of connected cells in series and parallel. The main consideration was how to design circuits with a number of cells and panels. Al-Hasan, A., (1998) investigated the effect of sand dust layers on beam light transmittance on a photovoltaic module through experimental and mathematical approaches. Light transmittance plays a key role in carrying sun's rays to solar cells to

generate electricity. The author analyzed the correlation between light transmittance and the amount of beam solar radiation. Jiang, H. el al (2011) conducted an experimental investigation on the impact of airborne dust deposition on the performance of solar photovoltaic (PV) modules. They investigated the transmittance of solar cells, which affects degradation of conversion efficiency with PV panels, and analyzed dust accumulation onto different types of solar PV panels. Abiola-Ogedengbe, el al (2015) conducted an experimental study on wind effects on a stand-alone photovoltaic (PV) module using four different wind directions. The module's surface pressure filed was investigated using the four wind directions with various inclination angles of the PV module.

Shah, el al. (2011) studied diagnostics of thin-film silicon solar cells and solar panels with variable intensity measurements (VIM). The VIM method was used for identifying the problem pertaining to a defective cell or module. Sumitomo, Huang, and Zhou (2011) presented deformation and material removal in a nanoscale multi-layer thin film solar panel using nanoscratch. They investigated the deformation and material removal characteristics of the panel using nano-mechanical testing. Potnuru, Pattabiraman, and Ganesan (2015) presented the positioning of PV panels for reduction in line losses and mismatch losses in a PV array. The relationships between mismatch losses and partial shading were analyzed. The mismatch losses were dependent on the shading pattern and configuration of shaded modules in the array. Rosa-Clot el al. (2010) investigated the performance submerged of photovoltaic solar panels. This paper showed the behavior of a photovoltaic panel submerged in water and its varying power production characteristics.

- Literature review of the PV array

The optimum PV array orientation depends on the location under certain weather conditions at the array system level. The maximum energy output is obtained when the tilt angle of an array is perpendicular to the sun's rays and as horizontal as possible to the surface of the array. Weinstock (2004) and Hu (2009) described the optimal design of stationary flat-plate solar collectors with geometric parameters of array and land through mathematical optimization techniques. However, neither researcher considered the conversion efficiency and power output relevant to the size of a solar cell and panel module, which are intrinsically related to the power output of a solar PV collector system. Also, a sequential quadratic programming method was used to investigate the optimal design results without consideration of mixed-integer parameters such as the number of arrays. As a result, it is difficult to find accurate and global optimal results for a stationary PV collector system. Tang and Wu (2004) researched a reasonable estimation of the optimal tilt angle of a fixed collector for maximizing its energy collection using mathematical techniques. They considered monthly diffuse radiation for calculating the optimal tilt angle of a collector in China.

Kacira, M., Simsek, M., Babur, Y. and Demirkol, S. (2004) investigated the performance of a PV panel related to its orientation and tilt angle with a horizontal surface in Turkey. They considered monthly and seasonal characteristics for optimum tilt angles for fixed and two-axis solar tracking systems. Chang (2009) concentrated on calculating the sun's position for determining the optimal tilt angle for a solar collector in Julian, Taiwan. Qasaimeh (2012) endeavored to optimize the angle of inclination of solar cells in Jordan. Solar energy was subsequently optimized each season with a specific tilt angle of inclination derived from the supplied information regarding solar energy, sun shine hours,

and temperature. Murtaza el al. (2014) investigated a maximum power point tracking technique based on bypass diode mechanism for PV arrays under partial shading. The effects of partial shading are caused by multiple PV arrays and environmental conditions. From this paper, several critical observations were pointed out by using two comprehensive PV models in which two types of diodes (bypass and blocking). The most critical factor was how to install PV arrays considering bypass diodes from partial shading.

Orozco-Gutierrez el al. (2014) presented a method for simulating large PV arrays that include reverse biased cells. They showed an effective algorithm for simulating a large mismatched PV array using inverse Jacobian matrix and observed the array behavior at a cell level in order to accurately predict power production and detect or diagnose dangerous situations for the PV array. Rhodes el al. (2014) investigated a multi-objective assessment of the effects of solar PV array orientation and tilt on energy production and system economics. The paper considered both total energy production through solar PV array and economic value given a particular location with electricity market prices and structure rates. This approach considered the AC electricity produced by a solar PV array system and electricity prices on a national scale in order to show how local electricity markets influence the economic value of solar placement on a national level. Kouchaki el al. (2013) conducted a new maximum power point tracking strategy for PV arrays under uniform and non-uniform insolation conditions based on the current and voltage characteristics of PV arrays for finding the maximum power point. Sivakumar el al. (2015) investigated the analysis and enhancement of PV efficiency with incremental conductance Maximum Power Point Tracker (MPPT) technique under non-linear loading

conditions. To do so, they conducted both simulation and experiment for the evaluation of the PV panel under non-linear loading conditions.

Sivestre el al. (2015) conducted a study on the analysis of current and voltage indicators in grid connected PV systems working in faulty and partial shading conditions. The paper showed how the analysis of the current and voltage indicators is focused on the detection of temporary faults from the effects of partial shading in the PV array or disconnection of the inverter in case of grid fluctuations of voltage. Ya'acob el al. (2013) calculated the electrical and thermal characteristics of multiple PV array configurations in pursuance of defining the electrical characteristics and temperature equation of a PV array installed in the tropics for the performance of PV modules. Camps el al. (2015) attempted to optimize the size of grid-connected PV systems (GCPVS). They validated the optimal PV-to-inverter sizing ratio value by using a custom workbench and a solar array simulator for mathematical models. Sivakumar and Arutchelvi (2014) investigated the composite power controller of grid converters for PV array excited wind-driven induction generators with variations in irradiation, wind and consumer demand (power requirement). They proposed a new control algorithm for grid connected inverter fed by PV array excited wind-driven induction generator for unbalanced nonlinear load at the point of common coupling. Martinez-Moreno el al. (2010) developed on experimental model to estimate shading losses in PV arrays. Simply, they showed a mathematical model to estimate shading losses in PV arrays with capabilities to calculate power. Parkak (2014) studied PV array reconfiguration methods under partial shading conditions. The paper proposed that each row of an array is formed by connecting the panels with a circuit design.

Configuration scanning algorithms were used to determine the possible configurations utilizing the short circuit current values.

Brecl and Topic (2011) presented an analysis of self-shading losses of fixed free-standing PV arrays. They evaluated the effects of the row distance on the PV array system considering the irradiation and shading losses. Zheng el al. (2014) investigated shading and bypass diode impact on energy extraction of PV arrays under different converter configurations. The paper compared the energy extraction characteristics of a PV array for different converter systems and showed how energy extraction characteristics of a PV system are altered by partial shading and different bypass diode arrangements. Kaushika el al. (2005) implemented a simulation model for the sizing of a stand-alone solar PV system with an interconnected array. They considered the electricity generation in the array and its storage in the battery for non-taking PV system and single-axis tracking aperture array systems. Richardson and Harvey (2015) studied strategies for correlating solar PV array production with electricity demand. The paper evaluated the correlations between PV energy production and electricity demand given a specific location for finding optimal orientation of PV modules.

- Literature review of uncertainty analysis

The aim of uncertainty analyses is to be able to predict the performance of engineering systems involving uncertain parameters for the analysis of environments characterized by unexpected circumstances such as workplace environments, manufacturing production conditions related to operation and production tolerances. Nowadays, there is a growing

interest in uncertainty analysis and optimal design among researchers from various disciplines.

Cabral el al. (2010) studied a stochastic method for stand-alone photovoltaic system sizing. The determination of the optimal size of a PV system requires the characterization of solar radiation. Therefore, they conducted stochastic optimization with random characteristics of solar radiation and compared the results obtained using the average measured and simulated monthly average daily global radiation on an inclined panel module. Zhou el al. (2013) focused on a two-stage programming model for the optimal design of distributed energy systems. The paper used a stochastic programming approach. The methodology was implemented during the planning of a distributed energy system in a hotel. The mathematical model was used for the design of a distributed energy system by classifying it into three different sections: energy generation section, energy conversion section, and energy storage section. The solution strategy for the two-stage stochastic optimization problem was based on genetic algorithms.

Hengsritawat (2012) investigated a probabilistic approach to designing an optimal-sized photovoltaic model in a distribution system. In this paper, the objective of the technique was to minimize average active power loss of the system while considering power quality constraints, such as voltage and current using probabilistic variations for power, and voltage with normal distributions. The I-V characteristics of PV models were studied to determine the optimal size of a PV model. Zulkifli el al. (2014) presented a probabilistic analysis for the solar photovoltaic output based on historical data. A probability distribution function-based analysis was used for solar photovoltaic generation considering the randomness of solar radiation. Moharil el al. (2010) investigated the

reliability analysis of a solar photovoltaic system using hourly mean solar radiation data. The estimation of solar photovoltaic power was conducted using various amounts of solar radiation. Gautam el al. (2002) calculated the reliability evaluation of solar photovoltaic arrays using the probability theory. The array performance was analyzed by considering circuit design for solar cells using panel interconnections in series and parallel systems.

The fuzzy set theory was introduced by Zadeh (1965). Nowadays, this theory is being applied to countless fields within and beyond the scope of conventional engineering. Bellman amd Zadeh (1970) extended fuzzy set theory to the fuzzy set-based optimization with decision-making in a fuzzy environment. Xiong and Rao (2004) presented fuzzy nonlinear programming for mixed-discrete design optimization through hybrid genetic algorithms. They proposed a mixed-discrete fuzzy nonlinear programming approach that combines the fuzzy λ-formulation with a hybrid genetic algorithm using mathematical techniques for finding the minimum cost design of a welded beam. Eman (2006) investigated a fuzzy approach for a bi-level integer non-linear programming problem (BLI-NLP) which consists of the higher-level decision-maker (HLDM) and the lower-level decision-maker (LLDM). The paper was focused on two planner integer models and a solution method for solving the problem using the concept of tolerance membership function and a set of Pareto optimal solutions. Liang (2008) studied fuzzy multi-objective production/distribution planning decisions with multi-product and multi-time period in a supply chain. The paper was focused on a fuzzy multi-objective programming model (FMOLP) with linear membership function to solve integrated multi-product and multi-time period production/distribution planning decision (PDPD) problems with fuzzy objectives.

- Literature review of multi-objective optimization

Most real-world optimization problems have multiple-objectives that are often conflicting. The goal of multi-objective optimization is to optimize the conflicting single-objectives with decision making, simultaneously. Li, Liao, and Coit (2009) proposed a two-stage approach for solving multi-objective system reliability optimization problems using a Pareto optimal solution set. To find a solution, a multiple object evolutionary algorithm (MOEA) was applied. Basic trade-offs for the Pareto optimal solution set were investigated. Merino, Jones, Clements and Miller (2003) described fuzzy compromise programming with precedence order in the criteria. They introduced a new multi-objective decision making (MODM) method in which the decision-making is allowed to include fuzziness in the information, but it is not forced to provide specific values for the weighting factors of the objectives . This means that the decision-maker is not required to assign specific values of weights to the objectives. Homburg (1998) proposed a hierarchical procedure for solving decision problems with multiple objectives. The suggested procedure includes two levels including top and base levels. In the top level, general information was provided to enable consideration of the base-level for determining a compromise solution. The author adopted the Zionts-Wallenius algorithm (ZW), which is an interactive procedure. The ZW algorithm is meant to reduce the set of possible weighting vectors until an optimal decision is made.

Ibrahim (2010) strived to solve multi-level multi-objective linear programming (ML-MOLP) problems through fuzzy goal programming approach using mathematical programming techniques. This paper showed a fuzzy programming model contrived to minimize the group retreat of degree of satisfactions of all the decision makers. There

were two proposed algorithm group of the membership functions for the defined fuzzy goals of the objective functions. Mahmoud and Ibrahim (2007) studied a multi-level multi-objective decision-making (ML-MODM) problem with linear or non-linear constraints. The objective functions at each subsystem were maximized or minimized at three levels of hierarchy structure for solving a three-level multi objective decision making problem. Osman, Abo-Sinna, Amer, and Emam (2004) investigated a three-level non-linear multi-objective decision-making (TLN-MODM) problem with linear or non-linear constraints. The paper proposed the concepts of tolerance membership function and multi-objective optimization at each level in order to develop a fuzzy decision model.

Shih, Lai, and Lee (1996) studied multi-level programming techniques for solving decentralized planning problems with multiple decision makers in a hierarchical system. They used the concepts of tolerance membership functions and multiple-objective optimization to develop a fuzzy approach for solving the problem and adopted Bard's grid search algorithm for obtaining an efficient solution. Chaudhuri and Deb (2010) presented an interactive evolutionary multi-objective optimization and decision-making procedure. In this paper, they suggested an interactive procedure for performing a complete multi-objective optimization and decision-making task using a set of Pareto optimal solutions and evolutionary methods.

Within CPC PV systems, any radiation within the collector acceptance angle enters through the aperture and finds its way to the absorber surface by multiple internal reflections. Improving the efficiency and reducing the cost of these solar collectors is a hot research topic in the field of solar collectors. Abdul-Jabbar and Salman (1988) concluded through a series of experiments in the Middle East that the CPC solar

collectors with double axis tracking system can get up to 75% more insolation. Kim and Han (2008) used both numerical and experimental methods to achieve the thermal efficiency of a CPC solar collector with a single-axis tracking system of about 14.9% higher than a stationary CPC solar collector. The compound parabolic concentrator (CPC), first proposed by Winston and Hinterberger (1975), has the capability of reflecting all the insolation to the absorber over a relatively wide range of angles.

Mills and Giutronich (1977) concluded, based on a comparative study of symmetrical and asymmetrical parabolic concentrators, that an asymmetrical design could collect higher and more stable energy. Trupanagnostopoulos, Papaefthimiou, and Zafeiratos (2000) compared the performance of three small CPC units and one large CPC unit with the aperture area of the larger unit equal to three times more than that of the smaller units through experiments and confirmed that the three smaller units performed better than the large unit. Mallick (2004) designed, constructed and experimentally tested a prototype asymmetric CPC solar collector. For the same receiving area, the power output of the CPC collector was found to be 1.62 times more than that of a flat plate photovoltaic panel. Other researchers focused on the design of different types of receivers.

Weinstock and Appelbaum (2007) compared the energy outputs of stationary flat plate solar collectors and flat plate solar collectors with various tracking systems. They found that the East-West horizontal axis multi-row PV panels with a North-South tracking performed 16% better than the stationary PV panels while the North-South horizontal axis PV panels with an East-West tracking system could provide 17% extra power compared to the stationary PV panels. However, when cost is a primary factor, a

stationary solar collector system is the most economical choice compared to the solar collectors with any tracking system.

In the case of cost analysis, Bony et al. (2010) made a report of industry workshop recommendations for near-term balance of system cost reductions. The report showed a physical system design for minimizing levelized cost, business process for reducing cost and uncertainty, and industry scale for ensuring rapid growth and innovation while satisfying customer-specific requirements. Goodrich et al. (2012) proposed a summary of residential, commercial, and utility-scale photovoltaic (PV) system prices in the United States. They investigated the PV system market values and analyzed bottom-up installed systems. Also, their report detailed 2010 benchmark system prices for residential and commercial rooftop systems and utility-scale ground-mount systems. Antoniadis (2009) presented high efficiency, low cost solar cells manufactured using 'silicon ink' on thin crystalline silicon wafers. The paper showed the optimization of high efficiency emitter formation and cell light absorption and ink-jet and screen printing optimization for a high throughput cell production. Also, all-back doping and multi-crystalline solar cells were considered and demonstrated. Nold et al. (2012) presented a cost model for silicon solar cell production along the PV value chain. The paper showed a cost calculation model for the economic comparison of different silicon solar cell production technologies with respect to the impact of cell efficiency improvement based on watt peak. They considered the cost model to be composed four components: cost of cell production, cell cost, module cost, and system cost for the economic evaluation of silicon solar cell technologies with regard to each level of the PV system. Paap et al. (2013) presented the cost analysis of flat plate concentrators employing microscale photovoltaic cells. The cost

model included the module cost, BOS cost, tracker cost, installation cost, and operation and maintenance cost. The sum of subcomponent costs denoted the total installed PV system cost including operation and maintenance costs.

1.5 Present Work

It can be seen from a comprehensive literature review that the following aspects related to solar PV system design have not yet been studied. These aspects are investigated in the present work.

- Optimal design of a solar PV system

The cell performance depends on solar cell structure, top contact design, and cell size. The correlations between cell structure and top contact design are investigated. Also, the correlations between cell size and top contract design are investigated. As a result, the solar cell structure, materials, light intensity, cell size, and top contact design have an influence on solar cell performance that can be quantified in terms of conversion efficiency and power output. Two single-objective problems are considered, separately, and a multi-objective problem is also formulated in order to find a compromise solution between conversion efficiency and power output with geometric design parameters. By including practical constraints, the solar cell design can be conducted using mathematical optimization techniques.

The optimization of PV panel module is dependent on the optimal design of individual solar cells and optimal design of the array system with power requirements. The role of the PV panel module is interactive between solar cells and the array system and is

composed of a number of solar cells and panel modules. Thus, a proper size and a number of panels should be considered in the design of a PV panel module.

In designing a solar PV array system with cost considerations, the costs of subsystems such as cell, panel, and array become important. By considering at each level, cost activity is related so that the costs of all subsystems are considered simultaneously and the entire PV array system is optimized for minimum cost. Each PV system has separate characteristics so that the costs of the PV system includes those associated with material of wafer, cell and panel module production, construction, installation site, and inverter system. Thus, the geometric design factors at each level will be reflected in the overall cost of the solar PV system.

- Multi-objective optimization

Interactive design factors are necessary for multilevel optimization with single-objective solutions at each level contributing to the non-tracking solar PV array system. The game theory and fuzzy set theory methodologies are used for finding the solution of the multi-objective optimization problem based on the results of single-objective problems. Orientation and inclination angle of a solar PV array system are critical factors for optimization with regard to the seasonal requirements of power. The characteristics of each season require a different installation design of a solar PV array system. Seasonal energy requirements are dependent on the specific location. When sunlight falls perpendicularly on a solar PV collector, the PV system's performance is maximized. As a result, the design of a solar cell and panel module can be adjusted accordingly to meet the requirements of seasonal characteristics with a consideration of costs. Also, solar cells

(with square or rectangular shapes) are interconnected and encapsulated for forming the optimal design of a PV panel module based on optimal performance of a solar cell. Thus, solar cell shapes should be taken into account when installing an optimal PV array system.

- Uncertainty analyses

Many researchers investigated the uncertainty of solar radiation. The design of solar PV systems with a consideration of all aspects of uncertainty has not been studied in the optimization of solar array systems. Uncertainty is known as error. In order to predict performance using uncertainty analysis, the performance object should be specified within a range of quantification of uncertainties in the relevant variables with respect to the interval confidence for finding how uncertainties propagate and estimating in numerical terms the magnitude of uncertainties in final results. In this work, uncertainties associated with the design parameters, including solar radiation, are considered in predicting the performance of solar PV systems using stochastic and fuzzy analysis methodologies.

The goal of this research is to simultaneously optimize both single-level PV systems and integrated solar PV array systems composed of solar cells, panel modules, and construction aspects while reducing both energy losses and costs through mathematical programming techniques. Single level PV systems are optimized sequentially through optimization techniques based on geometric design parameters.

Chapters 2 to 5 will take a detailed look into the processes and implications of this perspective.

Chapter 2 presents the optimal design of the various components of solar PV system including three different levels - solar cell, panel module, and array systems by considering conversion efficiency, power output, and incident solar energy based on the requirements of conversion efficiency and seasonal demands.

Chapter 3 presents the multi-objective optimal design of CPC and PV array systems based on the results of single-objective optimizations using modified game and fuzzy set theories. Multilevel optimization problems using game theory and fuzzy set theories are used for finding the compromise solution of six-objective optimization problems including conversion efficiency, power output, incident solar energy (annual, winter, and summer seasons), and cost with constraints on the power requirements of different seasons.

Chapter 4 considers the uncertainty based analyses and optimal design of a solar PV system through probabilistic and fuzzy set analysis methodologies. Uncertain parameters are treated as random variables or uncertain inputs to predict the performance. Probabilistic analysis method uses random variables containing both uncertain design parameters and/or uncertain design variables. The fuzzy membership functions are used for modeling the uncertain or imprecise design parameters of a solar PV system. Triangular membership functions are used to represent the uncertain parameters as fuzzy quantities. Fuzzy arithmetic operations and extension principle are used to find the membership functions of the fuzzy response parameters of the system.

Chapter 5 concludes and proposes arenas for future work.

CHAPTER 2

Optimal Design of Solar PV Systems

2.1 Overview

The purpose of photovoltaic (PV) systems is to collect as much solar energy as possible from the sun. The optimization of a solar cell involves two types of design parameters, namely, the intrinsic and extrinsic parameters. The cell geometric design involves the intrinsic parameters, such as the thicknesses of the emitter and base. The extrinsic parameters include quantities such as the geometric contact grid design parameters. Some parameters such as the doping level, properties of material and antireflective coating are assumed as specified data. Two steps are involved in the design of a solar cell. The first one is to optimize the performance of the solar cell by adjusting its thickness using the given data, especially the doping level, because it affects the thicknesses of the emitter and base. The second step is to minimize the power losses for maximizing the conversion efficiency of the solar cell under concentrated sunlight. Therefore, in order to achieve maximum conversion efficiency, it is necessary to optimize the structure of the solar cell as well as the collecting grid contact design under concentrated sunlight.

A panel module is constructed by connecting a number of solar cells, and it can be used as a component of a larger PV array system to generate electricity in order to satisfy the needed power requirements. Therefore, the optimization of the power output of a panel

module is dependent on the optimal design of individual solar cells used in the panel and can be determined by the size and number of cells and arrays in order to generate the maximum power output. All solar cells in practice have unique characteristics, and the power output of the panel module is limited by the solar cells having the lowest power output due to the mismatched cells. Solar panel modules are used in harsh and remote surroundings, so the panel module should be able to withstand environmental conditions such as dust, salt, sand, wind, snow, humidity, rain, condensation and evaporation of moisture, and seasonal temperature variations.

At the array system level, the installation of the PV array system is determined by the maximum amount of incident solar energy based on seasonal characteristics with shading effects associated with the number of arrays which, in turn, are associated with the seasonal characteristics of the flat plate PV array system. Therefore, the geographic characteristics influence the array system to collect the maximum solar energy. Also, cost is considered to each level of the solar cell, panel module, and array system including the raw materials, fabrication and production process used for the solar cells and panel modules. After factoring in the costs of solar cells and panel modules, the cost of a solar PV array system is influenced by the raw materials, equipment, labor, maintenance, facilities and installation site.

2.2 Optimization Problem and Solution

The formulation of an optimal design problem of solar PV systems involves an objective function, a set of constraints and design variables. The problem can be stated in a general mathematical form as

$$\text{Find} \quad \vec{X}=\begin{Bmatrix} x_1 \\ x_2 \\ . \\ . \\ . \\ x_n \end{Bmatrix} \tag{2.1}$$

to minimize or maximize the objective function f ($\vec{X}$)

subject to the constraints

$$g_i(\vec{X}) \leq 0, \qquad i = 1, 2, \dots, m \tag{2.2}$$

$$l_i(\vec{X}) = 0, \qquad i = 1,2, \dots, p \tag{2.3}$$

$$a_j \leq x_j \leq b_j, \qquad j = 1,2, \dots, l \tag{2.4}$$

where $g_i(\vec{X})$ and $l_i(\vec{X})$ are the inequality and equality constraints, respectively x_j is the j^{th} design variable, and a_j and b_j are the lower and upper bounds on the j^{th} design variables, respectively.

Sequential quadratic programming (SQP) is an iterative method for non-linear optimization. SQP methods can be used for the optimization of an objective function with constraints. The method has a theoretical basis and uses quadratic programming, sequentially.

The genetic algorithm (GA) is a method for solving both constrained and unconstrained optimization problems belonging to a natural selection process. Genetic algorithms (GAs) are rooted in Darwinian's theory of survival of the fittest in the principle of natural genetics for solving optimum design problems and implemented for mixed continuous-

discrete variables, discontinuous, and nonconvex design spaces. Also, GAs can be applied in non-linear problems for optimization. The program, *ga*, is suited for finding the global optimum solution with a high probability. GA begins with a set of design vectors and uses the basic ideas of reproduction, crossover, and mutation, and can be described by the following steps:

- A random population of trial design vectors is used for starting the procedure instead of a single design vector. In general, the size of the population is taken to be between 2n and 4n where n is the number of design variables.
- GA is used to find the values of the design variables to minimize or maximize only an unconstrained objective function. As such, the constrained optimization problem is to be converted into an equivalent unconstrained problem using the penalty function approach.
- Binary representation is used for coding the design vectors within GA. This indicates that the design variables are implemented by strings of binary variables that correspond to the chromosomes in natural genetics. This permits the search method to be applicable for solving discrete and mixed integer programming problems as well.
- The objective function value corresponding to the design vector plays the role of fitness in natural genetics.
- GA uses probabilistic transition rules, (not deterministic) because a new set of strings of design vectors is produced every new generation by using randomized parents selection and crossover from the old generation. They efficiently explore the new combinations with the available knowledge to find a new generation with better objective function value.

In the next three sections, solar cells, solar PV panel modules, and solar PV array systems are investigated along with their respective individual performance characteristics. At the cell level, the solar cell performance is investigated in terms of conversion efficiency and power output. At the panel level, the performance of a solar panel module is presented based on conversion efficiency. At the array level, the performance of solar PV array system is investigated based on the performance of its subsystems - the solar cell and the panel module – as well as the cost of the array system. The optimal design of an array system is characterized by six single-objective optimization problems.

2.3 Solar Cell

The solar cell structure, materials, light intensity, and top contact design have influence on the solar cell performance. The performance of a solar cell can be measured in terms of conversion efficiency and power output. The conversion efficiency of a solar cell is the ratio of its electrical output to the incident solar energy from sunlight. The power output may vary over a wide range of voltages and currents within the limited area of the solar cell.

2.3.1 Theoretical model

Silicon is the most common material used for converting sunlight into electrical energy. In a solar cell, one of the most important parts is the p-n junction. Solar cell performance can be given in terms of a simple model based on alloyed junction, epitaxial growth and thermal diffusion. The performance of a solar cell can be described in several steps based on the fundamental equations that describe semiconductor devices. This section briefly outlines how a typical solar cell model is developed using device

equations to predict the power output. The performance is dominated by a simple p-n junction cell consisting of an emitter, space-charge region, base with dopant concentration and illuminated sunlight. After considering the theoretical or ideal solar cell model with no losses, the conversion efficiency (η_c) under concentrated sunlight, with the power losses based on optical and omhic losses, needs to be considered. There are two parts in a solar cell structure and grid contact design for the optimization of a solar cell.

To determine the solar cell power output, the total current densities in three different regions- emitter, space charge region, and base, are to be considered using the values of structural parameters, such as dopant and intrinsic concentration, minor-carrier recombination velocity and the materials. Figure 2-1 shows a typical solar cell structure based on a single p-n junction.

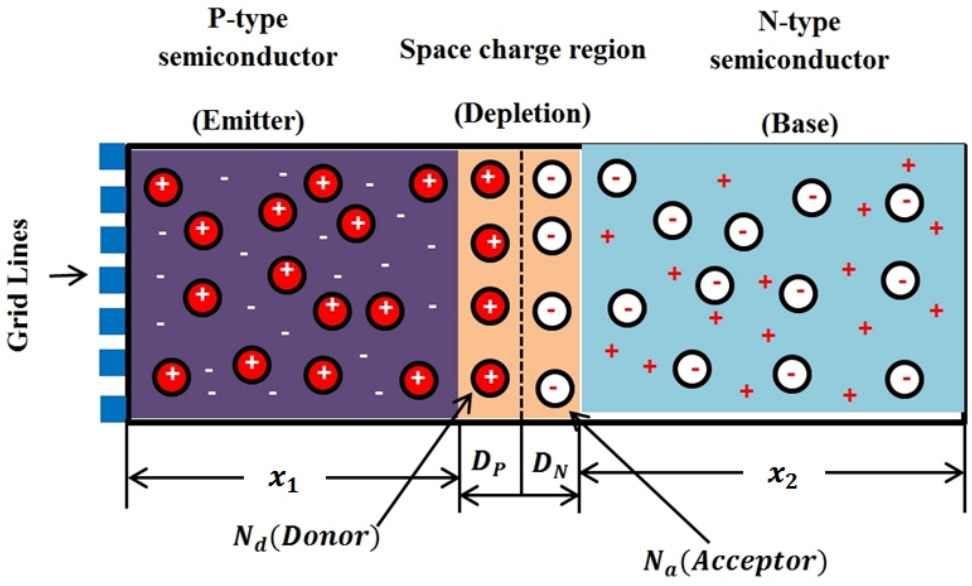

Figure 2-1 Basic solar cell structure

The current densities are generated in both the p and n sides of the junction. The electrons and holes generated within the diffusion length move to the space charge region. In the space charge region, the electrons and holes get separated in the strong electric region. The total current density (J_L) in the three regions can be computed as

$$J_L = J_E + J_{SCR} + J_B \tag{2.5}$$

where, the expressions for the individual values of J_E, J_{SCR}, and J_B are given in the publications of Jain, Heaselll, and Roulston (1986) and Singal (1980).

The current density in the emitter region (J_E) can be found using the dopant concentration of the emitter, recombination velocity of front surface, and thickness of the emitter as

$$J_E = qn_{ph}(1-R)\left[\frac{\alpha L_p}{{L_p}^2\alpha^2-1}\right] \times \left[\frac{\left(\left(\frac{S_p L_p}{D_p}\right)+\alpha L_p\right)-e^{-\alpha x_1}\left(\left(\frac{S_p L_p}{D_p}\right)\cosh\left(\frac{x_1}{L_p}\right)+sinh\left(\frac{x_1}{L_p}\right)\right)}{\left(\frac{S_p L_p}{D_p}\right)sinh\left(\frac{x_1}{L_p}\right)+cosh\left(\frac{x_1}{L_p}\right)} - \alpha L_p e^{-\alpha x_1}\right] \tag{2.6}$$

Similarly, the current density in the base region (J_B) can be determined using the dopant concentration, recombination of back surface and thickness of the base as

$$J_B = qn_{ph}(1-R)\left(\frac{L_n\alpha}{{L_n}^2\alpha^2-1}e^{(-x_1+x_2)\alpha}\right) \times \left[L_n\alpha - \frac{\left(\frac{S_n L_n}{D_n}\right)\left[cosh\left(\frac{x_2}{L_n}\right)-e^{-\alpha x_2}\right]+sinh\left(\frac{x_2}{L_n}\right)+L_n\alpha e^{-\alpha x_2}}{\left(\frac{S_n L_n}{D_n}\right)sinh\left(\frac{x_2}{L_n}\right)+cosh\left(\frac{x_2}{L_n}\right)}\right] \tag{2.7}$$

The current density in the space charge region (J_{SCR}) depends on the absorption coefficient of light (α) in the semiconductor device (emitter and base regions), the reflection coefficient of the anti-reflective coating (R), and the photon flux (n_{ph}) from the sunlight radiation. It is to be noted that the three variables (α, R, and n_{ph}) depend on the wavelength (λ) of the sunlight radiation as well as on the thicknesses of emitter and base (x_1 and x_2).

The current density (J_{SCR}) can be determined as

$$J_{SCR=}\ \mathrm{q}n_{ph}(1-R)e^{-x_1\alpha}(1-e^{-t_{scr}\alpha}) \tag{2.8}$$

t_{scr} is the depletion region width expressed as

$$t_{scr}=\sqrt{\frac{2K_s\varepsilon_0V_{bi}}{q}\frac{(N_a+N_d)}{N_aN_d}} \tag{2.9}$$

To calculate the total current density (J_L), the sub-parameter values must be established. Since the wavelength (λ) of absorption varies from 0.24 μm to 1.1 μm in silicon semiconductor materials, the photon flux density $n_{ph}(\lambda)$ and Si absorption coefficient were approximated with two linear curves (Liou and Wong, (1992)).

$$n_{ph}(\lambda)=C(19.7\lambda-4.7)\times10^{15} \qquad for\ 0.24\le\lambda\le0.47\ \mu\mathrm{m} \tag{2.10}$$

$$n_{ph}(\lambda)=C(-2.5\lambda+5.7)\times10^{15} \qquad for\ 0.48\le\lambda\le1.1\ \mu\mathrm{m} \tag{2.11}$$

The values of minority-carrier diffusion coefficients ($D_p\ and\ D_n$) can be derived in terms of the dopant concentrations of acceptor (N_a) and donor (N_d) as

$$D_p=\frac{1350V_T}{[1+81N_a/(N_a+3.2\times10^{18})]^{0.5}}\ cm^2/s \tag{2.12}$$

$$D_n = \frac{480V_T}{[1+350N_d/(N_d+1.05\times10^{19})]^{0.5}}\ cm^2/s \tag{2.13}$$

Moreover, the minority-carrier lifetimes ($\tau_p\ and\ \tau_n$) can be expressed as

$$\tau_p = \frac{12}{1+N_a/5.0\times10^{16}}\ \mu s \tag{2.14}$$

$$\tau_n = \frac{12}{1+N_d/5.0\times10^{16}}\ \mu s \tag{2.15}$$

and the minority diffusion lengths ($L_p\ and\ L_n$) can be obtained as

$$L_p = \left(D_p\tau_p\right)^{0.5} \tag{2.16}$$

$$L_n = (D_n\tau_n)^{0.5} \tag{2.17}$$

When a positive voltage is applied to the p-n junction, it decreases and overcomes the space charge region (J_{SCR}) thereby producing a current density. On the other hand, when a negative voltage is applied to the p-n junction, it increases the space charge region thereby preventing the production of current density. As a result, the diode equation gives an expression for the dark saturation current density (J_0) through the diode as a function of voltage.

When a positive voltage is applied to the p-n junction, it decreases and overcomes the space charge region (J_{SCR}) thereby producing a current density. On the other hand, when a negative voltage is applied to the p-n junction, it increases the space charge region thereby preventing the production of current density. As a result, the diode equation gives an expression for the dark saturation current density (J_0) through a diode as a function of

voltage. The reverse saturation current density (J_0) can be computed using the following equations, also known as the diode equations by Singal (1981).

$$J_{01} = qn_i{}^2 \left(\frac{D_n}{N_a L_n} + \frac{D_p}{N_d L_p}\right) \tag{2.18}$$

$$J_{02} = \frac{qn_i x_2}{2(\tau_n \tau_p)^2} e^{\left(\frac{\delta E_g}{2kT}\right)} \tag{2.19}$$

Details of the computational procedure for finding the short-circuit current density (J_{sc}) and open-circuit voltage (V_{oc}):

The short-circuit current density (J_{sc}) is a result of the generation and collection of light-generated carriers. Thus, the short-circuit current density (J_{sc}) depends on a number of factors, such as the total current density (J_L), the reverse saturation current density (J_0), the optical properties (α, R *and* n_{ph}), and the collection probability (D_p, D_n, τ_p, τ_n, L_p and L_n) and is given by Singal (1981).

$$J_{SC} = J_L - J_S = J_L - J_{01}\left[\left(e^{\frac{qV_{oc}}{kT}}\right) - 1\right] - J_{02}\left[\left(e^{\frac{qV_{oc}}{nkT}}\right) - 1\right] \tag{2.20}$$

The open-circuit voltage (V_{oc}) is not connected to any load, and as a result, it corresponds to the maximum amount of voltage from the solar cell which generates the net current density and is given by Singal (1981).

$$V_{oc} = (kT/q)\log(\frac{J_{sc}}{J_0} + 1) \tag{2.21}$$

The maximum operating power density (P_m) at one sun intensity can be found as

$$P_m = J_m V_m \tag{2.22}$$

where the maximum current (J_m) is given by Singal (1981).

$$J_m = J_L\left(1 - \frac{1}{\nu+1-\log(\nu)}\right)\ ,\ V_m = V_{oc}(1 - \frac{1}{\nu}\log(\nu + 1 - \log(\nu)))\ ,\ \nu = \frac{nkT}{q}V_{oc} \qquad (2.23)$$

For a sunlight concentration with intensity C, the equations for P_m, J_m and V_m can be obtained as given by Singal (1981):

$$P_m(C) = J_m(C)\, V_m(C) \qquad (2.24)$$

where $J_m(C)$ and $V_m(C)$ can be expressed by

$$J_m(C) = CJ_m \qquad (2.25)$$

$$V_m(C) = V_m + V_T\log(C) \qquad (2.26)$$

where the intensity of sunlight C can vary in the range of 1 to 100 suns and $V_T = \frac{nq}{KT}$ and the ideality factor (n), which is chosen to lie between 1 and 2 for simplicity, is a measure of how closely the diode follows the ideal diode equation. When a load is connected to the diode, a current will flow in the circuit as shown in Fig. 2-2.

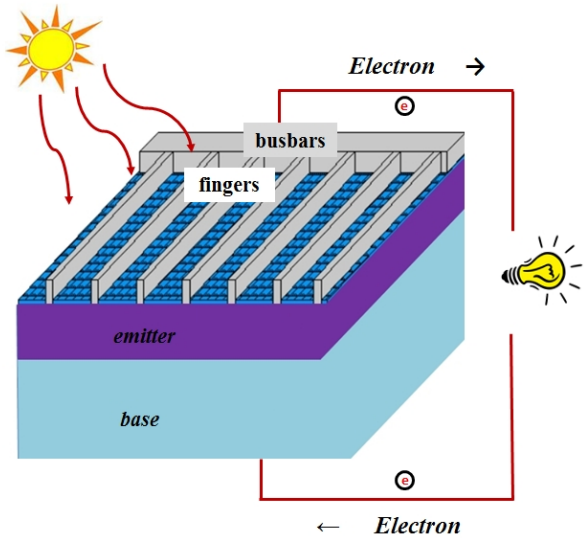

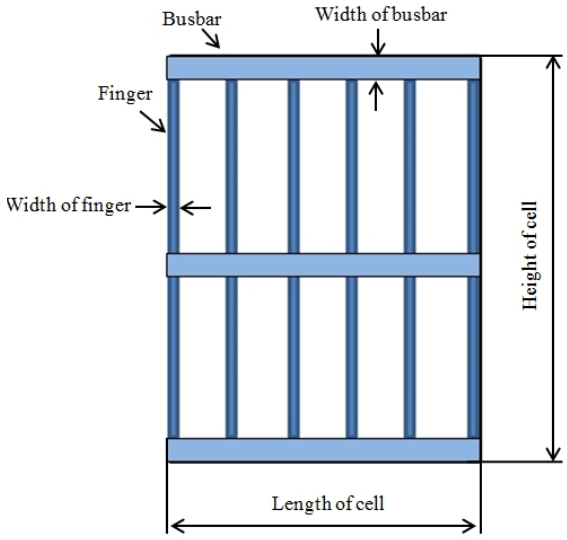

Figure 2-2 Simple solar cell structure with grid lines and top view of contact grid structure

Upon calculating the theoretical power output of solar cells, it is crucial to extract solar power without any power losses from the influence of the series parameters on concentrated sunlight (C) and dark J-V characteristic voltage and currents. However, if some power losses occur, they can be attributed to optical and electrical losses. The optical losses are a result of reflection, shadowing and unabsorbed radiation. In contrast, electrical losses can be divided into ohmic and recombination losses. In this work, shadowing and grid contact losses are considered in the optimization of solar cell design. The power losses are from the surface sheet (F_{sr}), contact (F_c), grid metal of fingers (F_f), busbars resistivity (F_b) and shadowing (F_s). The total fractional power losses (F_{sum}) can be expressed in terms of the individual fractional power losses given by Arturo (1984).

$$F_{sum} = F_{sr} + F_f + F_b + F_s + F_c \tag{2.27}$$

Based on sheet resistance (R_{sh}), the power loss can be calculated at the top contact point. When current is collected very close to the metallic grid lines, the power losses might be reduced in a solar cell. It is an important relationship between the fingers as well as the busbars. If the fingers are close to each other, the power losses will be reduced. On the other hand, if the fingers are too close, the solar cell cannot absorb enough sunlight due to blocking.

The calculation of total fractional power loss (F_{sum}) was explained by Shabana, Saleh, and Soliman (1988) and can be expressed as

$$F_{sum} = \sum_{i=1}^{n} \frac{P_{loss}}{P_{gneration}} = \sum_{i=1}^{n} \frac{\sum_{i=1}^{n} F_{sum} J_m V_m}{\sum_{i=1}^{n} J_m V_m} \tag{2.28}$$

The resistance of the sheet can be expressed in a differential from as

$$\mathrm{dR} = \left(\frac{Sheet\ resistance}{Distance\ \ along\ finger}\right) \text{Distance between two fingers.} \tag{2.29}$$

Thus the power loss due to sheet resistance can be calculated as

$$P_{loss\_sheet} = \int_0^{D/2} \frac{\mathrm{J_m}^2 \mathrm{L_f}^2 D^2 \mathrm{R_{sh}}}{\mathrm{L_f}} d_x = \frac{\mathrm{J_m}^2 \mathrm{L_f} \mathrm{R_{sh}}}{24} \tag{2.30}$$

The power generated is given by

$$P_{generation} = \mathrm{J_m} V_m (\mathrm{L_f} \frac{D}{2}) \tag{2.31}$$

The fractional power loss (F_{sr}) can be expressed as

$$F_{sr} = \frac{\mathrm{J_m R_{sh} D^2}}{12 \mathrm{V_m}} \tag{2.32}$$

Under normal circumstances, the contact resistance (R_c) can be considered, using the concept of transfer length (L_T), as

$$R_c = \frac{\sqrt{\mathrm{R}_{sh}R_c}}{\mathrm{L}_c}\ coth\left(\mathrm{L}_c\sqrt{\frac{\mathrm{R}_{sh}}{R_c}}\right) = \frac{2\mathrm{L}_T\mathrm{R}_{sh}}{\mathrm{L}_c}\ \cot\left(\frac{\mathrm{W}_f}{2\mathrm{L}_T}\right) \tag{2.33}$$

where $\mathrm{L}_T = \sqrt{\frac{R_c}{\mathrm{R}_{sh}}}$.

The specific contact resistance was described by Harrison and Reeves (1980) and the power loss of contact resistance can be found as

$$P_{losss\_contact} = I^2R_C = \left(\mathrm{J}_m\frac{\mathrm{L}_c}{2}\frac{\mathrm{D}}{2}\right)^2\left(\frac{2\mathrm{L}_T\mathrm{R}_{sh}}{\mathrm{L}_c}\ \cot\left(\frac{\mathrm{W}_f}{2\mathrm{L}_T}\right)\right) \tag{2.34}$$

Thus, the fractional contact loss (F_c) is given by

$$F_c = \frac{\mathrm{J}_m\mathrm{D}}{2\mathrm{V}_m}\mathrm{L}_T\mathrm{R}_{sh}\coth\left(\frac{\mathrm{W}_f}{2\mathrm{L}_T}\right) \tag{2.35}$$

The top of a solar cell has a series of arranged fingers intended to collect current. The corresponding resistive loss is given by

$$P_{generation} = \mathrm{J}_m V_m\left(\frac{\mathrm{L}_c}{2}D\right) \tag{2.36}$$

Because of symmetry, the equation is applied precisely at the midway along the length of finger to obtain

$$P_{loss\_finger} = I^2R_f = \int_0^{\frac{\mathrm{L}_f}{2}}\left(\mathrm{J}_m\frac{D}{2}\mathrm{L}_f\right)^2\left(\frac{\rho_m}{\mathrm{W}_f H_f}\right)d_x \tag{2.37}$$

Thus, the fractional power loss of finger (F_f) can be expressed as

$$F_f = \frac{J_m \rho_m (L_f)^2 D}{48 V_m W_f H_f} \tag{2.38}$$

The design of any metal contact should be considered to minimize the finger and busbar resistance. The ratio of width to thickness of a contact should be within the limits of the recommended aspect ratio, which is 0.23 ~ 0.25. Also, the fractional power loss of the busbars (F_b) is given by

$$F_b = \frac{J_m \rho_m B (L_b)^2}{6 V_m H_b W_b} \tag{2.39}$$

The width (W_b) and height (H_b) of the busbar are dependent upon the dimensions of the finger (W_f *and* H_f). If the dimensions of the finger (W_f *and* H_f) are determined, the width and height of busbar (W_f *and* H_f) can be determined and the scale factor (m) is subsequently applied.

The grid contact design maximizes transmittance from the sunlight and reduces optical loss. Thus, the vicinity of a solar cell contributes to reduced power losses. The fractional power loss of shadowing (F_s) is conditioned by the size and number of grid lines (N_f) because it prevents light from entering a solar cell.

$$F_s = \left(1 - \left(\frac{L_b L_f - (N_f W_f L_f + N_b W_b L_b - N_f W_f N_b W_b)}{L_c^2}\right)\right) \tag{2.40}$$

Arturo (1985) calculated the efficiency of a solar cell under concentrated sunlight (C) as

$$\text{Efficiency } (\eta_C) = \frac{J(C)_m V(C)_m}{P_{in} \cdot C} (1 - F_{sum}) \times 100 \tag{2.41}$$

where P_{in} is the incident power at 1 sun and is equal to 1 kW$/m^2$. In this work, the solar cell performance is optimized with considerations of fractional power losses (F_{sum}) and concentrated sunlight (C).

2.3.2 Formulation of optimization problems

The following step-by-step procedure is used for the computation of conversion efficiency of a solar cell:

1. Calculate the total current density (J_L) using Eqs. (2.6) – (2.9)
2. Compute the reverse saturation current density (J_0) using Eqs. (2.10) – (2.19)
3. Compute the short-circuit current density (J_{SC}) derived from the results of the total current density (J_L) and the reverse saturation current density (J_0) using Eq. (2.20)
4. Compute the open-circuit voltage (V_{oc}) using Eq. (2.21)
5. Compute the maximum power density: $P_m = J_m V_m$ using Eq. (2.23)
6. Compute the maximum power density with the intensity of sunlight: $P_m(C) = J_m(C)\, V_m(C)$ using Eqs. (2.25) – (2.26)
7. Calculate total fractional power loss (F_{sum}) using Eqs. (2.28) – (2.40)

The following procedure is used to compute the power output developed by the cell:

1. – 5. Steps 1 through 5 are same as those indicated for the computation of the conversion efficiency
6. Multiply the maximum power density in step 5 by the area of solar cell ($L_c \cdot H_c$) to find the maximum power generated by the solar cell.

The objective is to find the optimal design vector $\vec{X}$ for maximization of conversion efficiency (η) and power output (P_o) through minimization of the power losses under a solar intensity factor of *C* sums. The single-objective function of conversion efficiency can be expressed as

$$f_1(\vec{X}) = \text{conversion efficiency} = \frac{J(C)_m V(C)_m}{P_{in} \cdot C}(1 - F_{sum}) \times 100 \qquad (2.42)$$

To remove the dependence of power output of the solar cell on its area, it is more common to express the short-circuit current density as J_{sc} in mA/cm^2. Thus, the conversion efficiency of the solar cell will be related to short-circuit current (J_{sc}), open-circuit voltage (V_{oc}), incident power density (P_{in}) at 1 sun, concentrated sunlight of intensity of *C* suns, and the total fractional power loss (F_{sum}). The design vector of the problem, for a rectangular solar cell, is:

$$\overrightarrow{X} = \{T_e\ T_b\ L_c\ H_c\ W_f\ H_f\ N_f\ W_b\ H_b\ N_b\ C\}^T \equiv \{x_1\ x_2\ x_3\ x_4\ x_5\ x_6\ x_7\ x_8\ x_9\ x_{10}\ x_{11}\}^T \qquad (2.43)$$

The optimization problem is solved by placing the lower and upper bounds on the design variables as $x_j^{(l)} \leq x_j \leq x_j^{(u)}$; $j = 1\ to\ 11$, with the bounds indicated in Table 2-1:

Table 2-1 Lower and upper bounds on the design variables

j	1	2	3	4	5	6	7	8	9	10	11
$x_j^{(l)}$	0.1μm	100μm	0.5cm	0.5cm	20μm	4.6μm	2	100μm	4.6μm	2	1
$x_j^{(u)}$	8μm	450μm	5cm	5cm	200μm	50μm	100	4000μm	50μm	10	100

The constraints of the optimization problem include the required relationships between the heights of finger (H_f) and busbar (H_b) by considering the delivery to the busbars and the shading from the busbars, the ratio of width to height of the finger, and the spacing (D) between the fingers and the busbars:

$$D_f - \left(L_c - W_f \cdot N_f\right)/\left(N_f - 1\right) = 0 \tag{2.44}$$

$$W_f \cdot N_f - L_c \leq 0 \tag{2.45}$$

$$D_b - (H_c - W_b \cdot N_b)/(N_b - 1) = 0 \tag{2.46}$$

$$W_b \cdot N_b - H_c \leq 0 \tag{2.47}$$

$$0 \leq H_f - H_b \leq 1\mu\text{m} \tag{2.48}$$

$$0.23 \leq \frac{H_f}{W_f} \leq 0.25 \tag{2.49}$$

The power output (f_2) can be calculated from the maximum operating power density (P_m), which corresponds to the maximum operating voltage (V_m) and current density (J_m) including the total fractional power loss (F_{sum}), and the size of the solar cell.

$$\text{Maximize } f_2\ (\vec{X}) = \text{Power density } \left(\frac{W}{cm^2}\right) \times area\ of\ solar\ cell\ (cm^2) \tag{2.50}$$

The following additional constraint is considered while maximizing f_2. Conversion efficiency is chosen to be 80% of the maximum conversion efficiency ($\eta \geq 0.8\,\eta^*_{ma}$). The problem of maximization of conversion efficiency, $f_1 = (\eta^*_{ma})$, is investigated for two cases – one by maximizing the theoretical conversion efficiency of the solar cell (with no front contact material using only 8 design variables) and the other by maximizing the

practical conversion efficiency of the solar cell (with front contact material which causes ohmic and optical losses). In the case of maximization of power output, the problem is addressed by including a constraint that the conversion efficiency be at least a specified percentage of the maximum conversion efficiency and is investigated for different percentages of the maximum conversion efficiencies.

2.3.3 Validity and importance of the proposed optimization approach

As indicated in the literature review (chapter 1.4), most investigations aimed at the optimum design of solar cells by considering only subsystem designs. For example, some researchers considered only the top contact design by fixing the cell structure. Some investigators considered the cell structure design along with/without the intensity of sunlight as a design variable by fixing the top contact design variables. These sub-optimization approaches are not expected to yield the maximum possible conversion efficiency and the maximum power output of the solar cell. All investigators conducted their efforts at maximizing the conversion efficiency. The direct maximization of the power output of the solar cell was not considered in the literature. Hence the present approach, described in section 2.3.2, is proposed as the most comprehensive design for the solar cell. The optimization results (maximization of conversion efficiency) of the solar cell (using the present approach as described in section 2.3.1) are shown in Table 2-2.

Table 2-2 Optimization results of solar cell

Objective		Design variables											
		T_e (μm)	T_b (μm)	L_c (cm)	H_c (cm)	W_f (μm)	H_f (μm)	N_f	W_b (μm)	H_b (μm)	N_b	C	Conversion efficiency
Ini.	Sq.	6.0	200.0	3.0	3.0	60.0	10.0	20	600.0	8.0	4	12	15.01
	Rec.	6.0	200.0	3.0	3.0	60.0	10.0	20	600.0	8.0	4	12	15.01
$\overrightarrow{x^*}_{f_1}$	Sq.	7.3	244.4	0.81	0.81	20.0	5.0	18	100.0	6.0	2	6	20.28
	Rec.	7.5	208.0	2.45	0.50	20.0	5.0	12	100.2	6.0	3	6	20.54

In order to validate the superiority of the present approach, the following solar cell optimization problems are considered in this section.

a) Optimization of top contact design of the solar cell

In this case, only the design variables W_f, H_f, N_f, W_b, H_b, and N_b are selected as design variable and the remaining ones (namely T_e, T_b, L_c, H_c and C) are fixed at the values indicated in Table 2-2. The 6 – variable optimization problem is solved using the MATLAB program *ga* with the starting values given in Table 2-2. The results of optimization are shown in Table 2-3.

Table 2-3 Results of 6 – variable optimization problem

Objective		Design variables											
		T_e (μm)	T_b (μm)	L_c (cm)	H_c (cm)	W_f (μm)	H_f (μm)	N_f	W_b (μm)	H_b (μm)	N_b	C	Conversion efficiency
$\overrightarrow{x^*}_{f_1}$	Sq.	6.0	200.0	3.0	3.0	36.3	9.0	59	181.5	10.1	4	12	18.68
	Rec.	6.0	200.0	3.0	3.0	35.8	8.9	60	179.1	9.9	4	12	18.68

It can be seen that the optimization of only the top contact design yielded the maximum conversion efficiency of only 18.68 % while the proposed (present) approach gave the

maximum conversion efficiency of 20.28 % for a square cell. For a rectangular cell, the optimization of only top contact design yield the maximum conversion efficiency of 18.68 % while the proposed approach gave the maximum conversion efficiency of 20.54 %.

b) Optimization of cell structure design of the solar cell

In this case, only T_e and T_b are selected as design variables and the remaining ones (namely L_c, H_c, W_f, H_f, N_f, W_b, H_b, N_b, and C) are fixed at the values indicated in Table 2-2. The 2 – variable optimization problem is solved using the MATLAB program *ga* with the starting values given in Table 2-2. The results of optimization are shown in Table 2-4.

Table 2-4 Results of 2 – variable optimization problem

Objective		Design variables											
		T_e (μm)	T_b (μm)	L_c (cm)	H_c (cm)	W_f (μm)	H_f (μm)	N_f	W_b (μm)	H_b (μm)	N_b	C	Conversion efficiency
$\overrightarrow{x^*}_{f_1}$	Sq.	8.0	450.0	3.0	3.0	60.0	10.0	20	600.0	8.0	4	12	15.01
	Rec.	8.0	450.0	3.0	3.0	60.0	10.0	20	600.0	8.0	4	12	15.01

It can be seen that the optimization of only the cell structure design yields the maximum conversion efficiency of only 15.01 % while the proposed (present) approach gives the maximum conversion efficiency of 20.28 % for a square cell. For a rectangular cell, the optimization of only top contact design yields the maximum conversion efficiency of 15.01 % while the proposed approach gives the maximum conversion efficiency of 20.54 %.

c) Optimization of the size of cell and the intensity of sunlight

In this case, only L_c, H_c, and C (L_c= H_c for a square cell) for a rectangular cell are selected as design variable and the remaining ones (namely T_e, T_b, W_f, H_f, N_f, W_b, H_b, and N_b) are fixed at the values indicated in Table 2-2. The 3 – variable optimization problem is solved using the MATLAB program *ga* with the starting values given in Table 2-2. The results of optimization are shown in Table 2-5.

Table 2-5 Results of 3 – variable optimization problem

Design variables													
Objective		T_e (μm)	T_b (μm)	L_c (cm)	H_c (cm)	W_f (μm)	H_f (μm)	N_f	W_b (μm)	H_b (μm)	N_b	C	Conversion efficiency
$\overrightarrow{x^*}_{f_1}$	Sq.	6.0	200.0	4.02	4.02	60.0	10.0	20	600.0	8.0	4	1	18.31
	Rec.	6.0	200.0	5.00	1.76	60.0	10.0	20	600.0	8.0	4	4	19.00

It is evident that the optimization of only the cell structure design yieldes the maximum conversion efficiency of only 18.31 % while the proposed (present) approach gives the maximum conversion efficiency of 20.28 % for a square cell. For a rectangular cell, the optimization of only top contact design yields the maximum conversion efficiency of 19.00 % while the proposed approach gives the maximum conversion efficiency of 20.54 %.

It can be observed that the consideration of all the design variables indicated in section 3.2.1 is important in order to achieve the maximum possible conversion efficiency of the solar cell. Hence all the results shown in subsequent sections/chapters are based on the proposed (present) optimization approach.

2.3.4 Numerical results of the present optimization approach

a) Maximization of conversion efficiency of the solar cell

The maximization of the conversion efficiency (η_{ma}^{*}) of a solar cell can be considered in two stages - theoretical and practical conversion efficiency. Figure 2-3 (a) shows the variations of short-circuit current density in the emitter, base, space-charge regions (SCR) and the total current density with the thickness of the emitter over the range 0-8 μm (by solving a number of optimization problems by fixing the thickness of the emitter at one specific value at a time). The thickness of the base is fixed as 250 μm. The current density in the emitter is found to increase steeply from 0 to 2 μm with a slow variation beyond a value of 2 μm while the current density in the base is decreased within the same range. This means that the thickness of the emitter between 2 μm and 8 μm corresponds to a small variation of the total current density between 39.88 mA and 40.01 mA. In order to investigate the influence of base thickness over a wider range, the values of the short-circuit current density are found for a base thickness ranging from 1 to 450 μm, and the results are shown in Fig. 2-3 (b). In this case, several optimization problems are solved by fixing the thickness of the base at one specific value at a time while the thickness of the emitter is held at a constant value of 8 μm in all the cases. It can be observed that the short-circuit current density increases steeply as the base thickness increases from 1 μm to about 150 μm with no significant variation beyond a thickness of 150 μm. As a result, the variations in the thicknesses of the emitter and base will have a large influence on the total current density in specific ranges between 0.1 μm and 2 μm for the emitter and between 1 μm and 150 μm for the base of a solar cell. On the other hand, the range

between 2 μm and 8 μm for the emitter and between 150 μm and 450 μm for the base of a solar cell will have much less impact on the total current density.

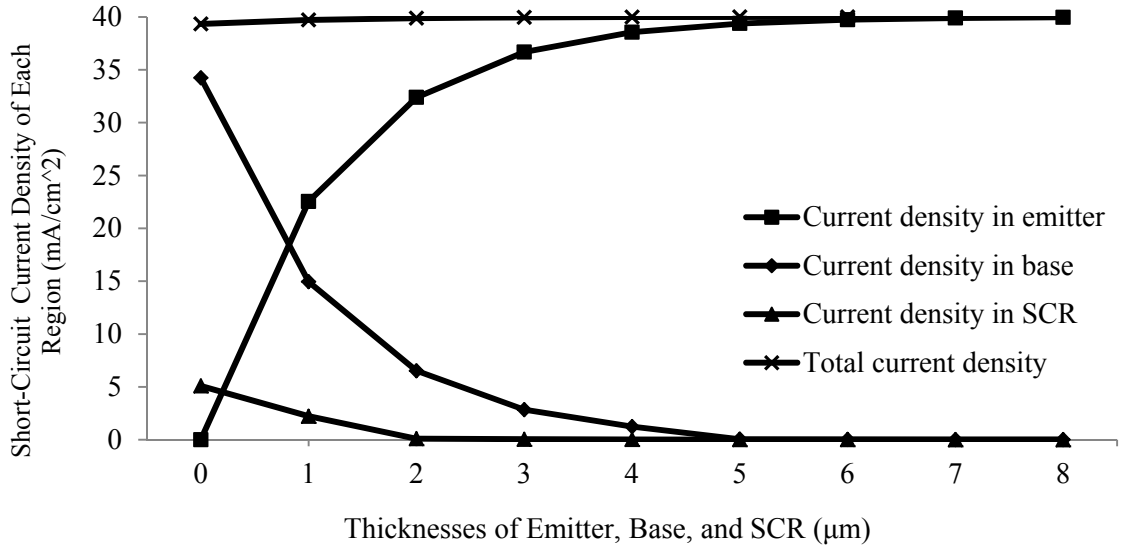

(a)

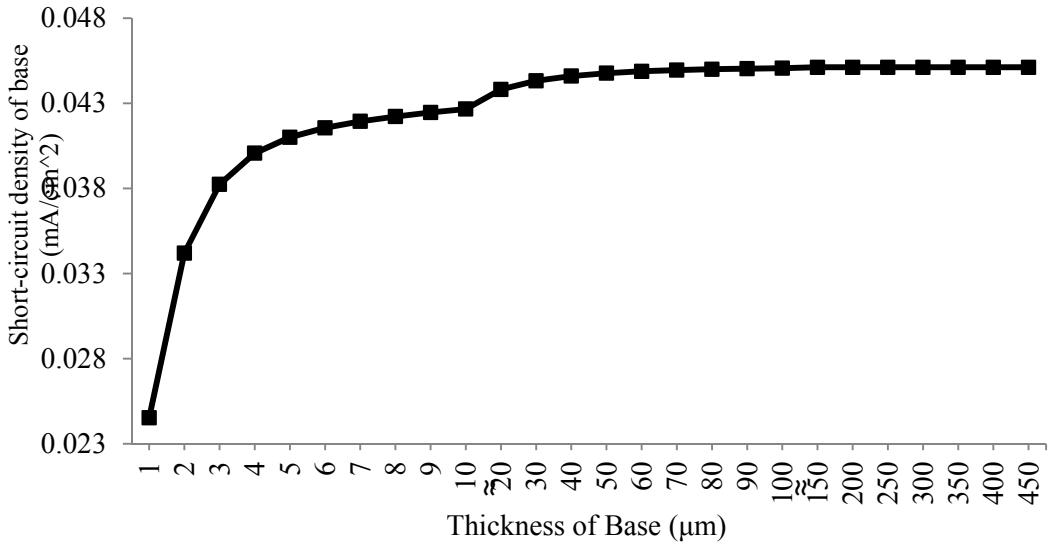

(b)

Figure 2-3 Relationships between short-circuit current density and thicknesses of emitter and base

To maximize the practical conversion efficiency of a solar cell, the grid variations of the contact design variables, namely, the length of the cell, width, height and number of the fingers, and the width, height and number of the busbars are to be considered. These variables lead to optical and ohmic losses that cause a reduction in the theoretical conversion efficiency. Two shapes- square and rectangular- are considered for the maximization of the practical efficiency of the solar cell. In the case of the square solar cell configuration, the width and height of the cell will be same; as such only ten design variables are considered by eliminating x_3 in the design vector of Eq. (2.43). A parametric study is conducted to find the influence of the concentrated sunlight on the open-circuit voltage of the solar cell. For this, the optimization problem stated in section 2.3.2 is solved several times by using only the first nine variables in the design vector, Eq. (2.43) with the value of the concentrated sunlight fixed at a different value each time. The variation of the optimal value of the objective function, the maximum practical efficiency, with the value of concentrated sunlight is shown in Fig. 2-4. The variation of the theoretical efficiency with the value of the concentrated sunlight is also shown plotted in Fig. 2-4 for comparison. It is to be noted that the practical efficiency of a solar cell is equal to the theoretical efficiency minus the contributions of optical and ohmic losses.

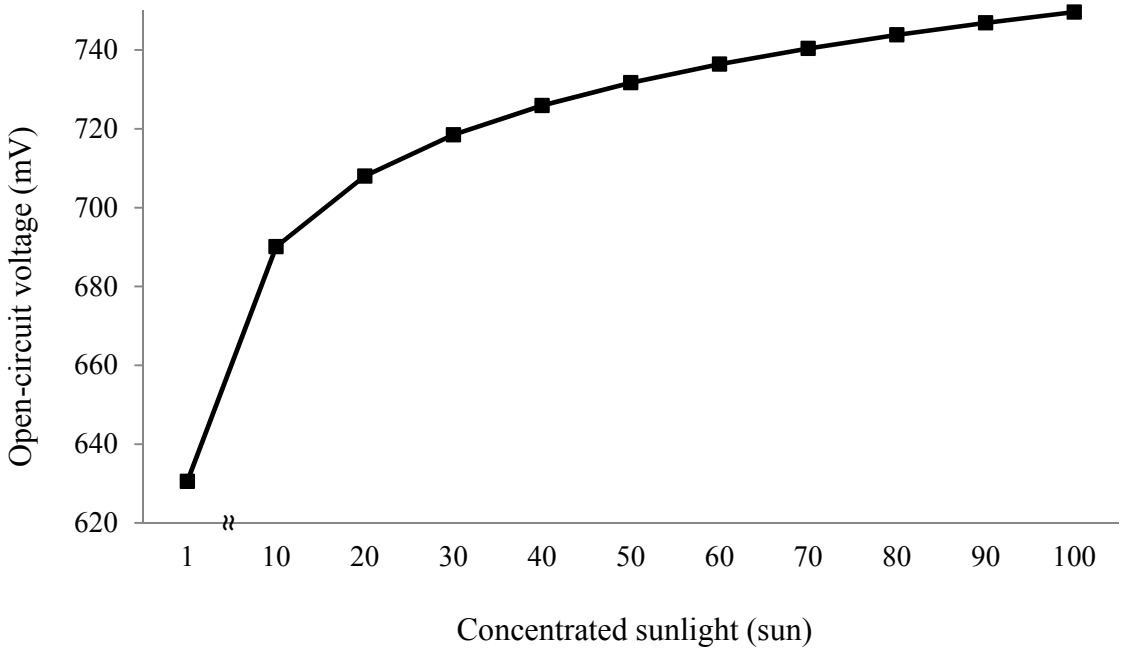

(a) Open-circuit voltage versus concentrated sunlight

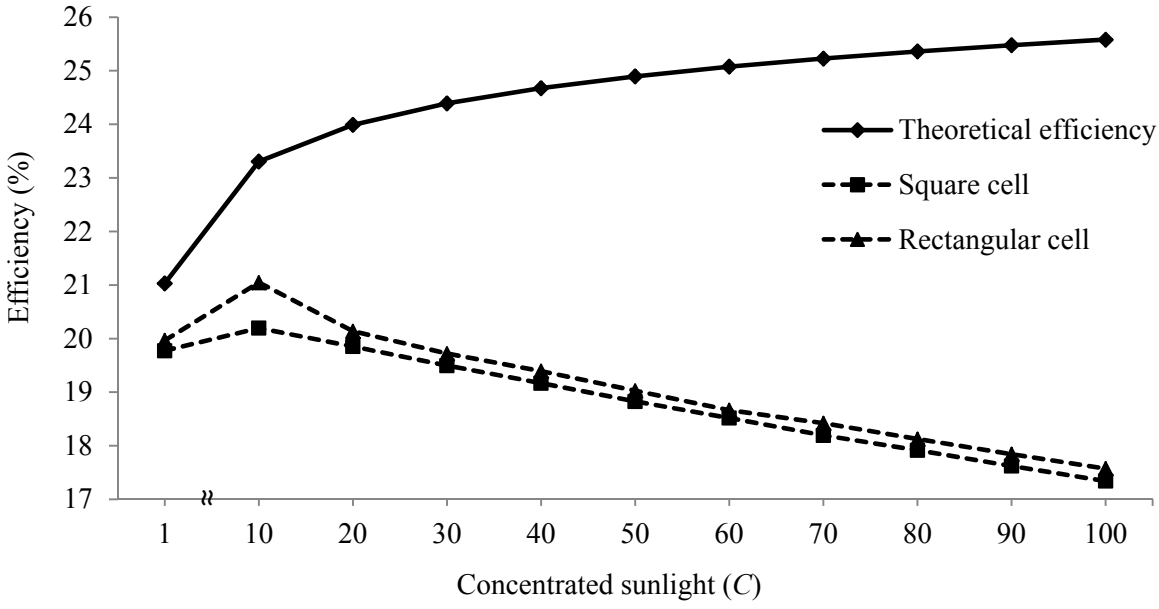

(b) Efficiency versus concentrated sunlight

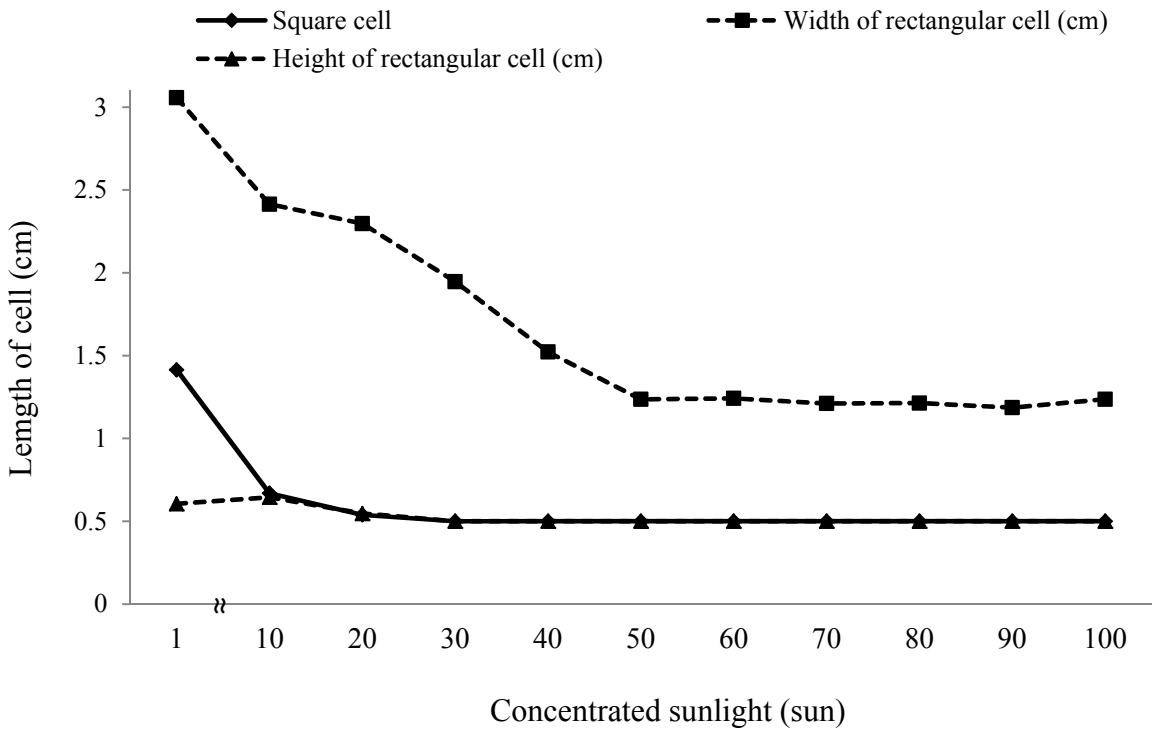

(c) Length of cell versus concentrated sunlight

Figure 2-4 Dependance of efficiency on concentration sunlight

- Theoretical conversion efficiency of the solar cell under a concentration ratio of one

The efficiency of a solar cell depends on a range of factors, such as materials, dopant concentrations (N_a and N_d), thickness of a solar cell (T_e and T_b), recombination velocity, and the variations associated with the fabrication process. An efficient solar cell consists of a thin emitter formed by low energy, low recombination velocity at the front surface, and enough base thickness for proper absorption from a wide range of wavelengths. However, if the thickness is thin enough, there is a limited recombination velocity of minority carriers toward the p-n junction. The emitter allows a solar cell to generate power. Heavily doped materials are the most important factors to determine the cell

performance because those minority-carrier diffusion coefficients (D_p and D_n), minority-carrier lifetime, and minority diffusion lengths (L_p and L_n) all influence the open-circuit voltage (V_{oc}) and short-circuit current (J_{sc}). Once the design factors of a solar cell's performance are determined, there are a number of potential methods that could be utilized based on a study of the performance characteristics at various concentrations of sunlight. The optimal design factor of cell thickness reduces material costs because it results in a thin solar cell, which is competitively priced to have significant impact on the size of large-scale power systems. If a solar cell has a smaller thickness, material is saved. At the same time, its performance is maximized. The objective function for the maximization of the theoretical conversion efficiency of a solar cell can be expressed as

$$\text{Maximize } f_1(\vec{X}), \% = \frac{J(C)_m V(C)_m}{P_{in} \cdot C} \times 100 \tag{2.51}$$

All the constraints stated in section 2.3.2, except those associated with the grid contact materials, are considered in the solution process. Note that the first three design variables in Eq. (2.43), which relate to the grid contact materials, are excluded from the design vector. The theoretical conversion efficiency is determined to find the characteristics of the solar cell using the values of structural parameters and pre-specified values of the cell thickness and concentrated sunlight. The thickness of base (T_b) is assumed as 250 μm, same as the value recommended in the literature (Singal (1980)) under a concentrated sunlight of 1 sun intensity. The input design factors used in this study are given by : dopant concentration of emitter = $2 \times 10^{17}\ cm^{-3}$, dopant concentration of base = $5 \times 10^{16}\ cm^{-3}$, recombination velocity of front surface = 1×10^2 cm/s , and recombination velocity of back surface = 1×10^4 cm/s. The charateristics of the solar cell at optimal

design, including the optimal values of the thicknesses of the emitter and base and the optimal conversion efficiency, are shown in Table 2-6. Next, a parametric study is conducted to find the influence of emitter thickness on the short-circuit current density.

Table 2-6 Characteristics of the optimal solar cell

Characteristic	Value
Thickness of emitter (T_e)	8 μm
Thickness of base (T_b)	250 μm
Concentrated sunlight (C)	1
Total short-circuit current (J_{sc})	40.01 mA/cm^2
Total open-circuit voltage (V_{oc})	630.56 mV
Maximum total current (J_m)	38.21 mA/cm^2
Maximum total voltage (V_m)	550.42 mV
Fill factor (FF)	83.35%
Conversion efficiency (η)	21.03%

- Maximization of practical conversion efficiency considering all ten design variables in Eq. (2.43)

The optimization problem stated in section 2.3.2 is solved by placing lower and upper bounds on all the design variables. As per to the works of Sharan (1986), Gessert (1992) and Djeffal (2012), the design data are assumed as $N_d = 2 \times 10^{17}\, cm^{-3}$, $N_a = 5 \times 10^{16} cm^{-3}$ (dopant concentrations of the emitter and base), $S_n = 1 \times 10^4 cm/s$, $S_p = 1 \times 10^2 cm/s$ (recombination velocities) to determine the thickness of the solar cell by

specifying grid contact resistance, sheet resistance , and metal resistivity for silicon as $R_c = 3 \times 10^{-3}\ \boldsymbol{\Omega}\cdot cm^2$, $R_{sh} = 100\ \boldsymbol{\Omega}/cm^2$, and $\rho_m = 1.6 \times 10^{-6}\ \boldsymbol{\Omega}\cdot cm$, respectively. The solution of the optimization problem yields the optimal values of the solar cell thickness (i.e., emitter and base thicknesses), grid contact design parameters, and the intensity of sunlight.

If the cell size is permitted to vary along with other design variables during optimization, the optimal values of the remaining design factors are expected to be different compared to the values found in the previous cases. Such a study is conducted in this section. The optimal values of the design variables, the value of the geometric grid lines, short-circuit current, open-circuit voltage, and the optimal theoretical and practical efficiencies of the solar cell obtained are shown in Table 2-7.

Table 2-7 Optimal design variables and other characteristics of the solar cell

Quantity	Square cell	Rectangular cell
Design variables :		
Thickness of emitter (T_e)	7.3 μm	7.6 μm
Thickness of base (T_b)	244 μm	208 μm
Size of the solar cell: ($Length_c$ for square cell and $L_c \times H_c$ for rectangular cell)	$0.81 \times 0.81\ cm^2$	$2.45 \times 0.5\ cm^2$
Width of finger (W_f)	20 μm	20 μm
Height of finger (H_f)	5 μm	5 μm
Number of finger (N_f)	18	12

Width of busbar (W_b)	100 μm	100.4 μm
Height of busbar (H_b)	6 μm	6 μm
Number of busbar (N_b)	2	3
Concentrated sunlight (C)	6	6
Characteristics of solar cell :		
Short-circuit current $(J_{sc}(C))$	240 mA/cm^2	240 mA/cm^2
Open-circuit voltage $(V_{oc}(C))$	676.9 mV	676.9 mV
Maximum current $(J_m(C))$	229.3 mA/cm^2	229.3 mA/cm^2
Maximum voltage $(V_m(C))$	596.7 mV	596.7 mV
Fill factor (FF)	84.2 %	84.2 %
Theoretical conversion efficiency (without power losses(η))	22.80 %	22.80 %
Optimal conversion efficiency (with power losses(η))	20.28 %	20.54 %

As can be seen from Table 2-3, the length of the cell and width of the finger approached their respective lower bound values. The maximum practical efficiencies of the square and rectangular cells with minimal power losses are found to be 20.28 % and 20.54 %, respectively. The corresponding theoretical efficiencies are found to be 22.80 % in both types of cells.

- Optimization with pre-specified cell size and width of fingers

The practical conversion efficiency of the solar cell is maximized by specifying the area of the cell as $1 \times 1\ cm^2$ for a square cell and $3 \times 2\ cm^2$ for a rectangular cell, and the width of the fingers as 80 μm. Thus, there will be only eight design variables left in Eq. (2.43) in the optimization problem. The results obtained from the solution of the optimization problem (using the program, *ga*) are shown in Table 2-8.

Table 2-8 Results of optimization with eight design variables

Quantity	Square cell	Rectangular cell
Design variables :		
Thickness of emitter (T_e)	8 μm	8 μm
Thickness of base (T_b)	304 μm	363 μm
Height of finger (H_f)	20 μm	20 μm
Height of busbar (H_b)	21 μm	21 μm
Width of busbar (W_b)	100 μm	415.6 μm
Number of finger (N_f)	10	17
Number of bus bar (N_b)	2	2
concentrated sunlight (C)	4	3
Characteristics of the solar cell :		
Short-circuit current ($J_{sc}(C)$)	160 mA/cm^2	120 mA/cm^2
Open-circuit voltage ($V_{oc}(C)$)	666.4 mV	659 mV
Maximum current ($J_m(C)$)	152.8 mA/cm^2	114.6 mA/cm^2
Maximum voltage ($V_m(C)$)	586.3 mV	578.8 mV

Fill factor (*FF*)	84 %	83.9 %
Theoretical conversion efficiency (without power losses(η))	22.4 %	22.4 %
Optimal conversion efficiency (with power losses(η))	18.17 %	19.17 %

It is noticed that the specification of the geometric parameters of the cell area and the width of a finger did not affect the thickness of the solar cell, short-circuit current and open-circuit voltage. The practical conversion efficiency has decreased from 20.28 % to 18.17 % and 20.54 % to 19.17 %, while the fractional power losses have increased from 11.09 % to 18.88 % and 9.93 % to 13.32 % for the square and rectangular cells, respectively, due to the optical and resistive losses. This shows that the change in the conversion efficiency is not proportional to the change in fractional power losses due to concentrated sunlight and interactions among the various geometric parameters.

b) Maximization of power output

The conversion efficiency of the solar cell is independent of the power output. It is only a factor when the solar cell is designed for maximum power output with a specified area. Thus, in order to find the maximum power output of the solar cell, a minimum constraint of 80 % of the maximum conversion efficiencies (in both square and rectangular cells) becomes necessary to prevent unrealistic conversion efficiencies resulting from the intensity of sunlight. Table 2-9 shows the values of design variables and other outputs

corresponding to maximum power output with a constraint of realizing at least 80 % of the maximum conversion efficiency in square and rectangular cells.

In the case of a square cell, the maximum power output is 9.46 W and the conversion efficiency is 16.22 % which is almost the minimum permissible value of 80 % of the maximum conversion efficiency. Since the power output is proportional to the size of the solar cell, the conversion efficiency has decreased due to an increase in the individual power losses ($F_{sr}, F_f, F_b, F_s \; and \; F_c$). The total power loss (F_{sum}) in a square cell for maximum power output is 32.88 %. The dominant power loss of 19.15 % is the fractional power loss due to shadowing from busbars and fingers (sunlight blockage). Thus, the maximum power output is given by the product of the power density, 0.389 $\frac{W}{cm^2}$ and the area of the solar cell, 24.3 cm^2 as 9.46 W, for a square cell.

In the case of a rectangular cell, the maximum power output is found to be 9.54 W with a conversion efficiency of 16.43 % which is close to the minimum permissible value of 80 % of the maximum conversion efficiency (20.54 %). The concentrated sunlight has reached a value of 40. The difference in total power loss between maximum conversion efficiency and maximum power output is 33.40 %, an indication that the total power loss in maximum power output is higher due to differing sizes of the solar cell. The main fractional power loss (20.26 %) is caused by shadowing from fingers and busbars because the number of fingers and busbars has increased from 12 to 64 and from 3 to 10, respectively. In addition, the widths of the finger and busbar associated with the power losses have increased from 40 μm to 65.80 μm and from 199.4 μm to 337.18 μm, respectively. With a consideration of cell structure, cell size, grid contact design, and

conversion efficiency, the power output of 9.54 W can be found as the product of density, 0.657 $\frac{W}{cm^2}$, and the area of the solar cell, 14.52 cm^2 for a rectangular cell. This indicates that the relationship between the conversion efficiency and power output plays a role in the optimization of the solar cell performance.

Table 2-9 Optimal design variables and other characteristics of the solar cell

Quantity	Square cell	Rectangular cell
Design variables :		
Thickness of emitter (T_e)	5.51 μm	5.18 μm
Thickness of base (T_b)	181.02 μm	282.17 μm
Size of the solar cell: ($Length_{cell}$ for square cell and $L_c \times H_c$ for rectangular cell)	$5 \times 5\ cm^2$	$5 \times 2.9\ cm^2$
Width of finger (W_f)	65.80 μm	65.80 μm
Height of finger (H_f)	17.88 μm	16.44 μm
Number of finger (N_f)	87	64
Width of busbar (W_b)	368.37 μm	337.18 μm
Height of busbar (H_b)	18.89 μm	17.43 μm
Number of busbar (N_b)	10	10
Concentrated sunlight (C)	24	40
Conversion efficiency (with power losses(η))	16.22 %	16.43 %
Maximum power output (P_o)	9.46 W	9.54 W

The single-objective optimization problems for maximum conversion efficiency provide a solar cell design having a maximum conversion efficiency of 20.28 % and 20.54 % for square and rectangular cells, respectively. In this section, the maximum power output of a solar cell is investigated by conducting sensitivity analysis by requiring the realization of different values of the maximum conversion efficiency (formulated as the ratio η/η_{ma}^{*}) in the range of 70 % to 100 %.

The difference between the lowest and highest power output of a solar cell is mainly caused by changes in power density, collected amount of sunlight, and total fractional power loss. An increase in the thicknesses of a solar cell emitter and base has the influence of improving the conversion efficiency (η). The widths of the fingers and busbars contribute to conversion efficiency and power density since they prevent collection of the proper amount of sunlight. Beyond a value of 90 % for minimum permissible value of the maximum conversion efficiency, the cell areas have steeply decreased from 22.81 cm^2 to 0.66 cm^2 for a square cell and from 13.44 cm^2 to 1.23 cm^2 for a rectangular cell. This indicates that an increase in the conversion efficiency and a decrease in the power output occur owing to changes in the geometric design and numbers of fingers and busbars; these are also associated with total power loss and power density.

Table 2-10 shows the variations of the conversion efficiency, total power loss, power density, cell area, and power output with respect to different minimum permissible values of constraint on the conversion efficiency in finding the maximum power output. The relationship between the conversion efficiency and power output has been observed through variations in power density and cell area associated with the geometric design

parameters, which indicated that the amount of power output has increased even though the power density has decreased by the reduction of the conversion efficiency. Thus, the area of a solar cell contributes to an increase in the total power output in both types of cells. This indicates that the behaviors of the conversion efficiency and power output are approximately opposite; hence a compromise solution is to be found in a practical solar cell design.

Table 2-10 Variations of conversion efficiency, power density, cell area, and power output with respect to maximum conversion efficiency ratio

Results						
$\frac{\eta}{\eta_{ma^*}}$		Conversion efficiency (%)	Total power loss (%)	Power density ($\frac{W}{cm^2}$)	Cell area (cm^2)	Power output (W)
70%	Square	14.20	42.81	0.6674	24.77	16.53
	Rect.	14.39	42.77	0.9207	17.56	16.17
75%	Square	15.24	37.82	0.5181	25.00	12.95
	Rect.	15.40	38.03	0.7393	17.21	12.73
80%	Square	16.22	32.88	0.3893	24.30	9.46
	Rect.	16.43	33.40	0.6572	14.52	9.54
85%	Square	17.24	27.29	0.2585	24.35	6.30
	Rect.	17.46	28.21	0.4888	13.33	6.51
90%	Square	18.25	20.96	0.1460	22.81	3.33
	Rect.	18.48	22.03	0.2772	13.44	3.73
95%	Square	19.26	16.56	0.1541	6.77	1.04
	Rect.	19.51	16.29	0.1951	8.33	1.63
100%	Square	20.28	11.09	0.1216	0.66	0.07
	Rect.	20.54	9.93	0.1232	1.23	0.15

2.4 Solar PV Panel Module

A solar PV panel module constitutes an assembly (with interconnections) of solar cells. The power output is the average power, in watts, produced as given by the product of the power density ($\frac{\mathrm{W}}{\mathrm{cm}^2}$) and the size of a solar cell (cm^2). The power output of a solar PV panel module can be determined by the characteristics of the power density of a single solar cell including materials, cell structure and front contact design, number of panel modules, and size of solar panel module comprised of cells. Figure 2-5 shows the configuration of a typical panel module interconnected by individual solar cells and a typical completed panel module with several components.

Solar cells with identical characteristics are connected and encapsulated to form panel modules, which are basic blocks of a solar PV array system. Ideally, the solar cells in a panel module would produce power output based on the number of identical solar cells used. However, in practice, all cells have unique characteristics, and the power output of a panel module is limited by the solar cells having the lowest output due to the connection of mismatched cells. Solar panel modules are used in harsh and remote surroundings, so the panel module should be able to withstand environmental conditions such as dust, salt, sand, wind, snow, humidity, rain, condensation, evaporation of moisture, and seasonal temperature variations.

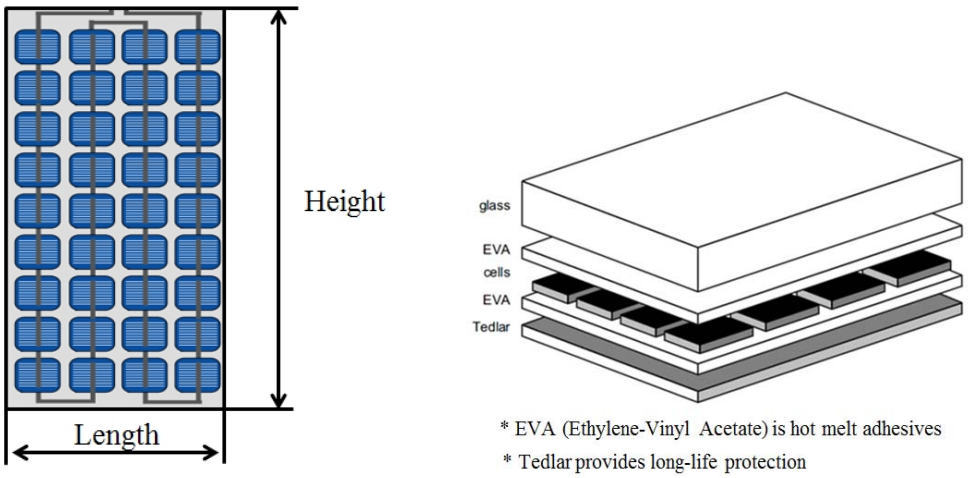

Figure 2-5 A typical panel module interconnected thorough a number of solar cells and encapsulated panel module structure

The top glass cover must have high transmission from sunlight to generate electricity and have good impact resistance and a hard surface. Also, the materials should be carefully selected to protect adhesion under extreme operating conditions. Therefore, the circuit design in series or parallel layout, module structure, environmental conditions, and mechanical protection are critical factors for reducing electrical and mechanical power losses in panel module performance. The power output can be calculated as the product of the power density associated with a cell's conversion efficiency and the size (area) of a panel module.

2.4.1 Formulation of optimization problems

To generate the solar conversion efficiency and power output in a panel module, the conversion efficiency (f_1) and power output (f_2) can be expressed as:

$$\text{Maximize: } f_1(\vec{X}) = \text{conversion efficiency} = \frac{J_m V_m}{P_{in} \cdot C}(1 - F_{sum}) \times 100\ (\%) \qquad (2.52)$$

The intensity of sunlight (C) is not treated as a design variable; it is fixed at a value of 1.

Maximize: $f_2(\vec{X})$ = P = power output of a solar PV panel module (W)

$$= L_p \times H_p\ (cm^2) \times Power\ density\ \left(\frac{W}{cm^2}\right)$$

$$= L_c \times H_c\ \times N_{c_l} \times N_{c_h} \times J_m \times V_m \tag{2.53}$$

where L_p is composed of the number of cells (N_{c_l}) and length of cells (L_c). Also, H_p is constructed by the number of cells (N_{c_h}) and height of cells (H_c). It is evident that the length and height of a panel module are associated with the size and number of solar cells.

The design vector of the problem is chosen as:

$$\vec{X} = \begin{Bmatrix} T_e \\ T_b \\ L_c \\ H_c \\ W_f \\ H_f \\ N_f \\ W_b \\ H_b \\ N_b \\ N_{c_l} \\ N_{c_h} \end{Bmatrix} \equiv \begin{Bmatrix} x_1 \\ x_2 \\ x_3 \\ x_4 \\ x_5 \\ x_6 \\ x_7 \\ x_8 \\ x_9 \\ x_{10} \\ x_{11} \\ x_{12} \end{Bmatrix} \tag{2.54}$$

The optimization problem is solved by placing lower and upper bounds on the design variables as $x_i^{(l)} \leq x_i \leq x_i^{(u)}$; $i = 1\ to\ 12$, with the bounds indicated in Table 2-11:

Table 2-11 Lower and upper bounds on the design variables of a panel module

j	T_e	T_b	L_c	H_c	W_f	H_f	N_f	W_b	H_b	N_b
$x_j^{(l)}$	0.1μm	100μm	10 cm	10 cm	20μm	4.6μm	2	100μm	4.6μm	2
$x_j^{(u)}$	8μm	450μm	20 cm	20cm	200μm	50μm	100	4000μm	50μm	10

j	N_{c_l}	N_{c_h}
$x_j^{(l)}$	1	1
$x_j^{(u)}$	100	100

The constraints of the optimization problem include the required relationships between conversion efficiency and power output. In order to obtain realistic conversion efficiency, a solar PV panel module is solved by placing the constraint on the minimum permissible conversion efficiency from 70 % of the maximum conversion efficiency (η_{ma}^*, 18.30 % for a square cell and a rectangular cell).

$$0.7\,\eta_{ma}^* - \eta \leq 0 \tag{2.55}$$

The size of a panel module can be constrained with the length of a cell and the number of cells.

$$L_{p\_min} \leq L_c \times N_{c_l} \leq L_{p\_max} \tag{2.56}$$

$$H_{p\_min} \leq H_c \times N_{c_h} \leq H_{p\_max} \tag{2.57}$$

Each panel module is typically rated from 40 W to 230 W, its area is mostly dependent on the rated power, and its conversion efficiency ranges from 12.80% ($\eta \geq 0.7\ \eta_{ma}^{*}$) to 18.30% based on single cell efficiency of a single panel module. The range of dimensions of the length and height for a panel module is shown in Table 2-12.

Table 2-12 Lower and upper bounds on a solar PV panel module design variables

Bound	L_p (cm)	H_p (cm)
Lower	50	50
Upper	90	160

2.4.2 Numerical results

In this work, the power losses of a panel module, including mechanical and electrical losses caused by mismatched cells and environmental conditions in a panel module system, are not considered. The total power losses in a panel module system are assumed to be less than 15 % (Electrical + Mechanical losses). Table 2-13 shows the results of the power output in a single panel module based on a square and a rectangular cell having the range of conversion efficiency from 18.11 % to 18.30 % in a square cell and from 17.91 % to 18.30 % in a square cell. The total power loss in a solar cell is with total power loss of 15 % in a single panel module. The power output of the panel containing rectangular cells is higher than the panel with square cells since the size of the panel module is more flexible and easier to adjust in the case of square cells (in the constrained size of panel) as shown in Table 2-13

Table 2-13 (a) Results of the power output of a panel module (design variables)

Objective		Design variables									
		T_e (μm)	T_b (μm)	L_c (cm)	H_c (cm)	W_f (μm)	H_f (μm)	N_f	W_b (μm)	H_b (μm)	N_b
Ini.	Sq.	5.00	200.00	15.00	15.00	60.00	30.00	40	420	30.00	5
	Rec.	5.00	200.00	15.00	15.00	60.00	30.00	40	420	30.00	5
$\overrightarrow{x^*}_{f_1}$	Sq.	5.90	407.22	10.00	10.00	6.81	17.04	61	36.13	18.05	10
	Rec.	6.59	183.97	10.24	10.00	7.12	17.81	60	35.69	18.81	10
$\overrightarrow{x^*}_{f_2}$	Sq.	7.57	310.83	11.25	11.25	90.78	22.69	61	453.93	23.70	9
	Rec.	7.85	305.63	18.00	12.31	78.00	19.50	74	725.63	20.51	10

Objective		Design variables			
		N_{c_l}	N_{c_h}	η_c (%)	Power output (W)
Ini.	Sq.	7	8	15.56	166.68
	Rec.	7	8	15.56	166.68
$\overrightarrow{x^*}_{f_1}$	Sq.	5	5	18.30	38.88
	Rec.	6	5	18.30	47.79
$\overrightarrow{x^*}_{f_2}$	Sq.	8	14	18.11	218.18
	Rec.	5	13	17.91	219.14

Table 2-13 (b) Results of the maximum power output of a panel module (other outputs)

Level		Design variables				
		L_p (cm)	H_p (cm)	η (%)	Power density ($\frac{W}{cm^2}$)	Power output (W)
Panel	Sq.	90	157.5	18.11	0.0154	218.18
	Rec.	90	160.0	17.91	0.0152	219.14

2.5 Solar PV Array System

2.5.1 Performance of a solar PV array system

A solar PV array system is comprised of the following components: (1) solar cells, (2) panel modules, and (3) an array system. A PV panel module consists of a number of interconnected solar cells encapsulated into a stable panel module, and an array is constructed with a number of panel modules. Also, a multi-row array system should be considered with possible shading effects between adjacent rows using proper orientation and inclination angle of the multi-row array system as shown in Fig. 2-6 while reducing cost at a specific location. Thus, the performance of a solar PV array system should be considered in terms of the conversion efficiency, power output, amount of incident solar energy with different seasonal requirements, and cost. In section 2.3, the conversion efficiency and power output of solar cells are investigated. In section 2.4, the power output of panel module is considered, with considerations of the conversion efficiency and power output, incident solar energy in different seasons, and cost being thoroughly investigated for their role in the optimization of a solar PV array system.

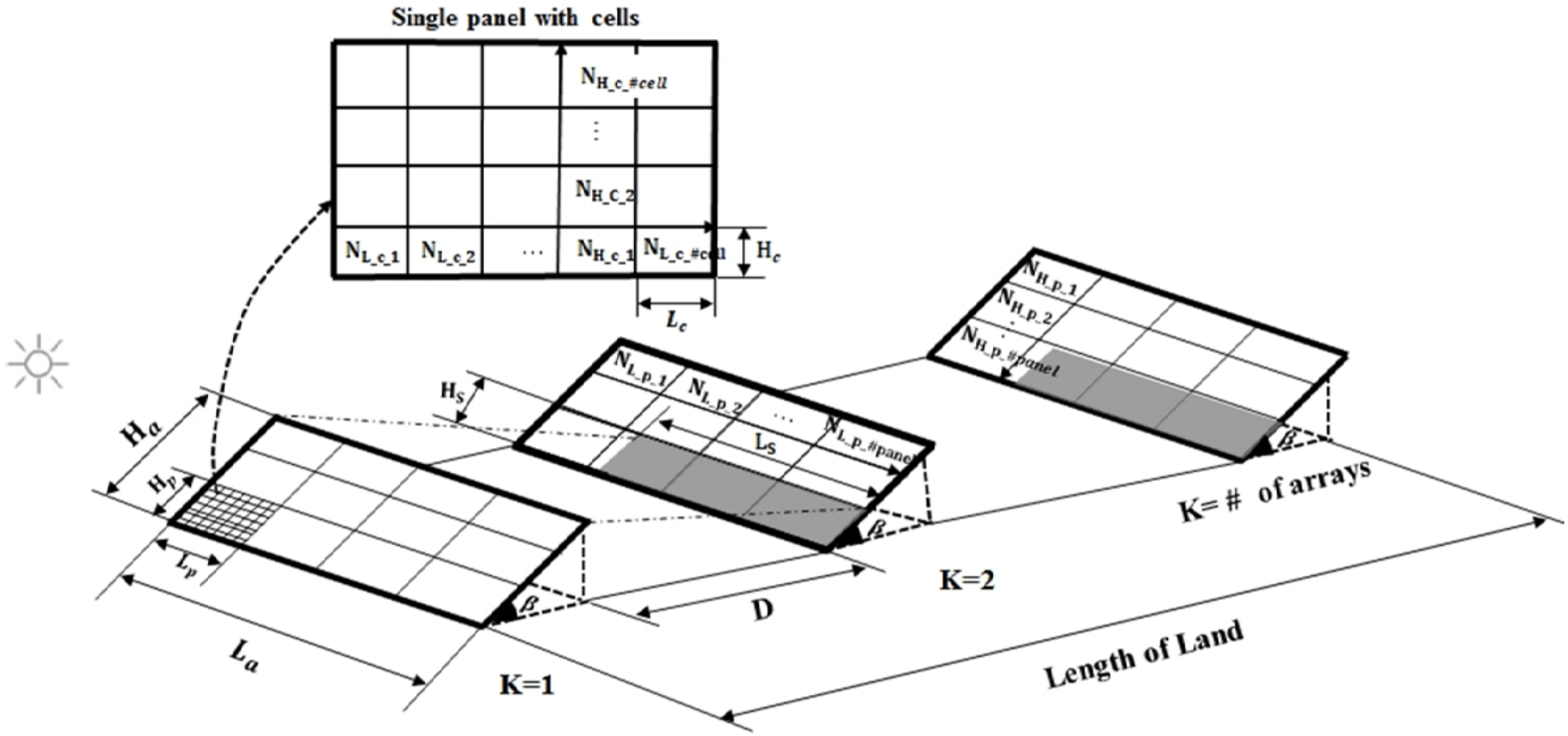

Figure 2-6 Solar PV array system with solar cells and panels

Computation of incident solar radiation

When solar radiation passes through a solar PV collector, a large portion of solar energy should be absorbed by the PV collector. When a single array system is installed, the tilt angle of the system should be determined to collect maximum solar energy. It is difficult to accurately estimate the amount of solar radiation because the amount of solar radiation can be affected by the presence and extent of clouds. Therefore, it is essential to classify a standard sky and estimate the hourly radiation that would be received on a horizontal collector surface under these standard conditions at a particular location. Hottel (1976) explained a method of estimating the beam radiation transmitted through clear atmosphere, which takes into account the zenith angle and altitude for a standard atmosphere and for the four climate types as shown in Fig. 2-7. Accordingly, the atmospheric transmittance for beam radiation τ_b is given by:

$$\tau_b = a_0 + a_1 \exp\left(\frac{-k}{cos\theta_z}\right) \tag{2.58}$$

where the constants a_0, a_1 and k for the standard atmosphere with 23 km visibility are found from the values a_0^*, a_1^* and k^* corresponding to altitudes less than 2.5 km:

$$a_0^* = 0.4237 - 0.00821(6 - A)^2 \tag{2.59}$$

$$a_1^* = 0.5055 + 0.00595(6.5 - A)^2 \tag{2.60}$$

$$k^* = 0.2711 + 0.01858(2.5 - A)^2 \tag{2.61}$$

where A is the altitude at a given location in kilometers

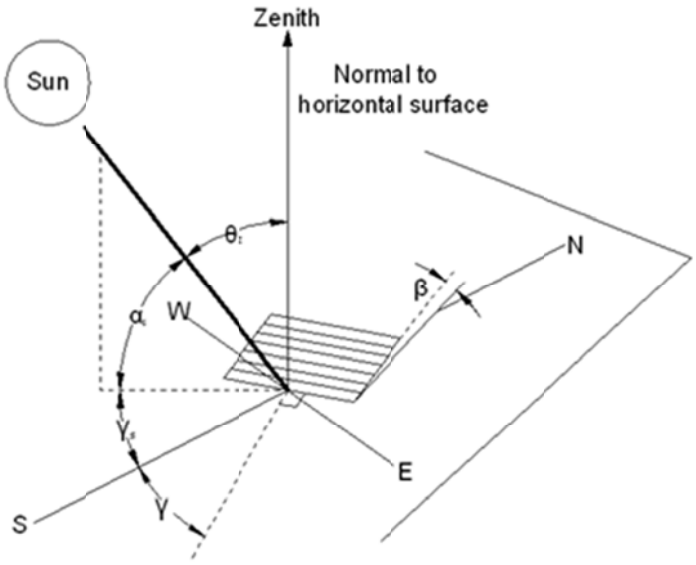

Figure 2-7 Zenith angle, slope, surface azimuth angle and solar azimuth angle for a tilted surface

Table 2-14 Correction factors for different climate types

Climate Type	r_0	r_1	r_k
Tropical	0.95	0.98	1.02
Midlatitude summer	0.97	0.99	1.02
Subarctic summer	0.99	0.99	1.01
Midlatitude winter	1.03	1.01	1.00

For different climate types, Table 2-14 gives the correction factors $r_0 = a_0 / a_0^*$, $r_1 = a_1 / a_1^*$ and $r_k = k / k^*$. Thus the transmittance of the standard atmosphere for beam radiation can be determined for any zenith angle and any altitude up to 5 km. The clear-sky beam radiation is given by:

$$G_{cnb} = G_{on}\tau_b \tag{2.62}$$

where

$$G_{on} = G_{sc}\,(1 + 0.033\,cos\frac{360\,n}{365}) \tag{2.63}$$

and G_{sc} is the solar constant. The clear-sky horizontal beam radiation can be determined as

$$G_b = G_{on}\tau_b \cos\theta_z \tag{2.64}$$

Liu and Jordan (1960) developed an empirical relationship between the transmission coefficient for beam and diffuse radiation for clear days:

$$\tau_d = 0.271 - 0.294\,\tau_b \tag{2.65}$$

$$G_d = G_{on}\tau_d \cos\theta_z \tag{2.66}$$

The shaded and un-shaded irradiation per unit area are:

$$S = H\,L[q_b + q_d + (K-1)(q_b^{sh} + q_d^{sh})] \tag{2.67}$$

where the yearly beam irradiation per unit area of an unshaded collector (first row), q_b, is given by:

$$q_b = \sum_{n=1}^{12}\sum_{T=1}^{24} G_b\,cos\,\theta\,\Delta T \tag{2.68}$$

The yearly diffuse irradiation per unit area of an unshaded collector (first row), q_d, is given by (sum of hourly values of typical days of each month of the year):

$$q_d = \sum_{n=1}^{12}\sum_{T=1}^{24} G_{bdh}\,\Delta T \tag{2.69}$$

The average yearly beam irradiation per unit area of a shaded collector ((K-1) rows); q_b^{sh}, is given by:

$$q_b^{sh} = \sum_{n=1}^{12} \sum_{T=1}^{24} G_b \cos\theta \, (1 - a_s) \, \Delta T \tag{2.70}$$

and the average yearly diffuse irradiation per unit area of a shade collector ((K-1) rows); q_d^{sh}, is given by:

$$q_d^{sh} = F_d^{sh} \sum_{n=1}^{12} \sum_{T=1}^{24} G_{dh} \, \Delta T \tag{2.71}$$

where G_b is the direct beam irradiance on the collector perpendicular to solar rays and G_{dh} is the horizontal diffuse irradiance. The angle between the solar beam and the normal to the collector (θ) is given by:

$$\cos\theta = \cos\beta \sin\alpha + \sin\beta \cos\alpha \cos\gamma \tag{2.72}$$

The shape factors for un-shaded and shaded solar collectors are given by:

$$F_d = \cos^2(\beta/2) \tag{2.73}$$

$$F_d^{sh} = \cos^2(\beta/2) - 1/2[(d^2+1)^{1/2} - d]\sin\beta \tag{2.74}$$

where d is the normalized distance between two rows given by

$$d = D \,/\, (H \sin\beta) \tag{2.75}$$

The relative shaded area a_s is given by

$$a_s = l_s \, h_s \tag{2.76}$$

with

$$l_s = 1 - \frac{d\sin\beta + \cos\beta}{l} \frac{|\sin\gamma|}{\cos\beta\tan\alpha + \sin\beta\cos\gamma} \tag{2.77}$$

is the relative shadow length.

$$a_s \geq 0, \qquad |\gamma| \leq 90\ deg., \quad 0 \leq l_s \leq 1 \tag{2.78}$$

$h_s = 1 - \dfrac{d \sin\beta + \cos\beta}{\cos\beta + [\sin\beta \cos\gamma / \tan\alpha]}$ is the relative shadow width (2.79)

$$a_s \geq 0, \qquad |\gamma| \leq 90\ deg., \quad 0 \leq h_s \leq 1 \tag{2.80}$$

and

$l = L / (H\ sin\beta)$ is the normalized collector length. (2.81)

Thus, the incident solar energy of solar PV array system is given by:

$$Q = L_a \times H_a \times \left[q_b + q_d + (K-1)\left(q_b^{sh} + q_d^{sh}\right)\right] \tag{2.82}$$

For a single array system, there is no needed to consider the shading effects and hence only the tilt angle and the corresponding absorbed area are considered at the specific location. Figure 2-8 shows a configuration of a single PV array. The amount of incident solar energy depends on the design variables of height (H_a) and length (L_a) of a single array and the tilt angle in a solar PV array ($L_a \times H_a$), which can be expressed in terms of the number of cells and panels used.

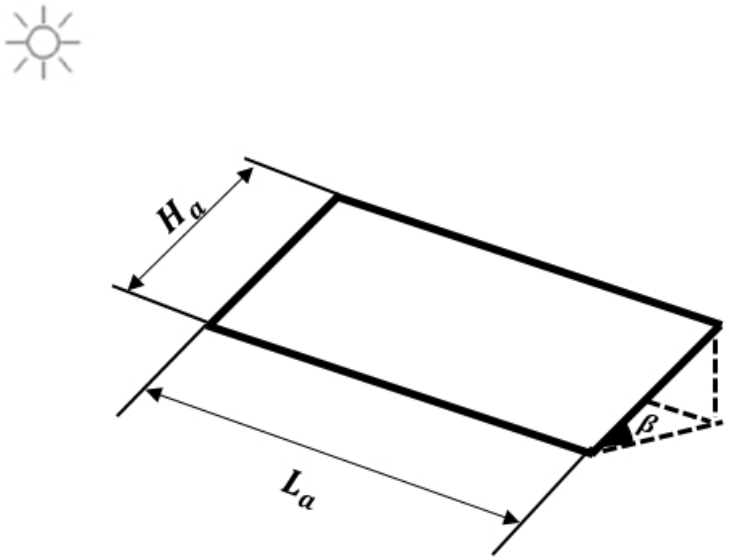

Figure 2-8 Configuration of a single PV collector to collect incident solar energy

However, when multi-PV array systems are installed in a limited area, the tilt angle and size of the solar PV collector system should be factored, including the shading effects from the adjacent rows of the array system.

The size of the PV array system is determined by the maximum amount of incident solar energy based on seasonal characteristics with shading effects associated with the number of rows or arrays. The seasonal characteristics in a non-tracking system are classified by the tilt angle of arrays from east in the morning to west in the evening to track the daily movement of the sun across the sky. The azimuth angle is linked to these seasonal characteristics as it determines the array's orientation with respect to establishing a line perpendicular to the equator.

In a single array without consideration of conversion efficiency and multiple arrays, a single array is optimized within three different seasons.

- Formulation of an optimization problem for a single array without a consideration of conversion efficiency and multiple arrays

The objective is to find the optimal design vector $\vec{X}$ for the maximization of annual monthly average, lowest, and highest months incident solar energy.

Maximize:$f_1(\vec{X})$ = annual monthly average incident solar energy

$$= L_a \times H_a \times \left[q_b + q_d + (K-1)\left(q_b^{sh} + q_d^{sh}\right)\right] \tag{2.83}$$

Maximize:$f_2(\vec{X})$ = lowest month incident solar energy (2.84)

Maximize:$f_3(\vec{X})$ = highest month incident solar energy (2.85)

The design vector of the problem is chosen as:

$$\vec{X} = \begin{pmatrix} L_a \\ H_a \\ \beta \end{pmatrix} \equiv \begin{pmatrix} x_1 \\ x_2 \\ x_3 \end{pmatrix} \tag{2.86}$$

The lower and upper bounds placed on the design variables (side constraints) are shown in Table 2-15.

Table 2-15 Lower and upper bounds on single solar PV array design variables without consideration of conversion efficiency and multiple arrays

Bound	L_a (cm)	H_a (cm)	β (degree)
Lower	1500	50	0
Upper	3000	200	90

- Numerical results of single array

Table 2-16 shows the values of the optimized tilt angle of a single array system in Miami (Latitude 24.5°) for a size of 3000 cm × 200 cm (Length of array × Height of array). An optimal tilt angle of a single array shows different installation angles for optimization.

Table 2-16 Optimal installation of a single PV collector

Obj.	L_a (cm)	H_a (cm)	β (degree)	Collected incident solar energy (kW)
f_1	2999.92	199.85	22.10	13.2179057
f_2	2999.97	199.99	32.96	12.5665345
f_3	299.98	199.99	5.65	13.9996364

The incident solar energy is the total amount of solar radiation energy collected on a limited (or given) PV surface area during any specified time for generating electricity from sunlight. The amount of incident solar energy differs with the season.

2.5.2 Formulation of single-objective optimization problems

To collect the maximum amount of solar incident energy, a multi-PV array system should be designed using suitable design parameters. As stated earlier, a solar PV array system consists of a number of solar cells and panel modules. A single objective optimization problem is stated as:

Minimize or maximize the objective function, $f_p(\vec{X})$; p = 1, 2, 3, 4, 5, and 6

The following six single-objective functions are considered for the solar PV array systems.

f_1 : Maximization of conversion efficiency of the cells used in the panel modules (η_{ma}^*)

f_2 : Maximization of power output of the array system used in the panel modules (P_m^*)

f_3 : Maximization of annual monthly average of incident solar energy (Q_{am}^*)

f_4 : Maximization of incident solar energy in the lowest month (Q_{lm}^*)

f_5 : Maximization of incident solar energy in the highest month (Q_{hm}^*)

f_6 : Minimization of cost of the array system (C_m^*)

The design vector of the problem is chosen as:[+]

$$\vec{X} = \begin{Bmatrix} T_e \\ T_b \\ L_c \\ H_c \\ W_f \\ H_f \\ N_f \\ W_b \\ H_b \\ N_b \\ N_{c_l} \\ N_{c_h} \\ N_{p_l} \\ N_{p_h} \\ D \\ \beta \\ K \end{Bmatrix} \equiv \begin{Bmatrix} x_1 \\ x_2 \\ x_3 \\ x_4 \\ x_5 \\ x_6 \\ x_7 \\ x_8 \\ x_9 \\ x_{10} \\ x_{11} \\ x_{12} \\ x_{13} \\ x_{14} \\ x_{15} \\ x_{16} \\ x_{17} \end{Bmatrix} \tag{2.87}$$

+ Seventeen design variables are considered for the maximization of the conversion efficiency of a square cell and a rectangular cell. The intensity of sunlight is not treated as a design variable; it is fixed at a value of 1.

The lower bounds and upper bounds placed on the design variables (side constraints) are shown in Table 2-17.

Table 2-17 Lower and upper bounds on the design variables of a multiple PV array system (Note that the bounds on L_c and H_c are different in the array system design compared to the arrays used in solar cell design)

	T_e (μm)	T_b (μm)	L_c (cm)	H_c (cm)	W_f (μm)	H_f (μm)	N_f	W_b (μm)	H_f (μm)	N_b
Lower	0.1	100	10	10	4.6	4.6	2	100	4.6	2
Upper	8	450	20	20	50	50	100	4000	50	10

	N_{c_l}	N_{c_h}	N_{p_l}	N_{p_h}	D (cm)	β (degree)	K
Lower	1	1	1	1	80	5	2
Upper	100	100	100	100	200	65	200

2.5.3 Maximization of conversion efficiency (f_1)

A solar PV array system is comprised of a number of solar cells and panel modules. For the PV array system, conversion efficiency should be considered.

$$f_1\left(\vec{X}\right) = \frac{J_m V_m}{P_{in} \cdot C}(1 - F_{sum}) \times 100 \tag{2.88}$$

Constraints are used as the same as from Eqs. (2.44) - (2.49).

The constraints on the optimization include the minimum required value of annual monthly average incident solar energy in the solar PV array system. The required incident solar energy are chosen to be at least 70 % of Q_{am}^{*}.

$$0.7\, Q_{am}^{*} - Q \leq 0 \tag{2.89}$$

where Q_{am}^{*} = 9.8842 × 10^5 W for a square cell and Q_{am}^{*} = 9.8556 × 10^5 W for a rectangular cell.

2.5.4 Maximization of power output (f_2)

As with conversion efficiency, the power output depends on the number of solar cells and panel modules used in a solar PV array system. Thus, the power output is associated with the size of an array and the conversion efficiency of the solar cell being optimized. Table 2-17 shows the list of bounds used on the size of the panel module and the array system.

$$f_2\left(\vec{X}\right) = L_c \times H_c \times N_{c_l} \times N_{c_h} \times N_{p_l} \times N_{p_h} \times J_m \times V_m \times K \tag{2.90}$$

The length of an array (L_a) is constrained by restricting the length of a cell (L_c) and the number of cells (N_{c_l}) and panels (N_{p_l}). The height of an array (H_a) is constrained by restricting the height of a cell (H_c), the number of cells (N_{c_h}), and the number of panels (N_{p_h})

$$1500 \text{ cm} \leq L_c \times N_{c_l} \times N_{p_l} \leq 3000 \text{ cm} \tag{2.91}$$

$$80 \text{ cm} \leq H_c \times N_{c_h} \times N_{p_h} \leq 200 \text{ cm} \tag{2.92}$$

The conversion efficiency and the incident solar energy are chosen to be 70 % of Q_{am}^{*} and η_{ma}^{*} for finding a reasonable power output.

$$0.7\,\eta_{ma}^{*} - \eta \leq 0 \tag{2.93}$$

where η_{ma}^{*} = 18.30 % for a square cell and η_{ma}^{*} = 18.30 % for a rectangular cell.

2.5.5 Maximization of annual monthly average incident solar energy (f_3)

The optimization problem for the maximum collection of incident solar energy is solved by imposing the lower and upper bounds on the design variables of the multi-PV array system (including the shading effects).

The incident energy output is given by Rao, Lee and Hu (2014):

$$f_3\left(\vec{X}\right) = Q = L_a \times H_a \times \left[q_b + q_d + (K-1)\left(q_b^{sh} + q_d^{sh}\right)\right] \tag{2.94}$$

The total length of the PV array system should be less than or equal to the maximum length of the available area:

$$L_a \times H_a \times cos\beta + (K-1) \times D \leq \text{Maximum permissible length} \tag{2.95}$$

The height of the array should be limited based on the installation, inspection and maintenance needs:

$$H_a \times sin\beta \leq \text{Maximum permissible height} \tag{2.96}$$

where L_a consists of the length of a solar cell, the number of solar cells, and the number of panels in the length side row. H_a is composed of the height of a solar cell, the number of solar cells, and the number of panels in the height side row.

2.5.6 Maximization of lowest month incident solar energy (f_4)

Orientation of the sun has a major impact on the amount of incident solar energy on a solar collector. When sunlight reaches the collector perpendicularly, the amount of incidental solar energy will be maximized The angle between the absorbing surface of a collector on the ground and the ray's direction can be determined at any particular location in terms of the specific time of the year, and the longitude of the location. The design parameters of a solar PV array system are influenced by the elevation, declination, and azimuth angles for collecting the maximum amount of solar energy. PV collectors can obtain more incident solar energy in summer than in winter by virtue of the tilt angle of the Earth. The tilt angle varies seasonally as the rotation of the Earth shifts. Although the horizontal face of a PV system absorbs the solar energy for maximum performance in summer, the amount of solar radiation is not always maximized due to the specific location and seasonal characteristics.

$$f_4\left(\vec{X}\right) = Q = \text{lowest month incident solar energy} \tag{2.97}$$

2.5.7 Maximization of highest month incident solar energy (f_5)

Climate change and seasonal energy demands have an influence on solar energy systems because higher temperatures affect electricity use, while warmer winters decrease energy demand (for heating systems). According to U.S. National Climate

Assessment, the annual average temperatures have been higher than the long-term average. There have been increases in population-weighted cooling degree days, which result in increased air conditioning use, and decreases in population-weighted heating degree days. This indicates that more energy is needed to cool buildings in summer while less energy is required to heat buildings in winter.

$$f_5\left(\vec{X}\right) = Q = \text{ highest month incident solar energy} \tag{2.98}$$

2.5.8 Minimization of cost of solar PV array system (f_6)

The cost of performance of a solar PV array system can be estimated through peak watt ratings. The cost of electricity generated by a solar PV collector system can be found by adding the costs of all the subsystems used. The peak watt (W_p) rating is determined by measuring the maximum power output of a solar PV collector system. The costs can be divided into two parts: those associated with the solar PV panel module and the balance of the system (BOS), including array installation, inverter system, and site work.

Thus, the objective function corresponding to the cost can be expressed as:

$f_6\left(\vec{X}\right) =$ Panel module production (\$) + Balance of system (\$)

Panel module production (\$) = Wafer + Cell + Panel module

Balance of system (BOS,\$) = Array installation + Inverter system + Site work

(2.99)

The cost of a panel module can be separated into the costs of wafer, cell production, and panel production. A solar PV collector system costs are related to those associated with

panel module design, racking, and electrical system. Both panel module and array installation costs are directly related to the efficiency based on the cost of power ($/Watt). Thus, the costs of wafer, cell, and panel module production can be expressed by:

Cost of wafer and cell production = watt per peak* of wafer and cell production (%)

× single solar cell size (cm^2) × number of cells × power density $\left(\frac{W}{cm^2}\right)$ (2.100)

** watt per peak: Kilowatt peak (kWp) stands for peak power as nominal power; the value specifies power output achieved by a solar panel module*

Cost of panel production = watt per peak of wafer and cell production (%)

× single panel module size (cm^2) × number of panels × power density $\left(\frac{W}{cm^2}\right)$ (2.101)

Cost of array installation = watt per peak of array installation (%)

× single array size (cm^2) × number of arrays × power density $\left(\frac{W}{cm^2}\right)$ (2.102)

In this work, the number of inverter systems is associated with the number of arrays. Thus, the costs of inverter system and installation land can be expressed as:

Cost of Inverter system = watt per peak of wafer and cell production (%)

× array system size (cm^2) × number of inverters × power density $\left(\frac{W}{cm^2}\right)$ (2.103)

Cost of installation land = watt per peak of installation (%) × installed land size (cm^2)

× power density $\left(\frac{W}{cm^2}\right)$ (2.104)

Similarly, the performance a panel module considering watt per peak should be reflected. Thus, the conversion efficiency and the incident solar energy are chosen to be 70 % of Q_{am}^{*} and η_{ma}^{*} for finding reasonable cost.

$$0.7\, Q_{am}^{*} - Q \leq 0 \tag{2.105}$$

$$0.7\, \eta_{ma}^{*} - \eta \leq 0 \tag{2.106}$$

where Q_{am}^{*} = 9.8842 × 10^5 W for a square cell and Q_{am}^{*} = 9.8556 × 10^5 W for a rectangular cell. η_{ma}^{*} = 18.30 % for a square cell and η_{ma}^{*} = 18.30 % for a rectangular cell.

The solar PV cells are mono crystalline-silicon cells produced using standard fabrication and production techniques. Also, each step in the production process entails cost contributions from raw materials, equipment, labor, maintenance, facilities, and consumables. The process of panel module production includes several production steps, from wiring metal contacts of completed solar cells to sealing and assembling each component of the panel module. The manufacturing of a PV panel module can be divided into the production of the wafer, cell, and panel module as shown in Fig. 2-9.

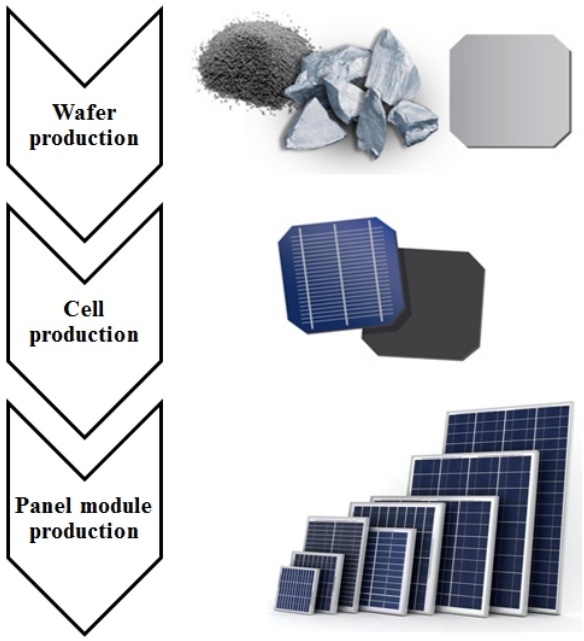

Figure 2-9 Production steps from silicon materials to PV panel module

In terms of materials, the first step includes raw silicon materials, ingot, and wafer slices. After the raw silicon materials are collected, oxygen is removed to produce metallurgical (semiconductor) grade silicon. The silicon is supplied in granular powder form which is then melted in a bath. The molten sand will become the source of silicon that will be the wafer. This crystal will produce large silicon ingot through a dominant technique known as the Czochralski (cz) method. Once a large ingot has been made, it is sliced up into wafers through cutting wires. Figure 2-10 shows the process from raw materials of a wafer to a completed wafer for a solar cell.

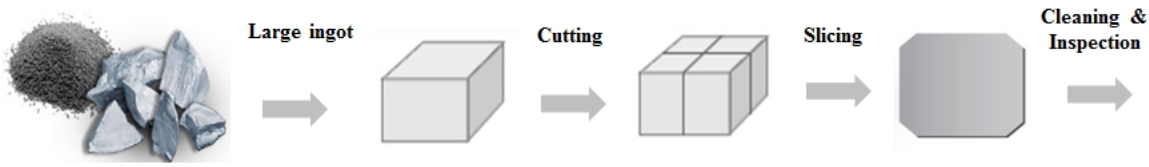

Figure 2-10 Process of wafer production

Cell production contains the manufacturing process from a wafer to the completed solar PV cell. Impurities are added to a silicon wafer with other materials such as boron and phosphorous for p-n junction formation called dopant concentration. Because pure silicon (c-Si) is shiny, it can reflect up to 35 percent of the sunlight. In order to reduce the amount of reflected sunlight, it is necessary to put an anti-reflection coating film on the silicon wafer with the buried grid front contact. Figure 2-11 shows the process of cell production from a completed wafer to a solar cell.

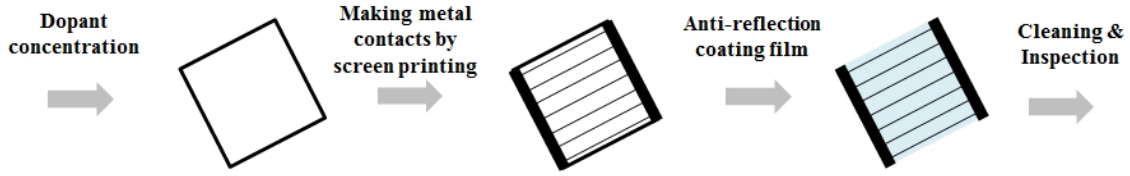

Figure 2-11 Process of cell production

Panel module production involves the manufacturing process from a solar cell to a finished panel module, including cell wiring, assembly and interconnection of a number of cells to establish a panel, lamination, sealing, framing, and terminal assembly to form a completed package. Figure 2-12 shows the process of production of a panel module from a number of solar cells connected electrically to a single panel module with different size cells.

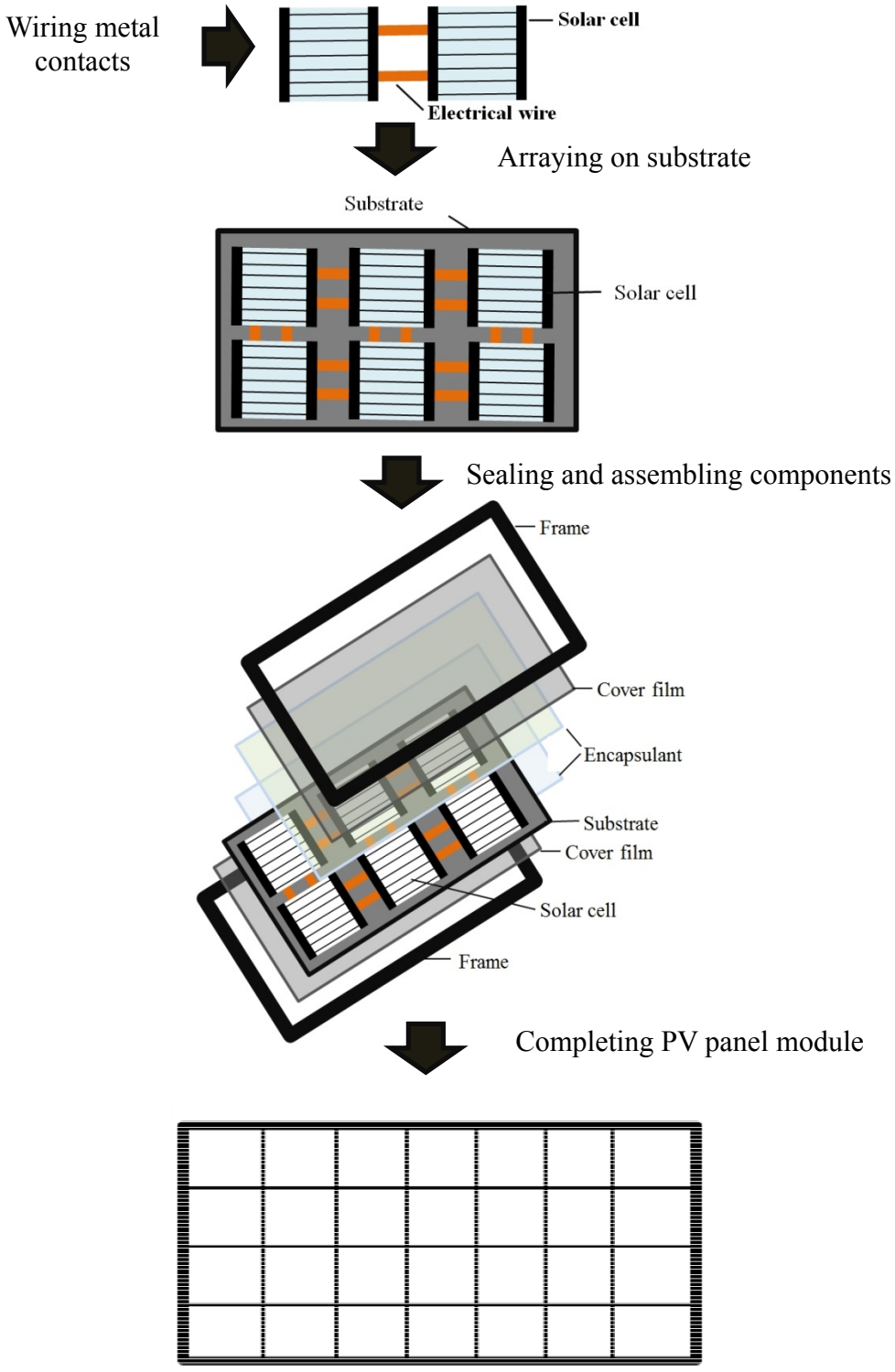

Figure 2-12 Process of PV panel module production

The balance of system (BOS) costs include all costs except the PV panel module costs, and are composed of the installed costs of the PV array system, inverter system, and installed land. The PV array system's design and construction, including manufacturing or purchasing components such as racking, wiring, foundations, inverters, labor, preparation of land, and installing and connecting the system related to the structure and electrical systems, constitutes a majority of balance of system (BOS) costs for a solar PV collector system. A solar PV inverter system functions to convert the variable direct current (DC) output obtained by solar PV collectors into a utility frequency alternating current (AC) output for commercial electricity. There are three different types of invertors- the stand-alone inverts, grid-tied inverters, and battery backup inverters. Figure 2-13 shows a configuration of a stationary fixed plate PV collector system, including cells, panels, arrays, an inverter system, and the installed land.

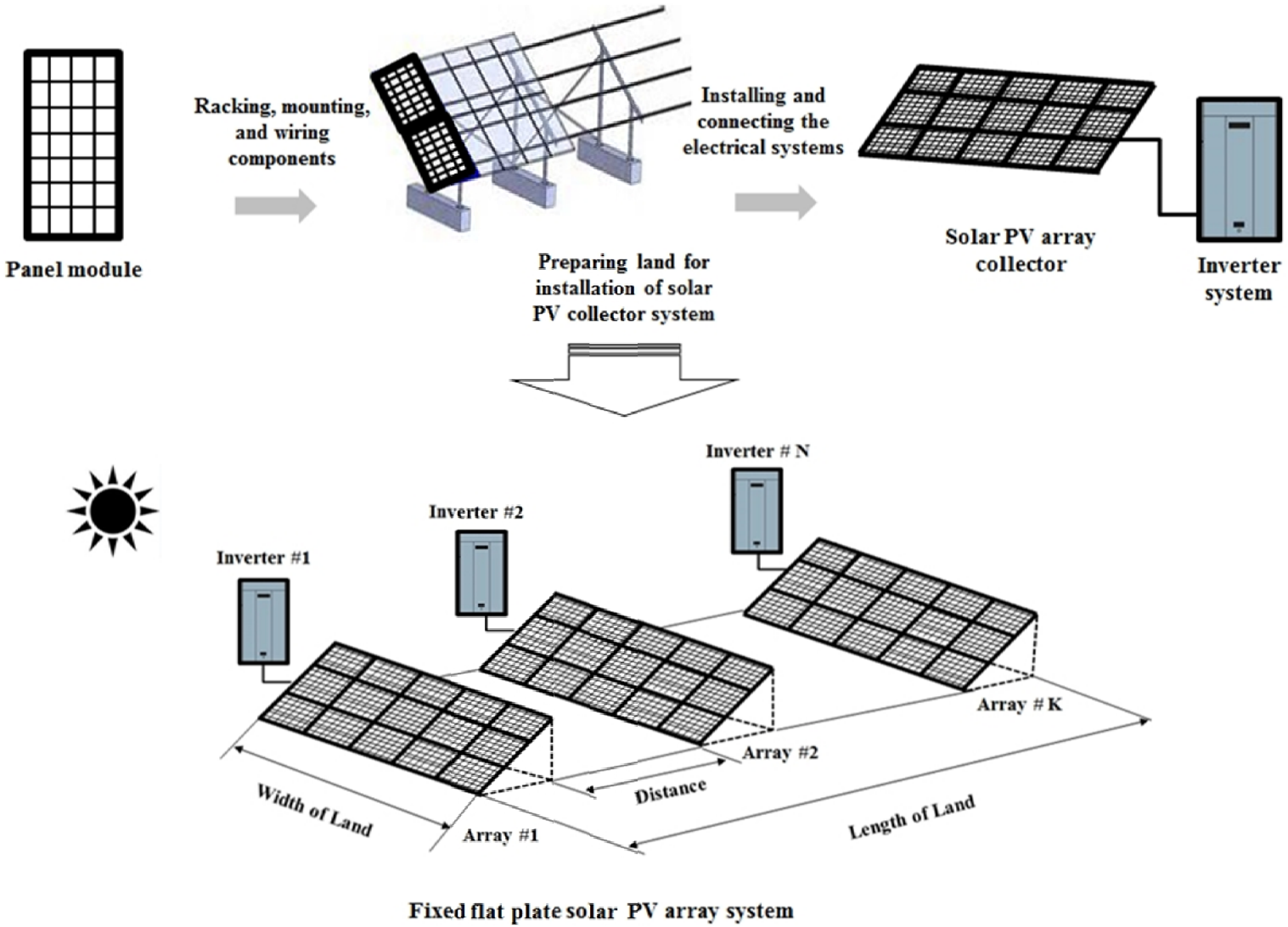

Figure 2-13 Configuration of a stationary flat-plate PV collector system

The cost of the balance of system (BOS) can also be broken down into power-proportional BOS costs related to the efficiency of a solar PV collector system and area-proportional BOS costs related to the mounting structure, labor, and wiring (Nold, 2012). In this work, therefore, the PV array installation costs are assumed to be proportional to the efficiency of a solar PV panel module, which includes installation labor such as electrical wage and labor content, general construction wage and labor contents, general and operating overhead and installation materials such as mounting hardware, wiring, conduit, and supply chain costs. The inverter system and site work costs are not considered in the efficiency of a solar PV array system. The cost of inverters system is determined by the number of PV arrays and the cost of site work is estimated by the size (area) of installation of a solar array.

The installation of a solar PV collector system can be divided into two types: (1) rooftop and (2) ground-mounted solar PV systems. The cost portion of a 100 kWp flat roof PV system installed in Germany and described by Nold (2012) is shown in Fig. 2-14. When the costs between rooftop and ground-mounted PV systems are compared, the costs of a rooftop PV system are approximately 14% higher than those of a ground-mounted PV system. This is in view of structural costs such as installation, racking, site preparation, and the general system development. In this work, the costs of flat roof and ground-mounted PV systems are assumed to be the same for simplicity.

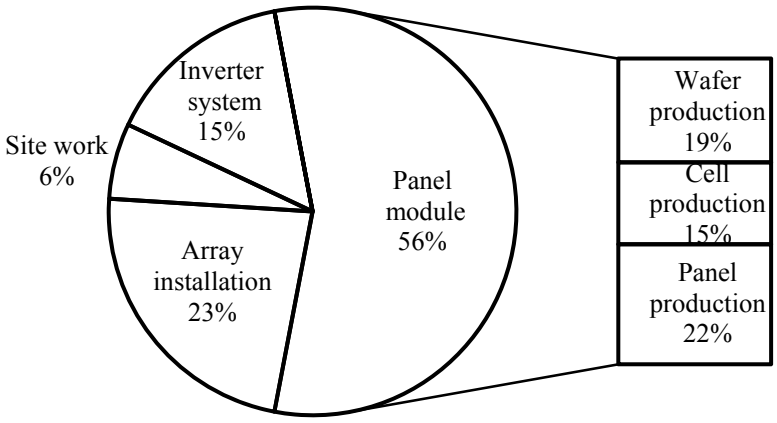

Figure 2-14 Portion of costs for a solar PV collector system

The costs of cell materials include silicon material, ingot and wafer. Cell production includes the costs of cell materials and the number of cells. Panel module production includes the assembly, component materials, and production process costs. Solar PV array installation costs can be broken down into 3 sections: array installation, inverter system, and land for installation.

2.5.9 Numerical results

The values of geometric design variables and single objective problems derived from a square and a rectangular cell are investigated. The optimization problems are solved using *ga* (MATLAB) with desired requirements on the capacity of a cell, panel, and array system for the purpose of finding the maximum values of six single-objective functions for a multi-PV collector system.

- Maximization of conversion efficiency (f_1)

The maximum conversion efficiencies (η^*_{ma}) in a single solar cell at cell level design reach 18.299 % in a square cell and 18.300 % in a rectangular cell within solar PV systems. Solar cell sizes are 10 × 10 cm^2 in a square cell and 10 × 10 cm^2 in a rectangular cell, respectively. The single panel module consists of 48 cells in a square cell and 40 cells in a rectangular cell. The single array is comprised of 94 panel modules and is sized at 2820.00 × 160.00 cm^2,($L_a \times H_a$) in a square cell; diversely, it is comprised of 124 panel modules and is sized at 2480.00 × 200.00 cm^2,($L_a \times H_a$) in a rectangular cell. Adhering to the specific requirements of a single panel module in terms of the number of cells, solar PV array systems are installed with a tilt angle of 45.67 ° and 84 arrays in a square cell and with a tilt angle of 11.79 ° and 65 arrays in a rectangular cell. It can thus be concluded that in undertaking to maximize the conversion efficiency, the conversion efficiency has almost the same values of 18.30 % between a square cell and a rectangular cell, but the optimal installation of the PV array systems shows different values in terms of the tilt angle and the number of arrays. Table 2-18 shows the results of maximization of conversion efficiency, design variables and single-objective functions.

Table 2-18 (a) Results of maximization of conversion efficiency, f_1 (design variables)

Objective		Design variables									
		T_e (μm)	T_b (μm)	L_c (cm)	H_c (cm)	W_f (μm)	H_f (μm)	N_f	W_b (μm)	H_b (μm)	N_b
Ini.	Sq.	4.0	220.0	12.0	12.0	80.0	7.0	40	480.0	8.0	5
	Rec.	4.0	220.0	12.0	12.0	80.0	7.0	40	480.0	8.0	5
$\overrightarrow{x^*}_{f_1}$	Sq.	6.2	145.9	10.0	10.0	71.3	17.8	60	356.8	18.8	10
	Rec.	6.3	195.3	10.0	10.0	69.2	17.3	61	346.2	18.3	10

Design variables									
Objective		N_{l_c}	N_{h_c}	N_{l_p}	N_{h_p}	D (cm)	β (degree)	K	η_c
Ini.	Square	7	10	30	1	90.0	30.0	70	14.12
	Rectangular	7	10	30	1	90.0	30.0	70	14.12
$\overrightarrow{x^*}_{f_1}$	Square	6	8	47	2	92.9	45.7	84	18.30
	Rectangular	8	5	31	4	91.9	11.8	65	18.30

Table 2-18 (b) Results of maximization of conversion efficiency, f_1 (six single-objective functions)

Results of single-objective optimization							
Objective		f_1(%)	f_2(W)	f_3(W)	f_4(W)	f_5(W)	f_6($)
Ini.	Sq.	14.66	1.7589E+05	3.0558E+05	2.7771E+05	3.2766E+05	3.5085E+05
	Rec.	14.66	1.7589E+05	3.0558E+05	2.7771E+05	3.2766E+05	3.5085E+05
$\overrightarrow{x^*}_{f_1}$	Sq.	18.30	5.8949E+05	7.2236E+05	6.1397E+05	8.2993E+05	9.5238E+05
	Rec.	18.30	5.0151E+05	6.9819E+05	5.3715E+05	7.9721E+05	8.0549E+05

- Maximization of power output (f_2)

For the maximum value of single-objective problems regarding power output, the conversion efficiencies are the second highest as 17.37 % in a square cell and 17.55 % in a rectangular cell from 18.30 % of $\eta_{ma}{}^*$ in both cells. The solar cell sizes are 12.45 × 12.45 cm^2 in a square cell and 19.23 × 13.33 cm^2 in a rectangular cell. The single panel consists of 40 cells in a square cell and 20 cells in a rectangular cell. The single array is comprised of 96 panel modules in the single array size at 2999.85 × 199.99 cm^2, ($L_a \times H_a$) in a square cell and 124 panel modules in the single array size at 2999.99 × 199.99 cm^2, ($L_a \times H_a$) in a rectangular cell. The largest size of a single array, 2999.99 × 199.99 cm^2, ($L_a \times H_a$), produces the maximum power output in a rectangular cell

explicable by the amount of generated power output that is dominant with the size of the solar PV collector (cm^2) and power density ($\frac{W}{cm^2}$). With 96 panel modules, solar PV array systems are installed with a tilt angle of 64.84 ° and 121 arrays in a square cell and with a tilt angle of 64.30 ° and 121 arrays in a rectangular cell. Thus, for maximization of power output, the values of power output reach 1.0636E+ 06 W in a square cell and 1.0639E+ 06 W in a rectangular cell as shown in Table 2-19, respectively.

Table 2-19 (a) Initial design and optimization results of f_2 (design variables)

		Design variables									
Objective		T_e (μm)	T_b (μm)	L_c (cm)	H_c (cm)	W_f (μm)	H_f (μm)	N_f	W_b (μm)	H_b (μm)	N_b
Ini.	Square	4.0	220.0	12.0	12.0	80.0	7.0	40	480.0	8.0	5
	Rectangular	4.0	220.0	12.0	12.0	80.0	7.0	40	480.0	8.0	5
$\overrightarrow{x^*}_{f_2}$	Square	3.9	204.0	12.5	12.5	197.2	47.8	51	995.4	47.8	3
	Rectangular	4.0	298.2	19.2	13.3	157.2	39.3	59	1674.7	40.3	4

		Design variables						
Objective		N_{l_c}	N_{h_c}	N_{l_p}	N_{h_p}	D (cm)	β (degree)	K
Ini.	Square	7	10	30	1	90.0	30.0	70
	Rectangular	7	10	30	1	90.0	30.0	70
$\overrightarrow{x^*}_{f_2}$	Square	5	8	48	2	81.0	64.8	121
	Rectangular	4	5	39	3	80.8	64.3	121

Table 2-19 (b) Initial design and optimization results of f_2 (six single-objective functions)

		Results of single objective optimization					
Objective		f_1(%)	f_2(W)	f_3(W)	f_4(W)	f_5(W)	f_6($)
Ini.	Sq.	14.66	1.7589E+05	3.0558E+05	2.7771E+05	3.2766E+05	3.5085E+05
	Rec.	14.66	1.7589E+05	3.0558E+05	2.7771E+05	3.2766E+05	3.5085E+05
$\overrightarrow{x^*}_{f_2}$	Sq.	17.37	1.0636E+06	9.3731E+05	6.6781E+05	1.2306E+06	1.7929E+06
	Rec.	17.55	1.0639E+06	9.4193E+05	6.7530E+05	1.2363E+06	1.7755E+06

- Maximization of the annual monthly average incident solar energy (f_3)

When annual monthly average incident solar energy is maximized, the conversion efficiencies are 15.84 % in a square cell and 15.00 % in a rectangular cell from 18.30 % of $\eta_{ma}{}^{*}$. The solar cell sizes are 16.67 × 16.67 cm^2 in a square cell and 19.18 × 14.13 cm^2 in a rectangular cell. The single panel consists of 16 cells in a square cell and 21 cells in a rectangular cell. The single array is comprised of 135 panel modules and is sized at 2999.77 × 199.98 cm^2,($L_a \times H_a$) in a square cell and 104 panel modules and is sized at 2992.51 × 197.88 cm^2,($L_a \times H_a$) in a rectangular cell.

Solar PV array systems are installed with a tilt angle of 38.18 ° and 84 arrays in a square cell and with a tilt angle of 30.99 ° and 80 arrays in a rectangular cell. In reference to the maximization of annual monthly incident solar energy (Q_{am}^{*}), the Q_{am}^{*} is maximized at the values of 9.8841E+ 05 W in a square cell and 9.855E+ 05 W in a rectangular cell as shown in Table 2-20, respectively.

Table 2-20 (a) Initial design and the optimization results of f_3 (design variables)

		Design variables									
Objective		T_e (μm)	T_b (μm)	L_c (cm)	H_c (cm)	W_f (μm)	H_f (μm)	N_f	W_b (μm)	H_b (μm)	N_b
Ini.	Square	4.0	220.0	12.0	12.0	80.0	7.0	40	480.0	8.0	5
	Rectangular	4.0	220.0	12.0	12.0	80.0	7.0	40	480.0	8.0	5
$\overrightarrow{x^*}_{f_3}$	Square	3.4	246.5	16.7	16.7	148.9	35.2	74	2167.9	35.2	9
	Rectangular	0.2	287.4	19.2	14.1	171.1	41.9	34	2666.5	42.5	9

Design variables								
Objective		N_{l_c}	N_{h_c}	N_{l_p}	N_{h_p}	D (cm)	β (degree)	K
Ini.	Square	7	10	30	1	90.0	30.0	70
	Rectangular	7	10	30	1	90.0	30.0	70
$\overrightarrow{x^*}_{f_3}$	Square	4	4	45	3	81.9	38.2	84
	Rectangular	3	7	52	2	81.4	31.0	80

Table 2-20 (b) Initial design and the optimization results, f_3 (six single-objective functions)

Results of single objective optimization							
Objective		f_1(%)	f_2(W)	f_3(W)	f_4(W)	f_5(W)	f_6($)
Ini.	Sq.	14.66	1.7589E+05	3.0558E+05	2.7771E+05	3.2766E+05	3.5085E+05
	Rec.	14.66	1.7589E+05	3.0558E+05	2.7771E+05	3.2766E+05	3.5085E+05
$\overrightarrow{x^*}_{f_3}$	Sq.	15.84	6.7873E+05	9.8842E+05	7.9968E+05	1.1447E+06	1.2543E+06
	Rec.	15.00	6.0420E+05	9.8556E+05	7.9368E+05	1.0986E+06	1.1629E+06

- Maximization of the lowest month for incident solar energy (f_4)

In reference to the maximization of the lowest month average incident solar energy, the conversion efficiencies are 13.25 % in a square cell and 17.54 % in a rectangular cell from 18.30 % of $\eta_{ma}{}^*$ of both cells. The solar cell sizes are 13.39 × 13.39 cm^2 in a square cell and 13.89 × 13.76 cm^2 in a rectangular cell. A single panel consists of 28 cells in a square cell and 28 cells in a rectangular cell. The single array is comprised of 112 panel modules and is sized at 2999.93 × 187.50 cm^2,($L_a \times H_a$) in a square cell and 104 panel modules and is sized at 2999.78 × 192.64 cm^2,($L_a \times H_a$) in a rectangular cell. Solar PV array systems are installed with a tilt angle of 47.80 ° and 95 arrays in a square cell and with a tilt angle of 49.33 ° and 93 arrays in a rectangular cell. Therefore, in

achieving the maximization of the lowest month incident solar energy (Q_{lm}^{*}), the Q_{lm}^{*} carries the values of 8.001E+ 05 W in a square cell and 8.007E+ 05 W in a rectangular cell, respectively. For avoiding shadow from the front rows of arrays, the values of tilt angles are raised to collect more solar energy. Solar radiation is less perpendicular on the surface of a PV collector during winter because the Earth is away from the sun (Earth's axial tilt: 23.5 °) so that the tilt angles of the multi-array system, which are intrinsically related to the direction of sunlight, become a primary factor in collecting more incident solar energy at this time of the year. The solar position in the hemisphere of the sky and geometrical relationship between the sun and the array surface fluctuate from season to season. It can be ascertained that the proper tilt angles combined with an exact number of arrays have a critical impact on the amount of incident solar energy collected, and they are needed to consider seasonal characteristics. Table 2-21 shows the results of the lowest month for incident solar energy.

Table 2-21 (a) Initial design and the maximization of the lowest month incident solar energy, f_4 (design variables)

		Design variables									
Objective		T_e (μm)	T_b (μm)	L_c (cm)	H_c (cm)	W_f (μm)	H_f (μm)	N_f	W_b (μm)	H_b (μm)	N_b
Ini.	Square	4.0	220.0	12.0	12.0	80.0	7.0	40	480.0	8.0	5
	Rectangular	4.0	220.0	12.0	12.0	80.0	7.0	40	480.0	8.0	5
$\overrightarrow{x^*}_{f_4}$	Square	5.9	252.5	13.4	13.4	140.9	33.6	37	2224.0	34.3	4
	Rectangular	5.1	354.6	13.9	13.8	107.3	26.5	77	1449.7	26.8	6

Design variables								
Objective		N_{l_c}	N_{h_c}	N_{l_p}	N_{h_p}	D (cm)	β (degree)	K
Ini.	Square	7	10	30	1	90.0	30.0	70
	Rectangular	7	10	30	1	90.0	30.0	70
$\overrightarrow{x^*}_{f_4}$	Square	4	7	56	2	85.5	47.8	95
	Rectangular	4	7	54	2	90.5	49.3	93

Table 2-21 (b) Initial design and the maximization of the lowest month incident solar energy, f_4 (six single-objective functions)

Results of single-objective functions							
Objective		f_1(%)	f_2(W)	f_3(W)	f_4(W)	f_5(W)	f_6($)
Ini.	Sq.	14.66	1.7589E+05	3.0558E+05	2.7771E+05	3.2766E+05	3.5085E+05
	Rec.	14.66	1.7589E+05	3.0558E+05	2.7771E+05	3.2766E+05	3.5085E+05
$\overrightarrow{x^*}_{f_4}$	Sq.	13.25	6.0190E+05	9.5561E+05	8.0018E+05	1.1520E+06	1.3343E+06
	Rec.	17.54	8.0130E+05	9.4654E+05	8.0071E+05	1.1460E+06	1.3428E+06

- Maximization of the highest month for incident solar energy (f_5)

In single-objective function for the highest month incident solar energy, the conversion efficiencies are 16.82 % in a square cell and 17.26 % in a rectangular cell from 18.30 % of $\eta_{ma}{}^*$ in both cells. The solar cell sizes are 11.11 × 11.11 cm^2 in a square cell and 16.67 × 13.33 cm^2 in a rectangular cell. The single panel consists of 30 cells in a square cell and 20 cells in a rectangular cell. The single array is comprised of 162 panel modules and is sized at 2999.96 × 200.00 cm^2, ($L_a \times H_a$) in a square cell and 135 panel modules and is sized at 2999.75 × 199.91 cm^2, ($L_a \times H_a$) in a rectangular cell.

Solar PV array systems are installed with a tilt angle of 62.00 ° and 113 arrays in a square cell and with a tilt angle of 63.70 ° and 117 arrays in a rectangular cell. The main

rationale for why the tilt angle of the multi- PV array system is increased is that the higher number of arrays and the longer time of collecting solar radiation stimulate the collection of more solar energy compared to the optimal installation angles of annual monthly average and lowest month. As an outcome, a more direct angle to the collector surface and shorter shadow allow the adjacent arrays to be tightly compacted in the system and is conducive to collecting the maximum amount of solar energy. Thus, in the case of the maximization of annual monthly incident solar energy (Q_{hm}^{*}), the Q_{hm}^{*} has the values of 1.2346E+ 06 W in a square cell and 1.236E+ 06 W in a rectangular cell as shown in Table 2-22, respectively.

Table 2-22 (a) Initial design and optimization results, f_5 (design variables)

		Design variables									
Objective		T_e (μm)	T_b (μm)	L_c (cm)	H_c (cm)	W_f (μm)	H_f (μm)	N_f	W_b (μm)	H_b (μm)	N_b
Ini.	Square	4.0	220.0	12.0	12.0	80.0	7.0	40	480.0	8.0	5
	Rectangular	4.0	220.0	12.0	12.0	80.0	7.0	40	480.0	8.0	5
$\overrightarrow{x^*}_{f_5}$	Square	4.7	312.2	11.1	11.1	35.2	84.2	78	398.5	9.4	6
	Rectangular	6.6	157.7	16.7	13.3	171.4	42.5	70	1816.3	43.4	4

		Design variables						
Objective		N_{l_c}	N_{h_c}	N_{l_p}	N_{h_p}	D (cm)	β (degree)	K
Ini.	Square	7	10	30	1	90.0	30.0	70
	Rectangular	7	10	30	1	90.0	30.0	70
$\overrightarrow{x^*}_{f_5}$	Square	5	6	54	3	83.9	62.0	113
	Rectangular	4	6	45	2	83.0	63.7	117

Table 2-22 (b) Initial design and optimization results, f_5 (six single objective functions)

Results of single objective optimization							
Objective		f_1(%)	f_2(W)	f_3(W)	f_4(W)	f_5(W)	f_6($)
Ini.	Sq.	14.66	1.7589E+05	3.0558E+05	2.7771E+05	3.2766E+05	3.5085E+05
	Rec.	14.66	1.7589E+05	3.0558E+05	2.7771E+05	3.2766E+05	3.5085E+05
$\overrightarrow{x^*}_{f_5}$	Sq.	16.82	9.6936E+05	9.4628E+05	6.9869E+05	1.2346E+06	1.6893E+06
	Rec.	17.26	1.0297E+06	9.4651E+05	6.8982E+05	1.2364E+06	1.7477E+06

- Minimization of cost (f_6)

In regards to cost, the smaller size in both solar cells contributes to higher conversion efficiencies, prompting power output to generate more electricity. As well, the smaller the size of the solar cell in a multi-PV array system, the lower the cost because cell materials significantly influence cost without a consideration of manufacturing points. On the other hand, a higher number of cells, panels, and arrays increase costs of the entire PV collector system, including costs of production, BOS, and site work. The conversion efficiencies of each 15.09 % for a square cell and 15.48 % for a rectangular cell are adjusted to the size of a multi-array system to collect the required amount of incident solar energy while considering the constraints on the permissible 70% of $Q_{am}{}^*$ ($Q \geq 0.7\ Q_{am}{}^*$) and $\eta \geq 0.7\ \eta_{max}{}^*$ in order to find the practical cost. The solar cell sizes are 14.31 × 14.31 cm^2 in a square cell and 12.71 × 13.43 cm^2 in a rectangular cell. The single panel consists of 30 cells in a square cell and 35 cells in a rectangular cell. The single array is comprised of 74 panel modules and is sized at 2647.16 × 171.71 cm^2, ($L_a \times H_a$) in a square cell and 135 panel modules and is sized at 2415.39 × 188.00 cm^2, ($L_a \times H_a$) in a rectangular cell. Solar PV array systems are installed with a tilt angle of

18.96 ° and 70 arrays in a square cell and with a tilt angle of 19.35 ° and 70 arrays in a rectangular cell, respectively. Table 2-23 shows the results of the optimization for cost.

Table 2-23 (a) Initial design and optimization results of f_6 (design variables)

		Design variables									
	Objective	T_e (μm)	T_b (μm)	L_c (cm)	H_c (cm)	W_f (μm)	H_f (μm)	N_f	W_b (μm)	H_b (μm)	N_b
Ini.	Square	4.0	220.0	12.0	12.0	80.0	7.0	40	480.0	8.0	5
	Rectangular	4.0	220.0	12.0	12.0	80.0	7.0	40	480.0	8.0	5
$\overrightarrow{x^*}_{f_6}$	Square	0.1	205.8	14.3	14.3	167.1	40.1	41	2665.4	40.7	8
	Rectangular	0.1	252.4	12.7	13.4	172.8	42.3	50	2353.4	42.8	8

		Design variables						
	Objective	N_{l_c}	N_{h_c}	N_{l_p}	N_{h_p}	D (cm)	β (degree)	K
Ini.	Square	7	10	30	1	90.0	30.0	70
	Rectangular	7	10	30	1	90.0	30.0	70
$\overrightarrow{x^*}_{f_6}$	Square	5	6	37	2	81.9	19.0	70
	Rectangular	5	7	38	2	96.0	19.3	70

Table 2-23 (b) Initial design and optimization results, f_6 (single objective functions)

		Results of single objective optimization					
Objective		f_1(%)	f_2(W)	f_3(W)	f_4(W)	f_5(W)	f_6($)
Ini.	Sq.	14.66	1.7589E+05	3.0558E+05	2.7771E+05	3.2766E+05	3.5085E+05
	Rec.	14.66	1.7589E+05	3.0558E+05	2.7771E+05	3.2766E+05	3.5085E+05
$\overrightarrow{x^*}_{f_6}$	Sq.	15.09	4.0811E+05	6.9545E+05	5.6781E+05	7.6333E+05	7.8265E+05
	Rec.	15.48	4.1828E+05	6.9545E+05	5.7226E+05	7.6160E+05	7.8309E+05

Table 2-24 shows the results of initial design parameters and six single-objective optimization results including conversion efficiency (f_1), power output (f_2), annual

monthly average incident solar energy (f_3), lowest month incident solar energy (f_4), highest month incident solar energy (f_5), and cost (f_6).

Table 2-24 Initial design parameters and single-objective optimization results (objective functions)

Results of single objective optimization							
Objective		f_1(%)	f_2(W)	f_3(W)	f_4(W)	f_5(W)	f_6($)
Ini.	Sq.	14.66	1.7589E+05	3.0558E+05	2.7771E+05	3.2766E+05	3.5085E+05
	Rec.	14.66	1.7589E+05	3.0558E+05	2.7771E+05	3.2766E+05	3.5085E+05
$\overrightarrow{x^*}_{f_1}$	Sq.	18.30	5.8949E+05	7.2236E+05	6.1397E+05	8.2993E+05	9.5238E+05
	Rec.	18.30	5.0151E+05	6.9819E+05	5.3715E+05	7.9721E+05	8.0549E+05
$\overrightarrow{x^*}_{f_2}$	Sq.	17.37	1.0636E+06	9.3731E+05	6.6781E+05	1.2306E+06	1.7929E+06
	Rec.	17.55	1.0639E+06	9.4193E+05	6.7530E+05	1.2363E+06	1.7755E+06
$\overrightarrow{x^*}_{f_3}$	Sq.	15.84	6.7873E+05	9.8842E+05	7.9968E+05	1.1447E+06	1.2543E+06
	Rec.	15.00	6.0420E+05	9.8556E+05	7.9368E+05	1.0986E+06	1.1629E+06
$\overrightarrow{x^*}_{f_4}$	Sq.	13.25	6.0190E+05	9.5561E+05	8.0018E+05	1.1520E+06	1.3343E+06
	Rec.	17.54	8.0130E+05	9.4654E+05	8.0071E+05	1.1460E+06	1.3428E+06
$\overrightarrow{x^*}_{f_5}$	Sq.	16.82	9.6936E+05	9.4628E+05	6.9869E+05	1.2346E+06	1.6893E+06
	Rec.	17.26	1.0297E+06	9.4651E+05	6.8982E+05	1.2364E+06	1.7477E+06
$\overrightarrow{x^*}_{f_6}$	Sq.	15.09	4.0811E+05	6.9545E+05	5.6781E+05	7.6333E+05	7.8265E+05
	Rec.	15.48	4.1828E+05	6.9545E+05	5.7226E+05	7.6160E+05	7.8309E+05

2.5 Conclusion

The optimal design of a solar PV array system is described with consideration of conversion efficiency, power output, solar radiation based on seasonal characteristics with shading effect from multiple array systems, and cost. The values of geometric design variables and single-objective problems are presented and investigated.

Conversion efficiency is reduced by the total power loss, mainly caused by fractional loss of shadowing effects from the fingers and busbars associated with the number of fingers and busbars dependent on the size of cells, panels, and arrays. To maximize the conversion efficiency and power output from sunlight to electricity in a solar cell, the

parameters of the solar cell structure and the mechanism of collecting solar energy are determined using mathematical programming approaches. A solar cell model has revealed that, in optimizing solar cell performance, a correlation exists between the cell structure and geometric design parameters for maximizing the conversion efficiency of a solar cell. The solar cell size, power density, and total power loss all influence the maximization of power output. Heavy doping levels reduce the open-circuit voltage and short-circuit current of a solar cell due to the emitter layer with resistive properties, while close spacing between fingers results in high power losses. This is the most decisive reason why optimal geometric design factors should be found for a solar cell for the maximum conversion efficiency. It is found that, in some cases, higher total power losses do not always correspond to maximum conversion efficiency on account of concentrated sunlight. Therefore, the correlation of cell structure parameters, grid contact design, cell size, conversion efficiency, and power output under intensity of sunlight should be deliberated by using optimum design procedure for a solar cell.

Power output is associated with the maximum number and tilt angle of arrays with the shortest distance between adjacent rows and is related to the maximum operating current and voltage, including the total power losses, power density, and size (area) of the solar PV collector. Larger-sized solar PV collectors collect more incident solar energy; the amount of power output is increased by the number of arrays, tilt angle, and distance between adjacent rows. Hence, the results of single power output at the panel level are determined by the size of a PV array system.

At the array level, with a consideration of the conversion efficiency and power output, the maximum amount of incident solar energy is investigated for optimal installation

according to three different types of seasonal demands- annual monthly average, lowest, and highest month for incident solar energy. Costs are minimized through an accurate tilt angle and the number of cells, panels, and arrays in a solar PV collector, which are associated with materials and production in a cell and panel module, inverter system, and installation site for a solar PV collector. It is necessary to constrain the conversion efficiency and incident solar energy for finding the practical value because the smallest size of a PV collector for conversion efficiency and cost is dominant to the minimization of cost.

CHAPTER 3

Multi-objective Optimal Design of Solar PV Array Systems Using Game and Fuzzy Set Theories

3.1 Overview

The electrical energy output of a solar photovoltaic (PV) collector in a non- tracking system depends on the PV array system, which generates electricity through photovoltaic effect. The installation of the PV collector is based on using proper orientation, inclination angle and the manner of mounting of the array (with self-shading losses) for collecting the maximum amount of solar energy at a specific location. Stationary solar PV array systems can be of two types – flat plate PV collector systems and compound parabolic PV collector systems- based on the method of collecting concentrating sunlight.

A solar PV array system is comprised of the following components: (1) solar cells, (2) panel modules, and (3) array system. The solar cells are interconnected in series and in parallel to generate electricity from sunlight. The energy conversion process is a main concern in deciding the design factors. A PV panel module consists of a number of interconnected solar cells encapsulated into a stable panel module. Solar cells require not only encapsulation, but also capability to provide power output without mechanical or electrical losses. The encapsulated frame provides mechanical rigidity to protect the brittle and interconnected solar cells as well as to prevent mechanical damage. In addition, it provides protection from metallic contacts, from corrosive factors, and permits

generating of electrical voltage by the panel. The durability of the assembled encapsulation, including front surface materials, encapsulant, rear surface, and frame, determine the ultimate operating life of the panel module. A PV array system consists of a number of PV panel modules, mounted and electrically connected on an installation structure to supply energy output for a particular requirement. As with the connection of a multitude of cells to form a panel module, a number of panel modules are connected in a series or parallel string to increase the energy. Matching of interconnected modules with respect to their outputs can maximize the efficiency of the array system. The main function of a mounting structure is to support the panel modules, and mechanical and electrical components. The orientation of the array system with respect to the sun determines the intensity of energy as well as the energy output of the array system. The maximum power output varies considerably with the seasons. Since the winter typically demands higher power requirements than that of the summer, it is best to design and install an array system according to winter orientation; this ensures an adequate supply of solar power year round. This means that time, including day, month, and season, can influence the optimization of the array installation because the energy output depends on the correct sunlight levels.

Geometric design relations should be considered in a solar PV array system, including solar cells, panel modules, and arrays for integrated optimization because geometric relationships are necessary for interaction within each level of a solar cell, panel module, and array, and for integration of a solar PV array system. After solar cells are determined based on conversion efficiency and panel modules are designed to maximize the power output with optimized solar cells, then the PV array system is optimized by using both the

solar cell and panel module designs as well as other parameters in sequential form. However, in this work, it is shown that within an integrated PV system, a solar cell, panel module, and array system can be simultaneously optimized through mathematical programming.

Similarly, CPC PV collector systems focus on small concentration ratio truncated CPC solar collectors without a tracking system used in practice. Since the higher part of the parabola will prevent radiation during some specific times, it will make the overall performance of the CPC solar collectors poor. Truncated CPC solar collectors are usually applied because a large portion of the reflector area can be eliminated in order to save the cost without seriously reducing the concentration.

3.2 Multi-objective Optimization Problem

The goal of optimization is to obtain the best performance of a particular system under given restrictions using mathematical programming techniques. A multi-objective optimization problem is solved as an equivalent single objective optimization problem using genetic algorithms (GA), as stated in chapter 2 (based on the results of single-objective optimization problem using the MATLAB program *ga.* Thus, MATLAB programming can implement the optimization of a solar PV array system performance using program, *ga,* which finds mixed-integer values by minimizing a scalar function of several variables starting from an initial set of values of the design parameters. Genetic algorithms (GA) are suitable for the optimization of complex nonlinear problems to find global optimum solutions with a high probability.

3.2.1 Overview

A solar PV array system consists of a number of individual solar cells interconnected in series or parallel to produce panels, and panel modules are used to produce an array system, and also an inverter system. Thus, the performance of a solar collector is determined by the following factors: (1) amount of solar radiation energy, (2) design of the solar PV array system (including PV cell, panel and array system considering photovoltaic effects), and (3) the inverter system including a controller, inverter, and battery, with functionality to deliver electrical power to points of demand from the solar collector system. Figure 3-1 shows the configuration of a solar PV array system.

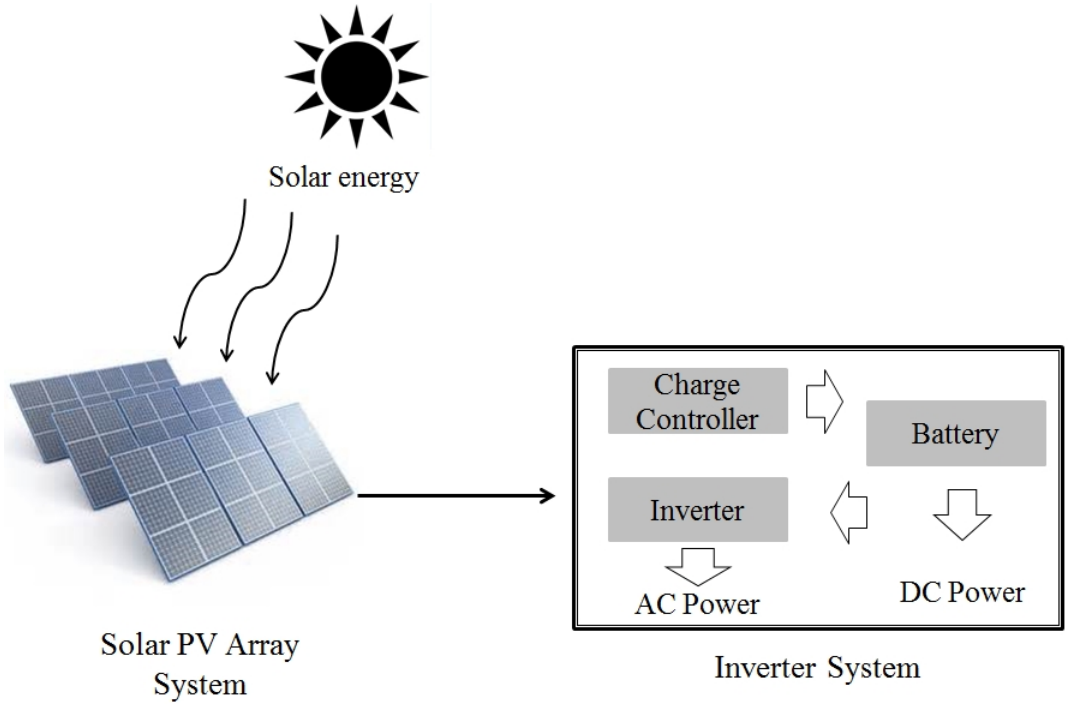

Figure 3-1 Overview of a solar PV array system

A solar PV array system is designed to supply certain amounts of electricity contingent on solar PV cells and panel modules by interconnected electrical wires. The type and

amount of electricity can be determined by the photovoltaic effect on the performance of individual subsystems: (1) conversion efficiency (%), (2) power output (W), and (3) energy output (W). Figure 3.2 highlights the division of a solar PV array system into its three subsystems: cell, panel module, and array.

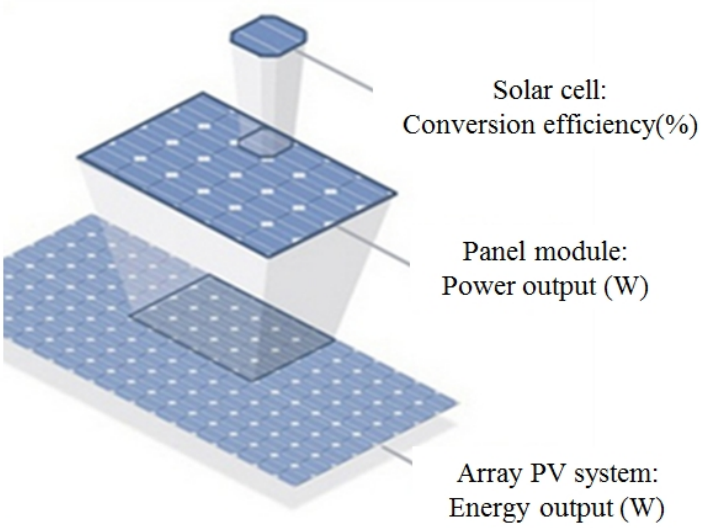

Figure 3-2 Subsystems of a solar PV array system

In a solar compound parabolic collector PV system, the reflector can be cylindrical to ensure focus on a receiver. Figure 3-3 shows a type of parabolic reflector.

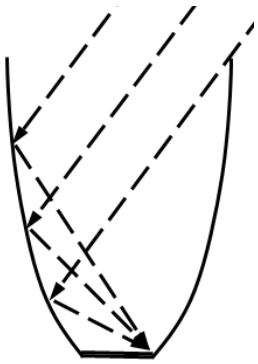

Figure 3-3 CPC PV reflector

Compound parabolic concentrators (CPCs) are a part of concentrating collectors, which contain parabolic reflectors and planar receivers. CPC applications are dependent on the concentration ratio. This ratio is an area concentration ratio defining as the ratio of the area the aperture to that of the receiver. A larger concentration ratio indicates a higher temperature, and hence more solar energy can be delivered. Low concentration ratio applications of CPC collectors can be classified into thermal and optical CPC collectors. In the case of thermal CPC collectors, the main concern is to improve the performance by reducing heat losses. In the case of an optical CPC collector, a higher solar cell operating temperature and a non-uniform illumination of the solar cell have the influence of reducing the performance of photovoltaic solar cell.

3.2.2 Game theory

In game theory, one-objective function is associated with each player. If the players in a game act independently without cooperating with each other, the game is said to be a non-cooperative game and the resulting solution is called a Nash equilibrium solution. The solution of a cooperative game is represented in terms of Pareto-optimal solution. A feasible solution X is called a Pareto optimal solution if there exists no other feasible solution $\vec{Y}$ such that $f_i(\vec{Y}) \leq f_i(\vec{X})$ for $i = 1, 2, \ldots, k$ with $f_j(\vec{Y}) < f_i(\vec{X})$ for at least one j. The cooperative game theory aims at determining a Pareto optimal solution that represents the best compromise among the k players (objective functions). For this, some rules of negotiation in the form of a supercriterion or bargaining model are to be specified before selecting a particular element from the Pareto optimal set.

The traditional game theory approach involves an iterative process and is implemented using the following steps presented by Rao and Hati (1979):

1. Start with an initial trial design vector, $\vec{X}$, and a set of weights $C_1, C_2, \ldots, C_{k-1}, C_k = 1 - C_1 - C_2 - \ldots - C_{k-1}$ for use in weighted objective function, *FC,* in Step 2.
2. Construct the weighted objective function, *FC,* as

$$FC = \sum_{i=1}^{k} C_i f_i(\vec{X}) \tag{3.1}$$

and generate a Pareto optimal solution, $\vec{X}_p$, by minimizing *FC*, including all the constraints, starting from the known weights and the design vector.

3. Starting from the solution $\vec{X}_p$, find the solution $\vec{X}_s$ that maximizes a predefined supercriterion *S*.
4. Test for the convergence of the process. For this, calculate

$$\left\| \vec{X}_s - \vec{X}_p \right\| \leq \varepsilon \tag{3.2}$$

where ε is a small number to ensure that $\vec{X}_s$ is almost the same as $\vec{X}_p$. If the inequality (3.2) is not satisfied, set $\vec{X} = \vec{X}_s$ and go to Step 2 and repeat Steps 2, 3 and 4 until the convergence criterion, Eq. (3.2), is satisfied.

For computational convenience, the iterative process indicated in Steps 1 – 4 above is simplified by minimizing the new objective function given by

$$F = FC - S \tag{3.3}$$

As can be seen, the minimization of F of Eq. (3.3) is expected to accomplish, approximately, the minimization of *FC* and the maximization of *S* in one step. This process is termed modified game theory, as introduced by Rao and Freiheit (1991). Noting that all multi-objective optimization approaches involve, in some fashion, the use of subjective information in selecting a Pareto optimal solution, the present approach can also be considered as an alternative method of multi-objective optimization.

In the proposed modified cooperative game theory approach, all the players presumably agree to find a compromise solution according to a mutually agreeable bargaining model or supercriterion. In this work, the supercriterion is assumed so as to maximize the deviation of the i^{th} objective function value from its worst (or maximum) possible value for each of the players *i* (*i* = 1, 2,…, *k*). There is a need to use an alternative procedure for the selection of the worst value of each objective function in order to apply modified game theory for multi-objective optimization. In the proposed (new) modified game theory (MGT), the selection of the worst value for each of the objective functions is made differently as indicated below.

Computational procedure

Find the design vector $\vec{X} = \{x_1 \ x_2 \cdots \ x_n\}^T$ to minimize the single-objective functions:

$$f_1(\vec{X}),\ f_2(\vec{X}), \dots,\ f_k(\vec{X});\ k = 1,2, \dots, t \tag{3.4}$$

subject to the constraints

$$g_j(X) \leq 0,\ j = 1,2, \dots, m \tag{3.5}$$

$$h_k(X) = 0,\ k = 1,2, \dots, p \tag{3.6}$$

$$x_i^{(l)} \leq x_i \leq x_i^{(u)} \quad i = 1,2,\dots,n \tag{3.7}$$

where $x_i^{(l)}$ and $x_i^{(u)}$ denote the lower and upper bounds on x_i.

1. Minimize each of the *k* objectives stated in Eq. (3.4) subject to the constraints of Eqs. (3.5) – (3.7) and find the corresponding optimal values of the objectives as $f_i(\vec{X}_i^*)$, i = 1, 2, … , k.
2. Find the maximum or worst value possible for each of the *k* objectives (F_{wi}) from the solutions obtained in Step 1. Construct matrix [P] as

$$[\mathrm{P}] = \begin{bmatrix} f_1(X_1^*) & f_2(X_1^*) & \dots & f_k(X_1^*) \\ f_1(X_2^*) & f_2(X_2^*) & \dots & f_k(X_2^*) \\ & \cdot & & \\ & \cdot & & \\ & \cdot & & \\ f_1(X_k^*) & f_2(X_k^*) & \dots & f_k(X_k^*) \end{bmatrix} \tag{3.8}$$

It can be found that the diagonal elements in the matrix [P] are the optimum value (best) in the respective columns.

3. Normalize each of the objectives so that no objective is favored by its magnitude and also assures that it lies between zero and one:

$$f_{ni}(\vec{X}) = \frac{f_i(\vec{X}) - f_i(\vec{X}_i^*)}{F_{wi} - f_i(\vec{X}_i^*)} \; ; \mathrm{i} = 1, 2, \dots, \mathrm{k}. \tag{3.9}$$

where F_{wi} is the worst value of the i^{th} objective function and $f_i(\vec{X}_i^*)$ is the optimum value (best) obtained in Step 1 of the i^{th} objective.

4. The Pareto optimal solution set can be found by formulating a weighted objective function, *FC*, as

$$FC = C_1 f_{n1}(\vec{X}) + C_2 f_{n2}(\vec{X}) + ... + C_{k-1} f_{n(k-1)}(\vec{X}) + (1 - C_1 - C_2 - .... - C_{k-1}) f_{nk}(\vec{X}) \tag{3.10}$$

and minimizing it under the stated constraints for all combinations of the weights C_1, C_2, …, C_{k-1} and $C_k = 1 - C_1 - C_2 - ... - C_{k-1}$, with $0 \le C_i \le 1$ and $\sum_{i=1}^{k} C_i = 1$.

The supercriterion, S, to ensure that each of the normalized objective functions, $f_{ni}(\vec{X})$, will be as far away as possible from its (normalized) worst possible value of 1 (for $i = 1, 2, \ldots, k$), can be expressed as

$$S = \prod_{i=1}^{k} \left[1 - f_{ni}(\vec{X})\right] \tag{3.11}$$

Then a new objective function, $F(\vec{Y})$, is created to find a Pareto optimal solution that represents a compromise solution as

$$F(\vec{Y}) = FC - S \tag{3.12}$$

where

$$\vec{Y} = \{x_1\ x_2 \cdots x_n\ C_1\ C_2 \cdots C_{k-1}\}^T \text{ with } 0 \le C_i \le 1,\ i = 1, 2, \ldots, k-1 \tag{3.13}$$

5. Minimize $F(\vec{Y})$ to find $\vec{Y}$ which yields the best compromise solution of the multi-objective optimization problem stated in Eqs. (3.4) – (3.7) as per the mutually agreeable bargaining model indicated in Eq. (3.11).

The single-objective optimization problem of each subsystem is solved using *ga* (MATLAB), which is a stochastic global search method. The solution of the multi-objective optimization gives a compromise solution under game theory method after

single-objective optimizations such as conversion efficiency, power output, and incident solar energy based on average, lowest, and highest months, are calculated.

3.2.3 Solar cell

The multi-objective optimization problem of a solar cell is conducted using the results of the individual single-objective problems of the maximization of conversion efficiency and power output.

3.2.3.1 Formulation of optimization problems

The results of optimization problems for a solar cell are used to formulate a multi-objective game theory optimization problem. The individual single-objective optimization problems of the maximization of conversion efficiency and power output are solved by using *ga* (MATLAB) to find the global minima in terms of mixed-integer variables starting from a set of initial design vectors as shown in Table 3-1.

Table 3-1 Values of design variables and single-objective optimizations

Objective		Design variables										
		T_e (μm)	T_b (μm)	L_c (cm)	H_c (cm)	W_f (μm)	H_f (μm)	N_f	W_b (μm)	H_b (μm)	N_b	C
Initial	Sq.	6.00	200	2	2	60	10	20	303	8	4	12
	Rec.	6.00	220	3	2	60	10	15	600	8	3	10
$\overrightarrow{x^*}_{f_1}$	Sq.	7.31	244.41	0.81	0.81	20.00	5.00	18	101.78	6.00	2	6
	Rec.	7.62	208.01	2.45	0.50	20.03	5.01	12	100.26	6.00	3	6
$\overrightarrow{x^*}_{f_2}$	Sq.	5.51	181.02	4.93	4.93	71.55	17.88	87	368.48	18.89	10	24
	Rec.	5.18	282.17	5.00	2.90	65.80	16.44	64	337.18	17.43	10	40

Objective	Square cell		Rectangular cell	
	f_1(%)	f_2(W)	f_1(%)	f_2(W)
Initial	17.84	0.8563	17.02	1.2010
$\overrightarrow{x^*}_{f_1}$	0.2028	0.0798	0.2054	0.1514
$\overrightarrow{x^*}_{f_2}$	0.1622	9.4615	0.1643	9.5448

3.2.3.2 Numerical results

A multi-objective optimization of a solar cell is investigated with the results of single-objective problems of the conversion efficiency and power output with intensity of *C* suns and solved by placing constraints on the minimum permissible conversion efficiency from 80 % for the maximum conversion efficiency (η^*_{ma}, 18.30 % for a square cell and a rectangular cell) and power output of 0.5 W for a square cell and a rectangular cell.

- Results with no constraint on the power output

Multi-objective optimization without consideration of constraint on power output is solved by the results of the maximum conversion efficiencies (η^*_{ma}), 20.28 % in a square cell and 20.54 % in a rectangular cell, and power output, 9.46 W in a square cell and 9.54 W in a rectangular cell, respectively. 80% of the maximum conversion efficiencies ($\eta \geq 0.8\,\eta^*_{ma}$) in both square and rectangular cells as a constraint are applied because intensity of sunlight is proportional to concentration ratio (*C*). The total power losses that reduce the theoretical conversion efficiency (21.03% in both a square cell and a rectangular cell) are 11.07 % for a square cell and 11.14 % for a rectangular cell. Also, main fractional power loss is from shadow of geometric metal parts of fingers and busbars, 6.82 % and 6.80 %, respectively. The power densities in both cells are calculated

by the maximum short-circuit current density (J_m) and open-circuit voltage (V_m) including the total power losses, 11.07 % and 11.14 %, and the results of power density are 0.122 $\frac{W}{cm^2}$ in both cells; they possess very similar values except for the collected areas from sunlight which offer different power output due to differing cell size such as 0.67 cm^2 for a square cell and 2.1 cm^2 for a rectangular cell. Thus, the power outputs can be derived by 0.081 W and 0.258 W, respectively. On other hand, the conversion efficiencies closely reach the highest efficiencies, 20.25 % and 20.26 % compared to 20.28 % and 20.54 %. An investigation on the variation of the weights of C_1 and C_2 used in the Pareto optimal solutions indicated that f_1 is the dominant problem in the case of multi-objective optimization. The results of multi-objective optimization are shown in Tables 3-2.

Table 3-2 (a) Results of multi-objective optimization problem (design variables)

Multi-objective Optimization		Design variables										
		T_e (μm)	T_b (μm)	L_c (cm)	H_c (cm)	W_f (μm)	H_f (μm)	N_f	W_b (μm)	H_b (μm)	N_b	C
Cell	Initial	4.00	120.00	1.50	1.50	60.00	10.00	25	300.00	8.00	5	30
	Sq.	7.97	267.88	0.82	0.82	20.19	5.02	18	100.93	6.02	2	6
	Rec.	7.77	265.71	3.75	0.57	33.71	8.43	10	168.54	9.44	2	6

Table 3-2 (b) Results single-objective function, new objective function, and weights

Results						
Multi-objective Optimization		f_1(%)	f_2(W)	New objective function	C_1	C_2
Cell	Initial	0.46	3.12	0.6045	0.30000	0.30000
	Sq.	20.25	0.081	0.0065	0.99213	0.00787
	Rec.	20.26	0.258	0.1221	0.92864	0.07136

- Results with constraint on the power output

With consideration of the permissible conversion efficiency, 80 %, ($\eta_c \geq 0.8\,\eta_{ma}^*$; η_{ma}^* = 20.28 % for a square cell and η_{ma}^* = 20.54 %) and power output, 0.5 W, the maximum operating power output can be estimated by the maximum operating current and voltage. The conversion efficiencies are decreased from 20.25 % to 17.56 % and from 20.26 % to 18.75 %, an implication that the total power losses in both cells are increased from 11.07 % to 19.25 % and 11.14 % to 15.24 % by increasing the values of geometric parameters in both cells. The changes in total power losses are 8.18 % and 4.1 %, which are mainly caused by the fractional power loss of shadowing 13.6 % for a square cell and 10.33% for a rectangular cell. In the case of the value of the geometric finger, the number of fingers is increased from 18 to 25 and from 10 to 19, and the thickness of width is increased from 20.19 μm to 200 μm and from 33.71 μm to 112.49 μm, which are attributed to a reduction in the conversion efficiencies in both cells. In the case of the value of the geometric busbar, the number of busbars is not changed from 2, but the thickness of width is dramatically increased from 100.93 μm to 1000 μm for a square cell and from 168.54 μm to 562.54 μm for a rectangular cell, which indicates that increasing the values of the

geometric busbar contributes to increases in the conversion efficiencies instead of increasing the number of busbars compared to fingers. The power output, which is calculated by operating power density, 0.0351 $\frac{W}{cm^2}$ and 0.0562 $\frac{W}{cm^2}$, and absorbed area of a solar cell from sunlight, 25 cm^2 and 12.9 cm^2, is 0.878 W for a square cell and 0.725 W for a rectangular cell, respectively. The value of single objective f_1 is still a dominant factor in both cell cases when compared to the results of weights of C_1 and C_2. The change in the value of weights of C_1 and C_2 used in the Pareto optimal solutions are different after applying the minimum value of power output 0.5 W as a constraint. In the case of weight of C_1, the value of weight of C_1 is increased from 0.99213 to 0.99998 for a square cell, but the value of C_1 is decreased from 0.92864 to 0.80496 for a rectangular cell. The values of weight of C_2 are decreased from 0.00787 to 0.00002 for a square cell. However, the values of weight of C_2 are increased from0.07136 to 0.19504 for a rectangular cell. Table 3-3 shows the results of multi-objective optimization.

Table 3-3 (a) Results of multi-objective optimization problem (design variables)

		Design variables										
Multi-objective Optimization		T_e (μm)	T_b (μm)	L_c (cm)	H_c (cm)	W_f (μm)	H_f (μm)	N_f	W_b (μm)	H_b (μm)	N_b	C
Cell	Initial	4.00	120.00	1.50	1.50	60.00	10.00	25	300.00	8.00	5	30
	Sq.	7.99	254.90	5.00	5.00	200.00	49.99	25	999.99	50.00	2	2
	Rec.	7.99	263.68	5.00	2.58	112.49	28.12	19	562.43	29.13	2	3

Table 3-3 (b) Results single-objective function, new objective function, and weights

Results						
Multi-objective Optimization		$f_1(\%)$	$f_2(W)$	New objective function	C_1	C_2
Cell	Initial	0.46	3.12	0.6045	0.30000	0.30000
	Sq.	17.56	0.878	0.6457	0.99998	0.00002
	Rec.	18.75	0.727	0.4995	0.80496	0.19504

3.2.4 Flat plate PV array system

The multi-objective optimization problem of a flat plate PV array is investigated using the results of the individual deterministic single-objective problems of maximization of conversion efficiency, power output, annual monthly average incident solar energy, lowest month incident solar energy, highest month incident solar energy and minimization of cost.

3.2.4.1 Formulation of optimization problems

A solar PV array system is needed to find the best performance considering photovoltaic effect, size and capacity of the solar collector at a particular location based on the desired requirements such as conversion efficiency, power output, incident solar energy with seasonal characteristics, and costs, so that one can specify the numbers of cells, panel modules, arrays, inverter system, and size of the entire PV collector using a multilevel approach. The basic problem of a multilevel design of a practical system involves a large number of elements or subsystems with multiple-load conditions, and a number of design variables and constraints. By administering the results of single-objective optimizations, a multilevel optimization problem is formulated and solved

using multiple objective functions. The problem of multi-objective optimization of the solar collector design can be stated in the following form:

Find the design vector $\vec{X} = \{x_1 \ x_2 \cdots \ x_n\}^T$ to minimize the single-objective functions:

$$f_1(\vec{X}),\ f_2(\vec{X}), \ldots,\ f_k(\vec{X});\ k = 1,2, \ldots, t \tag{3.14}$$

subject to the constraints

$$g_j(X) \leq 0,\ j = 1,2, \ldots, m \tag{3.15}$$

$$h_k(X) = 0,\ k = 1,2, \ldots, p \tag{3.16}$$

$$x_i^{(l)} \leq x_i \leq x_i^{(u)} \quad i = 1,2, \ldots, n \tag{3.17}$$

where $x_i^{(l)}$ and $x_i^{(u)}$ denote the lower and upper bounds on x_i. Most systems permit the partitioning of the vector $\vec{X}$ into two subvectors $\vec{Y}$ and $\vec{Z}$:

$$\vec{X} = \begin{Bmatrix} \vec{Y} \\ \vec{Z} \end{Bmatrix} \tag{3.18}$$

where the subvector Y denotes the coordination or interaction design variables between the subsystems and the subvector $\vec{Z}$ indicates the design variables confined only to subsystems. The vector $\vec{Z}$ can be partitioned as

$$\vec{Z} = \begin{Bmatrix} \vec{Z}_1 \\ \cdot \\ \cdot \\ \cdot \\ \vec{Z}_j \\ \cdot \\ \cdot \\ \cdot \\ \vec{Z}_K \end{Bmatrix} \tag{3.19}$$

where $\vec{Z}_j$ represents the design variables associated with only the j^{th} subsystem for each subsystem only and K denotes the number of subsystems in the entire system.

The design variables $\vec{Y}$ may appear in all the single-objective functions while the design variables $\vec{Z}_K$ appear only in the constraint sets $g^{(k)} \leq 0$ and $h^{(k)} = 0$. The bounds on the design variables, Eq. (3.17), can be expressed as

$$\vec{Y}^{(l)} \leq \vec{Y} \leq \vec{Y}^{(u)} \tag{3.20}$$

$$\vec{Z}_j^l \leq \vec{Z}_j \leq \vec{Z}_j^u \qquad j = 1,2,\dots,K \tag{3.21}$$

Thus, the objective function f(X) can be expressed as

$$\mathrm{f}(\vec{X}) = \sum_{j=1}^{K} f^j(\vec{Y}, \vec{Z}_j) \tag{3.22}$$

where $f^j(\vec{Y}, \vec{Z}_j)$ denotes the contribution of the j^{th} subsystem to the overall objective function. Note that a maximization type of objective function can be converted to a minimization type simply by changing the sign of the objective function.

Figure 3-4 shows a computational flow chart of the multi-objective optimization with the GMT optimization technique using the solution of single objective optimization problems based on genetic algorithm.

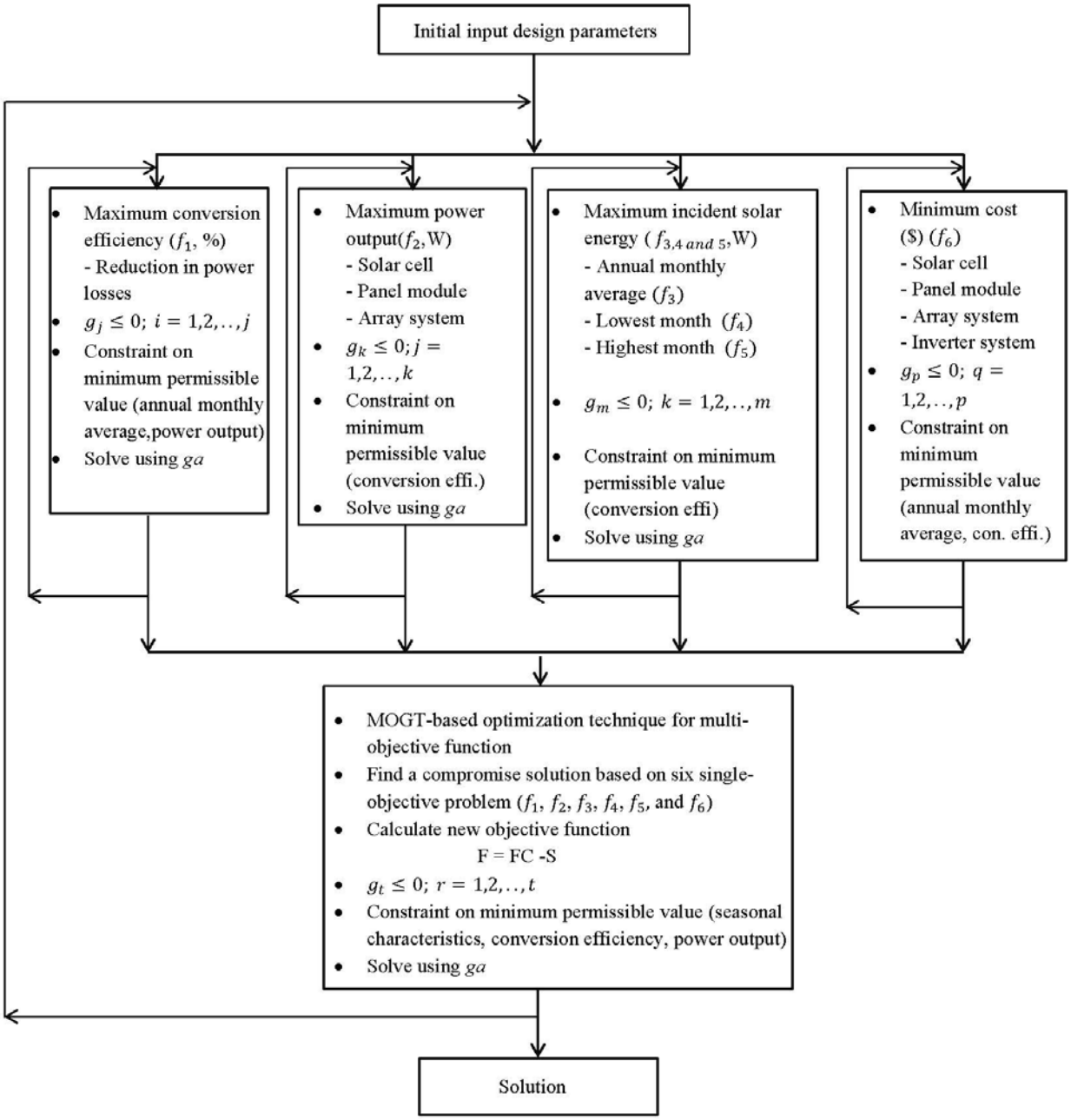

Figure 3-4 Computational flow chart of multi-objective optimization with single objective function based on genetic algorithm with the GMT optimization technique

3.2.4.2 Numerical results

Multilevel-objective optimization in flat plate PV array systems based on square and rectangular cells is implemented with no constraint and with constraints on the annual monthly average, lowest, and highest month incident solar energy. A multilevel-objective optimization problem is solved by using the new modified game theory method and the weighting method in Pareto optimal solutions with the results of single-objective optimization problems. A method for generating Pareto optimal solutions for multilevel criteria problems capable of being formulated is presented. The modified game theory method for generating the best compromise solutions (Pareto optimal solutions) is used in this work with illustrative and numerical results. The multilevel-objective optimization problem is solved by placing the constraints on permissible requirement values of conversion efficiency and maximum annual monthly average incident solar energy.

- Results with no constraint on the annual monthly average incident solar energy

Without consideration of incident solar energy, the multilevel objective optimization problem is investigated with the results of single-objective optimizations using *ga* (MATLAB). In the subsystem of a solar cell, objective optimization is the maximum conversion efficiency, and the constraint on the minimum conversion efficiency is applied to the permissible minimum conversion efficiency of 70 % for the maximum conversion efficiency, 18.30 %, ($\eta_c \geq 0.7\, \eta^*_{ma}$) in both square and rectangular cells. At the panel module level, the main optimization concern is to generate the maximum power output. In this work, the maximum-end power output of a solar PV array system is dependent on the size of the PV arrays, so that the power output of the panel module is determined by deciding the size of an array. At the array system level, the primary

inquiry is how much incident solar energy to collect under a particular condition to generate electricity from the panel module packages based on photovoltaic effects. Tables 3-3 are shown as the results of the multilevel-objective optimization problem without consideration of requirement of incident solar energy including annual monthly month, lowest, and highest month.

Conversion efficiencies of solar cells in both applications are 17.96 %, which is reduced by a total power loss of 14.49 %, especially from the fractional loss of shadow at 8.79 % and 18.12 %. This is decreased by a total power loss of 13.83 % from the main factor of the fractional loss of shadow at 8.02 %. The power densities are 0.01796 $\frac{W}{cm^2}$ and 0.01812 $\frac{W}{cm^2}$, respectively. A single panel module with a basic unit square power output of 2.2 W with 25 cells and rectangular power output of 1.98 W with 30 cells can generate electricity at 46.69 W and 50.54 W as a power output in the 2nd subsystem of the PV collectors. A single PV array system in both applications based on square and rectangular cells consists of the number of single panel modules with 56 and 46 panels and produces 2.615 kW and 2.325 kW of electricity, respectively.

The tilt angle of arrays based on square and rectangular cells are 30.39° and 53.03°, respectively. At an installed angle of 30.39°, the amount of the annual monthly average incident solar energy is higher than 53.03° because the value of weight C_1 based on square cells is higher than the value of weight C_1based on rectangular cells. Thus, the installation angles are associated with the size of the array, how much incident solar energy to collect, and minimizing costs.

The value of the weight of C_1 used in the Pareto optimal solutions is f_1, and it is the dominant factor in the case of multilevel objective optimization regarding square cells. In

contrast, the value of the weight of C_6 is the dominant factor for multilevel objective optimization regarding rectangular cells. The primarily dominant factors in both applications are the weight of C_1 and C_6 for multilevel objective optimization. Thus, the number of arrays reaches the lowest values on constraints in arrays in a square and rectangular cell as 2, respectively, by reason of the dominant factor of the weight of C_6 in both solar PV collector systems, as shown in Table 3-4.

Table 3-4 (a) Results of multi-objective optimization (design variables)

		Design variables									
Multi-objective optimization		T_e (μm)	T_b (μm)	L_c (cm)	H_c (cm)	W_f (μm)	H_f (μm)	N_f	W_b (μm)	H_b (μm)	N_b
Game theory	Square	3.41	356.97	11.06	11.06	55.47	13.37	75	642.16	13.45	9
	Rect.	5.08	234.33	10.94	10.00	49.26	12.23	73	837.70	12.77	6

		Design variables						
Multi-objective optimization		N_{c_l}	N_{c_h}	N_{p_l}	N_{p_h}	D (cm)	β (degree)	K
Game theory	Square	5	5	28	2	98.98	30.39	2
	Rect.	6	5	23	2	92.40	53.03	2

Table 3-4 (b) Results of single and multi-objective optimizations

		Results of single objective and multilevel-objective optimizations						
Single & Multi-obj. optimization		f_1(%)	f_2(W)	f_3(W)	f_4(W)	f_5(W)	f_6($)	New obj. opt.
Game theory	Sq.	17.96	5.23E+03	7.48E+03	7.15E+03	7.75E+03	8.73E+03	8.743
	Rec.	18.12	4.65E+03	5.75E+03	4.99E+03	6.24E+03	7.65E+03	7.591

Results of the weights								
Multi-obj. optimization		C_1	C_2	C_3	C_4	C_5	C_6	Total weights
Game theory	Sq.	0.167	0.019	0.075	0.236	0.027	0.476	1
	Rec.	0.562	0.099	0.036	0.054	0.083	0.166	1

Table 3-4 (c) Results of size of each level of cell, panel, and array

Results of size of each system										
Multi-obj. optimization		L_{Cell} (cm)	H_{Cell} (cm)	L_{Panel} (cm)	H_{Panel} (cm)	L_{Array} (cm)	H_{Array} (cm)	Cell area (cm^2)	Panel area (cm^2)	Array area (cm^2)
Game theory	Sq.	11.1	11.1	55.3	55.3	1548.3	110.6	122.2	3057.5	171222.1
	Rect.	10.9	10.0	65.6	50.0	1509.5	100.0	109.4	3281.5	150950.6

3.2.4.3 Sensitivity analyses

Multilevel-objective optimizations are separately investigated in a range from 50% to 95% of maximum amount of incident solar energy for an annual season for conversion efficiency and costs because the minimum requirements are necessary for interaction in a multilevel system. Tables 3-5 show the results of the multilevel-objective optimization problem with constraints on annual incident solar energy in the range of 50% to 95% from the maximum annual monthly average incident solar energy (Q_{am}^{*}).

In general, the results of sensitivity analysis are also expected to be useful when the numerically found values of the design variables are to be rounded to the nearest practically feasible (or available) values for producing real-life solar cells.

Sensitivity analysis is investigated with the constraints spanning from 50 % to 95 % of Q_{am}^{*} ; the permissible minimum constraint on annual monthly average incident solar energy in a range from 50 % to 95 % (Q $\geq Q_{am}^{*} = 9.8842E + 05\ W$ for a square cell and $Q_{am}^{*} = 9.8556E + 05\ W$ for a rectangular cell; P = from 50 % to 95 %).

The ranges of conversion efficiency under a different probability for multilevel objective optimization lie between 17.47 % and 15.71 % in a square cell, and between 17.67 % and 16.69 % in a rectangular cell, as a result of increases in total power losses from 16.94 % to 25.28 % and from 16.00 % to 20.62 % in both solar PV collectors based on square and rectangular cells, respectively. The primary factors for increases in the total power losses are larger solar cells and greater numbers and geometric dimensions of fingers, and busbars, so that the conversion efficiencies are decreased during increases in the higher amounts of annual monthly average incident solar energy from the minimum values of constraints from 50 % to 95 % of Q_{am}^{*} in order to collect higher amounts of incident solar energy. As a result, the power densities of a square and rectangular cell are decreased from 0.01747 $\frac{\mathrm{W}}{\mathrm{cm}^2}$ to 0.0157 $\frac{\mathrm{W}}{\mathrm{cm}^2}$ and from 0.01767 $\frac{\mathrm{W}}{\mathrm{cm}^2}$ to 0.0167 $\frac{\mathrm{W}}{\mathrm{cm}^2}$, respectively. The tilt angle of the solar PV collector is reduced from 24.90° to 18.36° for a PV collector based on a square cell, and from 22.77° to 17.44° for a PV collector based on a rectangular cell with adjustments made to the size and the number of arrays in order to collect maximum solar energy and minimize costs considering a compromise solution for deterministic multilevel objective optimization under a particular condition. In addition, the distance between adjacent rows of the arrays is decreased to reduce the cost of site work installation. Table 3-5 shows the results of deterministic multi-objective optimization with respect to a percent of annual monthly average solar incident energy.

Table 3-5 Results of deterministic multi-objective optimization with respect to a percent (P= 50 % ~ 95 %) of ($f_1 \sim f_6$) annual monthly average incident solar energy ($\eta \geq$ P η^*_{am})

Percent of annual incident energy		Design variables									
		T_e (μm)	T_b (μm)	L_c (cm)	H_c (cm)	W_f (μm)	H_f (μm)	N_f	W_b (μm)	H_b (μm)	N_b
50%	Square	5.69	370.02	10.10	10.10	199.99	49.99	40	1438.37	49.99	2
	Rectangular	7.57	290.42	19.74	10.28	196.74	49.16	42	983.70	49.77	5
60%	Square	5.81	256.00	10.14	10.14	192.47	48.12	41	963.39	49.10	3
	Rectangular	5.90	315.20	10.13	10.55	199.32	49.83	41	1074.88	49.96	3
70%	Square	7.26	384.16	10.03	10.03	199.37	49.82	40	997.33	49.98	3
	Rectangular	4.30	344.88	15.79	11.06	197.14	49.22	45	1012.70	49.62	5
80%	Square	1.73	269.96	10.00	10.00	199.97	49.94	44	1301.68	49.96	5
	Rectangular	2.50	215.94	19.61	13.33	199.99	49.99	50	1000.91	49.98	6
90%	Square	4.93	330.14	14.79	14.79	193.97	46.36	85	1724.90	47.16	2
	Rectangular	5.56	256.89	11.81	11.94	199.93	49.68	60	1446.73	49.91	4
95%	Square	4.00	246.14	14.01	14.01	194.90	47.69	100	1553.35	48.25	10
	Rectangular	5.75	377.32	11.07	18.80	199.52	48.06	67	1913.57	48.15	4

Percent of annual incident energy		Design variables						
		N_{c_l}	N_{c_h}	N_{p_l}	N_{p_h}	D (cm)	β (degree)	K
50%	Square	8	6	37	3	80.03	24.90	82
	Rectangular	4	6	38	3	80.44	22.77	80
60%	Square	8	6	37	3	81.01	23.81	81
	Rectangular	8	9	37	2	80.64	21.36	78
70%	Square	8	6	37	3	80.70	22.13	81
	Rectangular	5	9	38	2	81.90	21.05	75
80%	Square	5	6	52	3	81.99	22.29	78
	Rectangular	3	5	51	3	81.08	21.05	75
90%	Square	5	4	40	3	84.58	19.97	78
	Rectangular	5	5	49	3	82.74	19.61	79
95%	Square	5	7	42	2	80.36	18.36	75
	Rectangular	6	5	45	2	80.61	17.44	77

In variations of single-objective function, Pareto optimal solution (FC), supercriterion (S), and new objective function (F($\vec{Y}$)), the maximum conversion efficiencies in both square and rectangular cells are 18.30 % as a single objective function under constraints of the

permissible amount of 70 % from the maximum conversion efficiency (η_{ma}^{*}), 18.30 %, in both flat plate PV collectors. After the multilevel-objective optimization is applied to solve the best compromise solution in the solar PV collector systems, the reduction ratio of the obtained conversion efficiencies under a different probability to the maximum conversion efficiencies are decreased from 4.55 % at the permissible value of constraint 50 % based on Q_{am}^{*} to 14.13 % in the permissible value of constraint 95 % based on Q_{am}^{*} for a square cell. Likewise, a decrease is observed from 3.46 % at the permissible value of constraint 50% based on the permissible annual monthly average incident solar energy to 8.80 % at the permissible value of constraint 95 % of the maximum solar energy for a rectangular cell, respectively.

In a range between 50 % and 70 % of Q_{am}^{*}, the power output in a square cell is between 9.605E + 05 W and 9.446E + 05 W, but the power output with constraints on or above 80% of Q_{am}^{*} is rapidly decreased from 9.605E + 05 W to 7.945E + 05 W. Also, the power output gradually rises with the constraints on the increases in the amount of annual monthly average incident solar energy. In the case of a flat plate PV collector based on rectangular cells, the power output rapidly declines from 9.779E + 05 W to 8.9414E + 05 W due to the decreases in the size of the array at each probability.

In the case of costs, there are similar patterns with increases and decreases in power output, incident solar energy, and costs at the particular probabilities. The weighting method, the constraint method, and the minimum or maximum approaches of generating Pareto optimal set were used for a multilevel-objective optimization problem. The variations of supercriterion, Pareto optimal solution, and new objective optimization are investigated by placing weights (C_1, C_2, C_3, C_4, C_5, and C_6). The modified game theory

approach for generating the best compromise solutions is presented along with numerical examples.

The values of supercriterion in both flat plate PV collectors based on square and rectangular cells are slightly increased in the range of 50 % and 80 %. The value of supercriterion in the flat plate PV collector based on rectangular cells is dramatically increased up to 9.735, though the value of supercriterion in flat plate PV collector based on square cells is steeply decreased from 2.304 up to 1.572 because no feasible design variables exist which would decrease the single-objective function of power output without causing a simultaneous increase in at least one objective function. Figures 3-5 show the results of single-objective function, Pareto optimal solutions (FC), supercriterion (S), and new objective function ($F(\vec{Y})$) with respect to single objective function of ($f_1 \sim f_6$) annual monthly average incident solar energy.

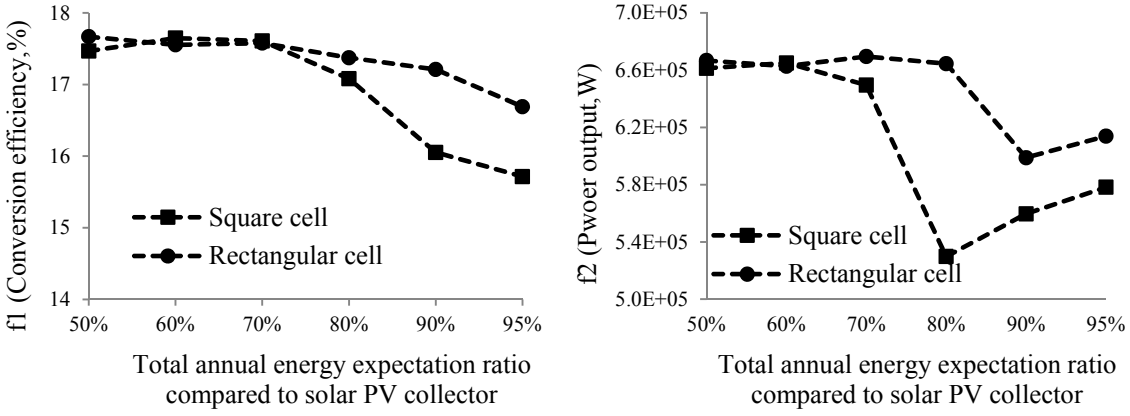

(a) (b)

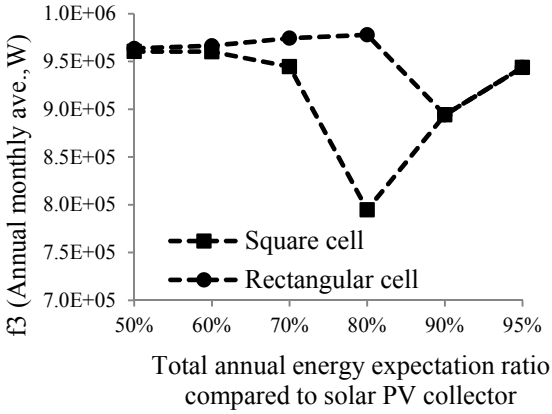
f3 (Annual monthly ave., W)
1.0E+06
9.5E+05
9.0E+05
8.5E+05
8.0E+05
7.5E+05
7.0E+05
Square cell
Rectangular cell
50%
60%
70%
80%
90%
95%
Total annual energy expectation ratio compared to solar PV collector

(c)

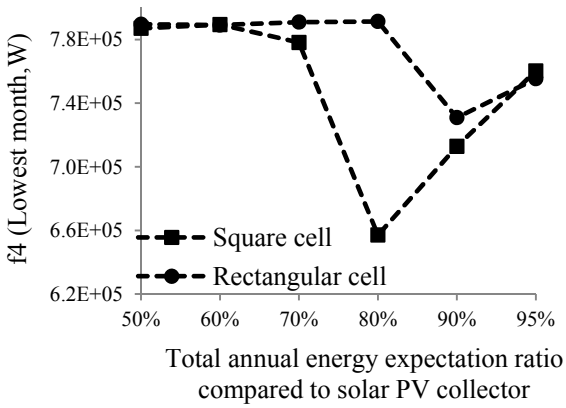
f4 (Lowest month, W)
7.8E+05
7.4E+05
7.0E+05
6.6E+05
6.2E+05
Square cell
Rectangular cell
50%
60%
70%
80%
90%
95%
Total annual energy expectation ratio compared to solar PV collector

(d)

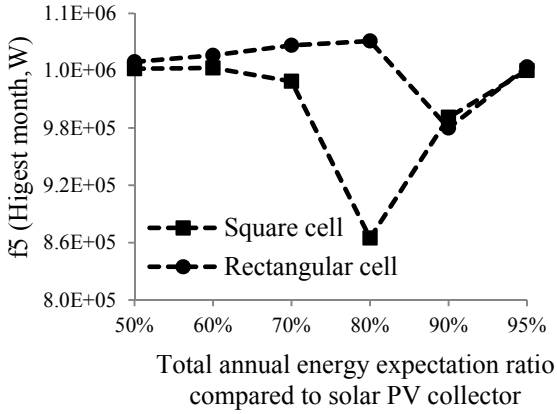
f5 (Higest month, W)
1.1E+06
1.0E+06
9.8E+05
9.2E+05
8.6E+05
8.0E+05
Square cell
Rectangular cell
50%
60%
70%
80%
90%
95%
Total annual energy expectation ratio compared to solar PV collector

(e)

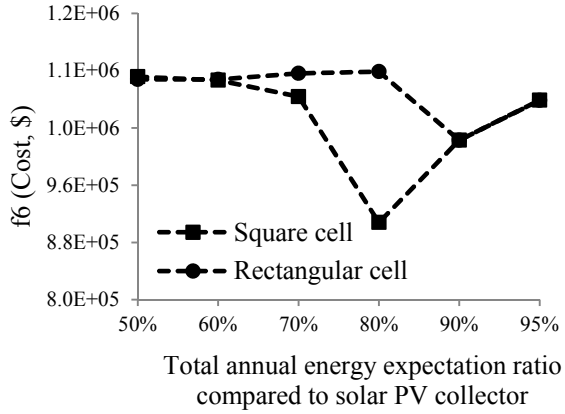
f6 (Cost, $)
1.2E+06
1.1E+06
1.0E+06
9.6E+05
8.8E+05
8.0E+05
Square cell
Rectangular cell
50%
60%
70%
80%
90%
95%
Total annual energy expectation ratio compared to solar PV collector

(f)

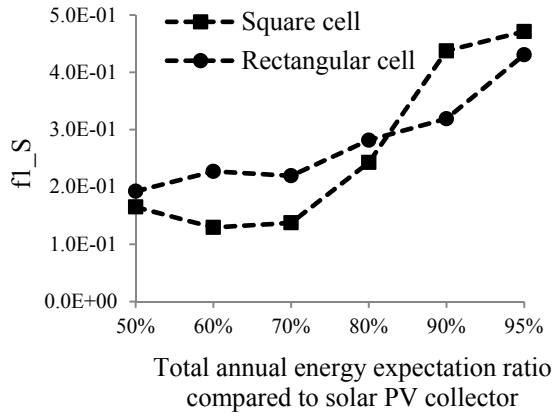
f1_S
5.0E-01
4.0E-01
3.0E-01
2.0E-01
1.0E-01
0.0E+00
Square cell
Rectangular cell
50%
60%
70%
80%
90%
95%
Total annual energy expectation ratio compared to solar PV collector

(g)

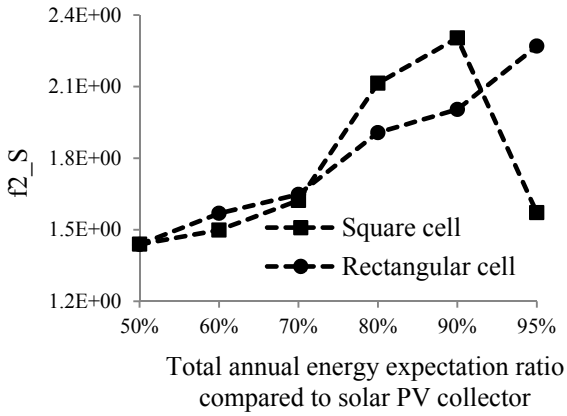
f2_S
2.4E+00
2.1E+00
1.8E+00
1.5E+00
1.2E+00
Square cell
Rectangular cell
50%
60%
70%
80%
90%
95%
Total annual energy expectation ratio compared to solar PV collector

(h)

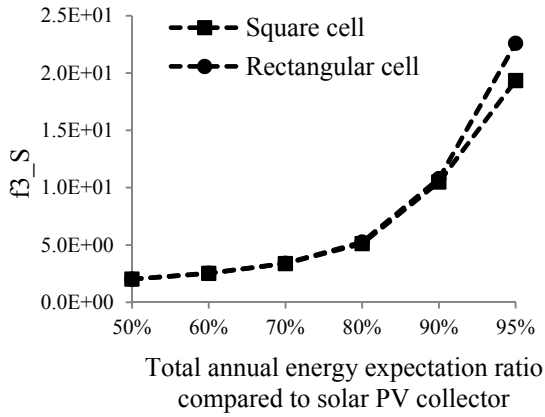
2.5E+01
2.0E+01
1.5E+01
1.0E+01
5.0E+00
0.0E+00
f3_S
Square cell
Rectangular cell
50%
60%
70%
80%
90%
95%
Total annual energy expectation ratio compared to solar PV collector

(i)

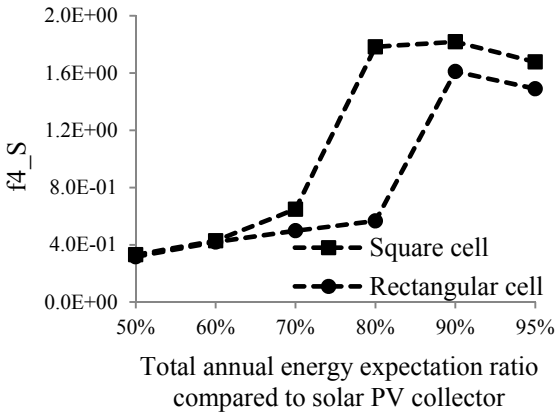
2.0E+00
1.6E+00
1.2E+00
8.0E-01
4.0E-01
0.0E+00
f4_S
Square cell
Rectangular cell
50%
60%
70%
80%
90%
95%
Total annual energy expectation ratio compared to solar PV collector

(j)

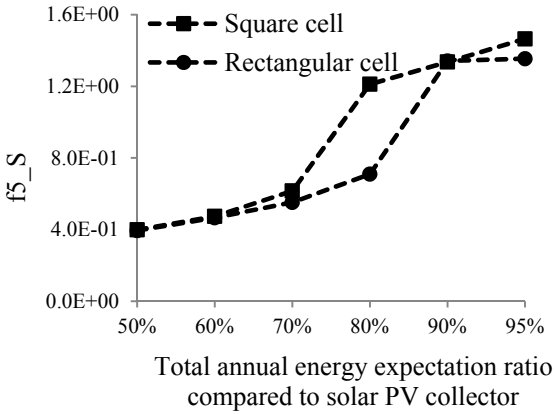
1.6E+00
1.2E+00
8.0E-01
4.0E-01
0.0E+00
f5_S
Square cell
Rectangular cell
50%
60%
70%
80%
90%
95%
Total annual energy expectation ratio compared to solar PV collector

(k)

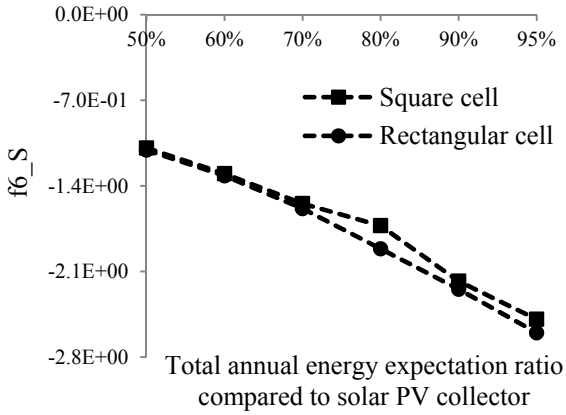
0.0E+00
-7.0E-01
-1.4E+00
-2.1E+00
-2.8E+00
f6_S
Square cell
Rectangular cell
50%
60%
70%
80%
90%
95%
Total annual energy expectation ratio compared to solar PV collector

(l)

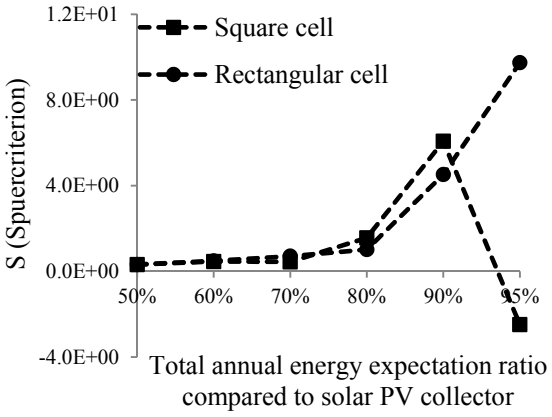
1.2E+01
8.0E+00
4.0E+00
0.0E+00
-4.0E+00
S (Spuercriterion)
Square cell
Rectangular cell
50%
60%
70%
80%
90%
95%
Total annual energy expectation ratio compared to solar PV collector

(m)

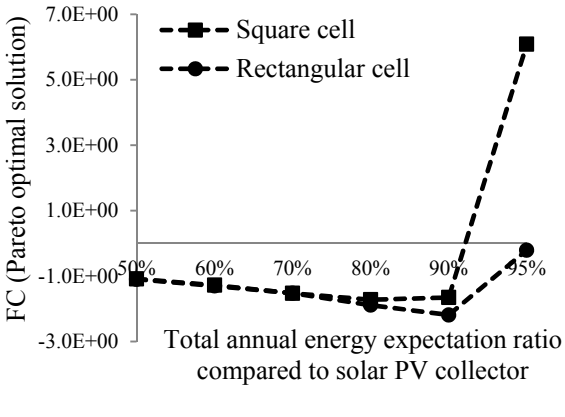
7.0E+00
5.0E+00
3.0E+00
1.0E+00
-1.0E+00
-3.0E+00
FC (Pareto optimal solution)
Square cell
Rectangular cell
50%
60%
70%
80%
90%
95%
Total annual energy expectation ratio compared to solar PV collector

(n)

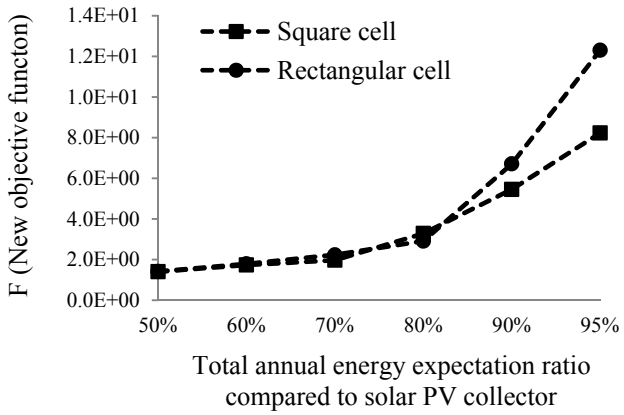

(o)

Figure 3-5 Variations of single objective function, Pareto optimal solution (FC), supercriterion (S), and new objective function ($F(\vec{Y})$) with respect to single objective function of (f1 ~ f6) annual incident solar energy

3.2.5 Compound parabolic concentrator (CPC) PV collector system

Solar CPC PV collector systems are capable of dealing with general situations under concentrated sunlight and issues resulting from higher cell operating temperatures; that is essential in utilizing concentrating systems as solar PV systems. Solar CPCs of PV concentrations have been considered for use in combination with solar cells.

3.2.5.1 Overview

The angle of incidence of the sun's ray on the concentrator is a main concern to collect as much sunlight as possible. Figures 3-6 show the geometry of a compound parabolic concentrator (CPC).

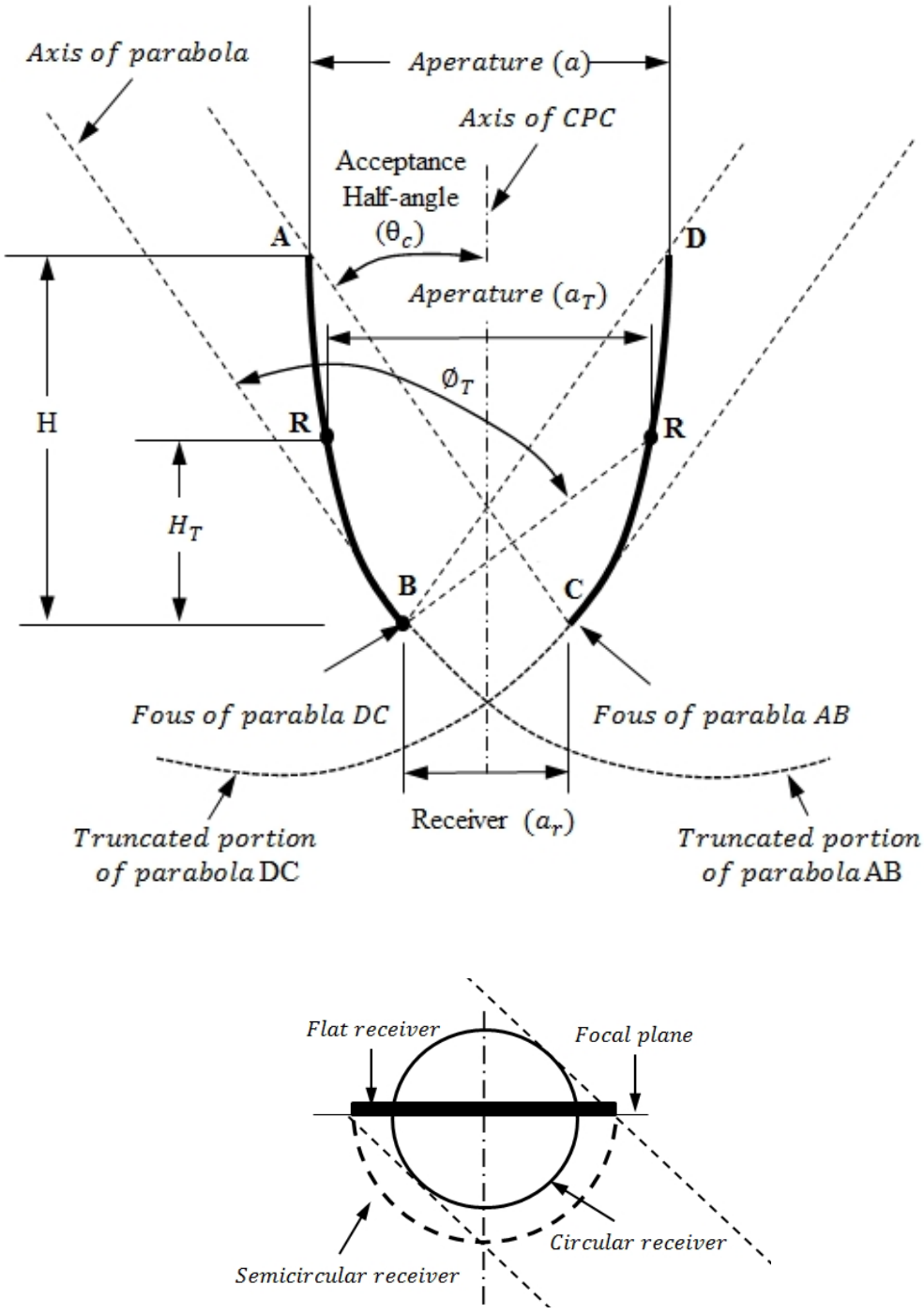

Figure 3-6 Cross section of compound parabolic concentrator and enlarged schematic of receiver with the different types of flat, circular, and semicircular shape

As seen in Fig. 3-6, the receivers of CPCs are largely divided into flat and circular shapes. In the case of a flat receiver, the geometry of CPC is designed by two main factors of the acceptance angle and the width of flat receiver. The relationships between the length of aperture and acceptance angle can be expressed by

$$\text{Length of aperture (a)} = \frac{\text{Width of flat recevier } (a_r)}{\sin(\text{acceptance angle } (\theta_c))} \tag{3-23}$$

and

$$\text{Height (H)} = \frac{\text{Width of flat recevier } (a_r) \times \left(1 + \frac{1}{\sin(\text{acceptance angle } (\theta_c))}\right)}{2\tan(\text{acceptance angle } (\theta_c))} \tag{3-24}$$

The focal length of the parabola can be written by

$$\text{Focal length of the parabola } (BC) = \frac{\text{Width of flat recevier } (a_r)}{2}(1 + \sin(a\text{cceptance angle } (\theta_c)) \tag{3-25}$$

Solar PV CPC is needed to reduce the depth of concentrator and the surface areas of reflection due to the cell performance because the reflected sections of the CPC are nearly parallel to the optical axis. Thus, the truncated CPCs attribute to an increase in the performance while decreasing the high cell operating temperature and ununiformed illumination from the sun.

Solar CPC PV collector systems are also used for increasing the intensity of sunlight for shake of improving the collector performance. Figure 3-7 shows that the number and size (area) of solar CPC PV collectors are associated with the installation area for the collectors.

In a multi-objective optimization of a solar CPC PV collector system, the main purpose of a solar CPC PV collector system design is to generate power obtaining maximum incident solar energy within a given (pre-specified) installation area. Thus, three single-objective functions can be designed as maximization of the annual monthly average incident solar energy (Q_{am}^{*}), maximization of the incident solar energy for the lowest month (Q_{lm}^{*}), and minimization of cost (C_{m}^{*}), - these are considered separately and simultaneously for a solar CPC PV array system.

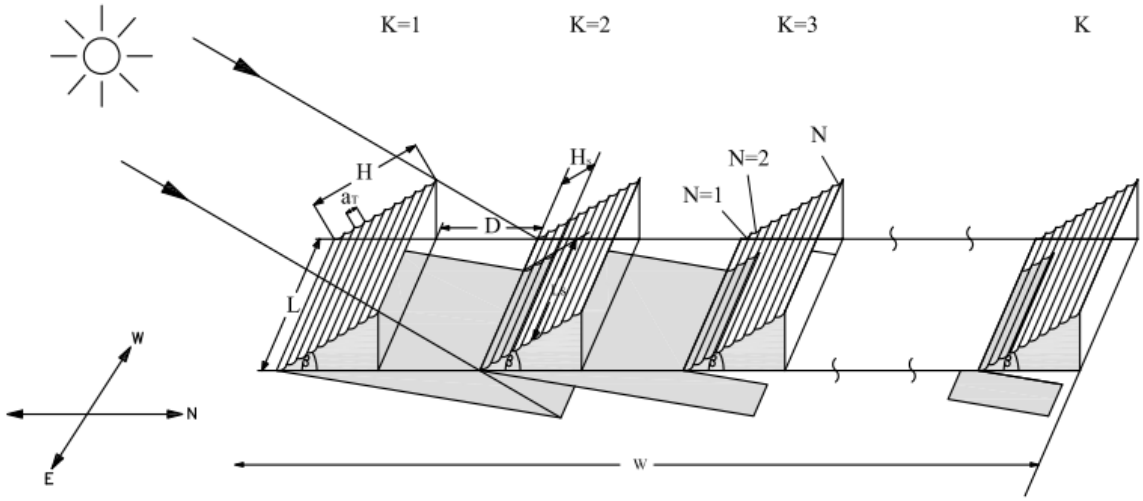

Figure 3-7 Multi-row CPC PV collector system in a given area

3.2.5.2 Formulation of optimization problems

The CPC unit for low concentration ratio has a receiver of length a_r, an acceptance angle of θ_c and is truncated at a height ratio r_T (the height of truncated CPC / the height

of full CPC). All the solar collectors are inclined at an angle β with respect to the horizontal. The design vector of the problem is given as:

$$\vec{X} = \{a_r \;\; \theta_c \;\; L \;\; \beta \;\; D \;\; K \;\; N \;\; r_T\}^T \tag{3.26}$$

The objective function for maximization is taken as:

$$Q = a_r \times L \times r_{cpc}^T \times N \times \left[q_b \tau_{cpc,b} + q_d \tau_{cpc,d} + (K-1)(q_b^{sh} \tau_{cpc,b} + q_d^{sh} \tau_{cpc,d})\right] \tag{3.27}$$

$$f_1(\vec{X}) = Q = \text{annual monthly average incident solar energy} \tag{3.28}$$

$$f_2(\vec{X}) = Q = \text{lowest incident solar energy} \tag{3.29}$$

where r_{cpc}^T can be calculated using Eqs. (3.30) ~ (3.37):

$$f = a_r(1 + sin\theta_c) \tag{3.30}$$

$$a = \; a_r / sin\theta_c \tag{3.31}$$

$$h = f cos\theta_c / sin^2\theta_c \tag{3.32}$$

$$a_T = \frac{f sin(\emptyset_T - \theta_c)}{sin^2(\emptyset_T/2)} - a_r \tag{3.33}$$

$$h_T = \frac{f cos(\emptyset_T - \theta_c)}{sin^2(\emptyset_T/2)} \tag{3.34}$$

$$r_T = \frac{h}{h_T} = \frac{\cos(\emptyset_T - \theta_c) sin^2(\emptyset_T/2)}{sin^2(\emptyset_T/2) cos\theta_c} \tag{3.35}$$

$$r_{cpc}^{full} = \frac{1}{sin\theta_c} = \frac{a}{a_r} \tag{3.36}$$

$$r_{cpc}^T = \frac{a_T}{a_r} \tag{3.37}$$

The expressions for computing $q_b, q_d,\ q_b^{sh}$ and q_d^{sh} are given Eq. (2.58) - Eq. (2.81) in chapter 2. For the constraints, the total length of individual collector (H) should be less than or equal to a given (specified) maximum value and the total width of the collectors should be less than or equal to the maximum width of the possible land:

$$KNa_T cos\beta + (K-1)D - W \leq 0 \tag{3.38}$$

The side constraints are taken as:

$$H = N \cdot a_T \leq H^{max} \tag{3.39}$$

$$a_r^{min} \leq a_r \leq a_r^{max} \tag{3.40}$$

$$\theta_c^{min} \leq \theta_c \leq \theta_c^{max} \tag{3.41}$$

$$0 \leq \beta \leq 90 \tag{3.42}$$

$$L_{min} \leq L \leq L_{max} \tag{3.43}$$

$$D_{min} \leq D \tag{3.44}$$

$$0 \leq r_T \leq 1 \tag{3.45}$$

$$1 \leq K \leq K_{max} \tag{3.46}$$

$$1 \leq N \leq N_{max} \tag{3.47}$$

$$1 \leq r_{cpc}^T \leq 3 \tag{3.48}$$

The cost objective function in the design of a solar CPC PV array system is formulated to include the costs of CPC PV collectors, reflectors and installation area. The cost objective function to be minimized can be expressed as:

$$f_3(\vec{X}) = \text{Cost} = \text{Cost}_{\text{PV}} + \text{Cost}_{\text{reflector}} + \text{Cost}_{\text{land}} \tag{3.49}$$

$$\text{Cost}_{\text{PV}} = \text{S}_1 \text{a}_{\text{T}} \text{L} \tag{3.50}$$

$$\text{Cost}_{\text{reflector}} = \text{S}_2 \text{A}_{\text{reflector}} \tag{3.51}$$

$$\text{A}_{\text{reflector}} = A_s(1 + \sin\theta_c)\left\{\frac{\cos\theta_c}{\sin^2\theta_c} + \log\left[\frac{(1+\sin\theta_c)(1+\cos\theta_c)}{\sin\theta_c[\cos\theta_c+\sqrt{2(1+\sin\theta_c)}]}\right] - \frac{\sqrt{2}\cos\theta_c}{(1+\sin\theta_c)^{1.5}}\right\} \tag{3.52}$$

$$\text{Cost}_{\text{land}} = \text{S}_3 \text{LW} \tag{3.53}$$

The optimal design of a solar CPC PV collector system is designed to efficiently collect and concentrate the sun's rays with the acceptance angle. Once the acceptance angle is adjusted, solar CPC PV collector systems are able to concentrate sunlight on the solar cells.

3.2.5.3 Numerical results

The single-objective optimizations of a solar CPC PV collector is illustrated by considering an illustrative example with the following data:

$a_r^{min} = 0.10\ (m)$, $a_r^{max} = 0.30\ (m)$, $\theta_c^{min} = 25\ (deg)$, $\theta_c^{max} = 90\ (deg)$, L_{min} = 15m, L_{max} = 30m, H_{min} = 0.5m, H_{max} = 2m, D_{min} = 0.8m, K_{max} = 150, N_{max} = 150, P = 80%, S_1 = 100 \$/m^2, S_2 = 20 \$/m^2, S_3 = 1/20/50 \$/m^2, $\tau_{cpc,b} = 1.0$, $\tau_{cpc,d}$ = 1.0

The solar CPC PV collector is assumed to face the equator (south) when being installed in a specific location, such as Miami (USA), where the latitude is 25.4°N and the altitude (A) is 5 m.

The starting design vector is given as:

$$\vec{X} = \{a_r \;\; \theta_c \;\; L \;\; \beta \;\; D \;\; K \;\; N \;\; r_T\}^T = \{0.10\ 40\ 25\ 40\ 1.0\ 70\ 10\ 0.5\}^T \qquad (3.54)$$

The results of the single-objective optimization problems, along with the initial design vector, are showed in Tables 3-6 (a) and (b).

Table 3-6 (a) Initial design and single-objective optimization results (design variables)

		Design variables							
Objectives		a_r (m)	θ_c (deg)	W (m)	β (deg)	D (m)	K	N	r_T
Initial		0.10	40.00	25.00	40.00	1.000	70	10	0.5000
Max f_1		0.11	89.54	30.00	52.98	0.806	100	9	0.0036
Max f_2		0.17	89.82	29.98	53.79	0.807	101	6	0.4160
Min f3	s_3=1	0.11	25.62	28.81	21.69	0.802	76	4	0.6136
	s_3=20	0.14	25.03	29.37	21.26	0.800	69	4	0.2622
	s_3=50	0.25	89.97	29.48	20.35	0.801	64	4	0.0012

Table 3-6 (b) Initial design and single-objective optimization results (objective functions and other outputs)

Objectives and other outputs						
Objectives		cpc ratio	f 1 $(10^6 \times W)$	f 2 $(10^6 \times W)$	f 3 $(10^6 \times W)$	f3/f1 ($/W)
Initial		1.4450	1.2675	1.0230	0.5517	0.4353
Max f_1		1	1.3790	1.1462	0.7190	0.5214
Max f_2		1	1.3778	1.1480	0.7257	0.5267
Min f_3	s_3=1	2.1921	1.1032	0.8421	0.3063	0.2776
	s_3=20	1.7963	1.1032	0.8833	0.4007	0.3632
	s_3=50	1	1.1032	0.8927	0.4689	0.4250

- Maximization of annual monthly average incident solar energy (f_1)

It can be seen that the optimum value of the truncation ratio (r_T) reaches zero value for the optimization problem involving the minimization of f_1; this indicates that the optimum solar CPC PV collector is entirely truncated. As a result, the optimum values of the design variables L, β, D, and K tend to be similar to the results of a flat plate solar PV array system those gained in the case of flat plate solar PV collectors.

- Maximization of lowest month incident solar energy (f_2)

The objective problem of lowest month incident solar energy (f_2) tends to derive similar results to the design variables of f_1 except for the value of the truncation ratio (r_T). The value of the truncation ratio for f_2 is larger than the value of the truncation ratio of

f_1 because seasonal characteristics are reflected in the CPC collectors as being less truncated.

- Minimization of cost (f_3)

In Tables 3-9 (b), the cost per unit watt ($/W), corresponding to the minimizations of f_1 and f_2 are 0.5214 and 0.5267, respectively, while the value reduces to 0.2776 in the case of minimization of f_3 for s_1=1. The outcomes mean that the significant objective in designing solar CPC PV collector systems is to reduce the cost per unit energy instead of collecting more solar energy.

With the results of single-objective optimizations, a multi-objective optimization problem is formulated and solved using the modified game theory.

- Results with no constraint on the CPC ratio

Using the results of single-objective optimization problems, the multi-objective optimization problem is generated and solved using the modified game theory approach and the results are listed in Tables 3-7. An observation on the variation of the weights (C_1, C_2, and C_3) used in the Pareto optimal solutions indicates that f_1 is dominant in the case of multi-objective optimization for s_3=1. However, f_2 is dominant in the multi-objective optimization for s_3 =20 and 50. In the solution of the multi-objective optimization problem with s_3=1 (shown in Table 3-10), the weights of f_2 and f_3 at the optimum are found to be between 0.54 % and 0.06 %, respectively. Hence, the results of the multi-objective optimization problem are distant from the optimum solutions given by the single-objective optimization problems of f_2 and f_3.

Table 3-7 (a) Results of multi-objective optimization (design variables)

Multi-objective	Design variables							
	a_r (m)	θ_c (deg)	W (m)	β (deg)	D (m)	K	N	r_T
s_3=1	0.14	89.95	30	36.15	0.805	84	7	0.0410
s_3=20	0.26	89.84	30	36.41	0.805	90	3	0.0543
s_3=50	0.17	89.86	29.84	35.08	0.887	79	6	0.0371

Table 3-7 (b) Results of multi-objective optimization (objective functions and other outputs)

Multi-Obj.	Objectives and other outputs							
	cpc ratio	f 1 ($10^6 \times W$)	f 2 ($10^6 \times W$)	f 3 ($10^6 \times W$)	Game theory			
					Overall	C_1	C_2	C_3
s_3=1	1	1.3710	1.1073	0.6146	0.19297	0.9939	0.0054	0.0006
s_3=20	1	1.3368	1.1011	0.5984	0.09476	0.0276	0.9664	0.0038
s_3=50	1	1.3228	1.0856	0.5879	0.08074	0.0798	0.9145	0.0057

- Results with a constraint on the CPC ratio

As observed earlier (from the results given in Tables 3-6 (a) and 3-6 (b)), the maximization of the annual monthly average incident solar energy results in nearly a flat plate solar collector as the best system. In order to achieve a solar CPC collector, the optimization problems are solved by adding more constraints to the CPC ratio so that the minimum ratio should be at least 1.2, along with the rest of the constraints.

Tables 3-8 (a) and (b) show the results of the three single-objective optimization cases, along with the values of initial design variables. It can be seen that the optimum values of the CPC ratio reach the value of lower bound of 1.2 in the minimizations of f_1 and f_2. Thus, the cost associated with the minimization of f_1 or f_2 has been slightly reduced compared to the corresponding optimum value without the additional constraint. The result of the minimization of f_3 shows the same result given in Table 3-8 (without the additional constraint). The cost per unit watt ($/W) of power associated with the minimization of f_3 is still much lower than those of the optimization of the first two objective functions for s_3=1.

Table 3-8 (a) Initial design and single-objective optimization results (design variables) (with constraint on CPC ratio)

		Design variables							
Objectives		a_r (m)	θ_c (deg)	W (m)	β (deg)	D (m)	K	N	r_T
Initial		0.10	40.00	25.00	40.00	1.000	70	10	0.5000
Max f_1		0.138	50.66	30.00	31.09	0.803	80	6	0.4107
Max f_2		0.202	37.32	30.00	48.08	0.882	92	4	0.1365
Min f_3	s_3=1	0.119	27.17	28.73	21.75	0.800	73	4	0.6610
	s_3=20	0.134	25.23	29.00	21.46	0.800	69	4	0.2638
	s_3=50	0.263	28.45	26.56	20.90	0.800	73	3	0.0683

Table 3-8 (b) Initial design and single-objective optimization results (objectives functions and other outputs) (with constraint on CPC ratio)

Objectives and other outputs						
Objectives		cpc ratio	f 1 $(10^6 \times W)$	f 2 $(10^6 \times W)$	f 3 $(10^6 \times W)$	f3/f1 ($/W)
Initial		1.4450	1.2675	1.0230	0.5517	0.4353
Max f_1		1.201	1.3404	1.0760	0.5204	0.3882
Max f_2		1.203	1.3021	1.0966	0.5685	0.4366
Min f_3	s_3=1	2.1054	1.1240	0.8451	0.3177	0.2826
	s_3=20	1.7878	1.0724	0.8614	0.3904	0.3640
	s_3=50	1.2096	1.0724	0.8735	0.4608	0.4297

The results of multi-objective optimization with the extra constraint are shown in Tables 3-9. The results show features that are different from those given in Tables 3-8 without the additional constraint on the CPC ratio. The values of the objective functions can be seen to increase slightly in the present case for $s_3 = 1$. However, for $s_3 = 20$ and 50, the objective functions of f_1 and f_2 increase and the objective function of f_3 decreases compared to those of Table 3-9. The objective function of f_3 is found to dominate in the multi-objective optimization solution in the cases of $s_3 = 20$ and 50. The values of the CPC ratio at the optimum point vary in the range of 1.24 – 1.76 in the present case.

Table 3-9 (a) Results of multi-objective optimization (design variables) (with constraint on CPC ratio)

Design variables									
Multi-objective		a_r (m)	θ_c (deg)	W (m)	β (deg)	D (m)	K	N	r_T
	s_3=1	0.145	52.94	30.00	40.77	0.84	91	5	0.8034
	s_3=20	0.102	26.05	29.07	21.95	0.80	73	5	0.2765
	s_3=50	0.224	29.75	29.13	14.16	0.95	70	3	0.1492

Table 3-9 (b) Results of multi-objective optimization (objective functions and other outputs) (with constraint on CPC ratio)

Objectives and other outputs								
Multi-Obje.	cpc ratio	f 1 ($10^6 \times W$)	f 2 ($10^6 \times W$)	f 3 ($10^6 \times W$)	Game theory			
					Overall	C_1	C_2	C_3
s_3=1	1.245	1.2848	1.0815	0.7297	0.09356	0.4018	0.4784	0.1198
s_3=20	1.766	1.0723	0.8702	0.5035	0.04386	0.0043	0.0225	0.9732
s_3=50	1.372	1.0743	0.8439	0.4839	0.33402	0.0733	0.0833	0.8434

3.2.5.4 Sensitivity analyses

In the single-objective optimization problem of f_1, the results provide almost a flat-plate solar PV array system design which has a maximum annual monthly average incident solar energy of $Q_{am}^{*} = 1.3790 \times 10^6$ W (the solar constant: 1367 W/m^2). The main reason for considering the optimum design of a solar CPC PV collector system is to reduce the overall cost and the cost per unit energy of a solar energy system. Thus, this section investigates the sensitivity analyses with respect to the energy output expectation

ratio or lower bound on Q (P), mathematically formulated as Q/Q^*_{am}, in the range of 70% to 100%. Sensitivity analyses with respect to lower values of P (less than 70%) have limited significance and, hence, are excluded from the present study. The price of installation land (s_3) will be various because these solar CPC PV collectors depend on a specific location (a rural place or an urban area). Three different levels of land prices—low with s_3 = 1 \$/m^2, medium with s_3 = 20 \$/m^2 and high with s_3 = 50 \$/m^2—are reflected and compared in the sensitivity analyses. Thus, the effects of the design variables as well as the CPC ratio and the cost are investigated in this section.

Figures 3-8 (a) – (h) show the variations observed in the optimum design variable values with respect to the changes in the value of P under different land prices, respectively. The vertical axis indicates the optimum values of different design variables and the horizontal axis represents the value of P in the range from 70% to 100%.

1. Variation of x_1

Figure 3-8 (a) presents the variation of design variable x_1, namely the length of the receiver, is presented in Figure 3-8 (a). In this figure, most of the optimum values stay at the top of the graph around a value of 0.167 m for s_3= 50. The optimum values of the length of the receiver for both s_3= 1 and s_3= 20 vary similarly as P varies from 70% to 100%. In particular, the value of a_r attains its lower bound value when P is in the range of 75% to 85%. When the values of P are close to 70% or more than 95%, larger values of the length of the receiver (and hence larger CPCs) are predicted.

2. Variation of x_2

The variation of the design variable x_2, namely half of the acceptance angle is shown in Fig. 3-8 (b). This design variable (angle) remains essentially constant at its lower bound

value (25 degree) when the value of P is less than about 85% for s_3= 1 and 20. When the value of P increases to 90% (for s_3= 20) and 95% (for s_3= 1), the optimum value increases dramatically and both the curves converge to a value of approximately 90 degrees at the value of P equal to 100%. However, for s_3= 50, the value of half the acceptance angle remains constant for all values of P at about 90 degrees.

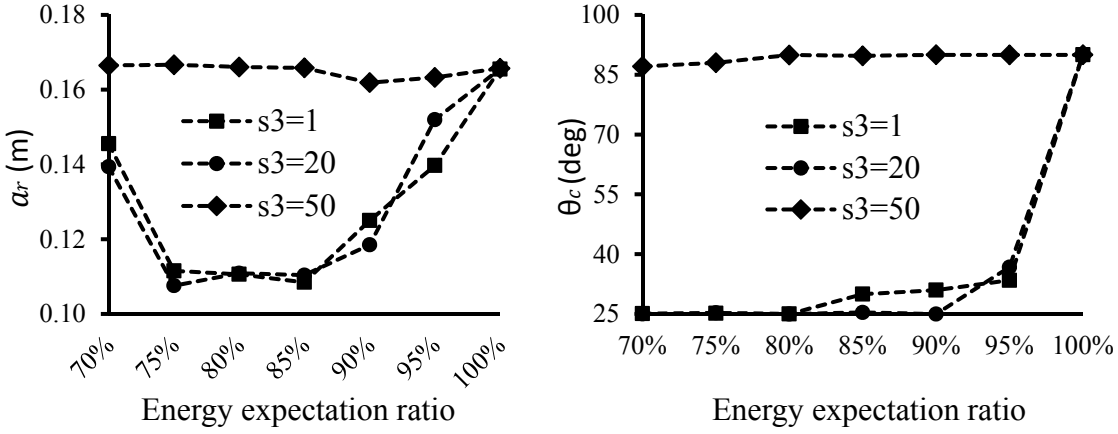

(a)

(b)

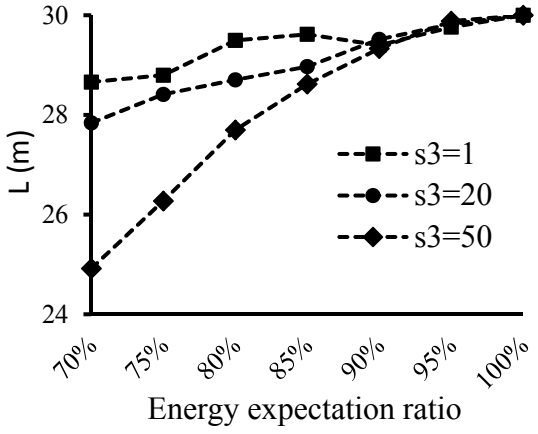

(c)

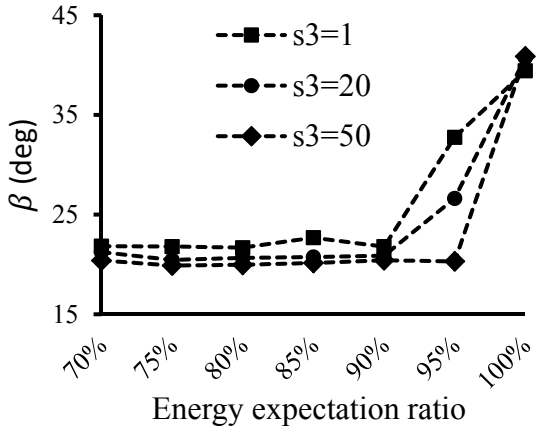

(d)

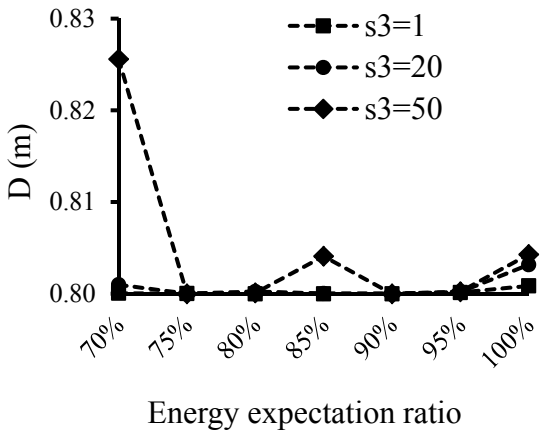

(e)

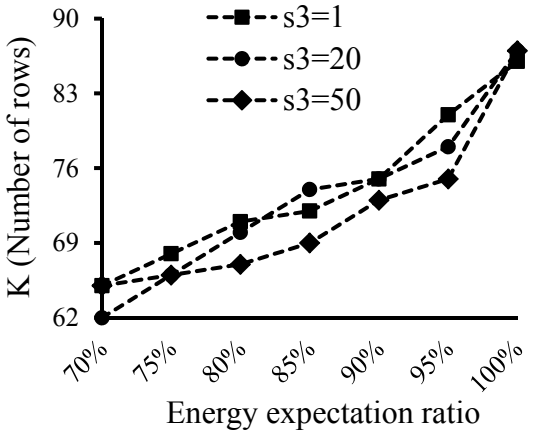

(f)

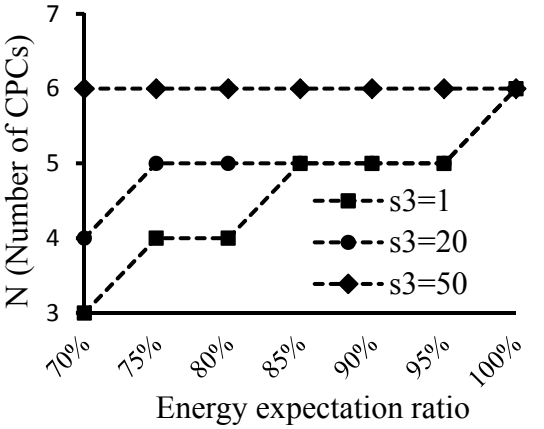

(g)

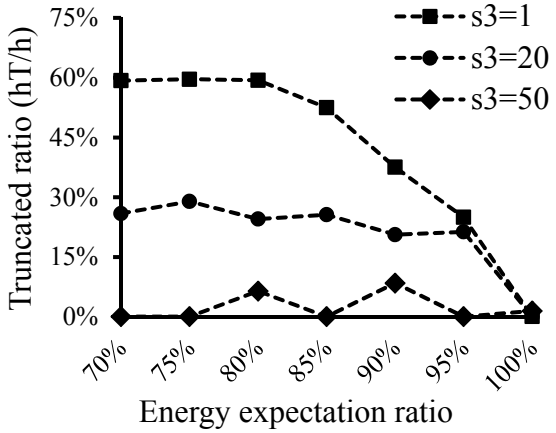

(h)

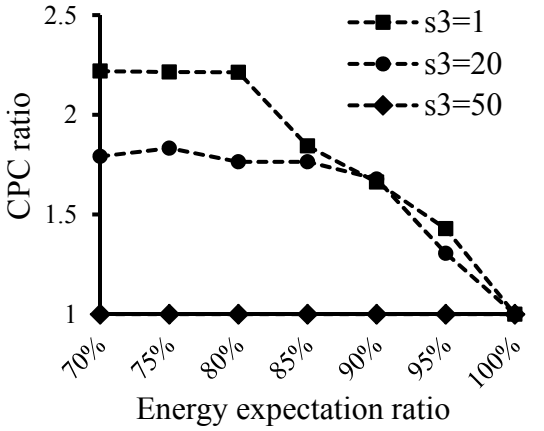

(i)

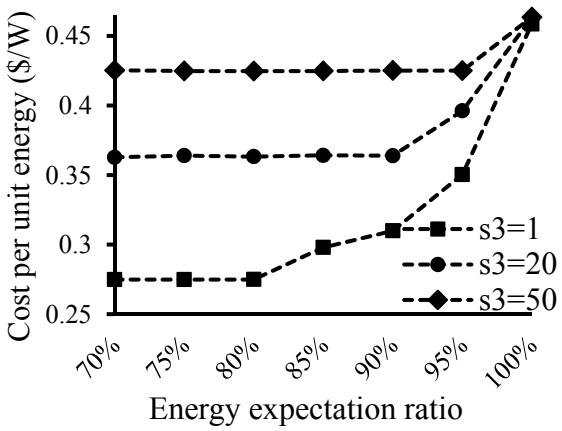

(j)

Figure 3-8 Sensitivity analysis with respect to P and s_3

3. Variation of x_3

Figure 3-8 (c) presents the variation of x_3, namely the width of the CPC solar panel. The results indicate that the design variable increases nearly linearly towards its upper bound value as the energy expectation ratio (P) increases from 70% to 100% for low to medium land prices (s_3= 1 and 20). However, when the unit price of land is high, the optimum values of x_3 no longer reach the upper limit at relatively lower energy expectation ratios. Thus, higher unit prices of land leads to lower optimum values of x_3 at any given energy expectation ratio (P) smaller than 90%.

4. Variation of x_4

Figure 3-8 (d) demonstrates the variation of the optimum values of the design variable x_4, the inclination angle β. When the energy expectation ratio lies between 70% and 90%, the optimum values of x_4 fluctuate in the range of 20 to 23 degrees for all values of the land price. As the energy output expectation ratio (P) approaches 100%, the optimum values tend to shift towards those of a flat plate solar collector design. As a result, the optimum values suddenly shoot to nearly 40 degrees, which is much larger than the values obtained for smaller values of P.

5. Variation of x_5

Figure 3-8 (e) presents the variation of the optimum values of the design variable x_5, namely the distance between two neighboring rows. It is clear that the optimum values remain essentially at the lower bound value when the unit price of land is low or medium. In contrast, when the unit price of land is high, the distance between two neighboring rows no longer adheres to the lower limit value; it rapidly decreases from a value of 0.83

m to 0.80 m as P increases from 70% to 75%. Beyond a value of P = 75%, the value of x_5 varies slightly about the lower bound value of 0.80 m.

6. Variation of x_6

Figure 3-8 (f) shows the variation of the optimum values of the design variable x_6, namely, the number of rows. With relatively lower energy output expectation ratios, fewer rows are needed for optimum design. The variation of the number of CPC units in one panel (x_7) is shown in Figure 3-8 (g).

7. Variation of x_7

For high land prices (s_3= 50), the design variable x_7 remains at its upper bound value of 6. For low and medium land values (s_3= 1 and 20), the values of x_7 increase from 4 to 6 and 3 to 6, respectively, as the value of P increases from 70 % to 100 %.

8. Variation of x_8

Figure 3-8 (h) provides the variation of the design variable x_8, namely truncation ratio of CPC. It is clear that the height of the truncated CPC is less than 30 % of the height of the full CPC when the land prices are low (s_3= 1) or medium (s_3= 20) for all values of P. However, for high land prices (s_3= 50), the truncation ratio of the optimum CPC units reduces from 60 % to nearly 0 % (flat plate) as P increases from 70 % to 100 %.

Figure 3-8 (i) gives the variation of the CPC ratio with respect to the optimum energy output expectation ratio under different unit prices of land. For high land prices (s_3= 50), the CPC ratio remains at 1 (corresponding to that of a flat plate collector) for all values of P. In the case of low and medium land prices (s_3= 1 and 20), the CPC ratio decreases from a value of 2.2 to 1 and 1.8 to 1, respectively, as the energy output expectation ratio

(P) increases from 70% to 100%. Finally, Figure 3-8 (j) presents the relationship between the cost per unit energy and the energy expectation ratio (P) under different unit prices of land. It can be seen that the three curves are nearly parallel to one another for values of P in the range 70 % to 80 %. For medium and high unit prices of land, the cost per unit energy is almost constant when the value of the energy output expectation ratio is smaller than 90%. Similarly, for a low land price, the cost per unit energy is constant for values of P up to 80%. As the value of energy output expectation ratio increases to more than 90 % (in the case of s_3= 20 and 50) and 80% (in the case of s_3= 1), the cost per unit energy starts to increase at a faster rate. The value continuously increases until it reaches a peak value, when the energy output expectation ratio (P) assumes a value of 100 %.

3.2.6 Fuzzy set theory-based optimization

Conventional optimization methods assume that the data are known, that constraints delimit as a crisp set of feasible decisions, and that objectives are defined and easy to formulate. The optimization process involves the selection of the design variables which optimize the objective function subject to the satisfaction of the constraints.

The crisp multi-objective optimization problem is stated as follows:

Find X

$$\vec{X} = [x_1, x_2, \ldots, x_l]^T \tag{3.55}$$

Which maximize or minimize the objective function f ($\vec{X}$)

subject to the constraints

$$g_i(\vec{X}) \leq 0, \qquad i = 1, 2, \dots, m \tag{3.56}$$

$$a_j \leq x_j \leq b_j, \qquad j = 1,2, \dots, l \tag{3.57}$$

where $g_i(\vec{X})$ and $l_i(\vec{X})$ are the inequality and equality constraints, respectively. x_j is the j^{th} design variable, and a_j and b_j are the lower and upper bounds on the j^{th} design variables, respectively.

The fuzzy domain corresponding to the objective functions and the constraints can be defined as

$$D = \left\{\cap_{i=1}^{k} \mu_{f_i}(X)\right\} \cap \left\{\cap_{j=1}^{m} \mu_{g_j}(X)\right\} \tag{3.58}$$

with

$$\mu_d(X^*) = \max \left\{\mu_{f_i}(X), \mu_{g_j}(X)\right\} \tag{3.59}$$

where $\mu_{f_i}(X)$ and $\mu_{g_j}(X)$ denote the membership functions of the jth constraint functions, respectively. The optimum solution X^* is selected such that

$$\mu_d(X^*) = \max \{\mu_D(X)\} \tag{3.60}$$

Computational procedure

The solution for the multi-objective fuzzy optimization problem can be found by (1) finding the solutions of the individual single-objective optimization problems, (2) determining the best and worst solutions possible for each of the objective functions, (3) using these solutions as boundaries of the fuzzy ranges in the corresponding fuzzy

optimization problem, and (4) solving the resulting fuzzy optimization problem. The details are indicated in the following step-by-step procedure.

1. Starting from design vector X_s, minimize the individual objective function $f_i(X)$ subject to the constraints $g_j(X) \leq b_j,\ j = 1,2,\dots,m$ using ordinary optimization procedures. Let the solution be $X_i^*,\ i = 1,2,\dots,k$.
2. Construct as matrix $[P]$ as

$$[\mathrm{P}] = \begin{bmatrix} f_1(X_1^*) & f_2(X_1^*) & \dots & f_k(X_1^*) \\ f_1(X_2^*) & f_2(X_2^*) & \dots & f_k(X_2^*) \\ & \cdot & & \\ & \cdot & & \\ & \cdot & & \\ f_1(X_k^*) & f_2(X_k^*) & \dots & f_k(X_k^*) \end{bmatrix} \tag{3.61}$$

   It can be found that the diagonal elements in the matrix [P] are the optimum value (best) in the respective columns.
3. The minimum and maximum possible values of the objective functions are identified as

$$\left.\begin{matrix} f_i^{min} = \min_j f_i(X_j^*) = f_i(X_i^*) \\ f_i^{max} = \max_j f_i(X_j^*) \end{matrix}\right\},\quad i = 1,2,\dots,k \tag{3.62}$$

4. From the extreme values of f_i determined in equation (3.56), the membership functions of the fuzzy objective functions are constructed as

$$\mu_{f_i}(X) = \begin{cases} 0, & if\ f_i(X) > f_i^{max} \\ \left(\frac{-f_i(X)+f_i^{max}}{f_i^{max}-f_i^{min}}\right), & if\ f_i^{min} < f_i(X) \leq f_i^{max} \\ 1, & if\ f_i(X) \leq f_i^{min} \end{cases} \tag{3.63}$$

5. The fuzzy constraints can be stated as

$$g_j(X) \leq b_j + d_j\ ,\ j = 1,2,\dots,m \tag{3.64}$$

where d_j denotes the distance by which the boundary of the jth constraint is moved. The membership function of the jth constraint can be defined as

$$\mu_{g_j}(X) = \begin{cases} 0, & if\ g_j(X) > b_j + d_j \\ 1 - \left\{\frac{g_j(X) - b_j}{d_j}\right\}, & if\ \ b_j \leq g_j(X) \leq d_j,\ \ j = 1,2,\dots,m \\ 1, & if\ g_i(X) \leq b_j \end{cases} \tag{3.65}$$

6. By considering the optimum solution as the intersection of the membership functions of the objective functions and constraints, the solution for the fuzzy multi-objective optimization problem can be found by determining X and λ, which maximize λ subject to

$$\left.\begin{matrix} \lambda \leq \mu_{f_i}(X),\ \ i = 1,2,\dots,k \\ \lambda \leq \mu_{g_j}(X),\ \ j = 1,2,\dots,m \end{matrix}\right\} \tag{3.66}$$

This problem can be addressed using ordinary single-objective non-linear programing techniques.

3.2.6.1 Formulation of optimization problems

- Solar cell

The results of deterministic optimization problems for a solar cell are used to formulate membership functions of the objectives for multi-objective fuzzy optimization. The individual deterministic single-objective optimization problems of the maximization of conversion efficiency and power output are solved by using *ga* (MATLAB) to find the

global minima in terms of mixed-integer variables starting from a set of initial design vectors. To prevent unreasonably small value of conversion efficiency, a lower bound on the conversion efficiency of 80 % of the maximum conversion efficiency ($\eta \geq 0.8\,\eta^*_{ma}$) is used as a behavior constraint on both square and rectangular cells. It is to be noted that due to the realized constraint on the minimum permissible conversion efficiency, the value of the maximum power output is restricted. The best and worst values of the single-objective optimization problems are found for constructing the membership functions used in formulating the constraints on the multi-objective fuzzy optimization of the solar cell. The constraints are given below. Table 3-0 shows the results of design variables of single-objective problems. Based on the results of two single-objective problems including conversion efficiency and power output of solar cells, the triangular membership function can be expressed as shown in Table 3-11.

Table 3-10 Values of design variables and objective functions of single-objective optimizations

Objective		Design variables										
		T_e (μm)	T_b (μm)	L_c (cm)	H_c (cm)	W_f (μm)	H_f (μm)	N_f	W_b (μm)	H_b (μm)	N_b	C
Initial	Sq.	6.00	200	2	2	60	10	20	303	8	4	12
	Rec.	6.00	220	3	2	60	10	15	600	8	3	10
$\overrightarrow{x^*}_{f_1}$	Sq.	7.31	244.41	0.81	0.81	20.00	5.00	18	101.78	6.00	2	6
	Rec.	7.62	208.01	2.45	0.50	20.03	5.01	12	100.26	6.00	3	6
$\overrightarrow{x^*}_{f_2}$	Sq.	5.51	181.02	4.93	4.93	71.55	17.88	87	368.48	18.89	10	24
	Rec.	5.18	282.17	5.00	2.90	65.80	16.44	64	337.18	17.43	10	40

Objective	Square cell		Rectangular cell	
	f_1(%)	f_2(W)	f_1(%)	f_2(W)
Initial	17.84	0.8563	17.02	1.2010
$\overrightarrow{x^*}_{f_1}$	0.2028	0.0798	0.2054	0.1514
$\overrightarrow{x^*}_{f_2}$	0.1622	9.4615	0.1643	9.5448

Table 3-11 Triangular membership function of objectives of solar cells

Objective		Membership function (Fuzzy)		
		$\mu = 0$	$\mu = 1$	d_i
f_1	Sq.	0.0798	0.2028	4.0539
	Rec.	0.1514	0.2054	4.1065
f_2	Sq.	0.1622	9.4615	9.3817
	Rec.	0.1643	9.5448	9.3934

For a square cell,

Constraints on the objective functions:

$$\mu_{f_1}(\mathrm{X}) = \begin{cases} 0 & if \quad f_1(x) \le 0.162189 \\ \frac{-f_1(x)+0.202728}{4.0539} & if \ 0.162189 < f_1(x) < 0.202728 \\ 1 & if \quad f_1(x) \ge 0.202728 \end{cases} \tag{3.67}$$

$$\mu_{f_2}(\mathrm{X}) = \begin{cases} 0 & if \quad f_2(x) \le 0.0798 \\ \frac{-f_2(x)+9.4615}{9.3817} & if \quad 0.0798 < f_2(x) < 9.4615 \\ 1 & if \quad f_2(x) \ge 9.4615 \end{cases} \tag{3.68}$$

Membership functions corresponding to the constraints and design variables:

$$\mu_{\sigma_i}(X) = \begin{cases} 0, & if\ \sigma_i(X) > b_i + d_i \\ 1 - \left\{\frac{g_i(X) - b_i}{d_i}\right\}, & if\ \ b_i \le \sigma_i(X) \le d_i,\ \ i = 1,2,\dots,10 \\ 1, & if\ \sigma_i(X) \le b_i \end{cases} \quad (3.69)$$

For a rectangular cell,

Constraints on objective functions:

$$\mu_{f_1}(\mathrm{X}) = \begin{cases} 0 & if \quad f_1(x) \le 0.16430 \\ \frac{-f_1(x) + 0.20537}{4.1065} & if\ 0.164303 < f_1(x) < 0.20537 \\ 1 & if \quad f_1(x) \ge 0.20537 \end{cases} \quad (3.70)$$

$$\mu_{f_2}(\mathrm{X}) = \begin{cases} 0 & if \quad f_2(x) \le 0.1514 \\ \frac{-f_2(x) + 9.5448}{9.3934} & if \quad 0.1514 < f_2(x) < 9.5448 \\ 1 & if \quad f_2(x) \ge 9.5448 \end{cases} \quad (3.71)$$

Membership functions corresponding to the constraints and design variables:

$$\mu_{\sigma_i}(X) = \begin{cases} 0, & if\ \sigma_i(X) > b_i + d_i \\ 1 - \left\{\frac{g_i(X) - b_i}{d_i}\right\}, & if\ \ b_i \le \sigma_i(X) \le d_i,\ \ i = 1,2,\dots,10 \\ 1, & if\ \sigma_i(X) \le b_i \end{cases} \quad (3.72)$$

It is observed that the results of maximum conversion efficiency (η^*_{max}) influence power output with decreases in the size of solar cells. The results tend to vary in terms of cost because of the restriction of minimum incident solar energy of average month as $\eta \ge 0.7\ \eta^*_{max}$. Between incident solar energies of annual monthly average and lowest month, the results of design variables show a significant gap in the values of design variables. Maximum power output and incident solar energy of highest month have similar variations in the results of respective single-objective optimization problem in order to collect the maximum amount of incident solar energy with a given size and number of

arrays. Similarly, the relationship between cost, power output and incident solar energy highest month is associated with the size of arrays.

- Flat plate PV array system

The solution for multi-objective fuzzy optimization problems according to the λ-formulation can be found after determining the results of single-objective optimization, as shown in Table 3-12, for formulating fuzzy membership functions. Table 3-13 shows the results of triangular membership function of objectives of a solar PV array system.

Table 3-12 Initial design parameters and single-objective optimization results

Results of single objective optimization							
Objective		f_1(%)	f_2(W)	f_3(W)	f_4(W)	f_5(W)	f_6($)
Ini.	Sq.	14.66	1.7589E+05	3.0558E+05	2.7771E+05	3.2766E+05	3.5085E+05
	Rec.	14.66	1.7589E+05	3.0558E+05	2.7771E+05	3.2766E+05	3.5085E+05
$\overrightarrow{x^*}_{f_1}$	Sq.	18.30	5.8949E+05	7.2236E+05	6.1397E+05	8.2993E+05	9.5238E+05
	Rec.	18.30	5.0151E+05	6.9819E+05	5.3715E+05	7.9721E+05	8.0549E+05
$\overrightarrow{x^*}_{f_2}$	Sq.	17.37	1.0636E+06	9.3731E+05	6.6781E+05	1.2306E+06	1.7929E+06
	Rec.	17.55	1.0639E+06	9.4193E+05	6.7530E+05	1.2363E+06	1.7755E+06
$\overrightarrow{x^*}_{f_3}$	Sq.	15.84	6.7873E+05	9.8842E+05	7.9968E+05	1.1447E+06	1.2543E+06
	Rec.	15.00	6.0420E+05	9.8556E+05	7.9368E+05	1.0986E+06	1.1629E+06
$\overrightarrow{x^*}_{f_4}$	Sq.	13.25	6.0190E+05	9.5561E+05	8.0018E+05	1.1520E+06	1.3343E+06
	Rec.	17.54	8.0130E+05	9.4654E+05	8.0071E+05	1.1460E+06	1.3428E+06
$\overrightarrow{x^*}_{f_5}$	Sq.	16.82	9.6936E+05	9.4628E+05	6.9869E+05	1.2346E+06	1.6893E+06
	Rec.	17.26	1.0297E+06	9.4651E+05	6.8982E+05	1.2364E+06	1.7477E+06
$\overrightarrow{x^*}_{f_6}$	Sq.	15.09	4.0811E+05	6.9545E+05	5.6781E+05	7.6333E+05	7.8265E+05
	Rec.	15.48	4.1828E+05	6.9545E+05	5.7226E+05	7.6160E+05	7.8309E+05

Table 3-13 Triangular membership function of objectives of solar PV array system

Obj.		Membership function (Fuzzy) $\mu = 0$	$\mu = 1$	d_i
f_1	Square	0.1325	0.1830	0.0478
	Rectangular	0.1501	0.1830	0.0330
f_2	Square	4.08110E+05	1.06365E+06	655537.519
	Rectangular	4.18284E+06	1.06389E+06	645606.026
f_3	Square	6.95449E+05	9.88416E+05	292966.883
	Rectangular	6.95450E+05	9.85558E+05	290107.739
f_4	Square	5.67810E+05	8.00180E+05	232374.701
	Rectangular	5.37152E+05	8.00711E+05	263558.941
f_5	Square	7.63325E+05	1.23462E+06	471294.601
	Rectangular	7.61597E+05	1.23636E+06	474764.089
f_6	Square	7.82650E+05	1.79293E+06	1010280.759
	Rectangular	7.83137E+05	1.77547E+06	992332.999

With the results of the best and worst solutions for individual single-objective functions, membership functions can be constructed and expressed.

For a square cell,

Constraints on objective functions:

$$\mu_{f_1}(\mathrm{X}) = \begin{cases} 0 & if \quad f_1(x) \le 0.1325 \\ \frac{-f_1(x)+0.1830}{0.0478} & if \quad 0.1325 < f_1(x) < 0.1830 \\ 1 & if \quad f_1(x) \ge 0.1830 \end{cases} \tag{3.73}$$

$$\mu_{f_2}(\mathrm{X}) = \begin{cases} 0 & if \quad f_2(x) \le 4.08110E{+}05 \\ \frac{-f_2(x)+1.06365E+06}{655537.519} & if \quad 4.08110E{+}05 < f_2(x) < 1.06365E{+}06 \\ 1 & if \quad f_2(x) \ge 1.06365E{+}06 \end{cases} \tag{3.74}$$

$$\mu_{f_3}(\mathrm{X}) = \begin{cases} 0 & if \quad f_3(x) \le 6.95449E{+}05 \\ \dfrac{-f_3(x)+9.88416E{+}05}{292966.883} & if \ 6.95449E{+}05 < f_3(x) < 9.88416E{+}05 \\ 1 & if \quad f_3(x) \ge 9.88416E{+}05 \end{cases} \tag{3.75}$$

$$\mu_{f_4}(\mathrm{X}) = \begin{cases} 0 & if \quad f_4(x) \le 8.00184E{+}05 \\ \dfrac{-f_4(x)+8.00184E{+}05}{232374.701} & if \ 5.67810E{+}05 < f_4(x) < 8.00184E{+}05 \\ 1 & if \quad f_4(x) \ge 5.67810E{+}05 \end{cases} \tag{3.76}$$

$$\mu_{f_5}(\mathrm{X}) = \begin{cases} 0 & if \quad f_5(x) \le 7.63325E{+}05 \\ \dfrac{-f_5(x)+1.23462E{+}06}{471294.601} & if \ 7.63325E{+}05 < f_5(x) < 1.23462E{+}06 \\ 1 & if \quad f_5(x) \ge 1.23462E{+}06 \end{cases} \tag{3.77}$$

$$\mu_{f_6}(\mathrm{X}) = \begin{cases} 0 & if \quad f_6(x) \le 7.82650E{+}05 \\ \dfrac{f_6(x)-7.82650E{+}05}{1010280.759} & if \ 7.82650E{+}05 < f_6(x) < 1.79293E{+}06 \\ 1 & if \quad f_6(x) \ge 1.79293E{+}06 \end{cases} \tag{3.78}$$

$$\mu_{\sigma_i}(X) = \begin{cases} 0, & if \ \sigma_i(X) > b_i + d_i \\ 1 - \left\{\dfrac{g_i(X)-b_i}{d_i}\right\}, & if \ \ b_i \le \sigma_i(X) \le d_i, \ \ i = 1,2,\dots,24 \\ 1, & if \ \sigma_i(X) \le b_i \end{cases} \tag{3.79}$$

For a rectangular cell,

Constraints on objective functions:

$$\mu_{f_1}(\mathrm{X}) = \begin{cases} 0 & if \quad f_1(x) \le 0.1501 \\ \dfrac{-f_1(x)+0.1830}{0.0330} & if \quad 0.1501 < f_1(x) < 0.1830 \\ 1 & if \quad f_1(x) \ge 0.1830 \end{cases} \tag{3.80}$$

$$\mu_{f_2}(\mathrm{X}) = \begin{cases} 0 & if \quad f_2(x) \le 4.182846E{+}05 \\ \dfrac{-f_2(x)+1.063891E{+}06}{645606.026} & if \ 4.182846E{+}05 < f_2(x) < 1.063891E{+}06 \\ 1 & if \quad f_2(x) \ge 1.063891E{+}06 \end{cases} \tag{3.81}$$

$$\mu_{f_3}(\mathrm{X}) = \begin{cases} 0 & if \quad f_3(x) \le 6.954506E{+}05 \\ \dfrac{-f_3(x)+9.855583E{+}05}{290107.739} & if \ 6.954506E{+}05 < f_3(x) < 9.855583E{+}05 \\ 1 & if \quad f_3(x) \ge 9.855583E{+}05 \end{cases} \tag{3.82}$$

$$\mu_{f_4}(\mathrm{X}) = \begin{cases} 0 & if \quad f_4(x) \le 5.37152E{+}05 \\ \frac{-f_4(x)+8.007113E+05}{263558.941} & if \ 5.37152E{+}05 < f_4(x) < 8.007113E{+}05 \\ 1 & if \quad f_4(x) \ge 8.007113E{+}05 \end{cases} \tag{3.83}$$

$$\mu_{f_5}(\mathrm{X}) = \begin{cases} 0 & if \quad f_5(x) \le 7.615971E{+}05 \\ \frac{-f_5(x)+1.236361E+06}{474764.089} & if \ 7.615971E{+}05 < f_5(x) < 1.236361E{+}06 \\ 1 & if \quad f_5(x) \ge 1.236361E{+}06 \end{cases} \tag{3.84}$$

$$\mu_{f_6}(\mathrm{X}) = \begin{cases} 0 & if \quad f_6(x) \le 7.83137E{+}05 \\ \frac{f_6(x)-7.83137E+05}{992332.999} & if \ 7.83137E{+}05 < f_6(x) < 1.77547E{+}06 \\ 1 & if \quad f_6(x) \ge 1.77547E{+}06 \end{cases} \tag{3.85}$$

$$\mu_{\sigma_i}(X) = \begin{cases} 0, & if \ \sigma_i(X) > b_i + d_i \\ 1 - \left\{\frac{g_i(X)-b_i}{d_i}\right\}, & if \ b_i \le \sigma_i(X) \le d_i, \ i = 1,2,\dots,24 \\ 1, & if \ \sigma_i(X) \le b_i \end{cases} \tag{3.86}$$

3.2.6.2 Numerical results

Multi-objective fuzzy optimization problems are conducted by finding a compromise solution for a solar cell and flat plate PV array system. For a solar cell, a multi-objective fuzzy optimization is implemented with the best and worst optimization results of conversion efficiency and power output of a solar cell. Furthermore, the conversion efficiencies are reached at the minimum values in a square cell and a rectangular cell. The fuzzy optimum solution indicates that the maximum levels of satisfaction that can be obtained in the presence of the stated uncertainty in the objectives and constraints are 0.9825 for a square cell and 0.9213 for a rectangular cell, respectively. The results of conversion efficiencies have been determined to be 16.24 % and 16.43 %, which lays to the low bound for preventing the lowest conversion efficiency as 80 % of the maximum

conversion efficiency. When considering power output, the results are reached at 0.242 W and 0.899 W, respectively. For a flat plate PV array system, a multi-objective fuzzy optimization is investigated with six single-objective problems. Design variables are changed in collecting more incident solar energy with the size of array systems and the number of arrays. Installation of many collector arrays is achieved by examining the distances between adjacent rows; they should be as close as 84.43 cm and 84.80 cm to collect larger amounts of incident solar energy. Tilt angles of flat plate PV array systems are associated with power output, amount of incident solar energy, and cost. Similarly, these tilt angles are approached to the upper bound of range of constraints. This means that a multi-objective fuzzy optimization tends to install a flat plate PV array system for generating more power output and collecting more incident solar energy.

The maximization of collecting incident solar energy of highest month contributes to increases in cost as a result of more installation requirements. Table 3-14 shows the results of deterministic design variables and multi-objective optimization.

Table 3-14 (a) Results of design variables and multi-objective optimization

Objective		Design variables										
		T_e (μm)	T_b (μm)	L_c (cm)	H_c (cm)	W_f (μm)	H_f (μm)	N_f	W_b (μm)	H_b (μm)	N_b	C
Fuzzy	Sq.	6.63	218.28	1.57	1.57	58.90	14.66	19	300.39	15.61	10	6
	Rec.	5.48	218.28	4.03	2.23	36.84	9.15	12	185.31	9.60	10	6

	f_1(%)	f_2(W)	λ
Sq.	0.1624	0.2417	0.98254
Rec.	0.1643	0.8990	0.92127

Table 3-14 (b) Results of multi-objective fuzzy optimization design variables

Design variables											
Objective		T_e (μm)	T_b (μm)	L_c (cm)	H_c (cm)	W_f (μm)	H_f (μm)	N_f	W_b (μm)	H_b (μm)	N_b
Fuzzy	Sq.	6.20	298.04	12.50	12.50	118.74	27.45	49	1400.78	27.61	9
	Rec.	5.70	303.08	11.76	13.33	119.98	29.85	62	1399.21	30.29	9

Design variables								
Objective		N_{c_l}	N_{c_h}	N_{p_l}	N_{p_h}	D (cm)	β (degree)	K
Fuzzy	Sq.	6	8	40	2	84.43	62.19	113
	Rec.	5	5	51	3	84.80	64.26	117

Table 3-14 (c) Results of single-objective optimization

Results of single-objective optimization								
Obj.		f_1(%)	f_2(W)	f_3(W)	f_4(W)	f_5(W)	f_6($)	λ
Fuzzy	Sq.	16.89	9.73E+05	9.44E+05	6.94E+05	1.23E+06	1.69E+06	0.898
	Re.	16.86	1.00E+06	9.36E+05	6.66E+05	1.23E+06	1.74E+06	0.974

3.3 Conclusion

The optimal design of a flat plate PV array and CPC collector systems are described with consideration of conversion efficiency, power output, solar radiation based on seasonal demands with shading effect in multiple array systems, and costs.

For game theory, the results of multi-level optimization suggest that there are optimal values for single-objection optimization at each subsystem level, but multi-objective optimization is conducted using the results of single-objective optimization, simultaneously using modified game theory. The optimal solutions are found under three different conditions: 1) without consideration of constraints on incident solar energy- (the numbers of arrays are approached to the lowest bound value in both square and rectangular cells because the dominant factor is f_6) in the case of multilevel-objective optimization 2) The deterministic multilevel optimization problem is solved by applying constraints on the minimum value of the annual monthly average incident solar energy in varying amounts in the range of 50 % to 95 % of the maximum amount of annual monthly average incident solar energy. Variations of design variables and sensitivity analysis are investigated by placing different values of constraints on annual monthly average incident solar energy for finding compromise solutions with different requirements.

In a solar CPC PV collector system, the maximization of the annual monthly average incident solar energy results in an optimum CPC solar collector that indicates that a flat plate solar PV collector is likely the best system. Since the price of a reflector is much cheaper in contrast to a solar cell, the primary objective of the CPC solar panel system

design is to reduce the area of a solar cell by increasing the area of reflectors. Therefore, steps to minimize the cost result in CPC solar collector designs that have CPC ratios in the range of 1.0 – 2.2. Sensitivity analyses are presented with respect to the total energy expectation ratio (compared to flat plate solar collectors) and different land prices. It is found that the cost per unit energy can be significantly reduced (as much as 41%) depending on different land prices if the total energy output can be sacrificed by about 20 % compared to the flat plate solar collector system. The minimization of f_1 is found to be dominant when $s_3 = 1$ and the minimization of f_3 is found to be dominant $s_3 = 20$ or 50 in the multi-objective optimization problem. Hence, the compromise solutions result in CPC solar collectors which have CPC ratios in the range 1.24 to 1.76 in the presence of an additional constraint on the CPC ratio.

For a fuzzy set based on a PV array system, the result of λ-formulation in the multi-objective fuzzy optimization indicates a quantitative representation of the degree of satisfaction of the intersection of the membership functions of the design variables, constraints and objective function. The optimum design of a solar PV collector system with fuzzy objective function and fuzzy constraints set is considered to illustrate the procedures. In a comparison of multi-objective optimization of game theory and fuzzy set theory, the results of conversion efficiency fall into a similar range above 90 % of maximum conversion efficiency. However, the results of power output, incident solar energy of annual monthly average, lowest, and highest months, and cost show very different outcomes when the two different theories are examined. Game theory for multi-objective optimization of a solar PV collector system attempts to minimize the costs of a

solar PV array system while fuzzy theory attempts to maximize the collected amount of incident solar energy.

As seen from the present results, a multilevel optimization problem is solved by finding a compromise solution in a solar PV array system consisting of three subsystems: cell, panel, and array. These are associated with conversion efficiency, power output, incident solar energy, and costs. Thus, this method is illustrated by utilizing the solar PV array system to highlight the optimal design of a processing system for finding the best compromise solution.

CHAPTER 4

Uncertainty Based on Analyses and Optimal Design of Solar PV Systems

4.1 Overview

The purpose of uncertainty analysis is to be able to predict the performance of solar PV systems more realistically through the quantification of uncertainties associated with various parameters. In this chapter, first the uncertainty analysis is investigated using stochastic (or probabilistic) and fuzzy approaches, and then the optimal design of solar PV systems is explored through probabilistic and fuzzy analyses.

Stochastic or probabilistic methods assume that the parameters of the problem are random variables with known probability distribution. Therefore, stochastic or probabilistic optimization methods involve random variables and, hence, the objective functions and constraints are also random variables. Random variables include uncertain design variables and/or uncertain design parameters or data. Also, probabilistic sensitivity analysis seeks the rate of change between the input and output in solar PV systems under uncertainties in probabilistic variables of the objective function. The stochastic techniques generate better results as compared to deterministic ones, and the optimal set of design and random variables are a means to produce maximum system performance. This study includes a review of stochastic optimization techniques implemented in finding the prediction of the performance of solar PV systems.

The geometric parameters are imprecise due to geometric dimensioning and tolerancing from machining settings during production and operator's error, assembling a product, and operating a system. The geometric values used in the optimal design are imprecise as a result of unpredictable engineering environments. Fuzzy sets include some degrees of membership that permit the gradual assessment of the membership of elements in a set.

The purpose of this chapter is to predict the performance of solar cell, flat plate PV array systems and CPC PV collector systems in the presence of uncertain parameters and/or to parametric design factors by considering probabilistic and fuzzy analysis methodologies.

4.2 Uncertainty Analysis of Solar PV Systems

Two different approaches to uncertainty analysis are considered based on stochastic (or probabilistic) and fuzzy analyses. When an uncertain quantity is described as a random variable with a known probability distribution, the probabilistic approach can be used to find the probabilistic response of the system. In some cases, an uncertain quantity is described vaguely in the form of linguistic statements such as "the intensity of sunlight is very high". In such cases, fuzzy analysis can be used to find the response of the system also in terms of linguistic terms.

The probabilistic analysis process is used for predicting performance in terms of a set of random variables. The random variables may be characterized by unexpected circumstances such as workplace environments, manufacturing production conditions related to operation, and production tolerances. The probabilistic analysis method uses random variables containing uncertain design parameters and/or uncertain design variables. Although a set of random variables is defined completely by the probability

mass function which is used for a function of the probability of discrete random variables, it is convenient to use the probability distribution function for continuous random variables. The probability of the random variables within a particular range of design parameters is expressed by the integral of the variable's density in confidence intervals for parameters. The normal probability distribution is very common to predict the performance of engineering systems. A set of random variables has the shape of a normal curve called a normal random variable. This random variable is to be normally distributed with mean value and standard deviation.

Fuzzy set analysis is the membership function in a set assessed in binary terms according to a bivalent condition with membership function values between 0 (an implication of complete comfort) and 1 (an implication of discomfort). The fuzzy set can provide solutions to a broad range of engineering problems. The membership function values indicate the degrees to which each object is compatible with the properties or features distinctive to the collection. The uncertainty in individual measurements of membership function is represented using simple triangular fuzzy numbers.

4.3 Probabilistic Optimization

Stochastic nonlinear programming deals with a general optimization problem with an objective f($\vec{X}$) and /or inequality constraints $g_j(\vec{X})$; j = 1 to m, where, at least one of the functions among f($\vec{X}$) and $g_j(\vec{X})$ is nonlinear in terms of $\vec{X}$ and some of the design variables and/or preassigned parameters are random variables. For simplicity, we assume that all the random variables are independent and follow normal distribution defined in

terms of their respective mean values and standard deviations. A probabilistic or stochastic programming problem can be stated as

Find $\vec{X}$ which minimizes $f(\vec{Y})$

subject to

$$P[g_j(\vec{Y}) \leq 0] \geq p_j, \quad j = 1,2,\dots,m \tag{4.1}$$

where $\vec{Y}$ is the vector of N random variables $y_1, y_2,\dots, y_N$ that might include the decision variable $x_1, x_2,\dots, x_l$. Eq. (4.1) indicates that the probability of realizing $g_j(\vec{Y})$ smaller than or equal to zero must be greater than or equal to the specified probability p_j.

In nonlinear stochastic programming, the objective function contains the uncertainty that depends on a set of random variables based on normal distribution. Thus, the objective function $f(\vec{Y})$ can be expanded as utilizing the mean values of y_i, $\overline{y_l}$, as

$$f(\vec{Y}) = f\left(\vec{\bar{Y}}\right) + \sum_{i=1}^{N}\left(\frac{\partial f}{\partial y_i}\middle|\vec{\bar{Y}}\right)(y_i - \overline{y_l}) + \text{higher} - \text{order derivative terms} \tag{4.2}$$

If the standard deviations of $y_i$and σ_{yi} are small, $f(\vec{\bar{Y}})$ can be approximated by the first two terms as:

$$f(\vec{\bar{Y}}) \cong f(\bar{Y}) - \sum_{i=1}^{N}\left(\left(\frac{\partial f}{\partial y_i}\middle|\vec{\bar{Y}}\right)y_i\right) + \sum_{i=1}^{N}\left(\left(\frac{\partial f}{\partial y_i}\middle|\vec{\bar{Y}}\right)y_i\right) = \psi(Y) \tag{4.3}$$

If all $y_i(i = 1,2,\dots,N)$ follow normal distribution, $\psi(Y)$, a linear function of Y, also follows normal distribution. The mean and the variance of ψ are given by

$$\bar{\psi} = \psi\left(\vec{\bar{Y}}\right) \tag{4.4}$$

$$\mathrm{Var}(\psi) = \sigma_{\psi}^{2} = \sum_{i=1}^{N} \left(\frac{\partial f}{\partial y_i}\middle|_{\bar{\vec{Y}}}\right)^{2} \sigma_{y_i}^{2} \tag{4.5}$$

since all y_i are independent. For the purpose of optimization, a new objective function $\mathrm{f}(\vec{Y})$ can be expressed as

$$\mathrm{f}(\vec{Y}) = k_1 \bar{\psi} + k_2 \sigma_{\psi} \tag{4.6}$$

where $k_1 \geq 0$ and $k_2 \geq 0$, and the numerical values of k_1 and k_2 include the important relationship of normal distribution (ψ) standard deviation (σ_{ψ}) for optimization.

Probabilistic constraints contain both deterministic and probabilistic variables that follow a known probability distribution. The constraints will be probabilistic and one would like to specify them with a certain minimum probability. The constraint inequality can be written as

$$\int_{-\infty}^{0} f_{gj}(g_j) dg_j \geq \int_{-\infty}^{z_1} f_z(z) d_z = p_j \tag{4.7}$$

where $f_{gj}(g_j)$ is the probability density function of the random variable, g_j, its range is assumed to be $-\infty$ to ∞. The constraint function $g_j(\vec{Y})$ can be expanded around the vector of mean values of the random variables, $\bar{\vec{Y}}$, as

$$g_j(\vec{Y}) \cong g_j\left(\bar{\vec{Y}}\right) + \sum_{i-1}^{N} \left(\frac{\partial g_j}{\partial y_i}\middle|_{\bar{\vec{Y}}}\right)(y_i - \bar{y}_{\imath}) \tag{4.8}$$

From Eq. (4.8), the mean value, $\overline{g_j}$, and the standard deviation, σ_{gj}, of g_j can be obtained as

$$\left(\frac{(g_j - \overline{g_j})}{\sigma_{g_j}}\right) > z_1 \tag{4.9}$$

$$g_j - \overline{g_j} - z_1\sigma_{g_j} \geq 0 \tag{4.10}$$

$g_j = 0$, thus $\overline{g_j} + z_1\sigma_{g_j} \leq 0$ (4.11)

$$\overline{g_J} = g_j\left(\vec{\bar{Y}}\right) \tag{4.12}$$

$$\overline{g_J} - \emptyset_j(p_j)\left[\sum_{i=1}^{N}\left(\frac{\partial g_j}{\partial y_i}\middle|\vec{\bar{Y}}\right)^2 {\sigma_{yi}}^2\right]^{1/2} \geq 0 \qquad j = 1,2,\ldots,\text{m} \tag{4.13}$$

By introducing the new variable

$$\theta = \frac{g_j - \overline{g_J}}{\sigma_{g_j}} \tag{4.14}$$

and noting that

$$\int_{-\infty}^{\infty} \frac{1}{\sqrt{2\pi}} e^{\frac{-t^2}{2}} dt = 1 \tag{4.15}$$

Eq. (4.7) can be rewritten as

$$\int_{-\frac{\overline{g_J}}{\sigma_{g_j}}}^{\infty} \frac{1}{\sqrt{2\pi}} e^{\frac{-\theta^2}{2}} d\theta \geq \int_{-\emptyset_j(p_j)}^{\infty} \frac{1}{\sqrt{2\pi}} e^{\frac{-t^2}{2}} dt \tag{4.16}$$

where $\emptyset_j(p_j)$ is the value of the standard normal variation corresponding to the probability p_j.

$$-\frac{\overline{g_J}}{\sigma_{g_j}} \leq -\emptyset_j(p_j) \tag{4.17}$$

or

$$-\overline{g_J} + \sigma_{g_j}\emptyset_j \leq 0 \tag{4.18}$$

Eq. (4.17) can be rewritten as

$$\overline{g_j} - \sigma_{g_j} \emptyset_j \left[\sum_{i=1}^{N} \left(\frac{\partial g_j}{\partial y_i} \middle| \vec{\bar{Y}} \right)^2 {\sigma_{g_j}}^2 \right]^{1/2} \geq 0 \tag{4.19}$$

Thus, the optimization problem of objective function f($\vec{Y}$) can be stated in its equivalent deterministic form.

4.3.1 Formulation of optimization problem

The new objective of the probabilistic optimization problem (F) is constructed by the combination of the mean value of the objective function ($\bar{f}$) and standard deviation of a solar cell and a solar PV array system (σ_f) with the weight values of k_1 and k_2 . By virtue of this, a new objective function (F) based on a set of random variables can be expressed as

$$\text{f(Y)} = k_1 \bar{f} + k_2 \sigma_f \tag{4.20}$$

The weighted mean $k_1 \bar{f}$ and the weighted variation $k_2 \sigma_f$ can be expressed as

$$k_1 \bar{f} \approx k_2 \sigma_f \tag{4.21}$$

and then rewritten as

$$k_2 \approx \frac{k_1 \bar{f}}{\sigma_f} \tag{4.22}$$

If the weight of the mean k_1 is equal to 1, the value of the weight of variation k_2 is decided by Eq. (4.22), and the value of the weight of variation, k_2, depends on the mean values of random variables and their coefficient of variations.

The deterministic optimization method is used to predict optimal cell (design) and solar PV array system design without considering the stochastic behaviors. Therefore, the stochastic approach presents more as complex and involves statistical processing for reliability.

4.3.2 Solar cells

To maximize solar cell conversion efficiency, maximum absorption and minimum recombination are necessary for high conversion efficiency of a solar cell. The objective is to find the optimal design vector $\vec{X}$ for the maximization of the conversion efficiency to reduce power losses under concentrated sunlight (C), and can be stated as a maximization problem as

$$\text{Maximize f}(\vec{X}) = \frac{J(C)_m V(C)_m}{P_{in} \cdot C}(1 - F_{sum}) \times 100 \tag{4.23}$$

Solar cell conversion efficiency is related to short-circuit current, open-circuit voltage, incident power density (P_{in}) at 1 sun, intensity of sunlight (C) and fractional power losses (F_{sum}). The power losses (F_{sum}) from metallic contacts largely consist of the surface sheet (F_{sr}), contact (F_c), grid metal of fingers (F_f), busbars resistivity (F_b) and shadowing (F_s). The total fractional power loss (F_{sum}) can be expressed in terms of the individual fractional power loss as

$$F_{sum} = F_{sr} + F_f + F_b + F_s + F_c \tag{4.24}$$

The design of the top contact considers geometric parameters of metal grids to minimize their resistance in addition to the overall reduction of power losses associated with the geometric grid contact factors. The main concerns in relation to geometric grid contact

factors are the finger and busbar spacing, the metal height-to-width aspect ratio, the minimum metal grid of width and height, and the resistivity of the metal. Accordingly, the design variables of the problem, for a rectangular solar cell, can be laid out as

$$\vec{X}=\begin{Bmatrix} T_e \\ T_b \\ L_c \\ H_c \\ W_f \\ H_f \\ N_f \\ W_b \\ H_b \\ N_b \\ C \end{Bmatrix} \equiv \begin{Bmatrix} x_1 \\ x_2 \\ x_3 \\ x_4 \\ x_5 \\ x_6 \\ x_7 \\ x_8 \\ x_9 \\ x_{10} \\ x_{11} \end{Bmatrix} \tag{4.25}$$

The random variable vectors are:

$$\vec{Y}=\begin{Bmatrix} T_e \\ T_b \\ L_c \\ H_c \\ W_f \\ H_f \\ W_b \\ H_b \\ P_{in} \\ \rho_m \\ \rho_c \\ R_{sh} \end{Bmatrix} \equiv \begin{Bmatrix} y_1 \\ y_2 \\ y_3 \\ y_4 \\ y_5 \\ y_6 \\ y_7 \\ y_8 \\ y_9 \\ y_{10} \\ y_{11} \\ y_{12} \end{Bmatrix} \tag{4.26}$$

Geometric design variables, except for integer values, such as the number of fingers (N_f), busbars (N_b), and intensity of sunlight (C), are considered random variables because these design factors are dependent on the manufacturing production conditions related to tolerances. The incident power density (P_{in}) varies in a particular location due to atmospheric effects. Furthermore, the metal property (ρ_m) of the fingers and busbars, the

contact resistivity (ρ_c), and the resistance of the sheet (R_{sh}) depend on the purity of materials and fabrication skills. Therefore, the random variables include design parameters except integer values, such as the number of fingers, busbars, and intensity of sunlight, and uncertain design parameters affecting the results of the objective function. Therefore, the random variables consist of 7 and 8 design parameters and all 4 uncertain design parameters, which include contact resistivity, sheet resistance, metal resistivity and incident power in a square cell and a rectangular cell, respectively. The solar constant is the rate of total solar energy at all wavelengths incident on a unit area normally exposed to the rays of the sun.

4.3.2.1 Numerical results

The MATLAB program can implement the optimization of solar PV array system performance based on the genetic algorithms (GA) method by using the function of *ga,* which finds mixed-integer values of the minimum of a scalar function of several variables, starting with an initial value of the design parameters.

The values of the coefficient are applied from 0.02 to 0.1 because there is no feasibility after the coefficient of variation exceeds 0.1. Table 4-1 and Fig. 4-1 show the values of k_2 and the variations of conversion efficiency in a square and a rectangular cell with a coefficient variation under the probability of a constraint satisfaction of 60 %. The conversion efficiencies (η_c) are steeply decreased from 20.284 % to 20.262 % at a coefficient of variation of 0.06 for a square cell and from 20.541 % to 20.525 % at a coefficient of variation of 0.08 for a rectangular cell. A detailed discussion of the

influences with various probabilities of constraint satisfaction and coefficient of variations is conducted in this section.

Table 4-1 Values of k_2 and the coefficient variations

Coefficient variation		0.02	0.04	0.06	0.08	0.1
k_2	Square	448	223	149	111	88
	Rectangular	582	291	193	143	115

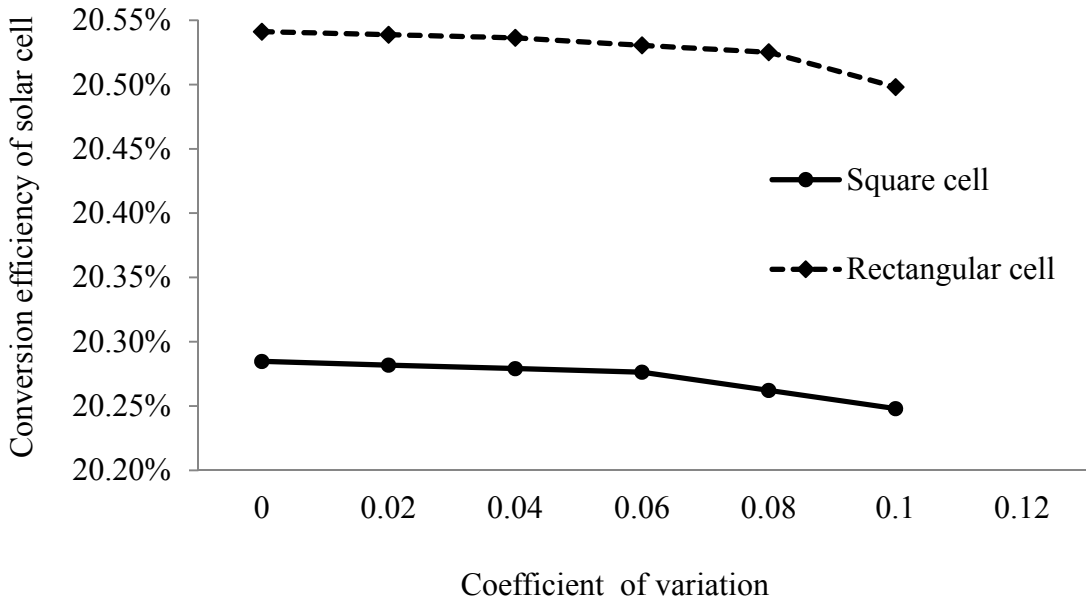

Figure 4-1 Comparison of conversion efficiency between square and rectangular cells under coefficient of variation

The influence of probability of constraint satisfaction and coefficient variation of random variables is observed. The new objective function, F, is maximized with different values of the probability of constraint satisfaction. The values of probability of constraint satisfaction are 50 %, 80 %, 90 %, 95 %, 99 %, and 99.997 % with 0.5 %, 1.0 %, 1.5 %,

and 2.0 % of coefficients of variation, respectively. Variations of mean conversion efficiency, $\bar{f}$, standard deviations, σ_f, and new objective function, F, are investigated through the design variables with respect to the probability of constraint satisfaction.

All design variables start to shift under different probabilities of constraint satisfaction and coefficients of variation. Figure 4-2 shows variations of design variables under varying values of coefficients of variation and probability of constraint satisfaction. Bear in mind that at a coefficient of variation of 0.005, both the variations of design variables and constraints at optimal design variables under different probabilities of constraint satisfaction are investigated. In contrast, when the variation of coefficient holds any value other than 0.005, only variations of design variables are investigated.

❖ 0.005 of coefficient of variation

- Square cell

The conversion efficiency is decreased from 20.284 % to 20.260 % as shown in Table 4-2 under a probability of constraint satisfaction between 50 % and 99.997 %. The value of standard deviation is decreased from 1.129E – 04 to 1.106E – 04. Individual design variables are examined below in further detail.

As shown in Figs. 4-2 (a) - (b), the thicknesses of the emitter and base are associated with a decrease in conversion efficiency; meanwhile, the probabilities of constraint satisfaction and variations of coefficient are increased. The thickness of the emitter is in a range between 7.56 μm and 7.78 μm, but the thickness of the base is dramatically decreased from 415 μm to 254 μm under a probability of constraint satisfaction between 50 % and 99.997 %, respectively.

The cell length (L_c) is increased from 0.80 cm up to 0.84 cm. The width of the fingers, as shown in Figs. 4-2 (d) and (e), is augmented from 20 μm to 20.43 μm at 99.997 % of probability of constraint satisfaction. Also, the width of the busbars is increased from 100 μm to 102.40 μm at 99.997 % of probability of constraint satisfaction. The heights of the fingers and busbars, as shown in Figs. 4-2 (f) and (g), are increased from 50 % to 99 % of probability of constraint satisfaction. However, after the probability exceeds 99 % of probability of constraint satisfaction, H_f is steeply increased from 4.91 μm to 4.97 μm . However, H_b is decreased from 6.01 μm to 5.82 μm because the number of busbars is modified. In selecting the number of fingers, the amount is reduced from 18 to 17, yet the number of busbars is constant at 2 as shown in Figs. 4-2 (h) and (i). The optimum value of intensity of sunlight is 6, though the larger cells begin to diminish in size as the intensity of sunlight reaches 5 at 99.997 % of probability of constraint satisfaction. This grants larger solar cells greater influence on the reduction of intensity of sunlight for conversion efficiency (η_c) as shown in Figs. 4-2 (j).

- Rectangular cell

The conversion efficiency is decreased from 20.541 % to 20.524 % as shown in Table 4-2 under a probability of constraint satisfaction between 50 % and 99.997 %. The value of standard deviation is increased from 8.807E – 05 to 8.947E – 04. A detailed discussion of the role of each design variable will follow.

As shown in Figs. 4-2 (a) - (b), the thickness of the emitter is in a range between 7.99 μm and 7.96 μm, but the thickness of the base is increased considerably from 252 μm to 406 μm under a probability of constraint satisfaction between 50 % and 99.997 %,

respectively. The cell length (L_c) is increased from 1.76 cm up to 2.44 cm; the length of height (H_c) is almost constant at 0.50 cm. Figures 4-2 (d) and (e) demonstrate a clear increase in the width of the fingers from 20.09 μm to 20.26 μm at 99.997 % of probability of constraint satisfaction. The width of the busbars is similarly increased from 100 μm to 101.31 μm at 99.997 % of probability of constraint satisfaction. As shown in Figs. 4-2 (f) and (g), the height of the fingers (H_f) is decreased from 5.00 μm to 4.92 μm under a probability of constraint satisfaction between 50 % and 99.997 %. The height of the busbars (H_b) is decreased from 6.01 μm to 5.82 μm as shown in Figs. 4-2 (h) and (i). In the case of the fingers, the number of fingers is the same at 12, but the number of busars is increased from 2 to 3 as shown in Figs. 4-2 (h) and (i). The optimum value of intensity of sunlight is 6 as shown in Figs. 4-2 (j).

Table 4-2 Mean values and standard deviations of objective of probability optimization under different constraint satisfaction and 0.005 of coefficient of variation

Coefficient variation Of standard deviation		Probability of constraint satisfaction	$\bar{f}$	F	σ_f
			Optimal	Optimal	Optimal
0.005	Square	50%	0.20284	0.40568	1.129E-04
	Rectangular		0.20541	0.41823	8.807E-05
	Square	80%	0.20282	0.40563	1.130E-04
	Rectangular		0.20539	0.41078	8.811E-05
	Square	90%	0.20281	0.40560	1.129E-04
	Rectangular		0.20538	0.41076	8.816E-05
	Square	95%	0.20280	0.40560	1.133E-04
	Rectangular		0.20537	0.41074	8.823E-05
	Square	99%	0.20277	0.40554	1.129E-04
	Rectangular		0.20534	0.41069	8.855E-05
	Square	99.997%	0.20260	0.40520	1.106E-04
	Rectangular		0.20524	0.41049	8.947E-04

Constraints at optimal design variables under a coefficient of variation case of 0.005 are further investigated. In assessing constraints for a square cell, the optimum values can be explained by an active change in g_1, g_2, g_3, g_4, and g_8 with a probability of constraint satisfaction and coefficient of variation. In assessing constraints for a rectangular cell, the optimum values can be explained by an active change in g_1, g_2, g_3, g_4, g_5, g_7, and g_9. The increment of constraints is derived from the percent of growth based on an optimum value of constraints.

1. Variations of g_1 and g_2

The constraints of g_1 and g_2 formulate the basis for the relationship between the height of the fingers and busbars, and are applied to the limited height between the finger and busbar. Table 4-3 shows the results of constraint of g_1 and g_2 at optimal design variables under a coefficient of variation case of 0.005.

- Square cell

The increment of g_1, calculated from the percent of growth based on an optimum value of g_1 under a probability of constraint satisfaction between 50 % and 99 % is less than 9.11 %, but the value of probability of constraint satisfaction at 99.997 % with 0.005 of coefficient of variation is increased up to 15.24 %. Additionally, the decrement of g_2 reaches 399.34 % at 99 % and 812.47 % at 99.997 % from the optimum value of constraint satisfaction.

- Rectangular cell

The increment of g_1 is under a probability of constraint satisfaction between 50 % and 99 % and is less than 8.85 %, but the value of probability of constraint satisfaction at 99.997 % with 0.005 of coefficient of variation is increased up to 15.11 %. The decrement of g_2 reaches 398.78 % at 99 % and 806.39 % at 99.997 % from the optimum value of constraint satisfaction.

Table 4-3 Constraint of g_1 and g_2 at optimal design variables under coefficient of variation of 0.005

Constraint	Probability of constraint satisfaction	Constraint	
		Square	Rectangular
g_1	50%	-1.00463E-04	-1.00441E-04
	80%	-9.71933E-05	-9.71222E-05
	90%	-9.54428E-05	-9.54983E-05
	95%	-9.40267E-05	-9.41244E-05
	99%	-9.13060E-05	-9.15524E-05
	99.997%	-8.51530E-05	-8.52683E-05
g_2	50%	-1.53226E-06	-1.51065E-06
	80%	-1.74992E-06	-1.81842E-06
	90%	-3.50152E-06	-3.44598E-06
	95%	-4.92172E-06	-4.82312E-06

2. Variations of g_3 and g_4

The constraints of g_3 and g_4 correspond to the relationship of the ratio of width to height of the finger ($\frac{H_f}{W_f}$). Table 4-4 shows the results of constraint of g_3 and g_4 at optimal design variables under a coefficient of variation of 0.005.

- Square cell

The increment of g_3 is attained to 22.47 % at 99 % constraint satisfaction and 34.50 % at 99.997 % constraint satisfaction, while the decrement of g_4 is increased to 1796.49 % at 99 % constraint satisfaction and 2902.58 % at 99.997 % constraint satisfaction, being mindful that these are associated with the aspect ratio of the width to height of the finger.

- Rectangular cell

The increment of g_3 is increased to 20.19 % at 99 % constraint satisfaction and 34.56 % at 99.997 % constraint satisfaction. The decrement of g_4 suddenly shoots up to 2145.53 % at 99 % of probability of constraint satisfaction and 3814.65 % at 99.997 % of the constraint satisfaction, recalling that these are associated with the aspect ratio of the width to height of the finger ($\frac{H_f}{W_f}$).

Table 4-4 Results of constraint of g_3 and g_4 at optimal design variables under coefficient of variation of 0.005

Constraint	Probability of constraint satisfaction	Constraint	
		Square	Rectangular
g_3	50%	-1.97389E-02	-1.96863E-02
	80%	-1.73517E-02	-1.80238E-02
	90%	-1.75115E-02	-1.75053E-02
	95%	-1.68602E-02	-1.68714E-02
	99%	-1.53038E-02	-1.57111E-02
	99.997%	-1.29281E-02	-1.28824E-02
g_4	50%	2.22575E-04	1.69805E-04
	80%	-2.16922E-03	-1.49585E-03
	90%	-2.00913E-03	-2.01540E-03
	95%	-2.66170E-03	-2.65052E-03
	99%	-4.22111E-03	-3.81302E-03
	99.997%	-6.68298E-03	-6.64727E-03

3. Variations of g_5 and g_6

The constraints of g_5 and g_6 are related to the length of a cell (L_c and H_c) and the width of the fingers and busbars. Table 4-5 shows the results of constraint of g_1 and g_2 at optimal design variables under a coefficient of variation of 0.005.

- Square cell

The increments of both g_5 and g_6 are almost unchanged as 4.53 % and 4.85 % under a probability of constraint satisfaction between 50 % and 99 %, respectively, because of a minor alternation to cell length (L_c) from 0.8 cm to 0.83 cm.

- Rectangular cell

Between 50 % and 99 % probability of constraint satisfaction, the decrement of g_5 sees little change; then it is swiftly increases to 38.70 % at 99.997 %. This is affected by the cell length associated with the fingers. However, the increment of g_6 is almost unchanged as 0.06 % because the length of height (H_c) is almost unchanged at 0.50 cm.

Table 4-5 Results of constraint of g_5 and g_6 at optimal design variables under coefficient of variation of 0.005

Constraint	Probability of constraint satisfaction	Constraint	
		Square	Rectangular
g_5	50%	-7.79361E-01	-1.73526E+00
	80%	-7.78383E-01	-1.72926E+00
	90%	-7.79185E-01	-1.72175E+00
	95%	-7.76206E-01	-1.72356E+00
	99%	-7.91565E-01	-1.72362E+00
	99.997%	-8.14669E-01	-2.40685E+00
g_6	50%	-7.63363E-01	-4.75661E-01
	80%	-7.62383E-01	-4.75673E-01
	90%	-7.63200E-01	-4.75770E-01
	95%	-7.60208E-01	-4.75645E-01
	99%	-7.75566E-01	-4.75586E-01
	99.997%	-8.00418E-01	-4.75374E-01

4. Variation of g_7

The constraint of g_7 is designated as the relationship between cell size and the geometric dimensions of the fingers and busbars because the length of the fingers and busbars is less than the length of the cells (L_c and H_c). The decrement of g_7 is increased to 39.57 % for a square cell and to 38.62 % for a rectangular cell under a probability of constraint satisfaction between 50 % and 99.997 % , which is affected by the cell length associated with the busbars as shown in Table 4-6.

Table 4-6 Results of constraint of g_7 at optimal design variables under coefficient of variation of 0.005

Constraint	Probability of constraint satisfaction	Constraint	
		Square	Rectangular
g_7	50%	-5.94936E-01	-8.25737E-01
	80%	-5.93427E-01	-8.22901E-01
	90%	-5.94674E-01	-8.19494E-01
	95%	-5.90079E-01	-8.20141E-01
	99%	-6.13911E-01	-8.20066E-01
	99.997%	-6.52076E-01	-1.14463E+00

5. Variations of g_8 and g_9

The constraints of g_8 correlate the distance between the fingers while g_9 is affiliated with the distance between the busbars. Table 4-7 shows the results of constraint of g_8 and g_9 at optimal design variables under a coefficient of variation of 0.005.

- Square cell

The decrement of g_8 is less than 1.60 % at 99 % constraint satisfaction, but the value of constraint is steeply increased to 11.41 % at 99.997 % constraint satisfaction compared to 99 %, and this is directly associated with the number of fingers.

- Rectangular cell

The increment of g_8 reaches 30.65 % at 99.997 % of the constraint satisfaction and is notably affected by the cell area associated with the numbers (N_f and N_b) and widths of the fingers and busbars.

Table 4-7 Results of constraint of g_8 and g_9 at optimal design variables under coefficient of variation of 0.005

Constraint	Probability of constraint satisfaction	Constraint	
		Square	Rectangular
g_8	50%	-4.49037E-02	-4.32419E-02
	80%	-4.48461E-02	-4.32430E-02
	90%	-4.48941E-02	-4.32518E-02
	95%	-4.47181E-02	-4.32404E-02
	99%	-4.56215E-02	-4.32351E-02
	99.997%	-5.00262E-02	-4.32158E-02
g_9	50%	-7.79361E-01	-1.73526E+00
	80%	-7.78383E-01	-1.72926E+00
	90%	-7.79185E-01	-1.72175E+00
	95%	-7.76206E-01	-1.72356E+00
	99%	-7.91565E-01	-1.72362E+00
	99.997%	-8.14669E-01	-1.20342E+00

❖ 0.01 of coefficient of variation

Table 4-8 shows the results of mean values and standard deviations of objective of probability optimization under different constraint satisfaction and coefficient of variation of 0.01.

- Square cell

The conversion efficiency is decreased from 20.284 % to 20.261 % as shown in Table 4-8 under a probability of constraint satisfaction between 50 % and 99 %. The value of standard deviation suddenly decreased from 2.032E – 04 to 1.915E – 04. It is necessary to consider the specific aspects of each of the design variables.

As shown in Figs. 4-2 (a) - (b), the thickness of the emitter is in a range between 7.78 μm and 7.76 μm. The thickness of the base is decreased from 414 μm to 235 μm under a

probability of constraint satisfaction between 50 % and 99 %, respectively. The cell length is increased from 0.80 cm up to 0.83 cm. The width of the fingers, as shown Figs. 4-2 (d) and (e), is augmented from 20 μm to 20.40 μm at 99 % of probability of constraint satisfaction. The width of the busbars sees an increase from 100 μm to 102.01 μm for a square cell at 99 % of probability of constraint satisfaction.

The heights of the fingers and busbars, as shown in Figs. 4-2 (f) and (g), are decreased from 50 % to 95 % of probability of constraint satisfaction. Once the probability exceeds 95 % of probability of constraint satisfaction, H_f undergoes a drop from 5 μm to 4.97 μm coupled with a decrease for H_b from 6.01 μm to 5.82 μm. Although the number of fingers is changed from 18 to 17, the number of busars remains at 2 as shown in Figs. 4-2 (h) and (i). The optimum value of intensity of sunlight is 6, but the larger cell size becomes smaller as the intensity of sunlight reaches 5 at 99.997 % of probability of constraint satisfaction, so that larger solar cells have an influence on the reduction of intensity of sunlight for conversion efficiency (η_c) as shown in Figs. 4-2 (j).

- Rectangular cell

The conversion efficiency is decreased from 20.541 % to 20.513 % as shown in Table 4-8 under a probability of constraint satisfaction between 50 % and 99.997 %. The value of standard deviation changed from 1.585E – 04 to 1.551E – 04. This will be explained below.

Figures 4-2 (a) - (b) reflect a thickness of the emitter that ranges between 7.99 μm and 7.38 μm, but the thickness of the base is vastly increased from 251 μm to 395 μm under a probability of constraint satisfaction between 50 % and 99 %, respectively. The cell

length (L_c) is increased from 1.76 cm up to 2.41 cm under a probability of constraint satisfaction between 50 % and 90 % while the cell length (L_c) is decreased from 2.41 cm to 1.77 cm under a probability of constraint satisfaction between 90 % and 95 %. Again, the cell length (L_c) is increased from 1.77 cm up to 1.81 cm under a probability of constraint satisfaction between 95 % and 99 %. The length of height (H_c) is the same at 0.50 cm. The width of the fingers, as shown Figs. 4-2 (d) and (e), is increased from 20.04 μm to 20.12 μm at 99 % of probability of constraint satisfaction. Also, the width of the busbars is increased from 102.43 μm to 106.03μm at 99 % of probability of constraint satisfaction. As shown in Figs. 4-2 (f) and (g), the height of the fingers (H_f) is decreased from 5.00 μm to 4.92 μm under a probability of constraint satisfaction between 50 % and 90 %. However, H_f is rapidly increased from 4.92 μm to 5.14 μm under a probability of constraint satisfaction between 90 % and 99 %. In the case of the height of the busbars (H_b), H_b is decreased from 6.00 μm to 5.84 μm under a probability of constraint satisfaction between 50 % and 90 %, H_b is increased from 5.84 μm to 5.98 μm under a probability of constraint satisfaction between 90 % and 95 % as shown in Figs. 4-2 (h) and (i). In the case of the fingers, the number of fingers is decreased from 12 to 11 under a probability of constraint satisfaction between 90 % and 95 %; on the other hand, the number of busbars is still the same at 2 as shown in Figs. 4-2 (h) and (i). The optimum value of intensity of sunlight is 6 as shown in Figs. 4-2 (j).

Table 4-8 Results of mean values and standard deviations of objective of probability optimization under different constraint satisfaction and 0.01 of coefficient of variation

Coefficient variation Of standard deviation		Probability of constraint satisfaction	$\bar{f}$	F	σ_f
			Optimal	Optimal	Optimal
0.01	Square	50%	0.20284	0.40568	2.032E-04
	Rectangular		0.20541	0.41823	1.585E-04
	Square	80%	0.20280	0.40560	2.034E-04
	Rectangular		0.20537	0.41075	1.587E-04
	Square	90%	0.20279	0.40559	2.036E-04
	Rectangular		0.20533	0.41066	1.593E-04
	Square	95%	0.20271	0.40541	1.913E-04
	Rectangular		0.20524	0.41047	1.608E-04
	Square	99%	0.20261	0.40523	1.915E-04
	Rectangular		0.20513	0.41027	1.551E-04

❖ 0.015 of coefficient of variation

Table 4-9 shows the results of mean values and standard deviations of objective of probability optimization under different constraint satisfaction and 0.015 of coefficient variation.

- Square cell

The conversion efficiency is decreased from 20.284 % to 20.243 % as shown in Table 4-2 under a probability of constraint satisfaction between 50 % and 95 %. The value of standard deviation suddenly decreased from 3.387E – 04 to 3.226E – 04. This section explores individual design variables.

As shown in Figs. 4-2 (a) - (b), the thickness of the emitter is in a range between 7.78 μm and 7.88 μm, but the thickness of the base drops from 414 μm to 219 μm under a probability of constraint satisfaction between 50 % and 95 %, respectively. The cell

length is increased from 0.80 cm up to 0.84 cm. The width of the fingers, as shown Figs. 4-2 (d) and (e), is significantly increased from 20 μm to 21.01 μm at 95 % of probability of constraint satisfaction. Also, the width of the busbars sees a vast growth from 100 μm to 105.11 μm for a square cell at 95 % of probability of constraint satisfaction. The heights of the fingers and busbars, as shown in Figs. 4-2 (f) and (g), are boosted from 50 % to 90 % of probability of constraint satisfaction. Upon 90 % of probability in excess of constraint satisfaction, H_f is steeply increased from 4.86 μm to 5.07 μm . Also, H_b is increased from 5.73 μm to 5.89 μm. The number of fingers is dropped from 18 to 17. As Figs. 4-2 (h) and (i) show, the number of busbars remains at 2. The optimum value of intensity of sunlight is 6, but the larger cell size becomes smaller as the intensity of sunlight reaches 5 at 90 % of probability of constraint satisfaction as shown in Figs. 4-2 (j).

- Rectangular cell

The conversion efficiency is decreased from 20.541 % to 20.516 % as shown in Table 4-9 under a probability of constraint satisfaction between 50 % and 95 %. The value of standard deviation suddenly declined from 2.643E – 04 to 2.553E – 04. Details are investigated below.

Figures 4-2 (a) - (b) establish that the thickness of the emitter ranges between 7.99 μm and 7.43 μm. The thickness of the base is in a range between 199 μm to 363 μm under a probability of constraint satisfaction between 50 % and 95 %, respectively. The cell length (L_c) is decreased from 1.76 cm to 1.71 cm under a probability of constraint satisfaction between 50 % and 90 % and then increases from 1.71 cm to 1.79 cm under a

probability of constraint satisfaction between 90% and 95 %. The length of height (H_c) is still 0.50 cm even though the conversion efficiency is decreased from 20.541 % to 20.516 %. The width of the fingers, as can be seen in Figs. 4-2 (d) and (e), is increased from 20.03 μm to 20.86 μm at 90 % of probability of constraint satisfaction; the width of the busbars is similarly increased from 100 μm to 104.45 μm at 90 % of probability of constraint satisfaction. As shown in Figs. 4-2 (f) and (g), the height of the fingers (H_f) is decreased from 5.00 μm to 4.87 μm under a probability of constraint satisfaction between 50 % and 90 %, followed by an increase in H_f from 4.87 μm to 5.04 μm under a probability of constraint satisfaction between 90 % and 95 %. The height of the busbars (H_b) is decreased from 6.00 μm to 5.73 μm under a probability of constraint satisfaction between 50 % and 90 % and then H_b is increased from 5.73 μm to 5.85 μm under a probability of constraint satisfaction between 90 % and 95 % as shown in Figs. 4-2 (h) and (i). The number of fingers is cut back from 12 to 11 under a probability of constraint satisfaction between 90 % and 95 %, but the number of busbars remains 2 as shown in Figs. 4-2 (h) and (i). The optimum value of intensity of sunlight is 6 as shown in Figs. 4-2 (j).

Table 4-9 Results of mean values and standard deviations of objective of probability optimization under different constraint satisfaction and 0.015 of coefficient of variation

Coefficient variation Of standard deviation		Probability of constraint satisfaction	$\bar{f}$	F	σ_f
			Optimal	Optimal	Optimal
0.015	Square	50%	0.20284	0.40568	3.387E-04
	Rectangular		0.20541	0.41823	2.643E-04
	Square	80%	0.20276	0.40552	3.412E-04
	Rectangular		0.20535	0.41070	2.647E-04
	Square	90%	0.20273	0.40546	3.180E-04
	Rectangular		0.20531	0.41062	2.657E-04
	Square	95%	0.20243	0.40487	3.226E-04
	Rectangular		0.20516	0.41033	2.553E-04

❖ 0.02 of coefficient of variation

Table 4-10 shows the results of mean values and standard deviations of objective of probability optimization under different constraint satisfaction and 0.02 of coefficient variation of standard deviation.

- Square cell

The conversion efficiency is decreased from 20.284 % to 20.243 % as shown in Table 4-2 under a probability of constraint satisfaction between 50 % and 90%. The value of standard deviation declines from 4.503E – 04 to 4.322E – 04. Details are investigated below.

As shown in Figs. 4-2 (a) - (b), the thickness of the emitter rests between 7.84 μm and 7.68 μm and the thickness of the base ranges between 420 μm to 302 μm under a probability of constraint satisfaction between 50 % and 90 %, respectively. The cell length is decreased from 0.80 cm down 0.79 cm under a probability of constraint

satisfaction between 50 % and 80 % and then increased from 0.79 cm to 0.84 cm under a probability of constraint satisfaction between 80 % and 90 %. The width of the fingers escalates from 20 μm to 21.02 μm at a probability of constraint satisfaction between 80 % and 90 %, an increase that is reflected in Figs. 4-2 (d) and (e). An increase is also observed in the width of the busbars; it shifts from 100 μm to 105.27 μm for a square cell under a probability of constraint satisfaction between 80 % and 90 %. The heights of the fingers and busbars, as shown in Figs. 4-2 (f) and (g), are increased from 50 % to 80 % of probability of constraint satisfaction. However, after the probability exceeds 80 % of probability of constraint satisfaction, H_f is steeply increased from 4.88 μm to 5.07 μm . Also, H_b is increased from 5.76 μm to 5.88 μm. The number of fingers drops from 18 to 17, but the number of busbars remains 2 as shown in Figs. 4-2 (h) and (i). The optimum value of intensity of sunlight is 6, but the larger cell size becomes smaller as the intensity of sunlight reaches 5 at 90 % of probability of constraint satisfaction as shown in Figs. 4-2 (j).

- Rectangular cell

The conversion efficiency is decreased from 20.541 % to 20.459 % as shown in Table 4-10 under a probability of constraint satisfaction between 50 % and 90 %. The value of standard deviation suddenly decreased from 2.642E – 04 to 2.616E – 04. An explanation for this is made below.

Figures 4-2 (a) - (b) illustrate the range for the thickness of the emitter to fall between 7.99 μm and 7.75 μm and the thickness of the base between 222 μm to 408 μm under a probability of constraint satisfaction between 50 % and 90 %, respectively.

Under a probability of constraint satisfaction between 50 % and 80 %, the cell length (L_c) is decreased from 1.76 cm to 1.72 cm; it is subsequently increased from 1.72 cm to 2.09 cm under a probability of constraint satisfaction between 80% and 95 %. The length of height (H_c) is the same at 0.50 cm. The width of the fingers, as shown Figs. 4-2 (d) and (e), climbs from 20.00 μm to 23.93 μm under a probability of constraint satisfaction between 80% and 90 %; furthermore, the width of the busbars is dramatically increased from 100 μm to 121.61 μm under a probability of constraint satisfaction between 80% and 90 %. As shown in Figs. 4-2 (f) and (g), the height of the fingers (H_f) is decreased from 5.00 μm to 4.88 μm under a probability of constraint satisfaction between 50 % and 80 %. H_f is then increased from 4.88 μm to 5.72 μm under a probability of constraint satisfaction ranging between 80 % and 90 %. Also, the height of the busbars (H_b) is decreased from 6.01 μm to 5.76 μm under a probability of constraint satisfaction between 50 % and 80 % and then H_b is increased from 5.76 μm to 6.47 μm under a probability of constraint satisfaction between 80 % and 90 % as shown in Figs. 4-2 (h) and (i). In the case of the fingers, the number of fingers is decreased from 12 to 10 under a probability of constraint satisfaction between 80 % and 90 %; in the case of the busbars, the number remains fixed at 2 as shown in Figs. 4-2 (h) and (i). The optimum value of intensity of sunlight is 6 as shown in Figs. 4-2 (j).

Table 4-10 Results of mean values and standard deviations of objective of probability optimization under different constraint satisfaction and 0.02 of coefficient of variation

Coefficient variation Of standard deviation		Probability of constraint satisfaction	$\bar{f}$	F	σ_f
			Optimal	Optimal	Optimal
0.02	Square	50%	0.20284	0.40568	4.503E-04
	Rectangular		0.20541	0.41823	2.642E-04
	Square	80%	0.20276	0.40551	4.544E-04
	Rectangular		0.20533	0.41065	2.650E-04
	Square	90%	0.20243	0.40485	4.322E-04
	Rectangular		0.20459	0.40917	2.616E-04

Without consideration of probability of constraint satisfaction and coefficient, the total power loss (F_{sum}) is 11.04 % for a square cell and 9.91 % for a rectangular cell including individual factors: the surface sheet (F_{sr}), contact (F_c), grid metal of fingers (F_f), busbars resistivity (F_b) and shadowing (F_s), and the maximum conversion efficiencies (η_c) are 20.284 % and 20.541 % in both cells. With the increments of the probability and coefficient variation, the total power losses (F_{sum}) are increased due to an increase in values of geometric design variables, which is associated with a decrease in conversion efficiency.

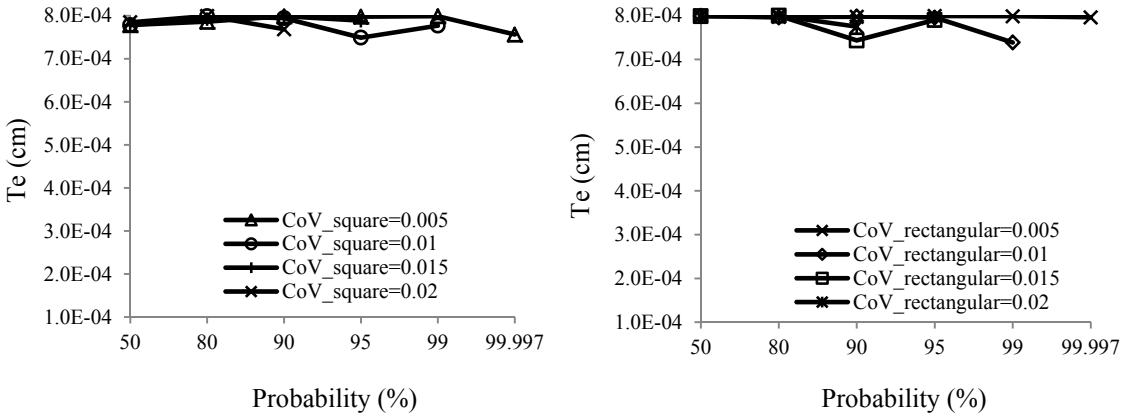
8.0E-04
7.0E-04
6.0E-04
5.0E-04
4.0E-04
3.0E-04
2.0E-04
1.0E-04
Te (cm)
CoV_square=0.005
CoV_square=0.01
CoV_square=0.015
CoV_square=0.02
50
80
90
95
99
99.997
Probability (%)
CoV_rectangular=0.005
CoV_rectangular=0.01
CoV_rectangular=0.015
CoV_rectangular=0.02

(a)

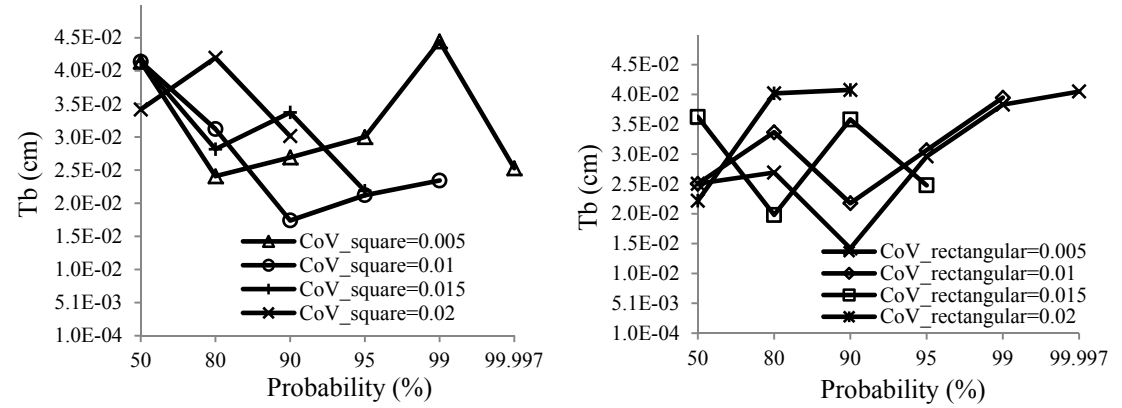
4.5E-02
4.0E-02
3.5E-02
3.0E-02
2.5E-02
2.0E-02
1.5E-02
1.0E-02
5.1E-03
1.0E-04
Tb (cm)
CoV_square=0.005
CoV_square=0.01
CoV_square=0.015
CoV_square=0.02
50
80
90
95
99
99.997
Probability (%)
CoV_rectangular=0.005
CoV_rectangular=0.01
CoV_rectangular=0.015
CoV_rectangular=0.02

(b)

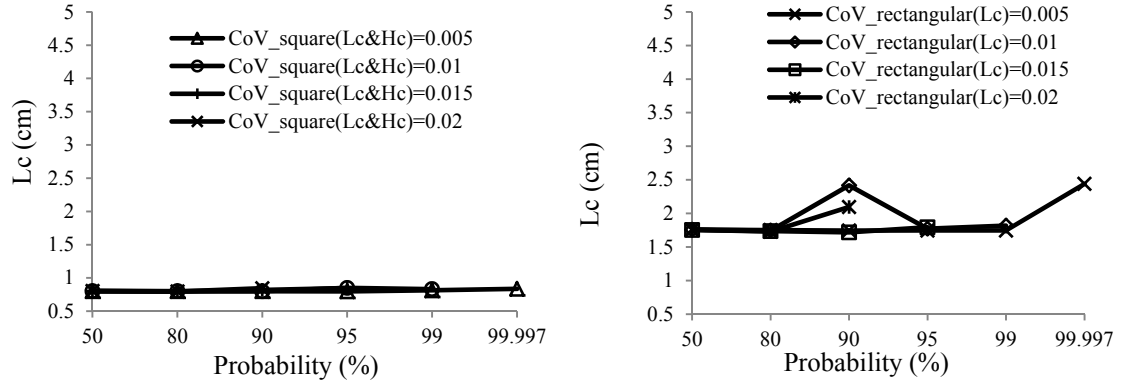
5
4.5
4
3.5
3
2.5
2
1.5
1
0.5
Lc (cm)
CoV_square(Lc&Hc)=0.005
CoV_square(Lc&Hc)=0.01
CoV_square(Lc&Hc)=0.015
CoV_square(Lc&Hc)=0.02
50
80
90
95
99
99.997
Probability (%)
CoV_rectangular(Lc)=0.005
CoV_rectangular(Lc)=0.01
CoV_rectangular(Lc)=0.015
CoV_rectangular(Lc)=0.02

(c) - 1

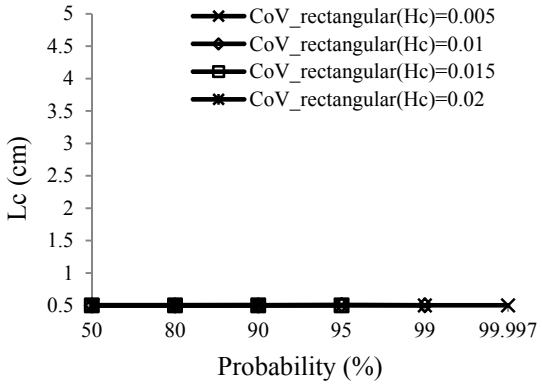
CoV_rectangular(Hc)=0.005
CoV_rectangular(Hc)=0.01
CoV_rectangular(Hc)=0.015
CoV_rectangular(Hc)=0.02
Lc (cm)
5
4.5
4
3.5
3
2.5
2
1.5
1
0.5
50
80
90
95
99
99.997
Probability (%)

(c) - 2

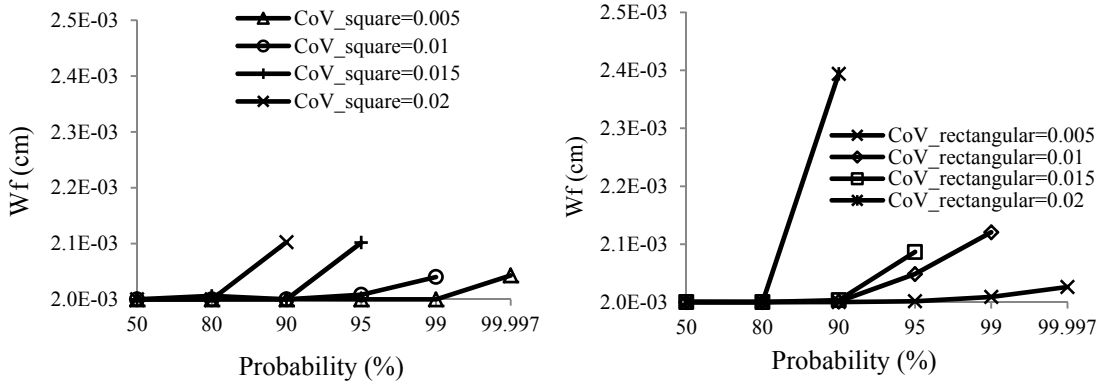
CoV_square=0.005
CoV_square=0.01
CoV_square=0.015
CoV_square=0.02
Wf (cm)
2.5E-03
2.4E-03
2.3E-03
2.2E-03
2.1E-03
2.0E-03
50
80
90
95
99
99.997
Probability (%)
CoV_rectangular=0.005
CoV_rectangular=0.01
CoV_rectangular=0.015
CoV_rectangular=0.02
Wf (cm)
2.5E-03
2.4E-03
2.3E-03
2.2E-03
2.1E-03
2.0E-03
50
80
90
95
99
99.997
Probability (%)

(d)

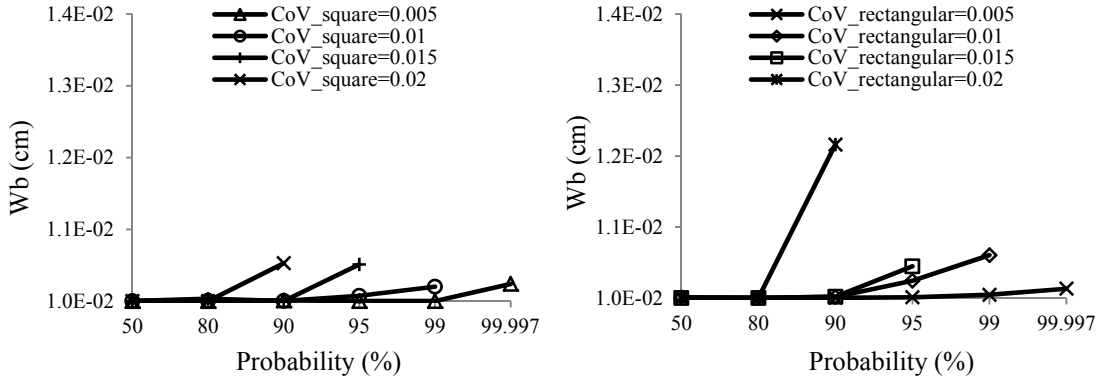
CoV_square=0.005
CoV_square=0.01
CoV_square=0.015
CoV_square=0.02
Wb (cm)
1.4E-02
1.3E-02
1.2E-02
1.1E-02
1.0E-02
50
80
90
95
99
99.997
Probability (%)
CoV_rectangular=0.005
CoV_rectangular=0.01
CoV_rectangular=0.015
CoV_rectangular=0.02
Wb (cm)
1.4E-02
1.3E-02
1.2E-02
1.1E-02
1.0E-02
50
80
90
95
99
99.997
Probability (%)

(e)

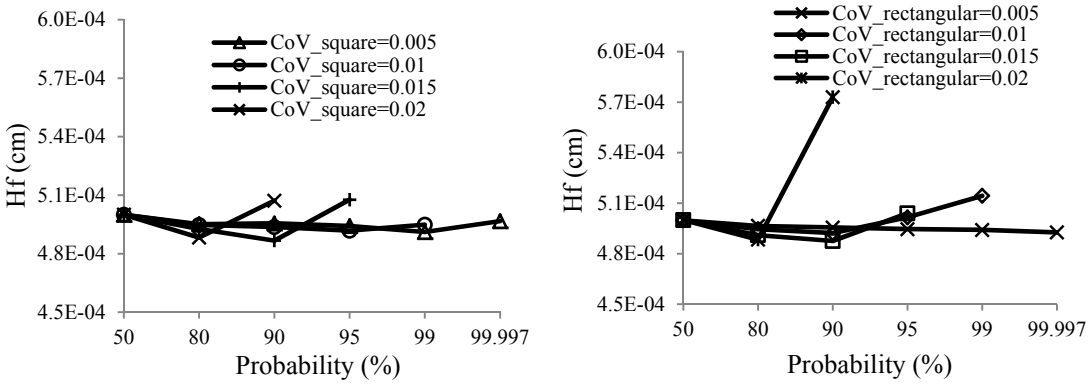
6.0E-04
5.7E-04
5.4E-04
5.1E-04
4.8E-04
4.5E-04
Hf (cm)
CoV_square=0.005
CoV_square=0.01
CoV_square=0.015
CoV_square=0.02
50
80
90
95
99
99.997
Probability (%)
CoV_rectangular=0.005
CoV_rectangular=0.01
CoV_rectangular=0.015
CoV_rectangular=0.02

(f)

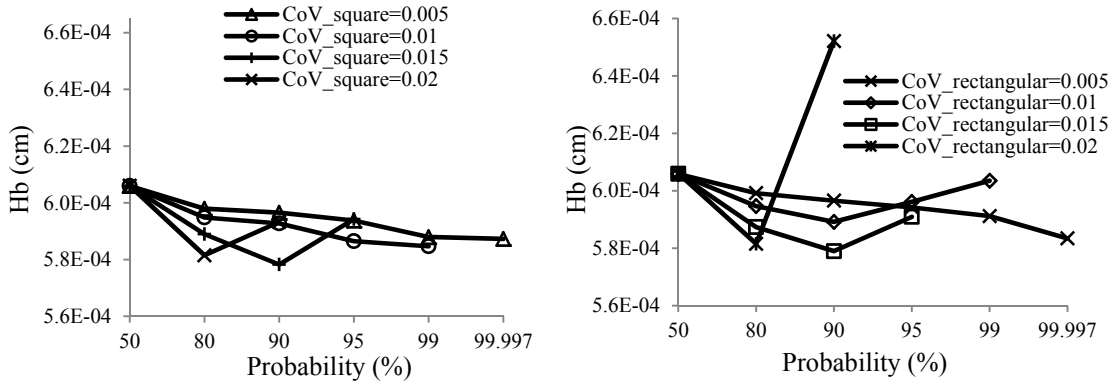
6.6E-04
6.4E-04
6.2E-04
6.0E-04
5.8E-04
5.6E-04
Hb (cm)
CoV_square=0.005
CoV_square=0.01
CoV_square=0.015
CoV_square=0.02
50
80
90
95
99
99.997
Probability (%)
CoV_rectangular=0.005
CoV_rectangular=0.01
CoV_rectangular=0.015
CoV_rectangular=0.02

(g)

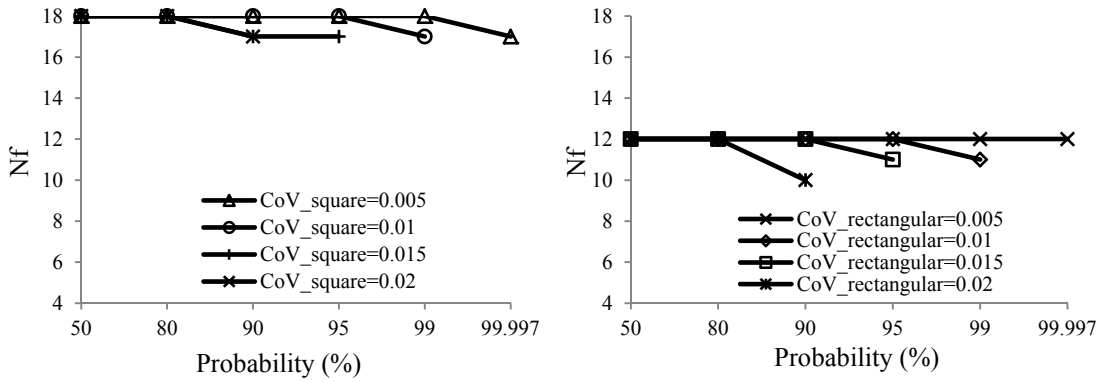
18
16
14
12
10
8
6
4
Nf
CoV_square=0.005
CoV_square=0.01
CoV_square=0.015
CoV_square=0.02
50
80
90
95
99
99.997
Probability (%)
CoV_rectangular=0.005
CoV_rectangular=0.01
CoV_rectangular=0.015
CoV_rectangular=0.02

(h)

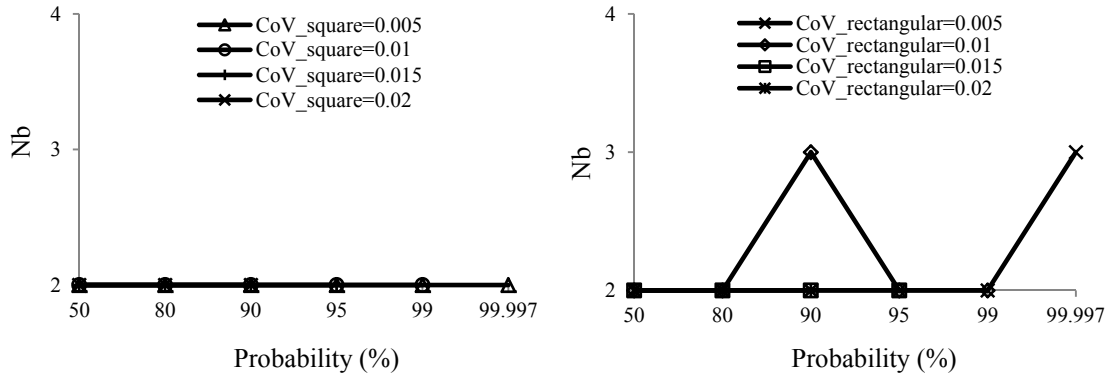

(i)

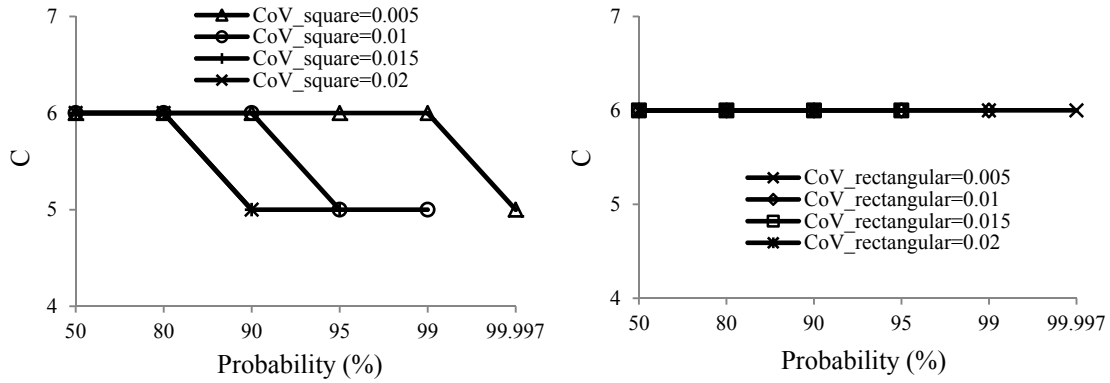

(j)

Figure 4-2 Results of design variables under coefficient variation and probability of constraint satisfaction

4.3.3 Flat plate solar PV array systems

The deterministic optimization method is used to predict optimal flat plate PV array system design without considering the stochastic behaviors. Therefore, the stochastic approach involves a higher level of complexity and involves statistical processing for reliability.

The conversion efficiency of a solar cell ($\overline{f_1} + \sigma_{f_1}$) is dependent on the size of the cells, geometric parameters and the number of fingers and busbars. Power output ($\overline{f_2} + \sigma_{f_2}$) and amount of annual monthly average incident solar energy ($\overline{f_3} + \sigma_{f_3}$) of a flat plate PV collector system is determined by the size of the cells, panels, and arrays and power density, which is associated with the conversion efficiency, distance between adjacent rows of the collectors, tilt angle of arrays, and number of arrays to maximize power output and incident solar energy under given constraints. Also, cost ($\overline{f_4} + \sigma_{f_4}$) is estimated by the results of the conversion efficiency ($\overline{f_1} + \sigma_{f_1}$), power output ($\overline{f_2} + \sigma_{f_2}$), and annual monthly average incident solar energy ($\overline{f_3} + \sigma_{f_3}$) considering subsystems – solar cell, panel module, and array. When the probability of constraint satisfaction is 50 %, all design variables maintain their values without regard to the coefficient of variation of the random parameters because the value of probability is applied to zero, which indicates the deterministic optimization results.

4.3.3.1 Numerical results

The uncertain parameters are assumed to be independent, normally distributed random variables with known mean and standard deviations. A new multi-objective problem is solved using the MOGT-based optimization technique pertaining to the results of four single-objective problems (maximum conversion efficiency, maximum power output, maximization of annual monthly average incident solar energy, and minimum cost) for finding a compromise solution.

Influences of probability of constraint satisfaction and coefficient variation of random variables are investigated. The results of multi-objective optimization using modified

game theory obtained with the different probability of constraint satisfaction varying from 50 % to 99.997 % are given in Table 4-11 (a) and coefficients of variation of random variables in a range between 0.5 % and 2 % are shown in Table 4-11 (b).

As the probability of constraint satisfaction is increased from 50 % to 99.997 %, the optimum values of design variables deviate from their optimum values. Table 4-11 shows the results of a flat plate PV collector design for different levels of probability of constraint satisfaction (CoV of all random variables =0.005).

1. Variation of T_e (x_1) and T_b (x_2)

The thickness of the emitter changes between 7 μm and 8 μm in both a square and a rectangular cell; as well, the thickness of the base increases from 258 μm to 435 μm for a square cell and from 260 μm to 380 μm for a rectangular cell. Higher thicknesses of the emitter and base contribute to increases in conversion efficiency, but the variations of thickness of the emitter and base in solar cells have only a mere impact on conversion efficiency. However, the geometric design variables of the fingers and busbars dominate the conversion efficiency.

2. Variation of L_c (x_3) and H_c (x_4)

The length of a square cell and a rectangular cell is decreased from 10.70 cm to 10.16 cm for a square cell as well as is decreased from 19.23 cm to 14.71 cm for the length and 13.32 cm to 11.55 cm for the height in a rectangular cell, which contributes to the geometry of the fingers and busbars.

3. Variation of W_f (x_5), H_f (x_6) and N_f (x_7)

The width of the fingers is decreased from 196.63 µm to 44.84 µm in a square cell as well as is decreased from 199.26 µm to 56.95 µm in a rectangular cell. The height of the fingers is decreased from 49.15 µm to 10.90 µm in a square cell and is decreased from 49.32 µm to 13.81 µm in a rectangular cell. The number of fingers is increased from 43 to 78 in a square cell and from 53 to 81 in a rectangular cell.

4. Variation of W_b (x_8), H_b (x_9) and N_b (x_{10})

The width of the busbars is decreased from 1619.48 µm to 459.62 µm in a square cell and from 999.10 µm to 683.70 µm in a rectangular cell. The height of the busbars is decreased from 49.97 µm to 11.59 µm in a square cell and from 49.76 µm to 14.38 µm in a rectangular cell. The number of busbars is increased from 2 to 10 in a square cell and from 6 to 10 in a rectangular cell.

The total power losses (F_{sum}) in both square and rectangular cells are associated with the conversion efficiency and explained with variations of parametric values of design variables. The total power loss in a square cell decreased from 17.12 % to 13.59 %, which indicates a rise in the conversion efficiency. The main parametric design variables contributing to increases in the conversion efficiency are the fingers and busbars because the decrease in geometric values of the fingers and busbars trigger increased individual power losses of grid metal of the fingers and busbars. On the other hand, while decreasing the geometric values of the fingers and busbars, the number of fingers and busbars is increased up to 10. This increase in the number of fingers and busbars results in trade-off between the geometric values and the numbers of fingers and busbars because the individual power losses of surface sheet (F_{sr}) and contact (F_c) are decreased

and the shadowing loss is likewise decreased. Similarly, the total power loss in a rectangular cell is decreased from 17.14 % to 14.84 % due to trade-off between the geometric values and the number of fingers and busbars. However, the difference between a square cell and a rectangular cell is that the side of length of a cell (L_c) is more flexible, so the fractional power loss of the fingers is higher than the fractional power loss of the busbars. As a result, conversion efficiencies of solar cells are increased from 17.42 % to 18.13 % in a square cell and from 17.42 % to 17.94 % in a rectangular one, explicable by a reduction of total power loss from the geometric variations in the number of fingers and busbars.

5. Variation of N_{l_c} (x_{11}) and N_{h_c} (x_{12})

The number of cells is increased from 5 to 8 in a square cell and varies between 3 and 5 in a rectangular cell for the side of length of a cell (L_c); notably, the number of cells is 6 in a square cell, but the number of cells is increased from 5 to 8 in a rectangular cell for the side of height (H_c), which consists of a single panel for an array system.

6. Variation of N_{l_p} (x_{13}) and N_{h_p} (x_{14})

The number of panels (N_{l_p}) is decreased from 56 to 36 in a square cell and from 58 to 39 in a rectangular cell for the side of length of a panel (L_p). The number of panels (N_{h_p}) is decreased from 3 to 2 in a rectangular cell for the side of height of a panel (H_p), but the number of panels (N_{h_p}) is constant as 3 in a square cell.

7. Variation of D (x_{15}) and β (x_{16})

The distance between adjacent rows and the tilt angle of arrays along with the size of cells, panels, and arrays is associated with the amount of incident solar energy. The distance between adjacent rows of the arrays is increased from 80.06 cm to 83.73 cm in a square cell and from 80.23 cm to 85.04 cm in a rectangular cell. The tilt angle of the arrays is increased from 22.93° to 26.52° in a square cell and from 20.19° to 24.18° in a rectangular cell.

8. Variation of K (x_{17})

The variations of cells and panels have an influence on the number of arrays, which is increased from 78 to 80 in a square cell and from 75 to 78 in a rectangular cell, under given constraints. In a range between 50 % and 95 %, the number of cells and panels is constant: 5 in length side of cells, 6 in height side of cells, 56 in length side of panels, and 3 in height side of panels with 78 arrays, but the distance between adjacent rows of arrays is gradually increased to generate maximum power output while modifying cell size to consist of panels and arrays under specified constraints. After the value of constraint satisfaction exceeds 95 %, the number of 57 in side of length of a panel (L_p) and 79 arrays starts to increase from 56 and 78, respectively, because the feasible ranges of the length and height of the cells, panels, and arrays are becoming restricted under different probabilities of constraint satisfaction. At 99.997 % of constraint satisfaction, the optimum design variables of the numbers of cells, panels, and arrays and new objective optimization are suddenly boosted to higher values, explicable by severely limited constraints.

Table 4-11 (a) Results of flat plate PV collector design for different levels of probability of constraint satisfaction (CV of all random variables =0.005)

Probability of constraint satisfaction		Design variables									
		T_e (μm)	T_b (μm)	L_c (cm)	H_c (cm)	W_f (μm)	H_f (μm)	N_f	W_b (μm)	H_b (μm)	N_b
50%	Sq.	7.74	258.76	10.70	10.70	196.63	49.15	43	1619.48	49.97	2
	Rec.	7.26	260.29	19.23	13.32	199.26	49.32	53	999.10	49.76	6
80%	Sq.	8.00	289.64	10.67	10.67	175.92	43.72	45	1708.67	44.46	2
	Rec.	8.00	225.06	17.50	13.28	187.26	46.54	54	943.62	47.27	6
90%	Sq.	8.00	357.36	10.65	10.65	125.18	31.01	51	818.02	31.74	4
	Rec.	7.97	225.61	17.13	13.09	135.74	33.63	61	984.85	34.33	6
95%	Sq.	7.64	428.88	10.63	10.63	98.60	24.37	56	788.81	25.09	5
	Rec.	8.00	328.66	17.10	13.10	124.27	30.71	63	1041.03	31.36	6
99%	Sq.	8.00	430.88	10.41	10.41	53.45	13.15	72	427.38	13.15	10
	Rec.	8.00	376.37	17.04	13.02	73.61	18.10	80	758.10	18.81	10
99.997%	Sq.	7.14	435.26	10.16	10.16	44.84	10.90	78	459.62	11.59	10
	Rec.	7.46	380.29	14.71	11.55	56.95	13.81	81	683.70	14.38	10

Probability of constraint satisfaction		Design variables						
		N_{l_c}	N_{h_c}	N_{l_p}	N_{h_p}	D (cm)	β (degree)	K
50%	Sq.	5	6	56	3	80.06	22.93	78
	Rec.	4	5	39	3	80.23	20.19	75
80%	Sq.	5	6	56	3	80.29	23.34	78
	Rec.	3	5	57	3	80.25	20.43	75
90%	Sq.	5	6	56	3	81.20	24.05	78
	Rec.	3	5	58	3	81.31	22.31	76
95%	Sq.	5	6	56	3	81.91	24.59	78
	Rec.	3	5	58	3	81.93	23.16	76
99%	Sq.	5	6	57	3	82.80	25.38	79
	Rect.	3	5	58	3	82.49	23.27	76
99.997%	Sq.	8	6	36	3	83.73	26.52	80
	Rec.	5	8	40	2	85.04	24.18	78

Table 4-11 (b) Results of flat plate PV collector design variables under probability of constraint satisfaction of 90 % with respect to coefficient of variation of random variable

Coefficient of variation		Design variables									
		T_e (μm)	T_b (μm)	L_c (cm)	H_c (cm)	W_f (μm)	H_f (μm)	N_f	W_b (μm)	H_b (μm)	N_b
0.05%	Sq.	8.00	357.36	10.65	10.65	125.18	31.01	51	818.02	31.74	4
	Rec.	7.97	225.61	17.13	13.09	135.74	33.63	61	984.85	34.33	6
1%	Sq.	7.61	360.38	10.52	10.52	100.51	24.68	55	502.58	25.24	7
	Rec.	8.00	263.24	17.02	13.16	97.55	23.95	70	865.20	24.52	8
1.5%	Sq.	8.00	260.18	10.33	10.33	50.17	12.21	74	436.35	12.88	10
	Rec.	7.97	343.04	17.52	12.21	73.35	17.85	76	825.18	18.37	9
2%	Sq.	8.00	304.75	10.37	10.37	32.04	7.73	100	544.59	8.45	10
	Rec.	5.83	331.51	18.75	13.00	56.98	13.75	95	912.26	14.25	10

Coefficient of variation		Design variables						
		N_{l_c}	N_{h_c}	N_{l_p}	N_{h_p}	D (cm)	β (degree)	K
0.05%	Sq.	5	6	56	3	81.20	24.05	78
	Rec.	3	5	58	3	81.31	22.31	76
1%	Sq.	5	6	56	3	82.78	24.61	78
	Rec.	3	5	58	3	80.83	23.68	76
1.5%	Sq.	5	6	57	3	84.36	24.29	78
	Rec.	3	5	56	3	81.89	22.95	79
2%	Sq.	6	8	47	2	88.07	25.78	83
	Rec.	4	4	39	3	83.42	25.74	88

The size of a single panel ($L_p \times H_p$) is increased from 3248.1 cm^2 to 4950.5 cm^2 in a square cell and from 3328.9 cm^2 to 6796.1 cm^2 in a rectangular cell, but the size of a single cell ($L_c \times H_c$) and single array ($L_a \times H_a$) is decreased from 114.5 cm^2 to 103.1 cm^2 and from 576,921 cm^2 to 534,658 cm^2 in a square cell, respectively. The size of single cell and single array is decreased from 256.1 cm^2 to 169.9 cm^2 and from 599,331 cm^2 to 543,691 cm^2 in a rectangular cell, respectively.

In a range between 50 % and 99 % of constraint satisfaction, the area of the flat plate PV collector system is decreased up to 2.49 % in a square cell and from up to 2.07 % in a rectangular cell, respectively. However, after exceeding 99 % of constraint satisfaction, the flat plate PV collector area is critically decreased up to 4.95 % in a square cell and 5.66 % in a rectangular cell because the length and height of the arrays are decreased up to 2.37 % and up to 5.08 % in a square cell and decreased up to 1.96 % and up to 7.74 % in a rectangular cell, which are associated with the area of the flat-plate PV collector system. Figure 4-3 shows variations of arrays including solar cells and panel modules under coefficient of variation of 0.005 with respect to different levels of probability of constraint satisfaction.

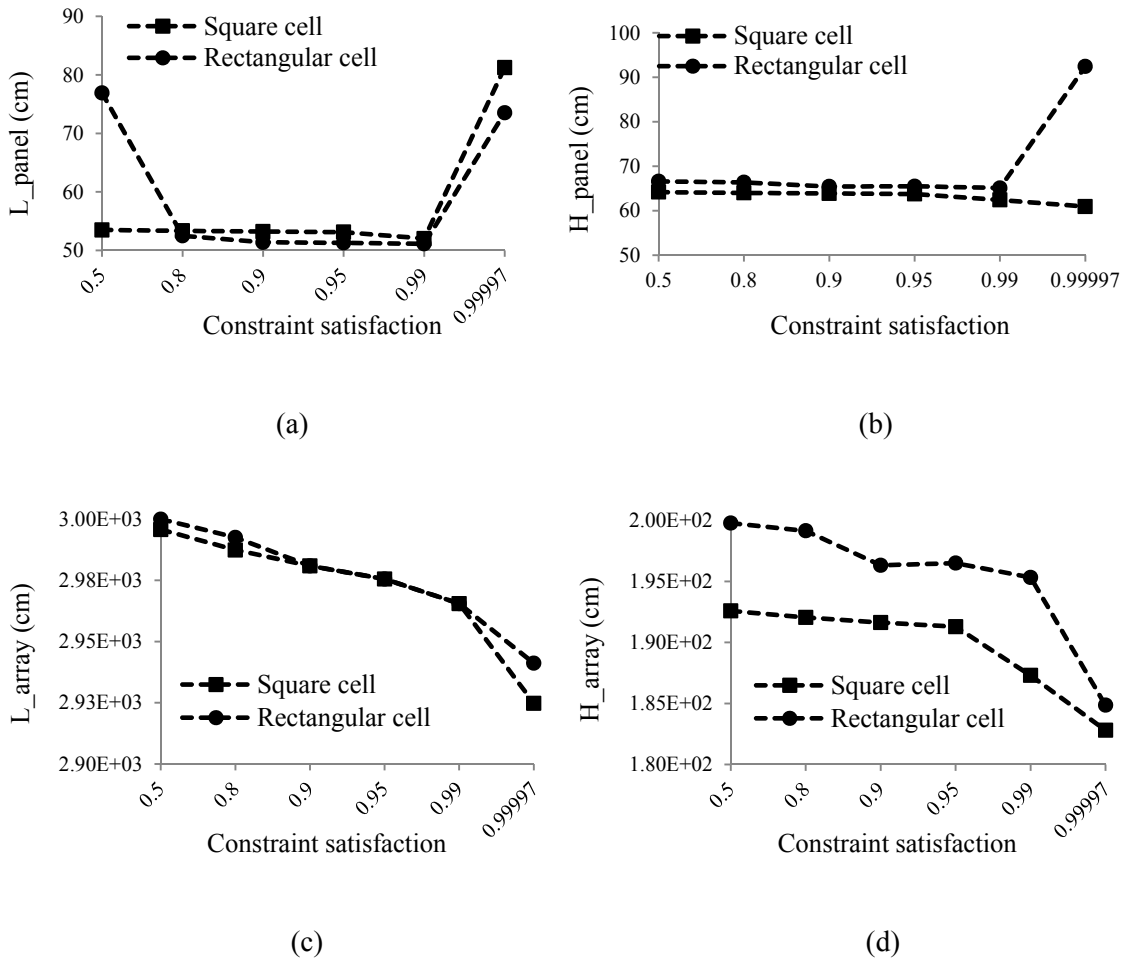

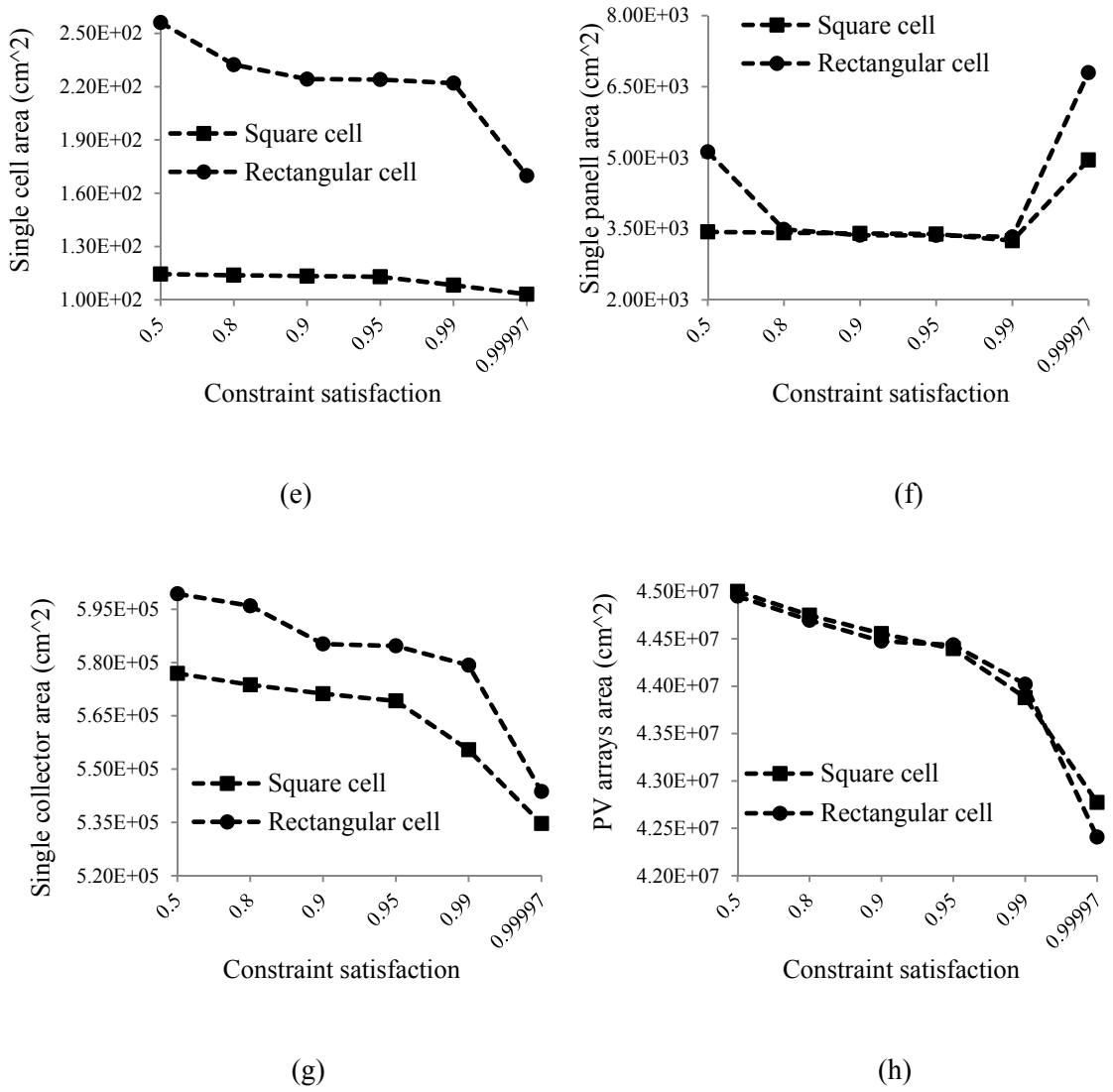

Figure 4-3 Variations of arrays including solar cells and panel modules under coefficient of variation of 0.005 with respect to probability of constraint satisfaction

As shown in Table 4-12, the maximum values of the new objective function, -(FC - S), decreased from 0.11826 to 0.02054 in a square cell and decreased from 0.13585 to -0.00143 in a rectangular cell under the probability of constraint satisfaction in a range from 50 % to 99.997 % with a coefficient variation of 0.005. An observation on the variation of the weights of c_1, c_2, c_3, and c_4 applied in the Pareto optimal solutions

indicated that f_3 is dominant in the multi-objective optimization in a square cell in a range between 50 % and 95 % of probability of constraint satisfaction. After the probability exceeds 95 %, the dominant factor in the multi-objective optimization switched from f_3 into f_1 in a range between 95 % and 99.997 %. On the other hand, when the probability of constraint satisfaction is 50 %, f_3 is dominant in the multi-objective optimization in a rectangular cell. In a range between 80 % and 90 %, f_4 is dominant because the number of arrays is increased from 75 to 76; in addition, in a range between 90 % and 95 %, f_3 is dominant because the values of distance between adjacent rows of the arrays and the tilt angle increases from 81.93 cm to 82.49 cm and from 23.16° to 23.27° with the number of arrays set at 76, respectively. When the probability of constraint satisfaction is above 99 %, f_1 is the dominant factor to optimize a multi-objective problem in a flat plate PV collector system explicable by tighter restrictions of geometric design parameters and the number of fingers and busbars. As a result, the conversion efficiencies of solar cells ($\overline{f_1}+\sigma_{f_1}$) are increased from 17.43 % to 18.13 % in a square cell and from 17.43 % to 17.94 % in a rectangular one due to reduction of total power loss from the geometric variations of the number of fingers and busbars. Power output ($\overline{f_2}+\sigma_{f_2}$) of a flat plate PV array system varies between 6.6682E + 05 W and 6.8230E + 05 W in a square cell and fluctuates between 6.6575E + 05 W and 6.6971E + 05 W in a rectangular cell. Annual monthly average incident solar energy ($\overline{f_3}+\sigma_{f_3}$) in the flat plate PV array system is decreased from 9.7428E + 05 W to 9.1889E+05 W in a square cell and decreased from 9.7813E + 05 W to 9.1925E + 05 W in a rectangular cell. The cost ($\overline{f_4}+\sigma_{f_4}$) varies between 9.5206E + 05 $ and 9.2100E + 05 $ in a square cell and between 9.3398E + 05 $ and 9.0217E + 05 $ in a rectangular cell.

Table 4-12 (a) Results of variation of constraint satisfaction probability on multi-objective optimization (Coefficient of variation of uncertain value: 0.005)

Coefficient variation of standard deviation		Probability of constraint satisfaction	Pareto optimal solution			Value of $\vec{f}=\begin{Bmatrix}\overline{f_1}\ (\%)\\ \overline{f_2}\ (W)\\ \overline{f_3}\ (W)\\ \overline{f_4}\ (\$)\end{Bmatrix}$ at $\vec{x^*}$
			FC (Weighted obj. function)	S (Supercriterion)	F = (FC – S) (New obj. function)	
0.005	Sq. Rec.	50%	0.04852	0.16678	-0.11826	$\begin{Bmatrix}17.43\\ 6.6682\text{E}+05\\ 9.7428\text{E}+05\\ 9.2988\text{E}+05\end{Bmatrix}$
			0.05117	0.18701	-0.13585	$\begin{Bmatrix}17.43\\ 6.6575\text{E}+05\\ 9.7813\text{E}+05\\ 9.2776\text{E}+05\end{Bmatrix}$
		80%	0.07133	0.16891	-0.09757	$\begin{Bmatrix}17.52\\ 6.6638\text{E}+05\\ 9.6767\text{E}+05\\ 9.2938\text{E}+05\end{Bmatrix}$
			0.11513	0.18547	-0.07034	$\begin{Bmatrix}17.49\\ 6.6457\text{E}+05\\ 9.7233\text{E}+05\\ 9.2618\text{E}+05\end{Bmatrix}$
		90%	0.10873	0.19882	-0.09009	$\begin{Bmatrix}17.97\\ 6.8040\text{E}+05\\ 9.6176\text{E}+05\\ 9.4919\text{E}+05\end{Bmatrix}$
			0.15645	0.19751	-0.04105	$\begin{Bmatrix}17.71\\ 6.6931\text{E}+05\\ 9.6439\text{E}+05\\ 9.3330\text{E}+05\end{Bmatrix}$
		95%	0.11014	0.19733	-0.08720	$\begin{Bmatrix}18.08\\ 6.8230\text{E}+05\\ 9.5692\text{E}+05\\ 9.5206\text{E}+05\end{Bmatrix}$
			0.17383	0.19636	-0.02252	$\begin{Bmatrix}\mathbf{17.73}\\ \mathbf{6.6971E+05}\\ \mathbf{9.6138E+05}\\ \mathbf{9.3398E+05}\end{Bmatrix}$

0.005	Sq. Rec.	99%	0.11189	0.19858	-0.08669	$\begin{Bmatrix} \mathbf{18.17} \\ \mathbf{6.7778E+05} \\ \mathbf{9.4471E+05} \\ \mathbf{9.4640E+05} \end{Bmatrix}$
			0.18089	0.18675	-0.00587	$\begin{Bmatrix} 17.79 \\ 6.6561E+05 \\ 9.5276E+05 \\ 9.2851E+05 \end{Bmatrix}$
		99.997%	0.15046	0.17100	-0.02054	$\begin{Bmatrix} 18.13 \\ 6.5907E+05 \\ 9.1889E+05 \\ 9.2100E+05 \end{Bmatrix}$
			0.13995	0.13852	0.00143	$\begin{Bmatrix} \mathbf{17.91} \\ \mathbf{6.4552E+05} \\ \mathbf{9.1925E+05} \\ \mathbf{9.0217E+05} \end{Bmatrix}$

Table 4-12(b) Results of variation of coefficient of variation on multi-objective optimization (Probability of constraint satisfaction: 90%)

Probability of constraint satisfaction		Coefficient variation of standard deviation	Pareto optimal solution			Value of $\vec{f}=\begin{Bmatrix}\overline{f_1}\ (\%)\\ \overline{f_2}\ (W)\\ \overline{f_3}\ (W)\\ \overline{f_4}\ (\$)\end{Bmatrix}$ at $\vec{x^*}$
			FC (Weighted obj. fun.)	S (Supercriterion)	F = (FC – S) (New obj. function)	
90%	Sq. Rec.	0.005	0.10873	0.19882	-0.09009	$\begin{Bmatrix}17.97\\ 6.8040\text{E}+05\\ 9.6176\text{E}+05\\ 9.4919\text{E}+05\end{Bmatrix}$
			0.15645	0.19751	-0.04105	$\begin{Bmatrix}17.71\\ 6.6931\text{E}+05\\ 9.6439\text{E}+05\\ 9.3330\text{E}+05\end{Bmatrix}$
		0.01	0.12545	0.19031	-0.06486	$\begin{Bmatrix}18.13\\ 6.7087\text{E}+05\\ 9.3955\text{E}+05\\ 9.3652\text{E}+05\end{Bmatrix}$
			0.19276	0.19965	-0.00689	$\begin{Bmatrix}17.79\\ 6.7208\text{E}+05\\ 9.5871\text{E}+05\\ 9.3692\text{E}+05\end{Bmatrix}$
		0.015	0.11387	0.17597	-0.06212	$\begin{Bmatrix}18.15\\ 6.5833\text{E}+05\\ 9.2415\text{E}+05\\ 9.1979\text{E}+05\end{Bmatrix}$
			0.19743	0.14329	0.05417	$\begin{Bmatrix}17.86\\ 6.4643\text{E}+05\\ 9.2534\text{E}+05\\ 9.0286\text{E}+05\end{Bmatrix}$
		0.02	0.17312	0.11249	0.06062	$\begin{Bmatrix}17.86\\ 6.1152\text{E}+05\\ 8.7439\text{E}+05\\ 8.5765\text{E}+05\end{Bmatrix}$
			0.24383	0.10726	0.13657	$\begin{Bmatrix}\mathbf{17.85}\\ \mathbf{6.3209\text{E}+05}\\ \mathbf{9.2534\text{E}+05}\\ \mathbf{9.0286\text{E}+05}\end{Bmatrix}$

4.4 Fuzzy Set Analysis

The mapping of uncertain input onto an uncertain response is called fuzzy set analysis. Fuzzy set theory provides gradual membership from the domain of quantitative and precise phenomena to vague, qualitative and imprecise conceptions. A fuzzy member can be represented using the concept of a range of interval confidence. The fuzzy set theory allows a gradual membership functions in relation to the set. This gradual membership is explained by a membership function. Membership in a classical subset A of X can be defined as a characteristic function μ_A from X to [0, 1] as

$$\mu_A(x) = \begin{cases} 1 \ \ if \ f \ x \ \in A \\ 0 \ if \ f \ x \ \notin A \end{cases} \tag{4.27}$$

A set A is called a fuzzy set if the valuation set is allowed to be the real interval [0, 1]. The fuzzy set A is completely characterized as

$$\mathrm{A} = \{(x, \ \mu_A(x)), \ x \in X\} \tag{4.28}$$

The membership function $\mu_A(x)$ quantifies the degree of membership of the elements x in A. The closer the value of $\mu_A(x)$ is to 1, the more x belongs to A. A is a fuzzy subset of X that has no sharp boundary. When X is a finite set $\{x_1, x_2, \dots, x_n\}$, a fuzzy set on X can be defined as

$$\mathrm{A}=\mu_A(x_1) + \mu_A(x_2) + \cdots + \mu_A(x_n) = \sum_{i=1}^{n} \mu_A(x_i) \tag{4.29}$$

The extension principle plays a key role in translating set-based concepts into fuzzy-set counterparts for transforming fuzzy sets through membership function. The α-level method is used for analyzing fuzzy set. All fuzzy input parameters are discretized using a

number of α-levels. In the α-level approach, the optimum solution is considered as one which has at least a certain degree of membership in the fuzzy feasible domain. The α-cut of α-level set of fuzzy set A is a set consisting of those elements of the universe X whose membership values exceed the threshold level α and can be expressed as

$$A_{\propto} = \{x \,/\, \mu_A(x) \geq \alpha\} \tag{4.30}$$

The membership function associated with a fuzzy set can be explained by its triangular shape. It is a fuzzy number represented with three points as follows: A = (a_1, a_2, and a_3) and shown in Fig.4-5. This representation is interpreted as membership functions and defined as

$$\mu_A(x) = \begin{cases} 0 & if \;\; x < a_1 \\ \frac{x - a_1}{a_2 - a_1} & if \;\; a_1 \leq x \leq a_2 \\ \frac{a_3 - x}{a_3 - a_2} & if \;\; a_2 \leq x \leq a_3 \\ 0 & if \;\; x > a_3 \end{cases} \tag{4.31}$$

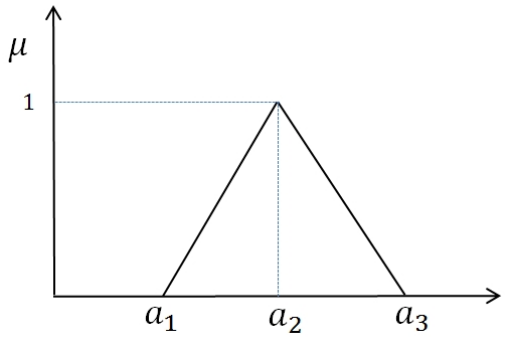

Figure 4-4 Triangular fuzzy number

The interval arithmetic method is used for applying the interval confidence of lower and upper bound values of uncertain input parameters and can be defined by the extension principle. The extension principle can be used to extend the four standard arithmetic

operators; addition, subtraction, multiplication, and division to be used with a fuzzy number. The lower and upper bound values are given by $y_i = y_i \pm \Delta y_i \; ; j = 1, 2, \ldots i$. y_i is the base value and Δy_i means the tolerance on y_i. A real number y is equivalent to an interval range [y, y], which has zero tolerance. The interval arithmetic method is used for creating the lower and upper bound values with the tolerance with interval arithmetic operations '•' (+, -, ×, ÷). Thus, the interval arithmetic value of X•Y can be formed from two intervals X = [$\underline{X}$, $\overline{X}$] and Y = [$\underline{Y}$, $\overline{Y}$]. The basic interval arithmetic operations are expressed as

$$\text{Addition: } X + Y = [\underline{X} + \underline{Y} \, , \overline{X} + \overline{Y}] \tag{4.32}$$

$$\text{Subtraction: } X - Y = [\underline{X} - \overline{Y}, \overline{X} + \underline{Y}] \tag{4.33}$$

$$\text{Multiplication: } X \times Y = \text{min. } [\underline{X} \times \underline{Y}, \; \underline{X} \times \overline{Y}, \overline{X} \times \underline{Y}, \overline{X} \times \overline{Y}],$$

$$\text{max. } [\underline{X} \times \underline{Y}, \; \underline{X} \times \overline{Y}, \overline{X} \times \underline{Y}, \overline{X} \times \overline{Y}] \tag{4.34}$$

$$\text{Division: } X \div Y = [\underline{X} \, , \overline{X}] \times [1/\overline{Y}, 1/\underline{Y}] \tag{4.35}$$

Solar PV array systems are analyzed through fuzzy set theory using a membership function in a fuzzy confidence interval. The deviation is determined by the difference between the membership function of the actual solar PV system performance and the crisp value of the PV system performance obtained using interval-valued fuzzy set and the membership function of the deterministic optimization of solar PV systems. The membership function of the actual performance of a solar cell placed Lb (low bound) for the left and Ub (upper bound) for the right segment. The membership function of the

crisp performance of a solar PV system is expressed as CP (crisp performance). The left side and right side errors can be calculated as

$$\Delta Lb = CP - Lb \text{ and } \Delta Ub = CP - Ub \tag{4.36}$$

The deviation of both sections can be derived from

$$\Delta Lb, \% = \left|1 - \frac{Lb}{CP}\right| \times 100 \quad \text{(deviation in lower bound section)} \tag{4.37}$$

and

$$\Delta Ub , \% = \left|1 - \frac{Ub}{CP}\right| \times 100 \quad \text{(deviation in upper bound section)} \tag{4.38}$$

Thus, the deviation as the percent absolute error with respect to solar PV system performance is calculated in both the lower bound and upper bound sections from the result of the crisp value of solar PV system performance. The α-cut interval levels of 0, 0.25, 0.50, 0.75, and 1 are applied to solar PV systems for prediction of deviations and variations.

4.4.1 Solar cells

The performance of a solar cell can be measured in terms of conversion efficiency and power output. The conversion efficiency and power output of a solar cell is investigated using fuzzy membership function.

4.4.1.1 Fuzzy analysis

The conversion efficiency is obtained by using the function of *ga* MATLAB program. The maximum conversion efficiencies (η_{ma}) are 20.28 % and 20.54 %, and the power

outputs are 9.46 W and 9.54 W in a square cell and a rectangular cell, respectively. The conversion efficiency in the fuzzy membership function is associated with geometric design parameters including the surface sheet, contact between the solar cell and grid metal contact, grid metal of fingers, busbars, and the shadowing from grid metal parts except for integer design values of a number of fingers and busbars, and intensity of sunlight. Thus, the uncertain input parameters, similarly, consist of 7 and 8 design parameters and all 4 uncertain design parameters in a square cell and a rectangular cell, respectively. As a result, the uncertain input parameters of the solar cell are applied to the fuzzy set analysis in the same way as uncertain input parameters.

The uncertain input parameters are

$$\vec{Y}=\begin{Bmatrix} P_{in} \\ \rho_m \\ R_c \\ R_{sh} \\ T_e \\ T_b \\ L_c \\ H_c \\ W_f \\ H_f \\ W_b \\ H_b \end{Bmatrix} \equiv \begin{Bmatrix} Y_1 \\ Y_2 \\ Y_3 \\ Y_4 \\ Y_5 \\ Y_6 \\ Y_7 \\ Y_8 \\ Y_9 \\ Y_{10} \\ Y_{11} \\ Y_{12} \end{Bmatrix} \tag{4.39}$$

±1 %, ±2 %, ±3 %, ±4 % and ±5 % of the fuzzy confidence intervals are applied to solar cell for observing the deviations varying the α-cut interval levels from crisp value.

4.4.1.2 Numerical results

- Conversion efficiency

In the case of a square cell, ±1 %, ±2 %, ±3 %, ±4 % and ±5 % of the fuzzy confidence interval, the percent deviations of solar cell conversion efficiency show the results of responses of 5.61 % and 25.15 % in the lower bound section and 5.90 % and 20.97 % to applying uncertain input parameters. Figures 4-5 (a) and (b) show the deviations from the crisp value in conversion efficiency and Figs. 4-6 (a) and (b) show the variations of the triangular shapes of a square cell and a rectangular cell. Conversion efficiency is associated with power losses, and the response to applying uncertain input parameters to a solar cell are observed with the example of ±2 % of fuzzy confidence interval in a square cell and a rectangular cell, respectively.

The crisp value of the total fractional power loss (F_{sum}) is 11.08 % at 20.28 % of the conversion efficiency. The total power loss (F_{sum}) becomes 2.38 % of the total power loss in the lower bound and 19.18 % of the total power loss in the upper bound. The total power loss reduced by the main individual fractional power loss is from the shadowing loss. The shadowing loss is 1.49 % in the lower bound and 14.64 % in the upper bound. These results indicate that the shadowing loss is caused by the size and number of fingers and busbars blocking sunlight.

In the case of ±2 % uncertain fuzzy confidence interval of the rectangular cell, the crisp value of the total fractional power loss (F_{sum}) is 9.93 % at 20.54 % of conversion efficiency. The total power loss becomes 1.39 % in the lower bound and 17.86 % in the upper bound. The main fractional power loss in the total power loss is from shadowing loss. The shadowing loss is 0.5 % in the lower bound and 13.69 % in the upper bound. Also, these results indicate that the shadowing loss is increased alongside any increases in

the cell size and number of fingers and busbars, which contribute to the blockage of sunlight.

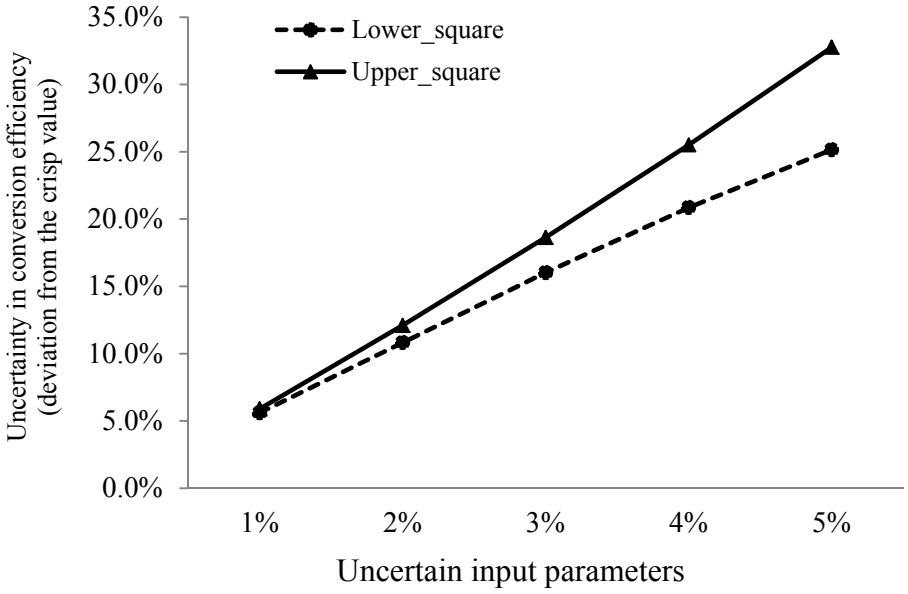

(a) Uncertainty in conversion efficiency of a square cell

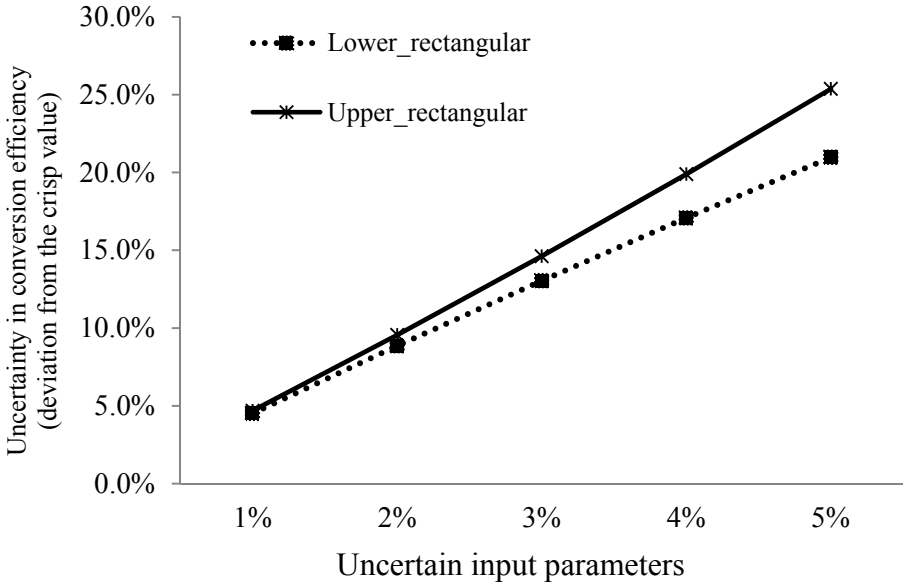

(b) Uncertainty in conversion efficiency of a rectangular cell

Figure 4-5 Variation of deviations from the crisp value in conversion efficiency

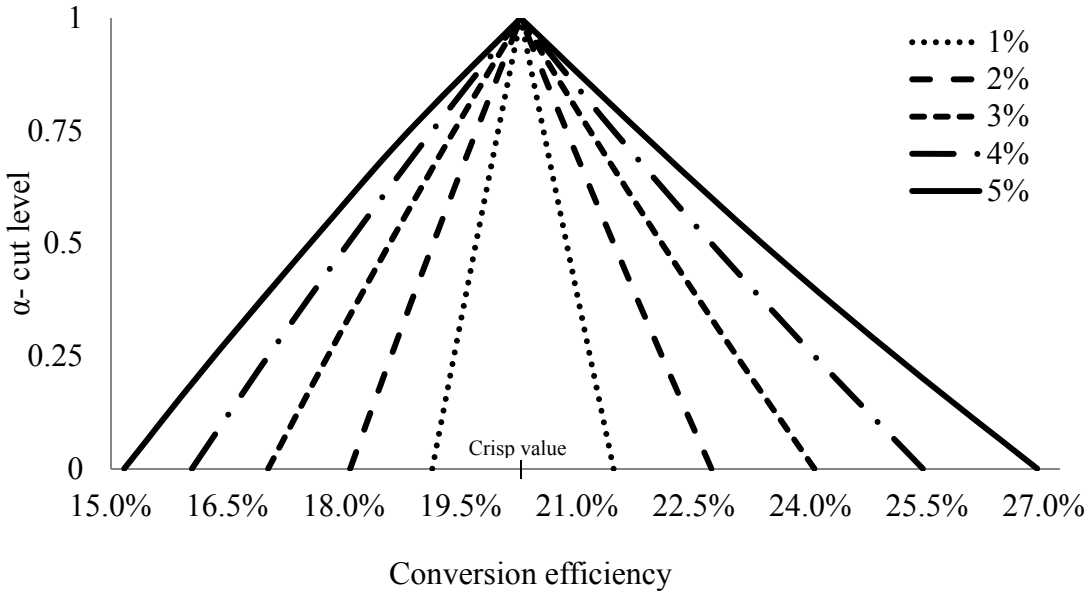

(a) Conversion efficiency of square cell

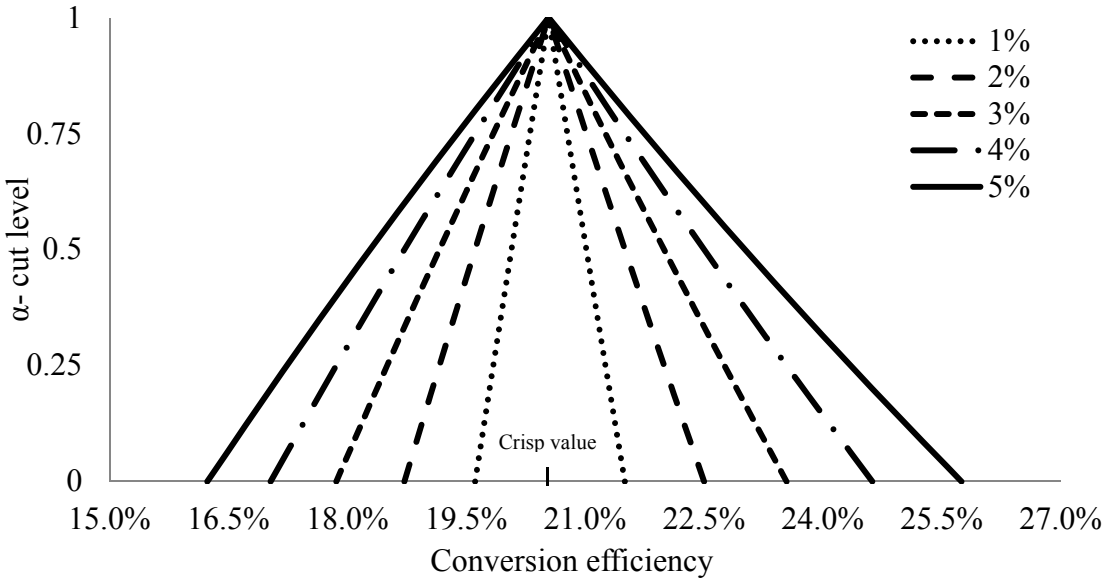

(b) Conversion efficiency of rectangular cell

Figure 4-6 Variation of triangular shapes from the crisp value in conversion efficiency with respect to a fuzzy confidence interval

- Power output

The response to applying uncertain input parameters with ±5 % uncertain fuzzy confidence interval in the solar cells show the deviations of 41.03 % in the lower bound and 52.98 % in the upper bound for a square cell and 39.96 % in the lower bound and 52.98 % in the upper bound for a rectangular cell from the crisp value of power output as shown in Fig. 4-7 (a) and (b), respectively. Also, Figs. 4-8 (a) and (b) show the change of the triangular shapes from the crisp value.

In the case of a square cell, at 0 of α-cut level, the fuzzy confidence intervals from ±1 % to ±5 % are applied to a solar cell for observing the deviations from the crisp value. The power output is associated with the cell size and the power density. The values of the power density applied by the fuzzy confidence interval are almost unaffected by the arithmetic operation of fuzzy analysis. However, the arithmetic operation has a significant impact on cell size (area). As a result, even though ±5 % of fuzzy confidence interval is applied, the response to uncertain input parameters increases significantly. For example, in the case of ±2 % uncertain fuzzy confidence interval of a square cell, the variations of deviation in the lower bound and the upper bound sections are different. With power densities of 0.579 ($\frac{\mathrm{W}}{\mathrm{cm}^2}$) in the lower bound and 0.581 ($\frac{\mathrm{W}}{\mathrm{cm}^2}$) in the upper bound from the crisp value of 0.580 ($\frac{\mathrm{W}}{\mathrm{cm}^2}$), these values of power densities indicate 0.198 % decreases and 0.1941 % increases from the crisp value, respectively. As a result, the cell size is a dominant factor for power output.

Similarly, in the case of ±2 % of uncertain interval confidence, with power densities of 0.984 ($\frac{\mathrm{W}}{\mathrm{cm}^2}$) in the lower bound and 0.989 ($\frac{\mathrm{W}}{\mathrm{cm}^2}$) in the upper bound from the crisp value of

0.986 ($\frac{W}{cm^2}$), these values of power densities indicate 0.245 % decreases and 0.179 % increases from the crisp value using the arithmetic operations. As a result, in terms of power output, the deviations are mainly affected by cell size.

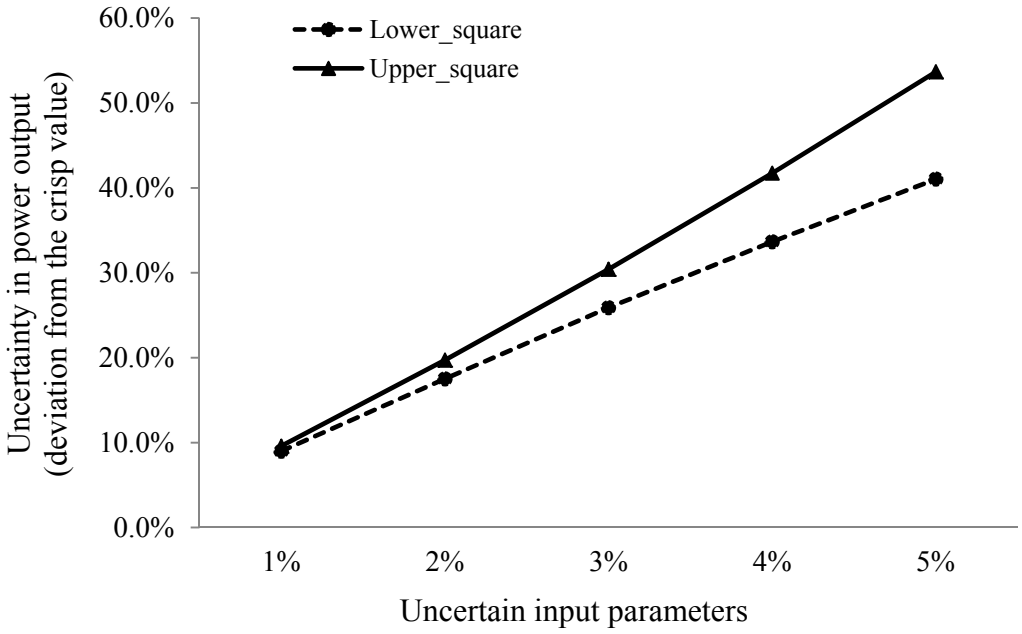

(a) Uncertainty in power output of a square cell

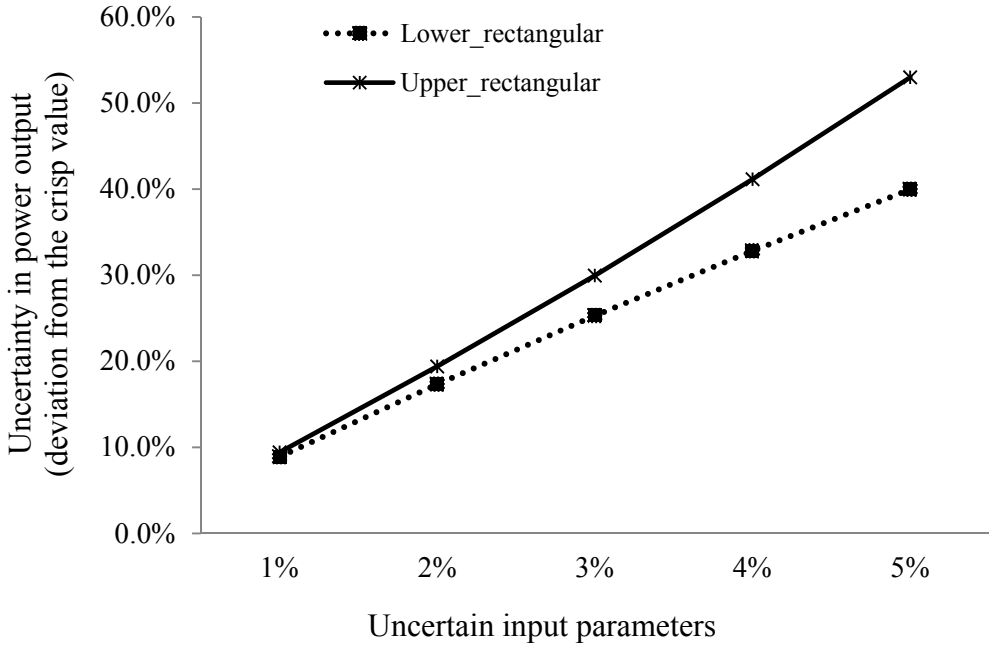

(b) Uncertainty in power output of a rectangular cell

Figure 4-7 Variation of deviations from the crisp value in conversion efficiency

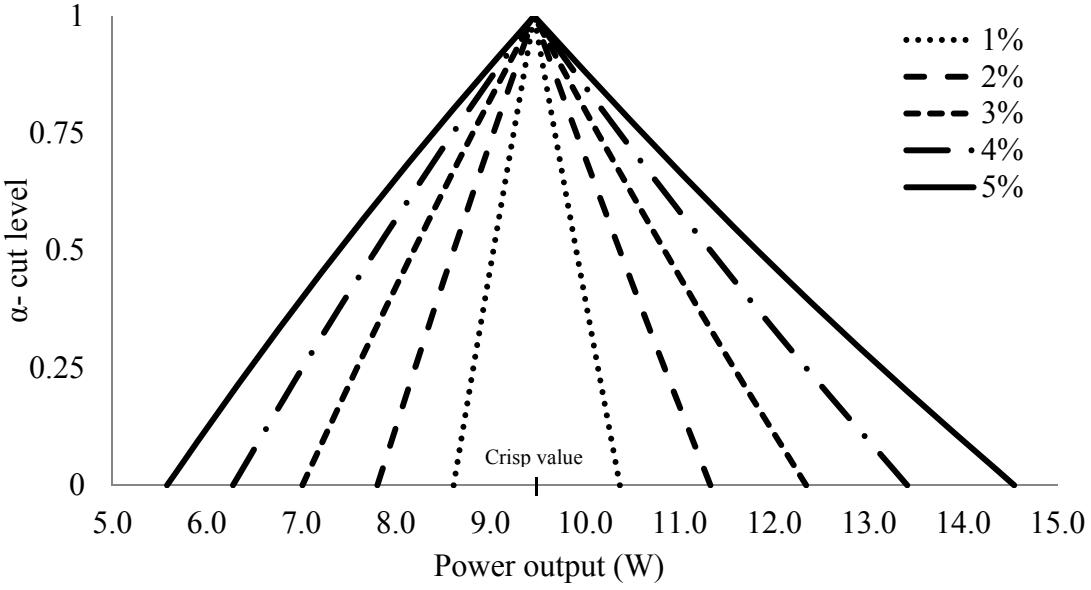

(a) Power output of square cell

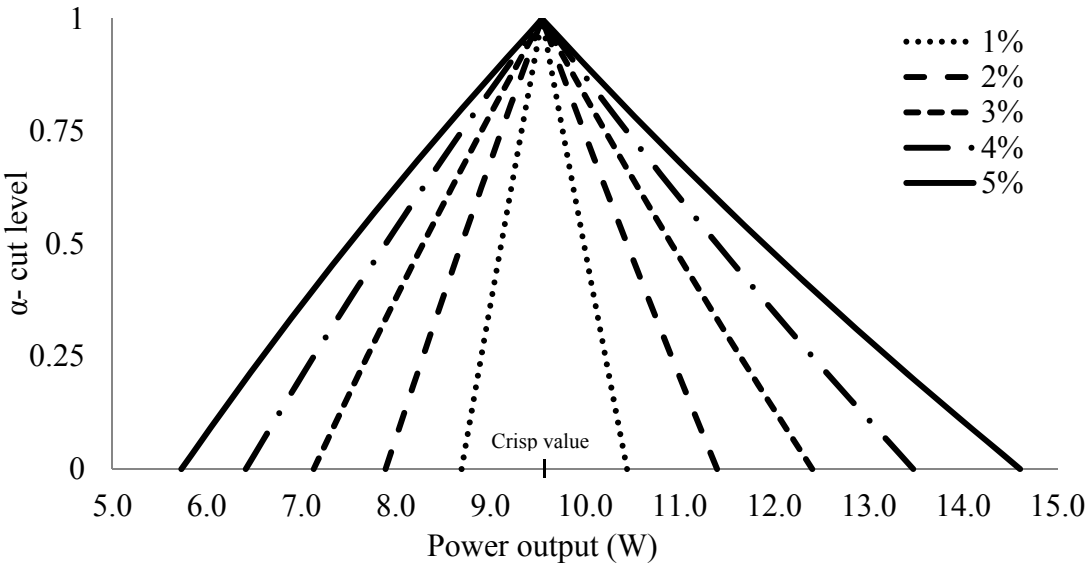

(b) Power output of rectangular cell

Figure 4-8 Variation of triangular shapes from the crisp value in power output with respect to a fuzzy confidence interval

When there is a ±5 % of fuzzy confidence interval and the a-cut level is equal to 0, one of the uncertain input parameters are applied to solar cells, but the remaining uncertain input parameters are fixed as a crisp value. The aforementioned individual uncertain parameter should be observed for variations in responses from the crisp value specifically for conversion efficiency and power output. This is intended to predict the performance of a solar cell because it can indicate which uncertain input parameters most contribute to performance.

- Conversion efficiency

In the case of the conversion efficiency, Y_1, and Y_7 of uncertain input parameters mainly influence the deviation of the conversion efficiency. Y_1 is constant solar energy and Y_7 is

the length of a solar cell in a square cell as shown in Fig. 4-9 (a). Similarly, Y_1, Y_7, and Y_8 are constant solar energy, and the length of a solar cell as shown in Fig. 4-9 (b).

In the case of the square cell, except for Y_1 and Y_8, other uncertain parameters contribute to the deviation at less than 1 %. Y_1 of an uncertain parameter is associated with the conversion efficiency ($\eta = \frac{J(C)_m V(C)_m}{P_{in}\ C}$ (1- F_{sum})). Thus, at ±5 % of the fuzzy confidence interval, 4.76 % and 5.26 % of deviations in both bounds are similar variations of uncertain input parameters, respectively. Y_7 of an uncertain input parameter is the main factor influencing the deviation of the conversion efficiency because the Y_7 parameter is associated with the fingers and busbars. The lengths of cells (L_c and H_c) are related to the length of the fingers and busbars in both a square cell and a rectangular cell. Similarly, in the case of the rectangular cell, at ±5 % of the fuzzy confidence interval, Y_1 is related to the conversion efficiency. Thus, the deviations of 4.76 % and 5.26 % are estimated. Y_7 and Y_8 of uncertain parameters are associated with the fingers and busbars, which are related to the contact power loss (F_c) between metallic fingers and busbars and solar cell surface and shadowing loss. When the lengths of the square and the rectangular cells increase from ±1 % to ±5 %, respectively, the deviation values become larger than the applied value of interval range. These results indicate that the fingers and busbars are related to the power losses of contact resistance (F_c), metal resistivity (F_f and F_b) and shadowing (F_s). When a single uncertain parameter is not incorporated with other uncertain input parameters, there is a small deviation, but with related factors between the length of the cells and the fingers or busbars, they significantly affect the deviation of the conversion efficiency.

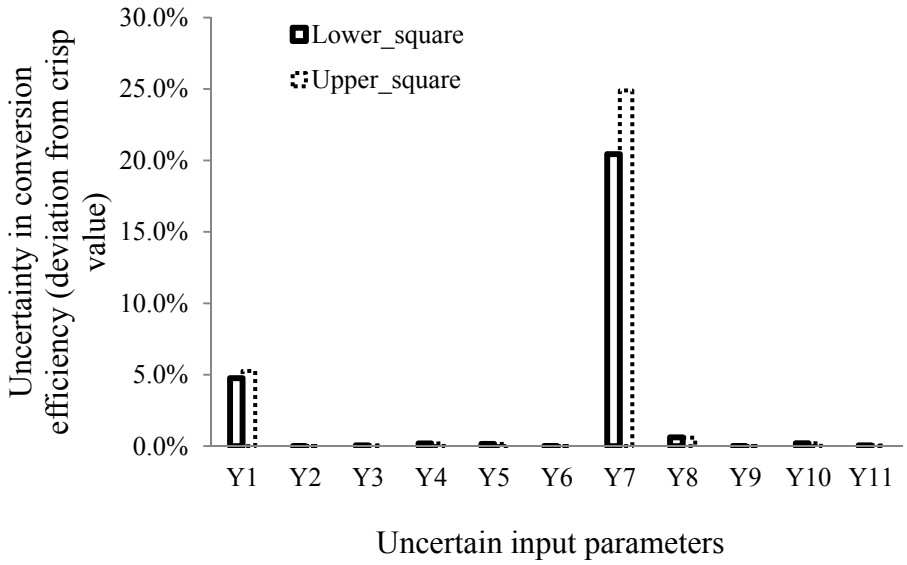

(a) Influence on conversion efficiency of square cell with respect to uncertain input parameters

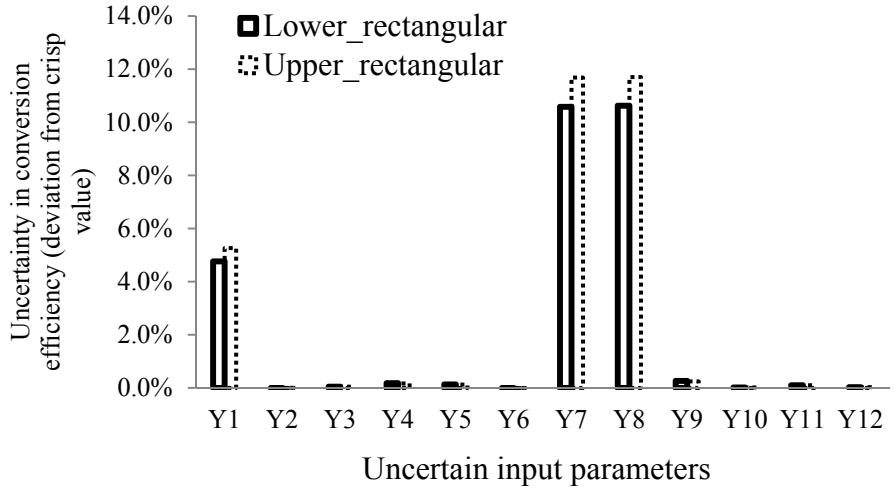

(b) Influence on conversion efficiency of rectangular cell with respect to uncertain input parameters

Figure 4-9 Influence on conversion efficiency with respect to uncertain input parameters

- Power output

In the case of square cell, at ±5 % of fuzzy confidence interval, the power density decreases 0.498 % in the lower bound and increases 0.488 % in the upper bound from the crisp value of the power density. These outcomes indicate that uncertain input parameters barely contribute to the deviation of power density including current and voltage. Figure 4-10 shows influence on power output with respect to uncertain input parameters. For square cells, 0.980 % of the power density decreases in the lower bound and 0.997 % of the power density in the upper bound. The total power losses (F_{sum}) are 6.90 % of the total power loss in the lower bound and 55.93 % of the total power loss in the upper bound from 32.88 % of the crisp value in a square cell. Also, the total power losses are 8.13 % of the total power loss in the lower bound and 55.42 % of the total power loss in the upper bound from 33.39 % of crisp value in a rectangular cell.

As a result, the power output is associated with the cell size (area), which is a major factor in solar cell design in a square cell (Y_7) and a rectangular cell (Y_7 and Y_8).

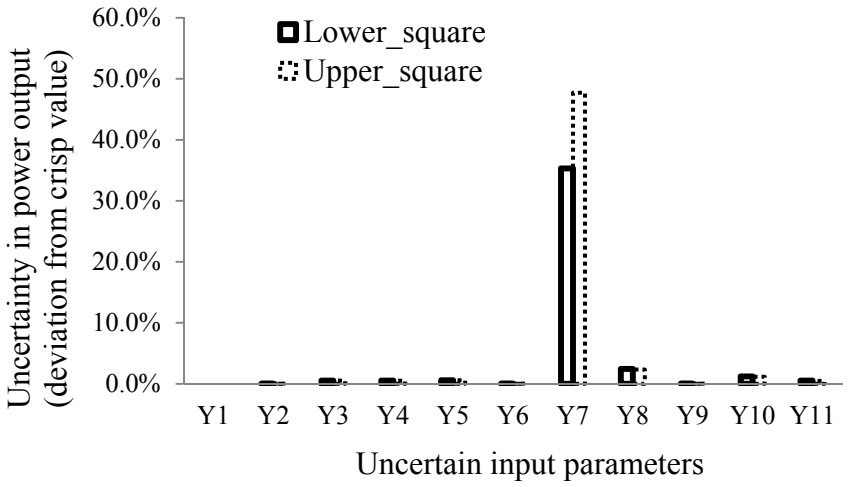

(a) Influence on power output of square cell with respect to uncertain input parameters

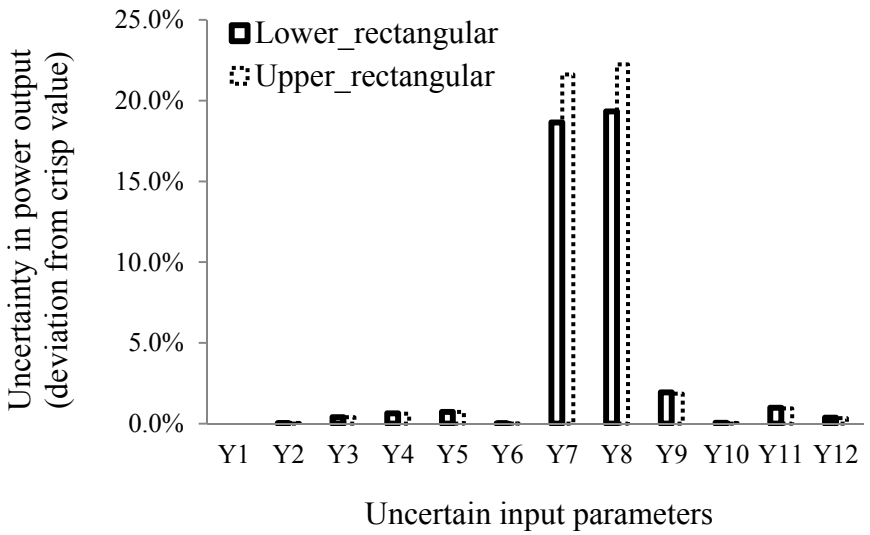

(b) Influence on power output of rectangular cell with respect to uncertain input parameters

Figure 4-10 Influence on power output with respect to uncertain input parameters

4.4.2 Solar CPC PV collector system

Solar CPC PV collector systems are used for the intensity of sunlight in order to improve the performance of photovoltaic (PV) solar collectors. There are three-objectives: the maximization of the average monthly incident solar energy (f_1), the maximization of the incident solar energy for the lowest month (f_2), and the minimization of cost (f_3). Each is considered separately.

4.4.2.1 Fuzzy analysis

Uncertain input parameters of the CPC collector unit has a receiver of length a_r, an acceptance angle of θ_c and is truncated at a height ratio r_T (the height of truncated CPC / the height of full CPC), dimensions L × W (length × width), and distance D between

adjacent rows. The solar collector is assumed to be installed in a specific location, Miami (USA), so the altitude (A) and solar constant (G_{sc}) are considered as uncertain input parameters. The uncertain input design parameters are:

$$\vec{S}=\begin{Bmatrix} a_r \\ \theta_c \\ L \\ \beta \\ D \\ r_T \\ A \\ G_{sc} \end{Bmatrix} \equiv \begin{Bmatrix} S_1 \\ S_2 \\ S_3 \\ S_4 \\ S_5 \\ S_6 \\ S_7 \\ S_8 \end{Bmatrix} \tag{4.40}$$

±1 %, ±2 %, ±3 %, ±4 % and ±5 % of the fuzzy confidence intervals are applied the solar CPC PV collector system for observing the deviations of three single-objective problems varying the α-cut interval levels from crisp value.

4.4.2.2 Numerical results

In the case of f_1 and f_2, the values of deviations of f_1 are 39.37 % in the lower bound and 52.02 % in the upper bound from the crisp value of f_1. The values of deviations of f_2 are 33.14 % in the lower bound and 22.39 % in the upper bound from the crisp value of f_2. These results indicate that uncertain input parameters are associated with collecting the amount of solar energy at a specified location and under seasonal characteristics as shown in Fig. 4-11.

Uncertain input parameters of S_1, S_2, S_3, S_4, and S_8 are main factors to influence the values of deviations in f_1. The other uncertain input parameters are less than 2 % as shown Fig. 4-11 (a). Four parameters of S_1, S_2, S_3, S_4, and S_8 contribute to the amount of average month incident solar energy. S_1 is the length of the cell receiver (a_r), which is

associated with S_2 (θ_c). The value of the deviation of a_r is the highest value for influencing the CPC PV performance because this factor helps determine the size of an array system. The value of S_2 contributes to the deviation of 7.92 % in the lower bound and 1.46 % in the upper bound. In this case, 1.46 % of the deviation from the crisp value of S_2 is lower than the deviation of the upper bound because this uncertain parameter influences the amount of solar energy, which means the lower bound section from the crisp value is more sensitive than the upper bound section. S_3 of a CPC collector contributes to 10 % of the deviation in both bounds. S_8 is 10 % in the lower bound and 9.98 % in the upper bound.

In the case of f_2, the deviation values are 42.34 % in the lower bound and 30.34 % in the upper bound from the crisp value of f_2. The values of deviation in uncertain input parameters are similar to f_1 except for θ_c and β. The tilt angle (β**)** is a critical factor in uncertain input parameters because the amount of incident solar energy fluctuates with varying tilt angles of an array due to Earth's axial tilt of 23.5°. Also, S_5 of an uncertain parameter contributes to 3.47 % of the deviation because the inclined arrays are sensitive to the distance between two adjacent rows with the Earth axial tilt angle at the lowest month (winter).

In the case of f_3, the deviation values are 25.24 % in the lower bound and 34.48 % in the upper bound from the crisp value of f3. Uncertain input parameters of S_1, S_2, S_3, S_4, and S_6 contribute to the results of the response of cost. S_1 and S_2 of the uncertain parameters influence mainly 9.64 % of the deviation in the lower bound 10.24 % in the upper bound because the cost of the CPC collector is estimated by the installation size (area) including

the solar receiver, land, and reflectors. Figures 4-11, 4-12, and 4-13 show the deviations of these three objective problems.

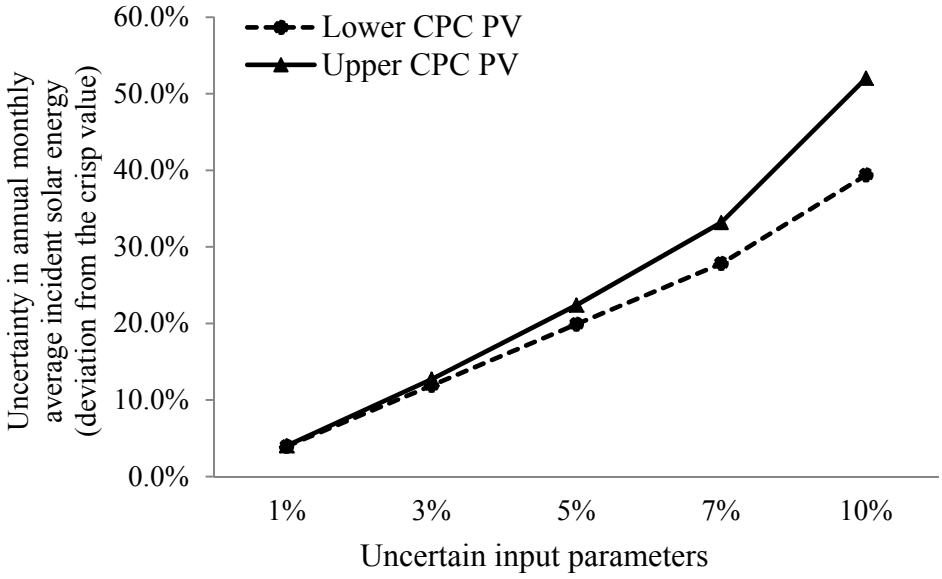

(a) Uncertainty in f1 of the solar CPC PV collector system

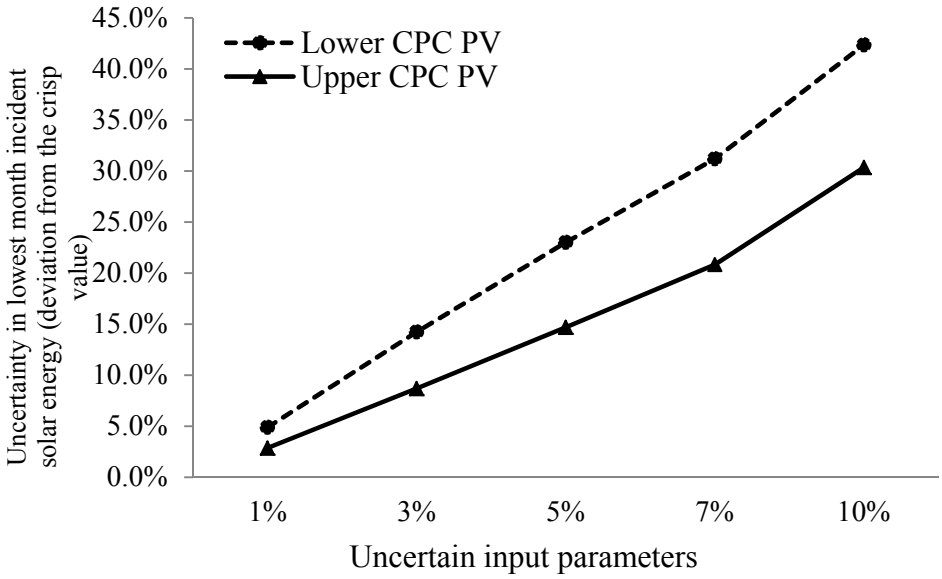

(b) Uncertainty in f2 of the solar CPC PV collector system

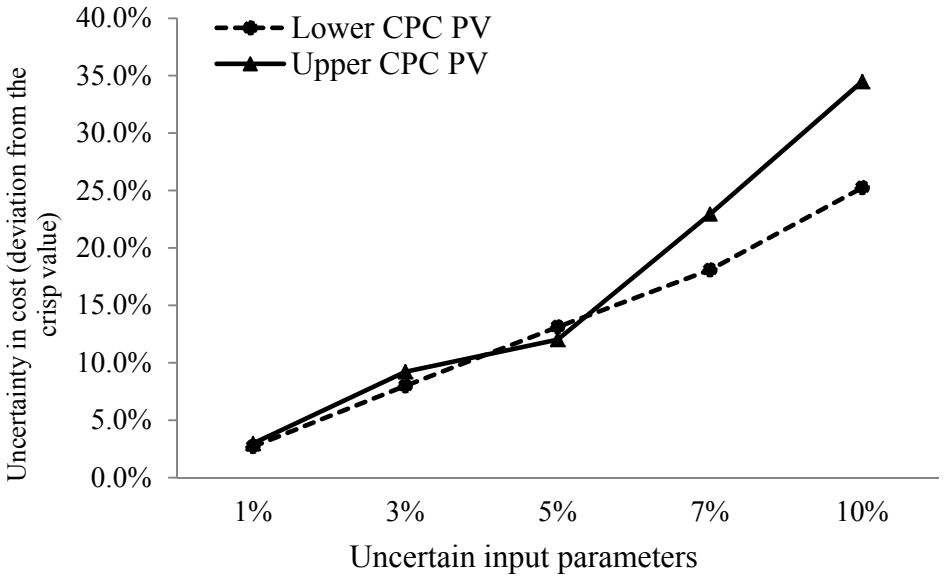

(c) Uncertainty in f3 of the solar CPC PV collector system

Figure 4-11 Variation of deviations of f_1, f_2 and f_3 from the crisp value with respect to a fuzzy confidence interval

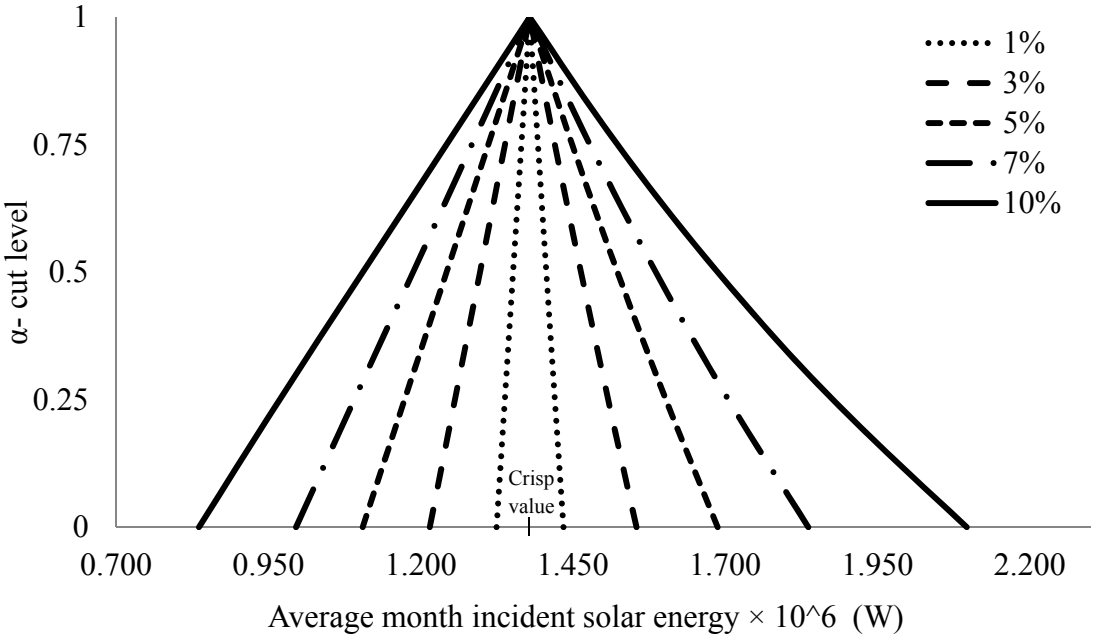

(a) Results of the influence on f_1

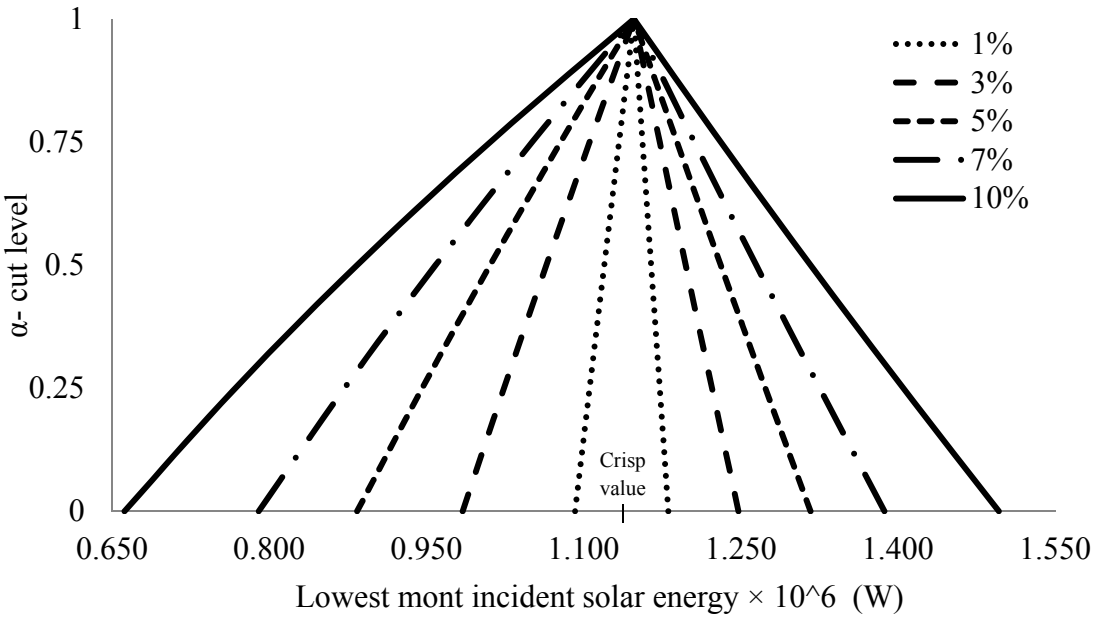

(b) Results of influence on f_2

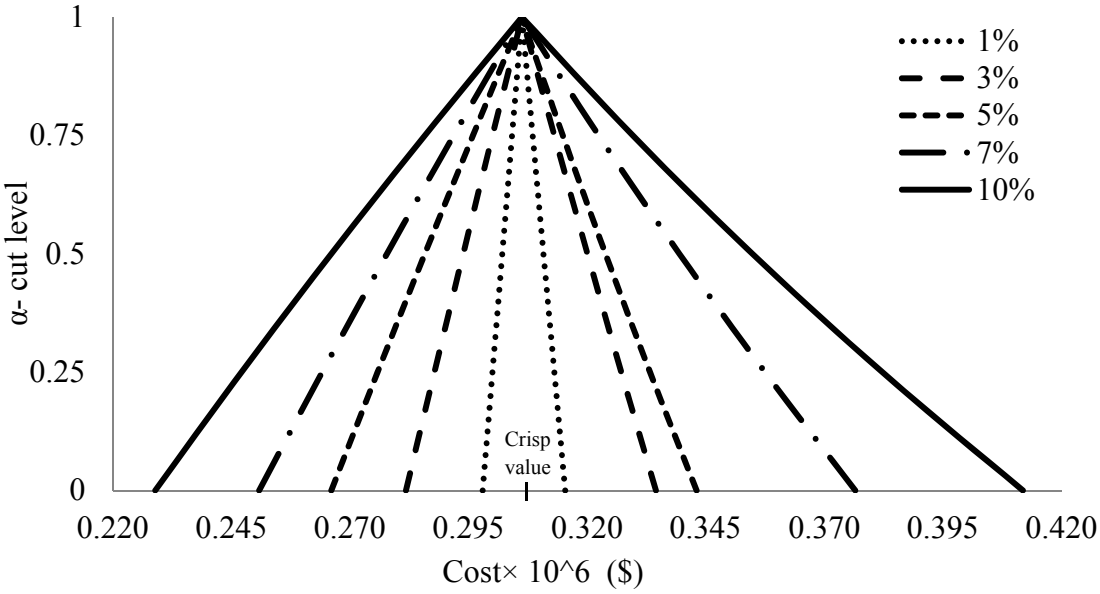

(c) Results of influence on f_3

Figure 4-12 Variation of triangular shapes of f_1, f_2 and f_3 with respect to a fuzzy set interval confidence

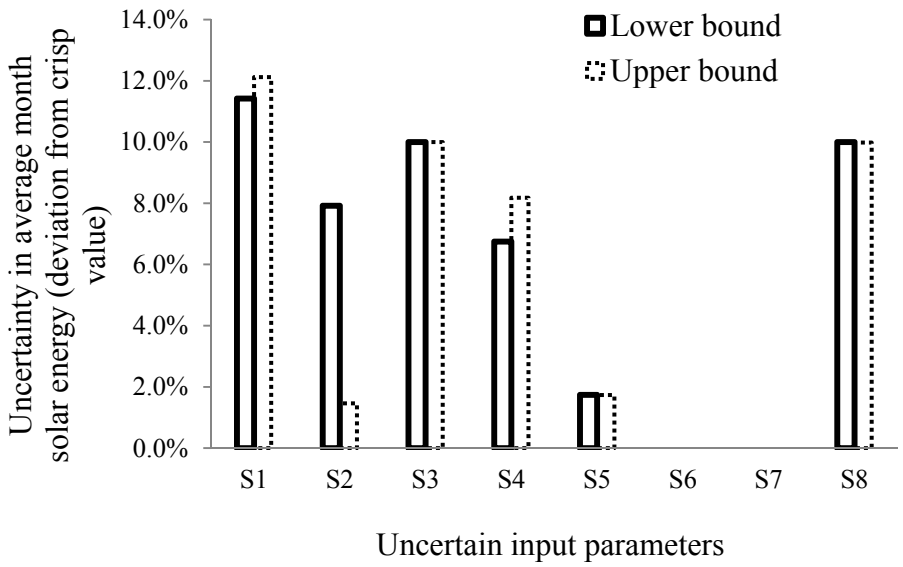

(a) Influence on average month incident solar energy of solar CPC PV collector with respect to uncertain input parameters

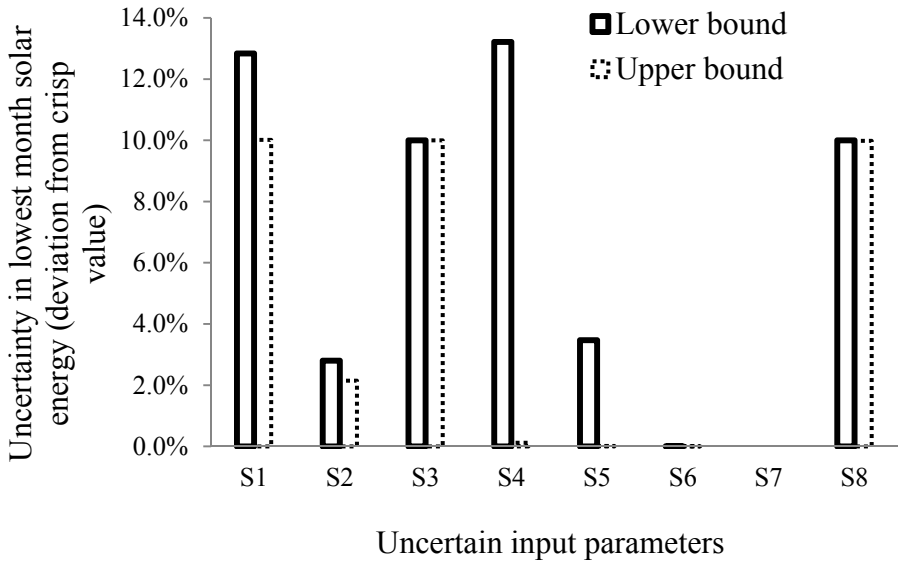

(b) Influence on lowest month incident solar energy of solar CPC PV collector with respect to uncertain input parameters

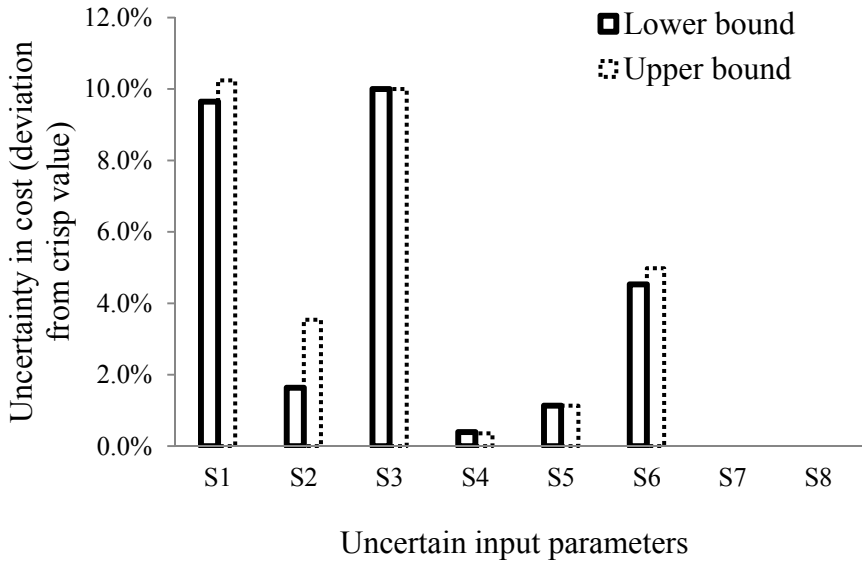

(c) Influence on cost of solar CPC PV collector with uncertain input parameters

Figure 4-13 Influence on cost of solar CPC PV collector with respect to uncertain input parameters

4.5 Conclusion

Probabilistic optimization and fuzzy set analysis techniques used in solar PV systems have been estimated. The results of probabilistic optimization are obtained by varying the values of levels of probabilities of satisfaction of constraints and coefficients of variation, and the results of fuzzy set analysis are gained by applying values of α-cut level and fuzzy confidence interval. This work illustrates the parametric study involved in the probabilistic performance of solar PV array systems.

- Solar cells

When the probability of constraint satisfaction is 50 %, all design variables have nearly the same results as the coefficients of variation of the random factors because the

probabilistic method retrogresses to deterministic optimization at different levels of uncertainty of the random variables. As the values of probability of constraint satisfaction increase from 50%, the constraints become more rigid, suggesting an optimization problem is solved by enforcing limited constraints compared to deterministic optimization conditions. The length of a cell, the height of the fingers and busbars, and the number of fingers are changed by applying different values of probability of constraint satisfaction and coefficient of variation in both cells. The change in geometric design variables has an influence on behavior constraints regarding the relationship between the height of the fingers and busbars, the aspect ratio of width to height of the fingers and busbars, and the numbers of fingers and busbars. As a result, most of the design variables start to vary considerably with varying coefficients of variation and probabilities of constraint satisfaction in both cells for observing the influence of uncertainty on the performance. In application, the change of probability of constraint satisfaction and coefficient of variation should be considered for solar cell design and manufacturing because randomness can lead to performance deviations in finding optimized solutions and obtaining effective performance uniformly across many data sets.

- Flat plate PV array system including the solar panel module

The standard deviation of each of the random parameters is varied from 0.5 % to 2 % of the respective mean values for observing the influence of uncertainty on optimization problem. The numerical results are given to show the influence of the level of probability of constraint satisfaction and the coefficient of variation of the random variables. Geometric parameters of the length of a cell, the height and width of the fingers and busbars, the number of fingers and busbars, and intensity of sunlight contribute to

reducing power losses, which improve the conversion efficiency while decreasing cell size. The size and number of the cells, panels and arrays attribute to the power output of an array system, amount of annual monthly average incident solar energy, and total cost of a solar PV array system considering the distance between adjacent rows and tilt angle. Under the application of different values of probability of constraint satisfaction and coefficients of variation of the random variables satisfaction, the conversion efficiency has increased due to tight constraints in both types of cells, respectively. These results indicate that variation values of conversion efficiency of a rectangular cell system are lower than a square cell system because the height and width of a rectangular cell is more flexible compared to a square cell. Also, there is trade-off between power density and the area of a flat plate PV array because the conversion efficiency is associated with power density, and the area of an array has decreased to limited values of constraints while the numbers of cells, panels and arrays have been adjusted. Based on changes in the conversion efficiency, the number of arrays, and the size of a flat plate PV array system, the maximum value of incident solar energy is optimized by the distance between adjacent rows and the tilt angle. Cost estimate is considered by peak per watt, which is associated with the power output and related sizes of cells, panels, arrays, and power density. In terms of cost, the cost of a work site has increased alongside an increase in the number of arrays, distance, and tilt angle, but the other cost factors, such as cell, panel, and array costs including materials, production, and installation are varied under different probability of constraint satisfaction and coefficient of variation. Thus, tradeoffs in a flat plate PV array system occur by the different values of probability of constraint satisfaction and coefficient of variation.

The fuzzy set theory is applied to solar PV systems using the membership function. Uncertain input parameters of different fuzzy confidence interval levels are applied to solar PV systems for observing the deviation from the crisp value.

- Solar cells

The deviations of solar cell performance including the conversion efficiency and power output are investigated. The design of a solar cell should be considered with top contact design. The conversion efficiency is associated with cell size and the geometric parameters of the fingers and busbars. As observed from the present results, the main considerations of optimal cell design are the cell size and metallic parts (fingers and busbars) because the total power loss is dominated by the contact loss between metallic parts and the size and number of fingers and busbars, which mainly cause shadowing loss. In the case of power output, the main uncertain parameter is the length of a solar cell. The power output is associated with the power density and cell size. The power density is small deviations for power output with ±5 % of the fuzzy confidence interval, but the variations of cell size significantly influence the deviation values.

As a result, consideration of the relationship between the conversion efficiency and power output is necessary for the optimal solar cell design.

- CPC PV collector systems

The optimal design of CPC PV collectors is investigated with a consideration of solar radiation with shading effect. It is observed that the average monthly incident solar energy (annual season) and incident solar energy for lowest month (winter) are different from the deviation values from the crisp values. As seen in the present results, when a

CPC PV collector system is installed in an annual season, the difference between the deviation value of the lower bound section and the value of the upper bound section is smaller than in winter. The main reason is that the CPC installation is sensitive to seasonal characteristics including solar radiation and with shading effect from the adjacent rows. Also, in the case of cost, the size of an array, cell receiver, and reflector should be reflected in a cost estimate as seen in previous results.

CHAPTER 5

Conclusion and Future Work

5.1 Conclusion

The aim of this work is to optimize solar PV systems at each level and solar PV array systems that are composed of solar cells and panel modules through mathematical programming techniques in order to seek optimum design parameters for improving the solar PV system performance while reducing cost. The genetic algorithms (GAs) method, modified game theory, and fuzzy set theory are implemented for solving the nonlinear programming of solar PV systems.

For optimal design of solar PV systems, six single-objective problems are formulated at various solar PV system levels considering the characteristics of a solar cell, panel module, and array system. In terms of increasing the conversion efficiency, the solar cell structure and top contact design are considered to improve the solar cell performance while reducing power losses. Solar cell structure contributes to voltage and current for calculating the performance through given parameters of materials, optical properties, and solar energy collection properties. The power losses are from top metallic contacts and blockage of sunlight. Relationships between current density and the thickness of cell structure of the emitter and base are investigated. For the purpose of maximizing solar cell performance, the contact grid variations (in terms of contact design variables) are considered. A parametric study is conducted to find the influence of emitter and base

thicknesses and relevant relationships among design variables. In considering maximization of the power output of an array system, the performance of individual solar cells, the number of solar cells and the complete system are considered. Power output is derived from power density and the size of a solar PV collector. With regards to incident solar energy, its amount is reliant on the size of the PV array system with consideration of seasonal variations of incident solar energy, shading effects associated with the use of multiple arrays and the tilt angle at a given installation area. The seasonal demands of a non-tracking system are determined by the tilt angle of arrays related to the sun's motion and position during a given time period. The position of the sun depends on the geographical location of a particular point on Earth. The motion of the sun has a major impact on the amount of power received by a solar collector in different seasons. Therefore, the amount of incident solar energy should be considered by variations in solar directions. In terms of cost, the cost of a solar PV array system is estimated through peak watt ratings. A solar PV panel module and balance of system (BOS) are considered to measure the maximum power output due to peak watt ratings. A solar PV panel module includes raw materials, fabrication, and production of solar cells in addition to the process of panel module production activities, such as wiring, sealing, and assembling each component. Also, balance of system (BOS) costs consists of the PV array system's design and construction activities, including manufacturing or purchasing of components.

The single-objective problems are solved using genetic algorithms (GAs). MATLAB programming can implement the optimization of a solar PV array system performance using the program, *ga,* which can find mixed-integer values of design variables by minimizing a scalar function starting from an initial set of values of the design parameters

for finding optimal values. Six single-objective optimization problems (maximizations of conversion efficiency of solar cell, power output of arrays, annual monthly average, lowest month's and highest month's incident solar energies, and minimization of cost) are investigated using *ga,* for finding optimal values.

Based on the results of single-objective optimization problems, a multi-objective optimization problem is formulated for a solar PV array system for finding a compromise solution in terms of its performance characteristics such as photovoltaic effect, size, and capacity of the solar collector and cost at a specified location through game and fuzzy set theories. Under game theory, multi-objective optimization problems of a solar cell, flat plate PV array system and CPC PV collector system are investigated. In the case of a solar cell, the multi-objective optimization problem of a solar cell is conducted using the results of the respective single-objective problems of the maximization of the conversion efficiency and power output and solved by placing on the minimum permissible conversion efficiency from maximum conversion efficiency and power output for finding a realistic compromise solution. In the case of a flat plate PV array system, the multi-objective optimization problem of the PV array system is formulated by six single-objective optimization problems which are related to the conversion efficiency of a solar cell, the power output of arrays, the annual monthly average incident solar energy, winter incident solar energy, summer incident solar energy and the total cost of the PV array system for finding a compromise solution in the process of the constraints stated. In the case of a CPC PV collector system, the multi-objective optimization problem of the CPC collector system is formulated by using the maximization of the annual monthly average incident energy, the lowest month's incident solar energy and cost. Also, with the results

of single-objective optimizations, the multi-objective optimization is investigated using the various CPC ratios and prices of installation land. In fuzzy set optimization, multi-objective optimization problems of a solar cell and flat plate array system are formulated by the results of the best and worst of single-objective optimization problems and found constructing the membership functions in a solar cell and solar PV array systems. A multi-objective optimization problem of a solar cell is formulated by the maximizations of the conversion efficiency and power output for finding a compromise solution and then the results are compared to the results of modified game theory. The multilevel optimization problem of a flat plate PV array system is constructed by six single objective optimization problems (the conversion efficiency of a solar cell, the power output of the arrays, annual incident solar energy, winter incident solar energy, summer incident solar energy and the total cost of the PV array system) and compared to the results of modified game theory. As a result, the multi-objective optimization problems of a solar cell, flat plate PV array system, and CPC PV collector system are for finding a compromise solution using modified game theory and fuzzy set theory.

The aim of uncertainty analysis is to predict the performance of a component or system in the presence of uncertain parameters. Uncertainty-based analyses and optimal design of a solar PV system are considered through probabilistic and fuzzy set analysis methodologies. Uncertain parameters are treated as random variables with known probability distributions in the probabilistic analysis. For the probabilistic analysis of a solar cell and flat plate PV array system, the random variables of a solar cell and flat plate PV array include geometric design variables (except for integer values; solar cell-a number of fingers and busbars, intensity of sunlight; panel module- a number of solar

cells; array system- a number of panels and arrays), design parameters of top metallic contact, and solar radiation. A solar cell and PV array system have been investigated by varying levels of probability of constraint satisfaction for prediction of performance. In the case solar cells, the length of a cell, the height of the fingers and busbars, and the number of fingers are changed by applying different values of probability of constraint satisfaction and coefficient of variation in both cells. These modifications in the geometric design variables have an influence on behavior constraints regarding the relationship between the height of the fingers and busbars, the aspect ratio of width to height of the fingers and busbars, and the numbers of fingers and busbars. Most of the design variables start to vary considerably with varying different levels of coefficients of variation and probabilities of constraint satisfaction in both cells for observing the influence of uncertainty on the optimization problem. In the case of solar PV array systems, random variables contribute to reducing power losses, which improve the conversion efficiency while cell size is decreased. The size and number of cells, panels and arrays attribute to the power output of an array system, amount of annual monthly average incident solar energy, and total cost of a solar PV array system considering distance between adjacent rows and the tilt angle.

The fuzzy membership functions are used for modeling the uncertain or imprecise design parameters of a solar PV system. Triangular membership functions are used to represent the uncertain parameters as fuzzy quantities. Fuzzy arithmetic operations and extension principles are used for finding the membership functions of the fuzzy response parameters of the system. In the case of a solar cell, the deviations of solar cell performance including the conversion efficiency and power output from the crisp value

are investigated by varying α-cut interval levels and uncertain input parameters of different fuzzy confidence intervals. In the case of a CPC PV collector system, the responses from applying uncertain input parameters of different fuzzy confidence interval levels are investigated by using the crisp values of the annual monthly average incident solar energy, lowest month incident solar energy, and cost. Also, the variations of three single-objective problems are represented by using a triangular shape with respect to various fuzzy interval confidence levels.

5.2 Future Work

In this dissertation, a non-tracking solar PV system is considered. It is possible to design a tracking system and its controls; but the cost of the resulting system will be very high.

Solar cell structure is made up of individual atoms bonded together in a regular structure to construct an arrangement. c-Si is a single PN junction material, but there are many different types of devices: hetero-junction devices, P-I-N and N-I-P devices, and multi-junction devices. Various junction devices should be considered to analyze a solar cell system using mathematical techniques pertaining to solar cell materials which are related to cell thickness, doping concentrations, and a metallic grid pattern of the surface that carry the current. For light intensity, only the top contact design is considered in this work as a design variable to minimize power losses including optical and electrical losses. However, in order to precisely reduce optical losses, anti-reflection coatings with different color, surface texture, material thickness, light trapping and rear reflectors can also be considered in a solar cell.

A PV panel module consists of a multitude of solar cells interconnected in series or parallel. To troubleshoot a PV panel module, the module circuit design should be considered. Notably, solar cell mismatch losses are caused by the interconnection of solar cells and modules. Analysis of the impact and power losses caused by mismatch should be investigated by considering various circuit designs in series and parallel. The packing density of solar cells in a PV panel module depends on the shape of the solar cells; for instance, square and circular shapes are obtainable. In this dissertation, c-Si solar cells are assumed in the form of square and rectangular shapes only. Most PV panel modules consist of a transparent top surface with glass, an encapsulant of EVA (Ethyl Vinyl Acetate), a rear and a frame. The front surface of a PV panel module plays a key role resulting from a high transmission from sunlight. Therefore, the top surface of the module needs a high transmission of light in the wavelength range based on respective characteristics of the solar cell materials. Different types of structural components of encapsulant, rear surface and frame of the module can be considered for enhanced optical transmission and thermal resistance with a consideration of wiring and assembling all components.

Within a solar PV array system, the operating temperature is a critical factor because the too low or too high operating temperature drops the energy efficiency of a solar PV array system including solar cell and panel module. It is important to know the temperature of a solar PV array system to predict its power output. Thus, temperature effects should be considered for estimating the performance of a solar PV array system.

REFERENCES

Abiola-Ogedengbe, A., Hangan, H., Siddiqui, K., 2015, Experimental investigation of wind effects on a standalone photovoltaic (PV) module, 2015, *Renewable Energy*, 75, pp.657-665

Abdul-Jabbar, N.K. and Salman, S.A., 1998, Effect of two-axis sun tracking on the performance of compound parabolic concentrators, *Energy Conversion and Management*, 39 (10), pp.1073–1079.

Al-Hasan, A., 1998, A new correlation for direct beam solar radiation received by photovoltaic panel with sand dust accumulated on its surface, *Solar Energy*, Vol.63, No. 5, pp.323-333

Annamdas, K.K. and Rao, S.S, 2009, Multi-objective optimization of engineering systems using game theory and particle swarm optimization, *Engineering Optimization*, Vol. 41, No. 8, pp. 737-752

Antoniadis, H., 2009, High efficiency, low cost solar cells manufactured using 'silicon ink' on thin crystalline silicon wafers, NREL/SR-5200-50824

Arturo, M.A, 1985, Optimum concentration factor for silicon solar cells, *Solar Cells*, Vol. 14, pp. 43-49.

Bellman, R.E., Zadeh, L.A., 1970, Decision making in a fuzzy environment, *Management Science*, 17, pp.141-164

Bony, L., Doig, S., Hart, C., Maurer, E., Newman, S., 2010, Achieving low-cost solar PV: Industry workshop recommendations for near-term balance of system cost reduction, *Rock Mountain Institute*

Brecl, K., and Topic, M., 2011, Self-shading losses of fixed free-standing PV arrays, *Renewable Energy*, 36, pp.3211-3216

Cabral, C.V., Filho, D.O., Diniz, A.S.A.C., Martins,J.H., Toledo, O.M., Vilhena,L., Neto, M., 2010, A stochastic method for stand-alone photovoltaic system sizing, *Solar Energy,* 84, pp.1628-1636

Camps, X., Velasco, G., Hoz, J.D.L., Martin, H., 2015, Contribution to the PV-to-inverter sizing ratio determination using a custom flexible experimental setup, *Applied Energy*, 149, pp.35-45

Chang, T. P, 2009, The Sun's apparent position and the optimal tilt angle of a solar collector in the northern hemisphere, *Solar Energy*, 83, pp.1274-1284

Chaudhuri, S. and Deb, K., 2010, An interactive evolutionary multi-objective optimization and decision making procedure, *Applied Soft Computing*, Vol. 10, pp.496-511

Goodrich, A., James, T., and woodhouse, M., 2012, Residential, commercial, and utility-scale photovoltaic (PV) system prices in the United States: Current rivers and cost-reduction opportunities, NREL.TP-6A20-53347

Dhingra, A.K., Rao, S.S., 1995, A cooperative fuzzy game theoretic approach to multiple objective design optimization, *European Journal of Operational Research*, Vol. 83, pp. 547-567

Djeffal, F., Bendib, T., Arar, D., Dibi, Z., 2012, An optimized metal grid design to improve the solar cell performance under solar concentration using multiobjective computation, *Materials Science and Engineering*.

Emam, O.E., 2006, A fuzzy approach for bi-level integer non-linear programming problem, *Applied Mathematics and computation*, 172, pp.62-71

Gautam, N.K., Kaushika, N.D., 2002, Reliability evaluation of solar photovoltaic arrays, *Solar Energy*, Vol. 72, No. 2, pp. 129-141

Hengsritawat, V., 2012, Optimal sizing of photovoltaic distributed generators in a distribution system with consideration of solar radiation and harmonic distortion, *Electrical Power and Energy Systems*, Vol. 39, pp.36-47

Hengsritawat, V., Tayjasanant, T., Nimpitiwan, N., 2012, Optimal sizing of photovoltaic distributed generators in a distribution system with consideration of solar radiation and harmonic distortion, 2012, *Electrical Power and Energy Systems*, 39, pp.36-47

Homburg, C., 1998, Hierachical multi-objective decision making, *European Journal of Operational Research*, 105, pp.155-161

Hottel, H.C., 1976, Simple model for estimating the transmittance of direct solar radiation through clear atmospheres, *Solar Energy*, **18**(2), pp.129-134

Hu, Y. and Rao, S. S., 2009, Game-theory approach for multi-objective optimal design of stationary flat-plate solar collectors, *Engineering Optimization*, 41(11), 1017 – 1035

Ibrahim A. Baky, 2010, Solving multi-level multi-objective linear programming problems through fuzzy goal programming approach, *Applied Mathematical Modelling,* Vol. 34 pp. 2377-2387

Jiang, H., Lu, L., Sun,K., 2011, Experimental investigation of the impact of aribone dust deposition on the performance of solar photovoltaic (PV) modules, *Atmospheric Environment*, 45, pp.4299-4304

Kacira, M., Simsek, M., Babur, Y. and Demirkol S., 2004, Determining optimum tilt angles and rientations of photovoltaic panels in Sanliurfa, Turkey, *Renewable Energy,* 29, pp.1265-1275

Kaushika, N.D., Gautam, N.K., Kaushik, K., 2005, Simulation model for sizing of stand-alone solar PV system with interconnected array, *Solar Energy Materials & Solar Cells*, 85, pp.499-519.

Kim, Y., Han, G. and Seo, T., 2008, "An evaluation on thermal performance of CPC solar collector," *International Communications in Heat and Mass Transfer*, 35(4), pp.446-457

Kouchaki, A, Iman-Eini, H., Asaei, B., A new maximum power point tracking strategy for PV arrays under uniform and non-uniform insolation conditions, *Solar Energy*, 91, pp. 221-232

Li, Z., Liao, H., and Coit, D., 2009, A two-stage approach for multi-objective decision making with applications to system reliability optimization, *Reliability Engineering and System Safety,* 94 pp.1585-1592

Liang, T.F., 2008, Fuzzy multi-objective production/distribution planning decisions with multi-product and multi-time period in a supply chain, *Computers & Industrial Engineering*, 55, pp.676-694

Liu, B.Y.H. and Jordan, R.C., 1960, Interrelationship and characteristic distribution of direct, diffuse and total solar radiation, *Solar Energy,* **4**(3), July, pp.1-19.

Mahmoud A. Abo-Sinna, Ibrahim A. Baky, 2007, Interactive balance space approach for solving multi-level multi-objective programming problems, *Information Sciences*, 177, pp.3397 – 3410

Martinez-Moreno, F., Munoz, J., and Lorenzo, E., 2010, Experimental model to estimate shading losses on PV arrays, *Solar Energy Materials & Solar Cells*, 94, pp.2298-2303

Merino, G.G., Jones, D.D., Clements, D.L., and Miller, D., 2003, Fuzzy compromise programming with precedence order in the criteria, *Applied Mathematics and Computation*, 134, pp.185-205

M.J. Chen, 1985, A new method for computer-aided optimization of solar cell structures, *Solid-State Electronics,* Vol. 28. No. 8. pp. 751-761

Moharil, R.M., Kularni, P.S., 2010, Reliability analysis of solar photovoltaic system using hourly mean solar radiation data, *Solar Energy*, 84, pp.691-702

Murtaza, A., Chiaberge, M., Sperino, F., Boero, D., Giuseppe, M. D., 2014, A maximum power point tracking technique based on bypass diode mechanism for PV arrays under partial shading, *Energy and Buildings*, 73, pp.13-25

Nold, S., Voigt, N., Friedrich, D., Weber, D., Haedrich, I., Mittag, M., Wirth, H., Thaidigsmann, B., Brucker, I., Hofmann, M., Rentsch, J., Preu, R., 2012, Cost modeling of silicon solar cell production innovation along the PV value chain, *EU PVSEC Program Planner*

O'Gallagher, J. J., 2008, Nonimaging optics in solar energy, Synthesis lectures on energy and the environment; technology, *science, and society*, Morgan & Claypool Publishers, San Rafael, CA.

Orozco-Gutierrez, M.L., Ramires-Scarpetta, J.M., Spagnuolo, G., Ramos-Paja, C.A., A method for simulating large PV arrays that include reverse biased cells, *Applied Energy*, 123, pp.157-167

Osman, M. S., Abo-Sinna, M. A., Amer, A. H., and Emam, O. E., 2004, A multi-level non-linear multi-objective decision-making under fuzziness, *Applied Mathematics and Computation*, 153 pp.239-252

Paap, S., Sandia Nat. Labs., Albuquerque, NM, Gupta, V. Cruz-Campa, J.L., Okandan, M., 2013, Cost analysis for flat-plate comcnetrators employing microscale photovoltaic cells, Photovoltaic Sepcialists Conference (PVSC),*IEEE*, 39, pp.3431-3434

Parlak, K.S., 2014, PV array reconfiguration method under partial shading conditions, *Electrical Power and Energy Systems*, 63, pp.713-721

Pelancheon, F., Mialhe, P., 1990, Optimization of solar cell performance, *Solid-State Electronics*, Vol.33, No.1, pp. 47-51

Potnuru, S.R., Pattabiraman, D., Ganesan, S. I., 2015, Positioning of PV panels for reductionin line losses and mismatch losses in PV array, *Renewable Energy*, 78, pp.264-275

Rao, S.S., 1987, Multi-objective optimization of fuzzy structure systems, *International journal for numerical methods in engineering*, Vol. 24, pp. 1157-1171

Rao, S.S., 1997, Analysis of uncertain structure systems using interval analysis, *AIAA*, Vol. 35, No. 4

Rao, S.S. and Hati, S.K., 1978, Game theory approach in multicriteria optimization of function generating mechanisms, *ASME*, pp. 78-87

Rao, S.S, Sundararaju,K., Prakash, B.G, and Balakrishna,C., 1992, Multiobjective fuzzy optimization techniques for engineering design, *Computers & structures*, Vol. 42, No. 1, pp. 37-44

Rao, S.S. and Freiheit, T.I, A modified game theory approach to multiobjective optimization, *ASME*, Vol. 113

Rao, Singiresu S., Hoe-Gil Lee, and Yi Hu, 2014, Optional Design of Compound Parabolic Concentrator Solar Collector System, *ASME J. Mechanical Design*, Vol. 136, No. 9, pp. 0914021-10.

Rao, Singiresu S., 2009, Engineering Optimization Theory and Practice, 4th Ed., *Wiley*, Hoboken.

Rault, F.K., 2002, A probabilistic approach to determine radiative recombination carrier lifetimes in quantum well solar cells, *Microelectronics Journal*, Vol. 34, pp.265-270

Rhodes, J.D., Upshaw, C.R., Cole, W.J., Holcomb, C.L., Webber, M.E., 2014. A multi-objective assessment of the effect of solar PV array orientation and tilt on energy production and system economics, *Solar Energy*, 108, pp.28-40

Richardson, D.B. and Harvey, L.D.D., 2015, Strategies for correlating solar PV array production with electricity demand, *Renewable Energy*, 76, pp.432-440

Rosa-Clot, M., Rosa-Clot, P., Tina, G.M., Scandura, P.F., 2010, Submerged photovoltaic solar panel: SP2, *Renewable Energy*, 35, pp.1862-1865

Shah, A.V., Sculati-Mellaud, F., Berenyi, Z.J., Ghahfarokhi, O.M., Kumar,R., 2011, Diagonostics of thin-film silicon solar cells and solar panels/modules with variable intensity measurements (VIM), *Solar Energy Materials & Solar Cells*, Vol. 92, pp.398-403

Shin, H.S., Lai, Y.J., Lee, E.S., 1996, Fuzzy approach for multi-level programming problems, *Computers & Operations Research*, Vol. 23, Issue 1, pp.73-91

Sivakumar, P., Kader, A.A., Kaliavaradhan, Y., Arutchelvi, M., 2015, Analysis and enhancement of PV efficiency with incremental conductance MPPT technique under non-linear loading conditions, *Renewable Energy*, 81, pp.543-550

Sivestre, S., Kichou, S., Chouder, A., Nofuentes, G., Karatepe, E., 2015, Analysis of current and voltage indicators in grid connected PV systems working in faulty and partial shading conditions, *Energy*, pp.1-9

Sivakumar, P, and Arutchelvi, M., 2014, Control of grid converters for PV array excited wind-driven induction generators with unbalanced and nonlinear loads, *Electrical Power and Energy Systems*, 59, pp.188-203

Sumitomo, T., Huang, H., Zhou, L., 2011, Deformation and material removal in a nanoscale multi-layer thin film solar panel using nanoscratch, *Intational Journal of Machine Tools & Manufacturer*, 51, pp.182-189

Tang, R. and Wu, T., 2004, Optimal tilt-angles for solar collectors used in China, *Applied Energy*, 79 pp.239-248

Tian, H., Mancilla-David, F., Ellis,K., Muljadi,E., 2012, A cell-to-module-to-array detailed model for photovoltaic panels, *Solar Energy*, 86, pp.2695-2706

Weinstock, D. and Appelbaum, J., 2007, " Optimization of economic solar field design of stationary thermal collectors," *Journal of Solar Energy Engineering*, 129, pp.363-370

Weinstock, D. and Appelbaum, J., 2004, Optimal solar field design of stationary collectors, *Journal of Solar Energy Engineering*, 126, pp. 898-905

Ya'acob, M.E., Hizam, H., Htay, M.T., Radzi, M. A.M., Khatib, T., 2013, Calculating electrical and thermal characteristics of multiple PV array configurations installed in the tropics, *Energy Conversion and Management*, 75, pp.418-424

Xiong, Y., Rao, S.S., 2004, Fuzzy nonlinear programming for mixed-discrete design optimization through hybrid genetic algorithm, *Fuzzy sets and systems*, Vol. 146, pp. 167-186

Zadeh, L., 1965, Fuzzy sets, Inform, Control 8, pp.338-353

Zhou, Z., Zhang, J., Liu, P., Li, Z., Georgiadis, M.C., Pistikopoulos, E. N., 2013, A two-stage stochastic programming model for the optimal design of distributed energy systems, *Applied energy*, 103, pp.135-144

Zulkifli, N.A., 2014, Probabilistic Analysis of Solar Photovoltaic Output Based on Historical Data, *IEEE 8th International Power Engineering and Optimization Conference*, pp.133-137

Zulkifli, N.A., Razali, M.M., Marsadek, M., Ramasamy, A.K., 2014, Probabilistic analysis of solar photovoltaic output based on historical data, *IEEE 8th international Power Engineering and Optimization Conference*, pp.133-137

Zheng, H., Li, S., Challoo, R., and Proano, J., 2014, Shading and bypass diode impacts to energy extraction of PV arrays under different converter configurations, *Renewable Energy*, 68, pp. 28-66